SECTION 4

Concrete Preparation and Initial Static Uniaxial Compression and Split Tensile Strength Testing

An initial step in this research was to first develop proper procedures for preparing consistent concrete for strength testing. To accomplish this the concrete was mixed and cured according to the MDOT modified mortar void method using a P1 mix design. This required that a procedure using the Michigan Tech lab equipment be established and used throughout this research. To establish this procedure as well as develop proficiency in the mixing process, a program was initiated to test concrete using three different coarse aggregate types. The program helped establish the concrete mixing. The second step was to investigate how different coarse aggregates, with a range of strengths, affect the compressive and tensile strength of the 28-day P1 concrete.

This section of the report presents the following results:

(1) A description of the MDOT modified mortar voids method used in this research,
(2) How the procedure was adapted at the Michigan Tech concrete laboratory and used to make concrete,
(3) The procedures used for handling and conditioning the coarse and fine aggregate,
(4) An analysis of three aggregate types to investigate how the MDOT mortar voids method varies with coarse aggregate types in uniaxial compression and split tensile testing, and
(5) A discussion concerning the results followed by conclusions and recommendations.

The research reported in this section was conducted by Bruce Hopkins at Michigan Tech and reported in a master's report titled "The Effect of Coarse Aggregate on Concrete Compressive and Tensile Strength." However, the thesis has been modified to a limited extent to conform to the overall report.

1 Introduction and Background

Traditionally, the coarse aggregate fraction of concrete has been made with natural aggregates such as gravels, carbonates, basalts and granites. Due to diminishing supplies of these aggregates, as well as the need to utilize by-product materials, a need exists to understand how the various material properties of the coarse aggregate affect the mechanical behavior of concrete. In general, the main performance criterion used in judging concrete quality is the 28-day uniaxial compressive strength test. To study how the compressive strength and split tensile strength of concrete varies with coarse aggregate, three aggregate types were compared. The coarse aggregates included in this study were basalt, natural gravel, and blast furnace slag. The selection of these material types was based primarily on the strength and shape of the three aggregates. The basalt was selected because it has the highest compressive strength and the most angular shape. The gravel has a relatively high compressive strength but a more rounded shape. Blast furnace slag is weaker in compression, but has a relatively rough surface (Vitton, 1998 b).

1.1 Background

A key portion (about 40 percent by volume) of concrete is the coarse aggregate, which is material larger than 4.75 mm (No. 4 sieve). In general, the material used as coarse aggregate varies from region to region, but typically must meet certain criteria for wear, absorption, and freeze-thaw durability. In this study crushed basalt, glacial gravel, and blast furnace slag were used to investigate how varying coarse aggregate properties may or may not affect concrete strength.

The basalt used in the study was obtained from an underground copper mining operation known as the Isle Royal Mines located near Houghton, Michigan. This mining operation ceased production in the 1930's. During the development of these mines, the basalt rock produced in the drilling and blasting for mine adits and drifts became known as "poor rock" due to the low concentrations of copper. These were considered as waste and were left stockpiled on the surface, termed as poor rock piles. Recently, these poor rock piles were purchased by local aggregate suppliers and crushed into various aggregate sizes.

Geologically, the basalt is of Precambrian age. It was formed as a flood basalt in association with the mid-continental rift zone. Due to the relatively quick cooling of the basalt as it flowed onto the surface of the earth; many gas bubbles were trapped as the lava cooled. Consequently, this basalt is known as amygdaloidal basalt, in which "amygdaloidal" is the term used for trapped gas bubbles. The flood basalts vary in thickness from a meter to ten meters. While the flood basalt was relatively uniform in composition, upon cooling, differentiation of minerals occurs with lighter minerals moving toward the top of the flow and denser minerals settling to the bottom of the flow. Therefore, obvious mineralogical differences occur in the basalt and subsequently in the crushed aggregate.

The glacial sand and gravel was obtained from an aggregate supplier in Hancock, Michigan. This operation mines sand and gravels from a glacial outwash, a deposit that formed during the last glacial episode. As is typical of glacial sand and gravel deposits, there is a very wide range of mineral types ranging from basalts to rhyolites to limestones. In general, rounded basalts and rhyolites dominate, with smaller quantities of limestone, indicative of the dominance of the local geology that consists of interbedded flood basalts and rhyolitic conglomerates. The sand portion, however consist primarily of quartz, with some feldspars present.

Blast furnace slag used in this study was from Detroit, Michigan. Slag is a co-product from the production of pig iron. In this process, iron ore, iron scrap, coke and either limestone or dolomite are added to the blast furnace. The coke combusts to produce carbon monoxide, which combines with the limestone and steel to form pig iron. Blast furnace slag is a nonmetallic byproduct, which contains mostly silicates, aluminosilicates, and calcium-aluminum-silicates.

Depending on the method of cooling, different forms of slag are produced, two of which are air-cooled and water quenched. A slag is formed when molten slag is placed in shallow beds and allowed to cool at ambient conditions in which a more crystalline structure is formed. This slag is typically referred to as air-cooled blast furnace slag (ACBFS). When liquid slag is cooled with the aid of water, it solidifies faster, due to increased thermal cracking of the material, producing a slag, which will be referred to as water quenched slag in this research. Physical properties of slag vary depending on the iron production process. For example higher unit weights are reported when slag contains more metals. This can result when more scrap iron is added to the blast furnace during the production of pig iron. The Federal Highway Administration (FHWA) reported a range of values for specific gravity from 2.0 – 2.5, compacted unit weight from 1120 – 1360 kg/m^3 (70 – 85 lbs/ft^3), and absorption ranging from one to six percent (FHWA, 1998).

ACBFS is used in granular bases, embankment and fills, and hot mix asphalt and Portland Cement Concrete (PCC) applications. While FHWA has user guidelines for these applications, the guideline for PCC only discusses ground granulated blast furnace slag. Currently, the FHWA does not address slag used as a coarse aggregate in PCC.

1.1.1 Previous Research

A study completed in 1933 used slag from two sources and gravel from one source as coarse aggregates for a strength comparison (Michigan State Highway Laboratory, 1933). In this study, the aggregates used were sieved into two uniform gradations and all mix designs were a six-sack mix. A sack is 43 kg (94 lbs) of cement. There were a total of four mixes with three of them containing the same blend of aggregate (one for each type of slag and one for the gravel) and the fourth had a finer blend of slag. This was done to show the effects of aggregate gradation on the strength of concrete. From each of the four mixtures, twenty beams and twenty cylinders were cast.

Axial compressive strength and modulus of rupture (MOR) tests were performed at 7 and 28-day periods on half the specimens made, i.e., ten tests per mix were performed at 7-days and then again at 28-days. In general, the results show slag had lower strengths for MOR and axial compressive strength at both test ages. Based on a 28-day cure, slag possessed an average of 11.6% lower axial compressive strength and a 5.1% less MOR strength than the concrete containing gravel. Also, there was no notable difference in strength when comparing the two slag mixes that contained different gradations. However, water-cement ratios were not consistent between the concrete mixes containing the different types of coarse aggregate possibly accounting for the variations in strength.

1.1.2 Mortar Voids Method

The Michigan Department of Transportation (MDOT) has been using a modified version of the mortar voids method to proportion concrete mix designs since 1928. Talbot and Richart first developed this method at the University of Illinois during the early 1920's (Shehan, 1970). Originally, the basic principal behind the mortar void theory was to seek minimum voids (air + water) in the concrete. Because coarse aggregate is assumed, for the most part, to consist of solid particles, the volume of voids in the concrete is said to be equal to the volume of voids in the mortar (sand, cement, air and water) for that concrete mix. The ratio between volume of voids and volume of cement is directly related to the strength of the concrete, if and only if the void spaces between the coarse aggregate particles are filled with mortar. It is known that the densest concrete mixture gives the highest strength concrete, but it is not necessarily the most durable. MDOT has specified air entrainment for all exposed concrete since 1942, which was done to improve durability. The recommended amount of entrained air specified is 6.5% with a tolerance of $\pm 1.5\%$ (MDOT, 1996). Due to the importance of void space for durability, the mortar void theory was altered to determine the minimum volume of water at the constant entrained air content.

The use of coarse aggregate in concrete is two fold, the first is to reduce volume change (reduce shrinkage) and the second is economy, since coarse aggregate is generally less expensive than cement. In addition, a concrete mixture should contain as much coarse aggregate as possible, while producing a workable mix. The limitation is that there must be enough mortar (sand, cement, air and water) to fill all the voids between the coarse aggregate particles.

The strength of hardened concrete depends upon the strength of the coarse aggregate as well as the strength of the mortar filling the void space between coarse aggregate particles. Two failure mechanisms are believed to be responsible when properly cured concrete fractures under an applied load. The first mechanism can be described as the break (or fracture mechanism), which is through or across the particles of coarse aggregate but not around them indicating that the coarse aggregate is weaker than the surrounding mortar (Shehan, 1970). The second failure mechanism is that "the break (or fracture) should be through some of the coarse aggregate particles with numerous particles pulled away from the mortar bond (as the fracture goes around the coarse aggregate)" (Grove, 1998). These fracture mechanics statements assume that the factors pertaining to the concrete mix remain constant and that the volume of coarse aggregate is not excessively high.

An MDOT laboratory procedure based on the above assumptions consists of a trial batch study using actual job materials. This laboratory procedure uses the job materials to determine the minimum voids at a constant entrained air content for the mortar. Results from the laboratory procedures determine several mix design parameters. After all laboratory work has been completed, a mix design is computed using the bulk dry specific gravity and absorption for both coarse and fine aggregates, as well as the dry loose unit weight of the coarse aggregate. The grade of concrete is also needed for the mix design. A complete description and detailed procedure of the mortar void method is discussed in the Mortar Voids Method of Proportioning Concrete, as used by the Michigan Department of State Highways (Shehan, 1970).

1.2 Research Objective

The main objective for this portion of the research was to determine the degree that the axial compressive and split tensile strength of concrete vary with coarse aggregate type using the MDOT Mortar Voids Method of Proportioning Concrete (Shehan, 1970). All of the concrete testing was conducted on 28-day concrete. To undertake this, three coarse aggregates were used representing a diverse selection of aggregate. The three aggregate types were basalt, glacial gravel, and blast furnace slag. An important issue in the research was to maintain a constant mix design with only the coarse aggregate as the variable (see Section 1.3). Consequently, MDOT guidelines and laboratory procedures were rigorously followed in this research program. This included a complete mixing procedure, as well as the testing methods for freshly mixed concrete.

1.3 Research Scope

Three types of coarse aggregate and one source of fine aggregate were considered in this research. Using a P1 mix design (MDOT, 1996, Section 601), three separate mix "recipes" were determined for the three different coarse aggregates because of the varying properties of each aggregate. This section provides the results for 28-day axial compressive and split tensile strength tests for the concrete made with each of the three types of coarse aggregates. Along with the testing results, the method for mixing the concrete used in this research, which was in accordance with MDOT specifications, is presented.

2 Materials and Casting Methods

The concrete tested in this project consisted of the following materials: cement, coarse and fine aggregates, air entrainer and water. There were no other admixtures used in any of the mix designs. Water used for all concrete was Houghton City water, which came directly from the tap located in the concrete mixing laboratory (B006) of Dillman Hall at Michigan Technological University (MTU). A measured quantity of water was placed in sealed five-gallon containers one day prior to casting a batch of concrete. This was done so the water would be at room temperature by the time a batch was mixed. Each of the remaining constituents is described in the following sections. ASTM procedures were followed with exceptions, where noted.

2.1 Cement

Lafarge (Alpena) Type I cement, which conformed to ASTM C 150-97, was used throughout the entire study. The manufacturer specified specific gravity used for all design calculations was 3.15. Cement was packaged in 43 kg (94 lbs) sacks. In order to eliminate as many variables as possible, care was taken in handling of cement. The cement was measured out to the exact amount needed to produce one batch of concrete (6 ft^3), then placed in moisture proof buckets with tight sealing lids and stored in the concrete mixing laboratory in Dillman Hall. An Ohaus electronic scale with a capacity of 100 kg (220 lb.) and a readability of 0.01 kg was used to weigh the cement.

2.2 Aggregates

As mentioned three types of coarse aggregate and one type of fine aggregate were used for this study. The coarse aggregates chosen included a basalt mine rock, glacial gravel and an iron blast furnace slag. The fine aggregate was natural silica sand. All aggregates were sampled at their sources and brought back to MTU for storage. MDOT source numbers, aggregate types and the reference name used in this report are listed in Table 2.1. A description of each type of aggregate follows herein.

Table 2.1 Aggregate Source Numbers and Reference Names

Reference Name	MDOT Source No.	Agg. Type	% crushed
CA-B	31 - 076	Moyle basalt	100
CA-G	31 - 045	Glacial gravel	50
CA-S	82 - 019	Levy blast furnace slag	100
FA-Y	31 - 045	Natural silica sand	-

In Table 2.1 the reference name listed, e.g., CA-B, will be used throughout this chapter to refer to the concrete made with each of the coarse aggregates. The "CA" stands for coarse aggregate, while the "B" stands for basalt and therefore CA-B would be concrete made with basalt as the coarse aggregate.

Two of the coarse aggregates used for this study were locally available from the Houghton/Hancock area of Michigan. A 100% crushed (highly angular) basaltic mine rock (Moyle, 31-076) was one of the chosen aggregates. This aggregate varied in color from a dark gray to a medium green and contains amygdaloidal inclusions or gas bubbles. In general, the mineralogy consists of pyroxenes and quartz. A 50% crushed glacial gravel (form the Superior Sand and Gravel company, 31-045) was the second coarse aggregate used for the study. The glacial gravel was non-uniform in color and contained a number of different minerals but was mostly composed of quartz and feldspars. These two aggregate types were chosen based on their characteristics, availability and location.

As mentioned, slag is a manufactured aggregate produced as a by-product in the production of pig iron and contains mainly silicates and calcium. The material floats to the top of the blast furnace and is released from the base of the blast furnace after the heavier pig iron has been removed. When the slag is poured into the yard it is generally water quenched but in the past has been air-cooled. Once the slag is cooled, it is broken up and brought to the aggregate pit where it was crushed down and sieved to the proper gradation for stockpiling. As discussed in Chapter 3 water-quenched slag was used in this project. The slag was also 100% crushed.

Sieve analysis was performed on both fine and coarse aggregates using the ASTM C 136-96a procedure. The coarse aggregates were mechanically sieved into four size fractions (1) 25.0 – 19.0 mm (1 – 3/4 in.), (2) 19.0 – 12.5 mm (3/4 – 1/2 in.), (3) 12.5 – 9.5 mm (1/2 – 3/8 in.) and (4) 9.5 – 4.75 mm (3/8 in. – No.4). Immediately after sieving, the aggregate was placed in plastic containers (one container for each size fraction), and covered with tight sealing lids to avoid contamination. A test blend was later created with 25% by weight of each size fraction. This test blend was chosen to produce a uniform gradation, which would pass the MDOT 6AA gradation limits. A standardized test blend also helped to eliminate any effect that various gradations might have on the results, i.e., the same test blend was used throughout the project. For example, specific gravity experiments used 5000 g (11.0 lb.) sample sizes, and the test blend would contain 1250 g (2.8 lb.) of each size fraction.

The fine aggregate was locally available natural silica sand from the Superior Sand and Gravel Company (31-045) in Hancock, Michigan. This fine aggregate was used throughout this study for the primary purpose of eliminating any effect that the use of several types may have had on the research results. Due to storage limitations, however, sand had to be obtained from the source three times. Grain size distribution charts with MDOT specified gradation limits for 6AA coarse and 2NS fine aggregates are provided in Figures 2.1 and 2.2, respectively (MDOT, 1996, Section 902). The grain size distribution curve for fine aggregate was an average of several sieve analyses performed. At least one sieve analysis was performed whenever new aggregate was obtained. The fine aggregate fell within the limits specified for a 2NS aggregate. The fine aggregate had an average fineness modulus of 2.67. To avoid contamination the sand was stored in large plastic containers with tight fitting lids.

Each aggregate in this study was tested to determine apparent specific gravity (G_S), bulk dry specific gravity ($G_{B(DRY)}$), bulk saturated surface dry specific gravity ($G_{B(SSD)}$), percent absorption, and unit weight. Samples of all coarse and fine aggregates were sent to MDOT, where specific gravity and absorption tests were conducted following ASTM C127 for coarse aggregate and C128 for fine aggregate. Companion tests were performed at MTU where specific gravities and absorption values for coarse aggregate were determined according to ASTM C127-88, while ASTM C 128-93, for measuring the specific gravity and absorption of the fine aggregate, respectively. In addition, the same properties were measured at MTU using automated methods (Vitton et al., 1998 a). Dry loose unit weights were also measured at MTU according to the shoveling procedure stated in ASTM C 29-97. Results from these tests are listed in Table 2.2.

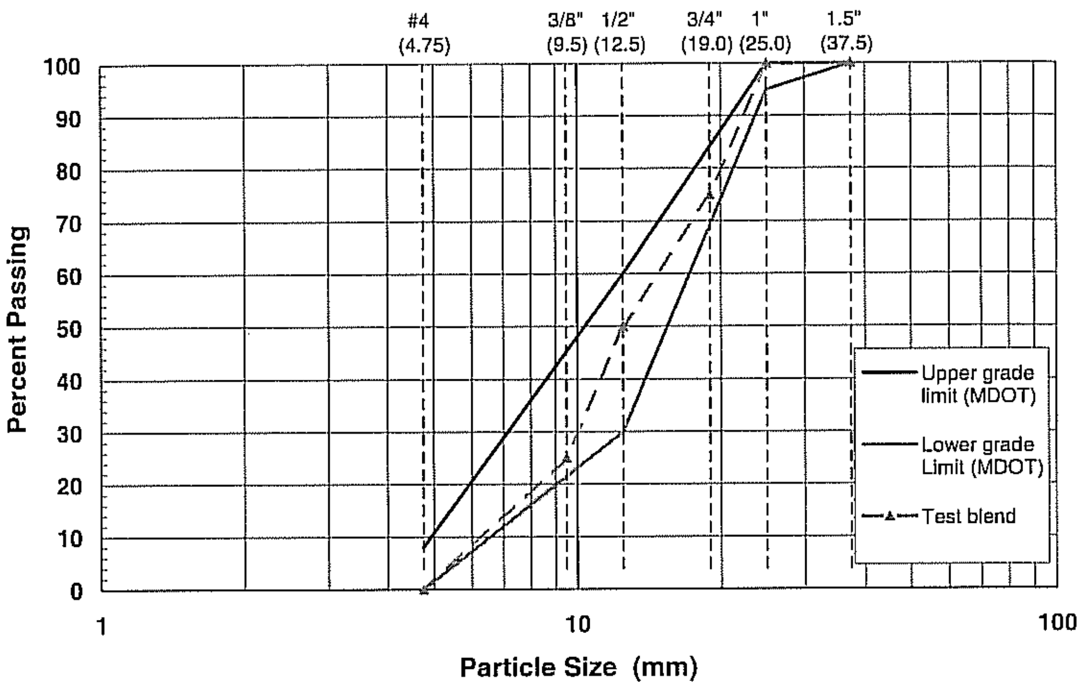

Figure 2.1. Grain Size Distribution for Test Blend 6AA Coarse Aggregate and MDOT Specified Grade Limits.

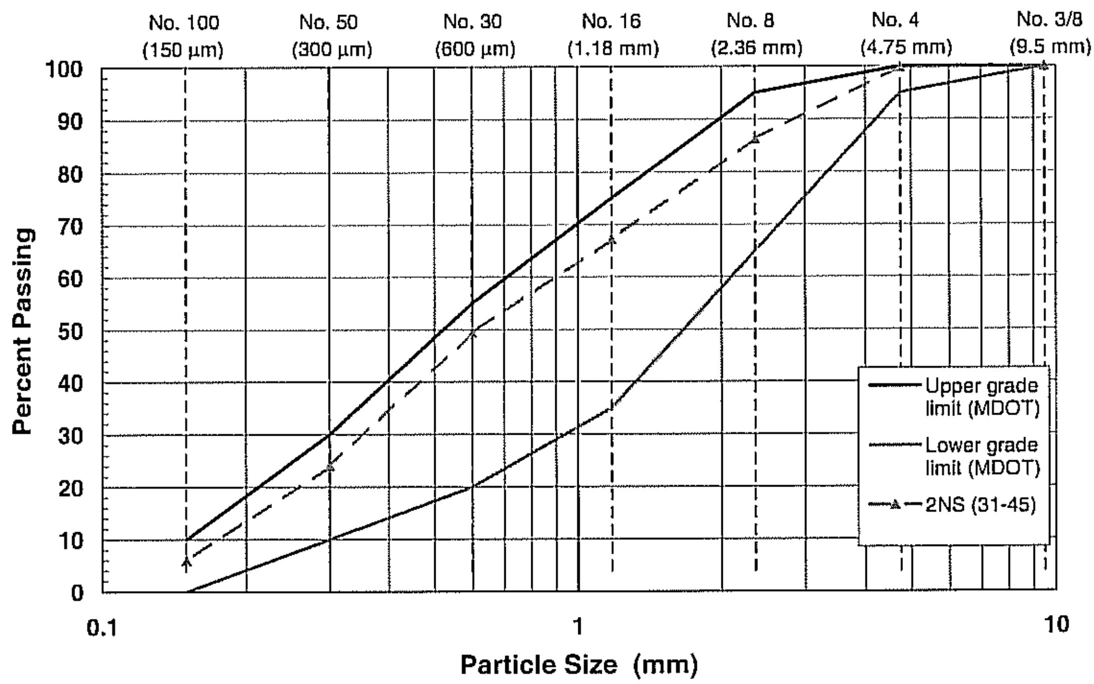

Figure 2.2. Grain Size Distribution for 2NS Fine Aggregate and MDOT Specified Grade Limits.

Table 2.2 Summary of Aggregate Properties

Aggregate Type	Tested by	Apparent Specific Gravity G_S	Bulk SSD Specific Gravity $G_{B(SSD)}$	Bulk Dry Specific Gravity $G_{B(DRY)}$	Absorption %	Unit Weight kg/m^3 (lb/ft^3)
CA-B (basalt)	MDOT	2.91	2.83	2.79†	1.45†	-
6AA Coarse Aggregate	MTU	2.91	2.82	2.78	1.54	1510 (94)†
Source # 31 – 76	Automated	2.89	2.82	2.78	1.44	-
CA-G (glacial gravel)	MDOT	2.83	2.76	2.73†	1.35†	-
6AA Coarse Aggregate.	MTU	2.83	2.76	2.72	1.48	1556 (97)†
Source # 31 – 45	Automated	2.79	2.72	2.69	1.46	-
CA-S (slag)	MDOT	2.47	2.35	2.27†	3.55†	-
6AA Coarse Aggregate.	MTU T1‡	2.68	2.56	2.49	2.74	1212 (76)†
Source # 82 – 19	MTU T2‡	2.71	2.44	2.29	6.76	
	Automated	2.85	2.49	2.29	8.49	-
FA-Y (silica sand)	MDOT	2.73	2.68	2.67†	.87†	-
2NS Fine Aggregate.	MTU	2.75	2.69	2.65	1.30	1728 (108)
Source # 31 – 45	Automated	2.72	-	-	-	-

† Used for mix designs.
‡ MTU Trials 1 and 2, respectively.

Worksheets for computing the specific gravity of the coarse and fine aggregates as tested by MTU are included in Appendix IV-A. For each aggregate, a minimum of three tests were performed to determine average values for G_S, $G_{B(SSD)}$, $G_{B(DRY)}$, and percent absorption. G_S is defined as the oven dry weight of coarse aggregate divided by the apparent volume (no permeable voids included in the volume). $G_{B(SSD)}$ is the saturated surface dry weight of the coarse aggregate divided by the envelope volume (permeable voids included). The oven dry weight of the coarse aggregate divided by the envelope volume is equal to $G_{B(DRY)}$. Each worksheet includes the raw data and the formulae used for computations as well as a summary of average values. These average values were listed in Table 2.2 under the heading MTU. For the case of CA-S, two trials were performed according to the optional procedures allowed by ASTM C127-88. The first trial used a gentle stream of moving air to bring the aggregate to the saturated surface dry condition. The procedure for trial two was to roll the aggregate on towels until the saturated surface dry condition was obtained. Results of each trial are tabulated in Table 2.2 and included in Appendix IV-A.

The three test methods (MDOT, MTU, and Automated) used to determine G_S, $G_{B(SSD)}$, $G_{B(DRY)}$, and absorption were in good agreement for both CA-B and CA-G. Test methods used to determine specific gravity and absorption values for slag did not compare well with one another even though an additional trial was performed by MTU. Because MDOT has more experience working with slag than does the author, and the three methods compared well for CA-B and CA-G, it was decided to use the MDOT values for specific gravities and absorption for both fine and coarse aggregates in the mix designs used in this study.

2.3 Mix Designs

The mortar voids method (Shehan, 1970) for proportioning concrete mixtures was used to determine all mix designs. A standard six-sack grade P1 Portland Cement Concrete (PCC) pavement mix (MDOT, 1996, Section 601) was used in this project. Quantities for each mix design constituent were calculated by MDOT (MDOT Form 1830, File 300, 1998 and included in Appendices B through D of this report). This method of mix design used bulk dry specific gravity for both coarse and fine aggregates. A workability factor (b/b_o) of 0.72, defined as the volume of dry loose coarse aggregate per unit volume of concrete was also used as a mix design parameter. A target slump of 51 - 76 mm (2 – 3 in.) and an air content of 5% ± 1.5% was considered an acceptable batch. The three mix designs, one for each type of coarse aggregate, are listed in Table 2.3.

Table 2.3 Mix Design Proportions, per m^3

	Coarse aggregate type		
	CA-B	CA-G	CA-S
Cement	335	335	335
Coarse agg. (dry)	1087	1120	873
Fine agg. (dry)	791	743	803
Water	165	162	181

Note: All quantities in kg/m^3 ($1\ kg/m^3 = 1.69\ lbs/yd^3$).

"Mixing Proportion" worksheets used for computing the proper amount of each constituent per batch of concrete are included as the first page in Appendices IV-B, IV-C, and IV-D corresponding to the three mix designs, CA-B, CA-G, and CA-S, respectively. There is one mix proportion worksheet for each type of coarse aggregate used in this project. MDOT provided values for each material used to make 1 m^3 of concrete (Table 2.3) are shown on each worksheet (MDOT Form 1830, File 300 and included in Appendices IV-B through IV-D of this report). These worksheets were developed to compute quantities for each constituent used to make a 0.078 m^3 (2.75 ft^3) batch of concrete as well as the total amount of absorbed water per m^3. Batch computation worksheets that follow the mix proportion worksheets in each of these appendices are discussed in Section 2.4.

2.4 Aggregate Preparation

A two-step preparation process was used for all coarse aggregate. First, forty-eight hours before mixing concrete, a specified amount of coarse aggregate was oven dried for 24 hours. Each size fraction was kept separate. A tare weight of pails used for soaking aggregate was measured and recorded on the batch computation worksheet. Because of batch size, two containers were used for soaking the coarse aggregate with two of the four size fractions in each container. Each individual size fraction of coarse aggregate was then measured in the dry condition and placed in a container. Finer material was placed at the bottom of the container and the coarser material on top, i.e., materials retained on the 4.75 mm (No. 4) and the 19 mm (3/4 in.) sieves were placed in the first pail with the 4.75 mm aggregate at the bottom of the container. This was done to help hold the finer material in place during the later decanting process of the coarse aggregate.

Second, the aggregate was soaked in water for 24 hours before it was used to make a batch of concrete, which is referred to as moisture conditioning. All aggregates were weighed using an Ohaus electronic scale with a capacity of 100 kg (220 lbs) with 0.01kg (0.01lbs) readability.

Third, the fine aggregate was moisture conditioned for 24 hours before it was used to make a batch of concrete. A fixed drum refractory mortar mixer (10 cubic foot capacity, 10 HP (220 volt), Anchor Manufacturing Co., Chicago, IL) was used for the conditioning. The fine aggregate was first placed in the mixer. While the mixer was running, water was added until the aggregate was moistened slightly above the saturated surface dry condition. A simple test was performed to determine if enough water had been added to the sand. This was accomplished by taking a handful of sand and squeezing it together then letting go. If enough water has been added the sand should just start to clump in the hand. After the sand was moisture conditioned, the mixer was covered with plastic bags and a tarp to help minimize evaporation of water from the sand.

All of the batch computations worksheets for the mixes used in this research are provided in Appendices IV-B, IV-C, and IV-D. Consequently, there is one worksheet for every batch of concrete made. Two batches are included for both CA-B (basalt) and CA-G (glacial gravel), while four batches are presented for CA-S (slag). Included in the coarse aggregate data block on each sheet are pail tare weights and the quantities of coarse aggregate per size fraction. The fine aggregate data block has values for moisture content and the total amount of sand per batch. First the moisture content was calculated then multiplied by the design quantity of fine aggregate to obtain the moisture (amount of water) in the fine aggregate. The moisture was then added to the design weight of fine aggregate. Design weight equals the total amount of aggregate needed to make a batch of concrete.

2.5 Air Entraining Admixture

The air-entraining admixture used for the project was Master Builders Neutralized Vinsol Resin Solution (MB VR) conforming to ASTM C 260-86, which was supplied by MDOT. MB VR admixture has no standard dosage rate, but the manufacturer recommends a dosage rate of 16 to 260 mL/100 kg (1/4 to 4-fl oz/100 lbs) of cement should be used for a trial mix to achieve the desired air content. There are many factors that affect the dosage rate of MB VR including cement type, slump, percent of fine materials, sand gradation, temperature, batch size and type of mixer. Due to the number of factors involved in proportioning air entrainment, a trial and error method was used for determining the proper amount of admixture for each mix design. A range between 19 to 28 ml was found to give the best results to achieve the target value for air content. Proper storage of MB VR was important because exposure to air will decrease its effectiveness. A one-gallon glass container with an airtight lid was used for storing air entrainer. Air entrainer was then measured immediately prior to batching using a plastic graduated cylinder with a least readable division of 1mL. The actual quantity used in each batch of concrete is included on the batch computation sheets in Appendices IV-B, IV-C, and IV-D for each of the three respective mixes.

2.6 Mixing and Casting

All concrete was made and cured at MTU in the concrete laboratory (B006) of Dillman Hall. A three-blade rotating drum mixer powered by a one horsepower (115 volt) electric motor with a six cubic foot capacity was used to make all concrete. A batch size of $0.078 m^3$ ($2.75 ft^3$) was used, which was enough concrete to cast eight cylinders and perform the following tests: one unit weight, one air content and one slump test. All concrete used for unit weight, slump, and air content testing was discarded in order to minimize the effects of aggregate segregation in casting the test cylinders.

Standard 152 x 305 mm (6 x 12 in.) plastic cylinder molds were used to form all concrete cylinders. These cylinder molds conformed to ASTM 470-94 with the exception that a hole was drilled in the bottom of all molds and some molds were reused. Prior to reuse, cylinder molds were visually inspected for defects such as rounding of edges and any cracks or scratches. If any defects were found, those molds were discarded. No molds were used more than twice. A small paper disk was placed inside the mold covering the hole at the bottom and a piece of duct tape was applied to the outside bottom over the hole. This was done to ensure no loss of moisture while the specimen was curing. Each mold was oiled at least 30 minutes prior to use with Clean Strip Form Release Oil.

Each batch of concrete was made in a buttered mixer. Buttering was accomplished by mixing a sand cement mixture with enough water added to make it about the same consistency as a batch of concrete. This mixture was then smeared on the inside the mixer coating it evenly. The excess material was scraped out so that no clumps existed on the inside of the mixer. During the three-minute rest period (discussed in Step

11 of Section 2.6.1) the mixer was scraped down to remove any material that had adhered to the sides. This was done to ensure thorough mixing of all constituents.

2.6.1 Mixing Procedure

The following mixing, casting and testing procedures were used. Batch computation worksheets for each batch were previously discussed. Reference to such worksheets is made in general terms.

1) Lay out all tools and equipment needed.
2) Paper, tape and oil cylinder molds.
3) Calculate moisture content of fine aggregate (FA), (ASTM C 566 microwave method). Multiply design weight of FA by the moisture content, to obtain the amount of water (moisture) in the FA. Add this value back to the design weight of FA to compute the total amount of FA needed for the batch. (See batch computations worksheet).
4) Weigh cement and reserve water.
5) Measure air-entraining admixture.
6) Decant water from coarse aggregate (CA). Weigh each container and add back the amount of water needed for the batch minus a known quantity of reserve water, e.g., 3 kg (6.61 lbs). Cover containers so that no moisture is lost. Use only room temperature water. (See water measurement data block on batch computation worksheet).
7) Weigh out FA from step 3. Cover containers as above.
8) Butter the mixer. Use three shovels full of FA and two scoops of cement (not from either the FA or cement already measured out). Add enough water to produce the same consistency as the batch to be made, i.e., a 51 – 76 mm (2-3 in.) slump. Coat the inside of mixer completely; scrap out excess material and discard.
9) Add materials to mixer in the following order.
10) CA with water (from CA containers, not reserve water).
11) Air entraining admixture- rinse graduated cylinder out completely using a portion of the reserve water and pouring this into the mixer as well.
12) Add FA.
13) Start mixer and add cement while starting timer as soon as all the cement is added.
14) Mix for 3 minutes. During the first 2.5 minutes, add enough reserve water to achieve the desired consistency, i.e., 51 – 76 mm (2-3 in.) slump. Add small quantities at a time, being careful to not add too much water. Concrete should fall off the blades and no concrete should be stuck to the sides of mixer. If there is any stuck to the sides, then more water is needed. No water should be added in the last 30 seconds of mixing time.

15) Rest for 3 minutes. Scrap down mixer if needed. Take temperature of concrete in accordance with ASTM C 1064-86(1993). Determine if more water needs to be added (if the mixer had to be scraped then more water is needed). Testing equipment for step 15 should be in the damp condition now.
16) Mix for 2 minutes. Add more water if needed in very small amounts. Again, no water should be added in the last 30 seconds of mixing time.
17) Weigh the remaining reserve water plus container (surplus + tare) and record on batch computations worksheet in reserve water data block.
18) Discharge concrete into a clean damp pan.
19) Perform tests on freshly mixed concrete.
20) Slump (ASTM C143-90a) completed in the first 2.5 minutes from discharge.
21) Unit weight (ASTM C 138-92).
22) Air content (ASTM C 173-94a).
23) Cast concrete cylinder specimens (ASTM C 192-90a). Cover with tight sealing lids and place in curing room.
24) Record all values (air entrainment used, temperature and test results from step 15) on batch computation worksheets as well as the time and date the batch was made.
25) Perform yield data calculations. (See Section 2.7).

2.7 Yield Data and Report of Test

"Yield Data" worksheets are provided in Appendices IV-B, IV-C, and IV-D of this report for the three respective mixes using three different coarse aggregates (basalt, glacial gravel, and iron blast furnace slag). Each worksheet includes yield data for all batches made using a specific aggregate. Yield data includes calculated values for unit weight of concrete, batch volume, cement used for 1 m^3 of concrete, net water used for 1 m^3 of concrete, and water-cement ratio for each batch that was cast. Formulae used for each computation are also included on the worksheets. A "Report of Test" worksheet follows the yield data sheet in each of the same appendices.

"Report of Test" worksheets include unit weight of concrete, actual cement content, slump, air content, and water-to-cement ratio (w/c) for each batch, in addition to an average value for each quantity. These average quantities are summarized in Table 2.4. Average values for both of these items are also included on the worksheet. A summary of coarse aggregate properties is shown there as well. Other test results listed on the "Report of Test" worksheets include compressive strength (discussed in Section 3.1), and split tensile strength (discussed in Section 3.2).

Table 2.4 Summary of Yield Data

	Coarse Aggregate Type		
	CA-B†	CA-G†	CA-S‡
Slump (mm)	67	64	59
Unit weight (kg/m^3)	2391	2377	2249
Actual cement content (kg/m^3)	334	336	342
Water/cement ratio (by weight)	0.47	0.46	0.46
Air content (%)	5.6	4.6	4.3
Compressive strength (MPa)	41.0	41.4	45.0
Split tensile strength (MPa)	3.49	3.54	3.95

(1 kg/m^3 = 1.69 lb./yd^3) (1 mm = 3.94 x 10^{-2} in.) (1 MPa = 145.0 psi)
† Average of two batches.
‡ Average of four batches.

2.8 Curing, Stripping, and Capping

Following cylinder casting (Step 16, Section 2.6.1), cylinders were immediately placed in a 100% humidity curing room. Cylinders were stripped 24 ± 8 hours after casting and labeled, then immediately returned to the curing room. The curing room was constantly maintained to ensure a 100% humid environment so that cylinders had free water on all sides during the 28-day curing period. When cylinders were taken to be capped or strain gagged, wet towels were wrapped around them to keep them moist. Capping took place when the cylinders were 26-days old in accordance with ASTM C 617-94. Forney Hi-Cap High–Strength capping compound was used for capping all cylinders. Cylinder caps were inspected daily for any defects such as debonding caused by shrinkage. If any such defects were found, cylinders were recapped and returned to the curing room until the time of testing.

3 Experimental Procedure and Results

The three mix designs used to make concrete tested for this project were the same with the exception of coarse aggregate type. All concrete was batched and cured in one location as discussed in Chapter 2. Because the curing facilities and testing laboratory were located in two separate buildings at MTU, cylinders were wrapped in wet towels and covered in heavy canvas for transportation and short-term storage. This was done to ensure cylinders were tested in the moist condition. It also helped to reduce surface shrinkage and residual stresses that could have caused premature failure. Experimental procedures and results for axial compression, splitting tensile strength and strain gaging are presented below.

3.1 Compressive Strength

Concrete cylinders were tested for compressive strength in the Rocks Mechanics Laboratory located in the Mining and Materials Building at MTU. A MTS load frame that had a capacity of 4448 kN (1,000,000 lbs) was used for all compression and split cylinder testing. The load frame has a mass of 6,360 kg and is considered a very stiff frame. Figure 3.1 illustrates the general configuration of the uniaxial testing. An Instron 8500 controller connected to a personal computer with Instron Series IX software operated the load frame. The compression machine hydraulically loaded a specimen in either displacement or load control and met the requirements of ASTM C 39-96.

Standard 152 x 305 mm (6 x 12 in.) concrete cylinders tested were at 28 days and followed ASTM C 39-96 procedure except for rate of loading. Actual load rate was 133 kN/min (30,000 lb./min), which was 12% slower than the minimum ASTM specified rate of 151 kN/min (34,000 lb./min). A shunt-cal calibration system was used to calibrate the machine before a precapped cylinder was placed on the bottom platen. The bottom platen, along with the specimen, was then raised until it was about 10 mm (0.4 in.) from the top platen where it was then centered in the machine. A seating load of

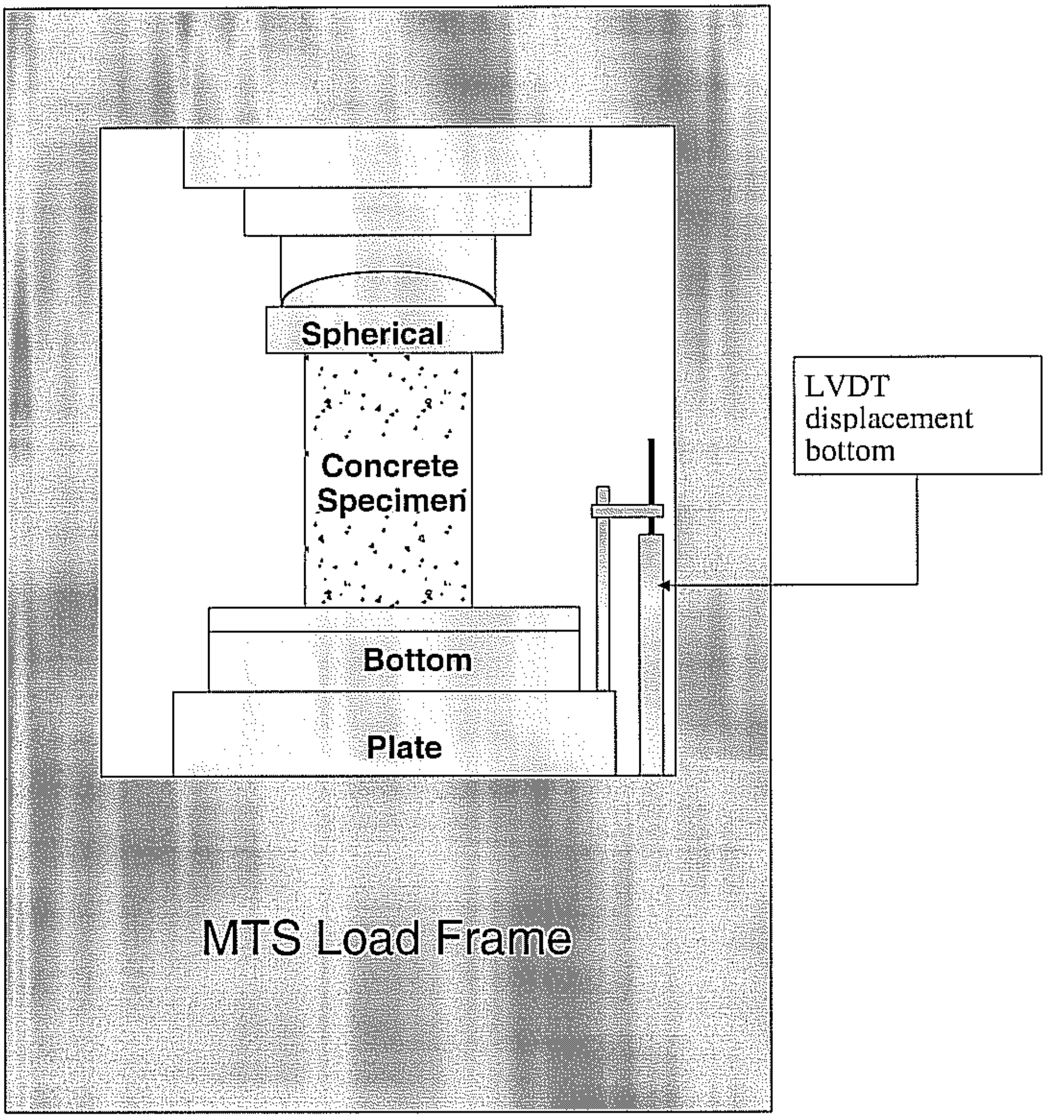

* Not to scale

Figure 3.1 MTS load frame with LVDT.

approximately 4.45 kN (1,000 lb.) was applied to the specimen using displacement control. The Instron Series IX software program automatically switched the machine from displacement control to load control and loaded the specimen until failure. Load and platen displacement were recorded continuously throughout each axial compression cylinder test.

Axial compression test results are shown as load versus crosshead displacement graphs in Figures 3.2 to 3.5. Each figure shows results from two batches of concrete made with the same coarse aggregate, i.e., Figure 3.2 has results from both batches of CA-B (basalt). Because four batches of CA-S (slag) were casted, two figures are included as Figures 3.4 and 3.5, respectively. Each figure contains all cylinders tested for that particular type of coarse aggregate along with the average curve for the group, with the exception of CA-S (slag), which has two figures with half the cylinders tested on each one. Load-displacement curves do not pass through the origin, because of the small seating load applied to each concrete specimen. These curves were not used to calculate modulus of elasticity because a stress-strain curve could not be readily obtained from the data. Instead, apparent stiffness was calculated from the load-displacement curves, and is discussed further in Section 3.1.1. Additionally, an estimated modulus of elasticity discussion is provided in Section 4.1.2.

Tables 3.1-3.3 include values for displacement at failure, apparent stiffness, maximum load, and stress for each cylinder tested. Also included for the same values are the averages and standard deviations per batch. Some cylinders (where noted) did not meet the requirements of ASTM C39-96, thus these cylinders were not included in the averages or standard deviations. Slump and percent air are reported also for ease of comparison. Test results show that the maximum average axial compressive strength for concrete mixes CA-B (41.0 MPa) and CA-G (41.8 MPa) varied by 2%, with CA-G being higher. Mix CA-S (45.0 MPa) showed a 9.8% increase in maximum stress when compared to concrete mix CA-B.

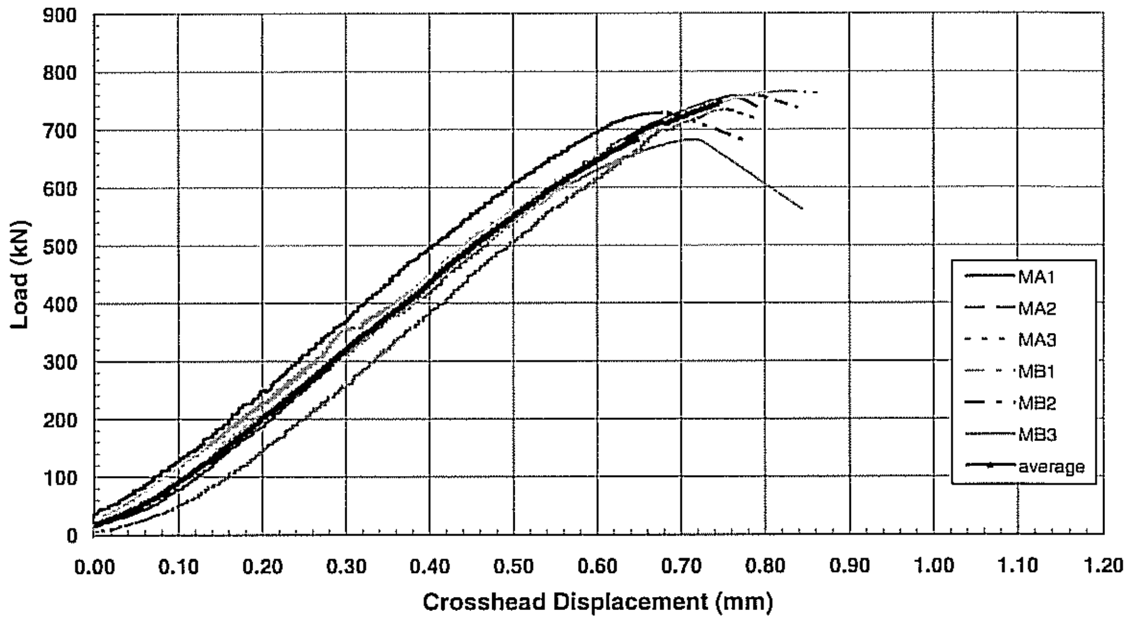

Figure 3.2. Axial Compressive Load versus Crosshead Displacement for Concrete Mix CA-B (basalt).

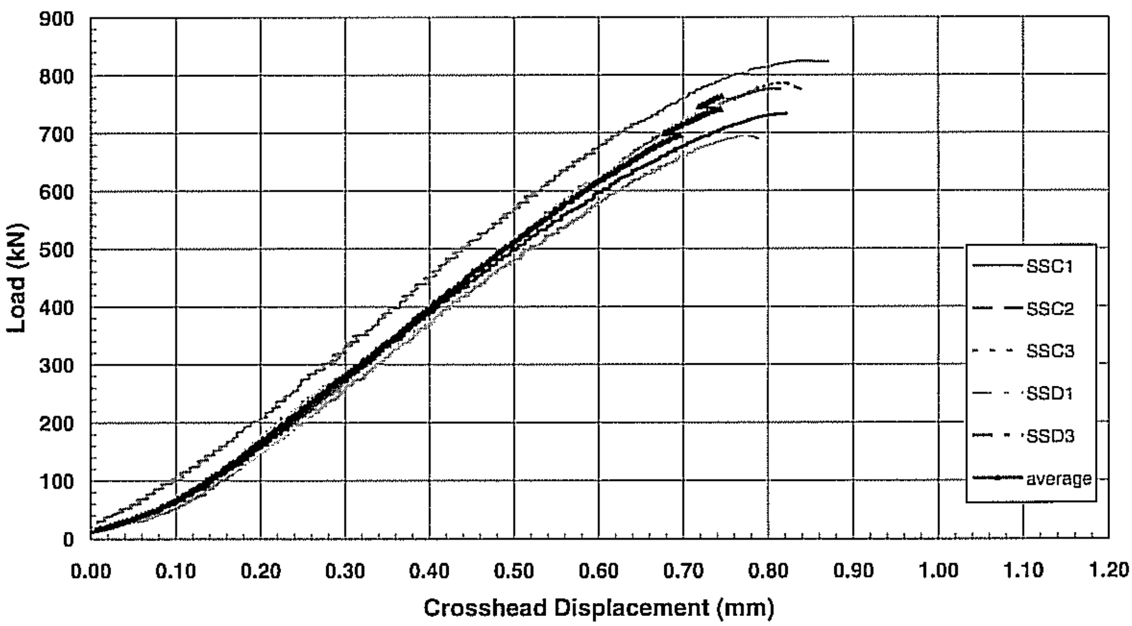

Figure 3.3. Axial Compressive Load versus Crosshead Displacement for Concrete Mix CA-G (glacial gravel).

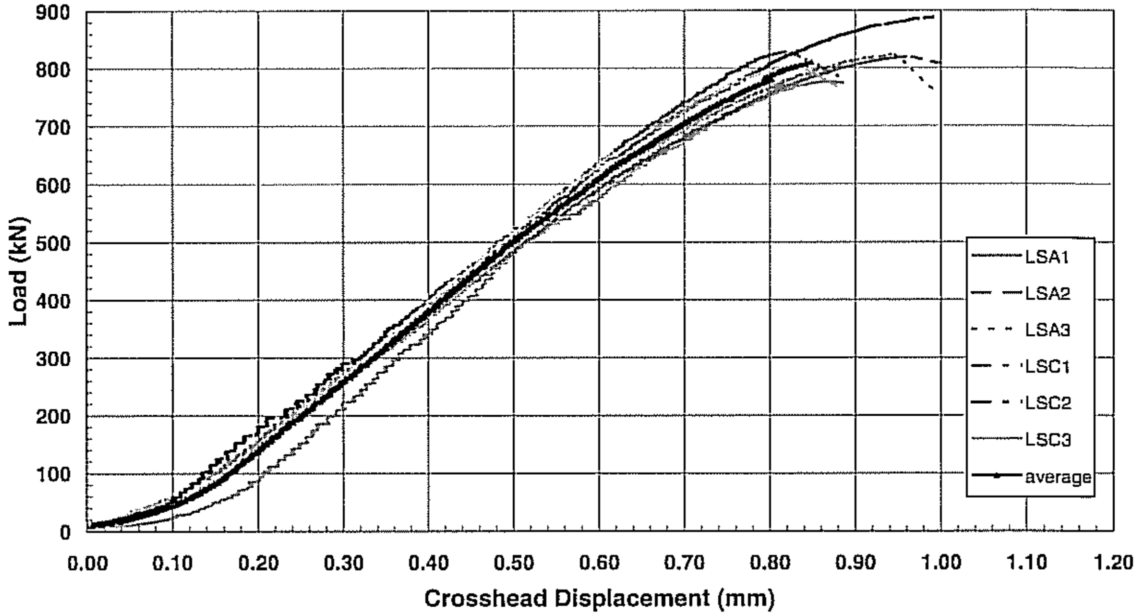

Figure 3.4. Axial Compressive Load versus Crosshead Displacement for Concrete Mix CA-S (slag), Batches LSA and LSC.

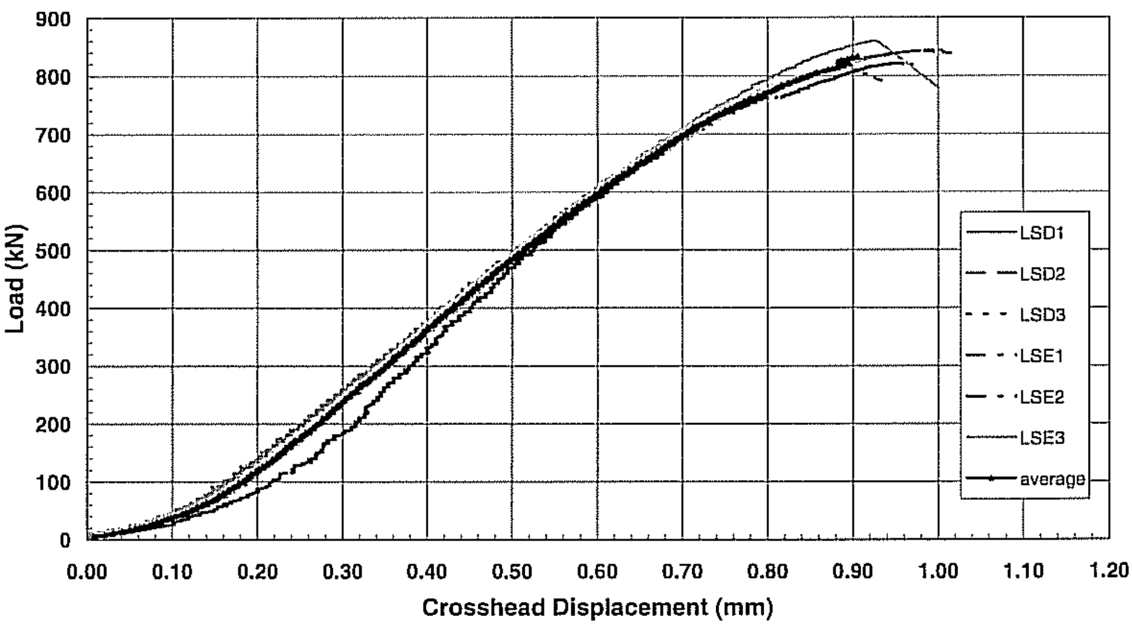

Figure 3.5. Axial Compressive Load versus Crosshead Displacement for Concrete Mix CA-S (slag), Batches LSD and LSE.

Table 3.1 Axial Compression Test Results for Coarse Aggregate CA-B Cylinders

Cylinder Identification	Maximum Load kN	Maximum Stress MPa	Displacement @ Failure mm	Apparent Stiffness kN/mm	Slump mm	Percent Air
Batch A						
MA1	756	41.4	0.756	1189	57.2	5.7 %
MA2	758	41.5	0.794	1130		
MA3	733	40.2	0.747	1142		
Avg.	**749**	**41.0**	**0.766**	**1154**		
STD	**13.7**	**0.8**	**0.02**	**31**		
Batch B						
MB1	765	42.0	0.827	1085	76.2	5.5 %
MB2	728	39.9	0.668	1177		
MB3†	681	37.3	0.712	1141		
Avg.	**747**	**40.9**	**0.747**	**1131**		
STD	**26.7**	**1.5**	**0.11**	**65**		

* 1 kN = 224.8 lb. 1 MPa = 145.0 psi 1 mm = 3.94 x 10^{-2} in.

† Not included in average or standard deviation.

Table 3.2 Axial Compression Test results for Coarse Aggregate CA-G Cylinders

Cylinder Identification	Maximum Load kN	Maximum Stress MPa	Displacement @ Failure mm	Apparent Stiffness kN/mm	Slump mm	Percent Air %
Batch C						
SSC1	824	45.2	0.839	1120	50.8	4.1
SSC2	776	42.6	0.806	1185		
SSC3	786	43.1	0.822	1134		
Avg.	**795**	**43.6**	**0.822**	**1146**		
STD	**25.2**	**1.4**	**0.02**	**34**		
Batch D						
SSD1	695	38.1	0.778	1045	76.2	5.1
SSD2	-	-	-	-		
SSD3	733	40.2	0.824	1115		
Avg.	**714**	**39.2**	**0.801**	**1080**		
STD	**27.0**	**1.5**	**0.03**	**49**		

* 1 kN = 224.8 lb. 1 MPa = 145.0 psi 1 mm = 3.94 x 10^{-2} in.

Table 3.3 Axial Compression Test Results for Coarse Aggregate CA-S Cylinders

Cylinder Identification	Maximum Load kN	Maximum Stress MPa	Displacement @ Failure mm	Apparent Stiffness kN/mm	Slump mm	Percent Air
Batch A						
LSA1	776	42.6	0.866	1287	57.2	4.2 %
LSA2	819	44.9	0.967	1150		
LSA3	821	45.0	0.949	1159		
Avg.	**805**	**44.1**	**0.927**	**1199**		
STD	**25.1**	**1.4**	**0.05**	**77**		
Batch C						
LSC1	827	45.3	0.825	1213	57.2	4.3 %
LSC2†	888	48.6	0.991	1092		
LSC3	803	44.0	0.834	1257		
Avg.	**815**	**44.7**	**0.830**	**1235**		
STD	**16.6**	**0.9**	**0.01**	**31**		
Batch D						
LSD1	857	47.0	0.918	1200	50.8	4.1 %
LSD2	842	46.2	0.985	1165		
LSD3	844	46.2	0.991	1136		
Avg.	**848**	**46.5**	**0.965**	**1167**		
STD	**8.3**	**0.5**	**0.04**	**32**		
Batch E						
LSE1	814	44.6	0.896	1214	69.9	4.5 %
LSE2	820	44.9	0.949	1286		
LSE3	813	44.6	0.890	1206		
Avg.	**816**	**44.7**	**0.912**	**1235**		
STD	**3.8**	**0.2**	**0.03**	**44**		

* 1 kN = 224.8 lb. 1 MPa = 145.0 psi 1 mm = 3.94×10^{-2} in.

† Not included in average or standard deviation.

3.1.1 Apparent Stiffness

Apparent stiffness, *K*, is defined herein as the ratio of the change in load to the change in crosshead displacement. Simply put, *K* is the slope of the load versus crosshead displacement curve. It is not the true stiffness of the specimen nor is it the modulus of elasticity of the concrete. It is the value obtained using the measured crosshead displacement readings and the actual load change. The LVDT mounted on the MTS load frame measured crosshead displacement that included both deformations of the specimen and that of the top platen system. Figure 3.1 is a sketch of the MTS load frame with the LVDT that measured crosshead displacement. Because this measure of total crosshead displacement was larger than the specimen displacement, the slope of each curve was less steep than anticipated causing the apparent stiffness to be smaller in magnitude than the true specimen stiffness. In this setup, the modulus elasticity of the concrete specimen is underestimated because the measured strain (and hence deflection) includes deflections of the loading system and platens.

Apparent stiffness was determined from the slope of the linear portion of the load versus crosshead displacement curve using a linear regression of each cylinder tested axially for ultimate compressive strength. The apparent stiffness of each cylinder is listed in Tables 3.1 to 3.3. The linear portion of the curve was defined between approximately 100 kN (22,480 lb.) to 40% of peak load. Because the stiffness of the top platen system was unknown the modulus of elasticity of the concrete specimens could not be determined directly, only general comparisons between the three types of coarse aggregates can be made from these results. However an attempt was later made to estimate the modulus of elasticity by conducting compliance tests using a steel cylinder. The method used to estimate the modulus of elasticity is discussed further in Chapter 4. In general, the apparent stiffness for concrete mix CA-G was 2.6% lower than CA-B. CA-S exhibited a 5.8% higher apparent stiffness than CA-B.

3.2 Splitting Tensile Strength

Splitting tensile strength was tested according to ASTM C 496-90 with the MTS load frame located in the Mining and Materials Building. On each end of the cylinders tested, diametrical lines were drawn lying in the same plane as the applied load with a jig specifically manufactured for that use. An aligning jig with the horizontally placed specimen was set on the bottom platen of the MTS load frame. The top-bearing block was then set into place and the specimen was aligned using the diametrical drawn lines on the specimen ends. Wood core paneling strips separated the specimen from both the top and bottom bearing blocks. The platen was then raised so that a small seating load was applied to the specimen and bearing blocks before the end plates were removed from the jig. The Instron Series IX program automatically switched the machine to load control and loaded the specimen until failure at a constant rate of 89 kN/min (20,000 lb./min). Load and crosshead (platen) displacement were recorded continuously.

Split cylinder test results are shown as load versus crosshead displacement plots in Figures 3.6 to 3.9. There is one graph for each coarse aggregate CA-B and CA-G with results from two batches included on each figure. Each graph contains all cylinders tested for that particular set of batches along with the average curve for the group. Two figures (Figures 3.8 and 3.9) are included for coarse aggregate CA-S because four batches of concrete were cast from this aggregate. These figures also contain average results from two batches.

Tables 3.4 - 3.6 include values for displacement at failure, apparent stiffness, maximum load, and maximum tensile stress for each cylinder tested in the split tensile test set-up. Also included for the same properties are the averages and standard deviations per batch. Slump and percent air are also reported. Comparing the maximum splitting tensile stress for the three mixes, CA-G is 1.4% higher than CA-B while CA-S showed to be 13.2% higher than CA-B. Slump and percent air as measured on the fresh concrete batches are also tabulated and show consistency independent of coarse aggregate.

3.2.1 Apparent Stiffness

Apparent stiffness is the slope of the linear portion of the load versus the crosshead displacement curve and was calculated using linear regression. The linear portion of the curve was defined between approximately 5 kN (1,124 lb.) and 40% of the peak load. Values for apparent stiffness have the same error associated with them as discussed above for axial compression test. Therefore, only general comparisons between the three types of coarse aggregates can be made from these results. In general, concrete mix CA-G and CA-S showed a 7.0% and a 9.6% decrease in apparent stiffness compared to mix CA-B, respectively.

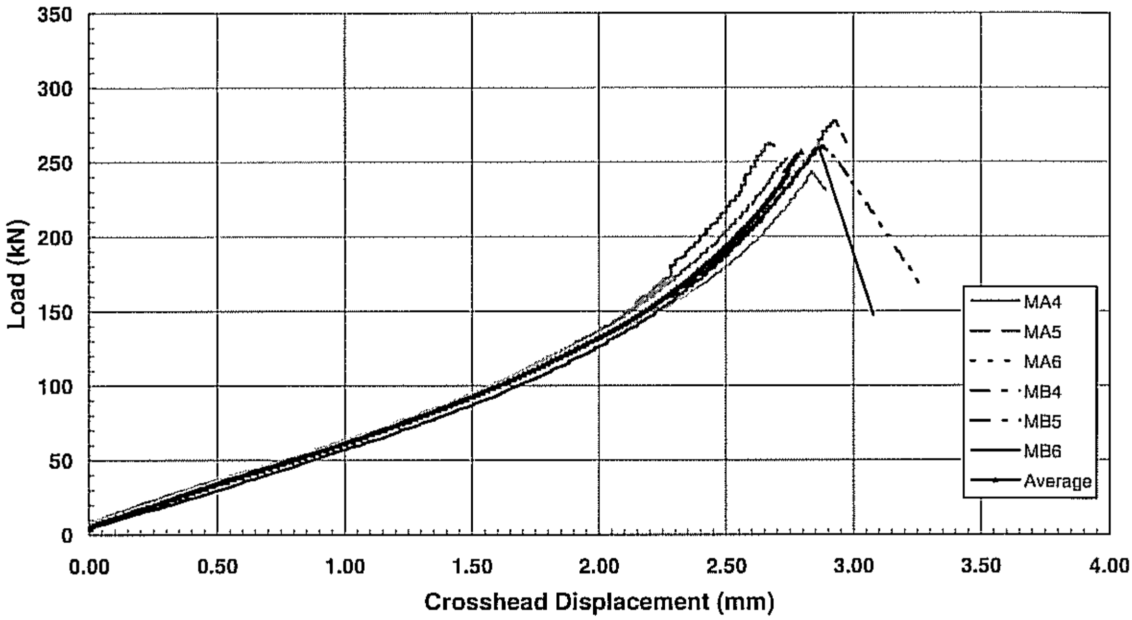

Figure 3.6. Split Tensile Load versus Crosshead Displacement for Concrete Mix CA-B (basalt).

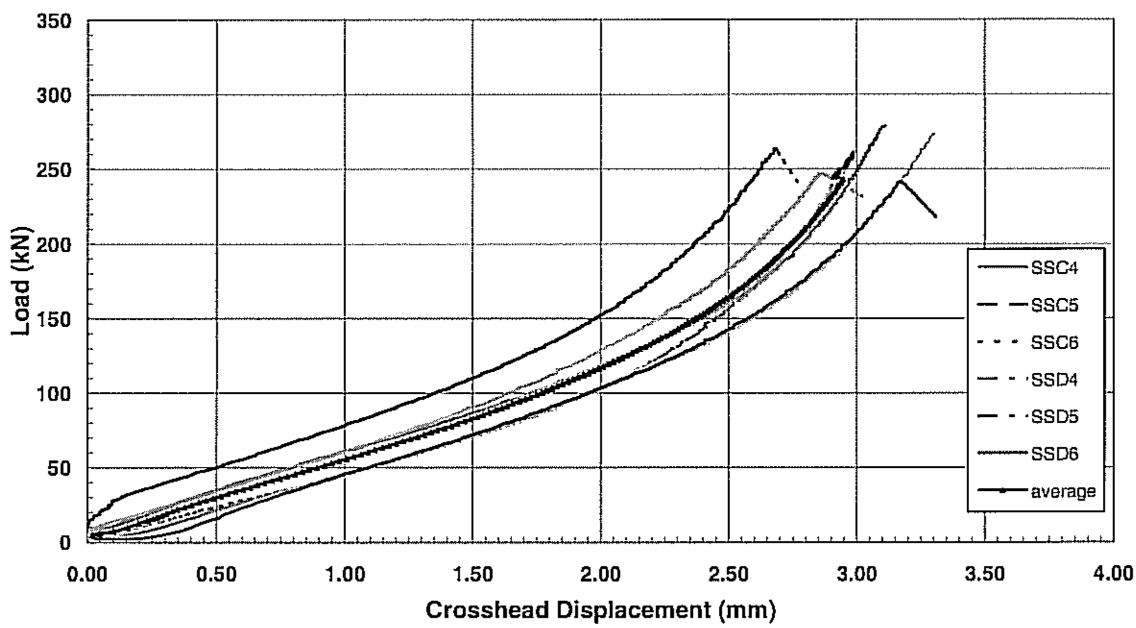

Figure 3.7. Split Tensile Load versus Crosshead Displacement for Concrete Mix CA-G (glacial gravel).

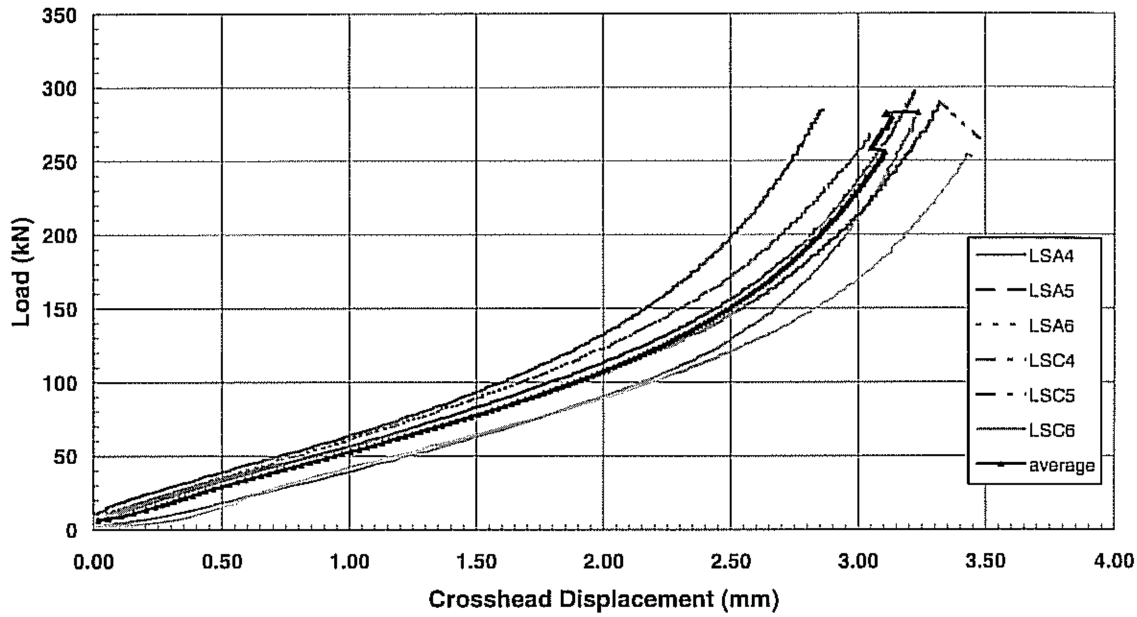

Figure 3.8. Split Tensile Load versus Crosshead Displacement for Concrete Mix CA-S (slag) Batches LSA and LSC.

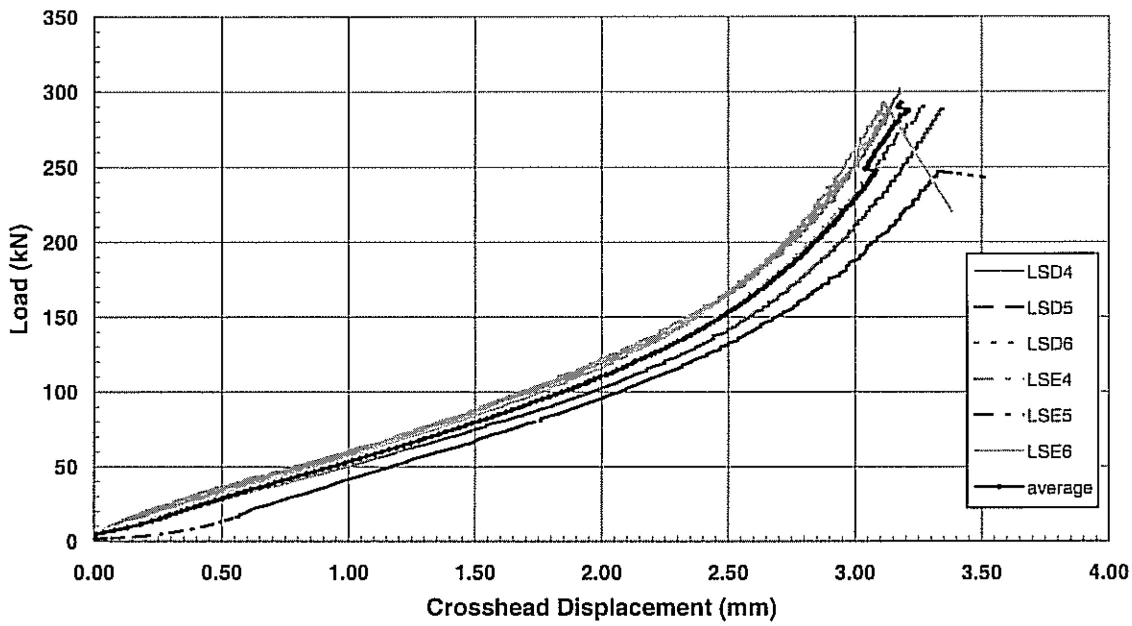

Figure 3.9. Split Tensile Load versus Crosshead Displacement for Concrete Mix CA-S (slag) Batches LSD and LSE.

Table 3.4 Split Tensile Strength Test Results for Coarse Aggregate CA-B Cylinders

Cylinder Identification	Maximum Load kN	Maximum Stress MPa	Displacement @ Failure mm	Apparent Stiffness kN/mm	Slump mm	Percent Air
Batch A						
MA4	243	3.33	2.836	57	57.2	5.7 %
MA5†	277	3.78	2.931	59		
MA6	252	3.47	2.737	59		
Avg.	**248**	**3.40**	**2.787**	**58**		
STD	**6.0**	**0.1**	**0.07**	**1.4**		
Batch B						
MB4	262	3.61	2.670	57	76.2	5.5 %
MB5	260	3.57	2.878	56		
MB6	259	3.54	2.866	58		
Avg.	**261**	**3.57**	**2.805**	**57**		
STD	**1.7**	**0.0**	**0.12**	**1.0**		

* 1 kN = 224.8 lb. 1 MPa = 145.0 psi 1 mm = 3.94×10^{-2} in.

† Not included in average or standard deviation.

Table 3.5 Split Tensile Strength Test Results for Coarse Aggregate CA-G Cylinders

Cylinder Identification	Maximum Load kN	Maximum Stress MPa	Displacement @ Failure mm	Apparent Stiffness kN/mm	Slump mm	Percent Air
Batch C						
SSC4	273	3.75	3.300	52	50.8	4.1 %
SSC5	279	3.82	3.111	54		
SSC6	262	3.61	2.994	50		
Avg.	**271**	**3.72**	**3.135**	**52**		
STD	**8.6**	**0.1**	**0.15**	**2.0**		
Batch D						
SSD4	247	3.36	2.857	55	76.2	5.1 %
SSD5†	263	3.61	2.683	60		
SSD6	241	3.29	3.174	55		
Avg.	**244**	**3.33**	**3.016**	**55**		
STD	**3.6**	**0.0**	**0.22**	**0.0**		

* 1 kN = 224.8 lb. 1 MPa = 145.0 psi 1 mm = 3.94×10^{-2} in.

† Not included in average or standard deviation.

Table 3.6 Split Tensile Strength Test Results for Coarse Aggregate CA-S Cylinders

Cylinder Identification	Maximum Load kN	Maximum Stress MPa	Displacement @ Failure mm	Apparent Stiffness kN/mm	Slump mm	Percent Air
Batch A						
LSA4	279	3.82	3.227	48	57.2	4.2 %
LSA5	284	3.89	2.866	54		
LSA6	267	3.68	3.044	54		
Avg.	**277**	**3.79**	**3.045**	**52**		
STD	**8.8**	**0.1**	**0.18**	**3.5**		
Batch C						
LSC4	297	4.06	3.225	52	57.2	4.3 %
LSC5	289	3.96	3.321	47		
LSC6†	254	3.47	3.426	48		
Avg.	**293**	**4.01**	**3.273**	**50**		
STD	**5.4**	**0.1**	**0.07**	**3.5**		
Batch D						
LSD4	302	4.13	3.176	54	50.8	4.1 %
LSD5	288	3.96	3.348	50		
LSD6	291	3.99	3.277	52		
Avg.	**294**	**4.03**	**3.267**	**52**		
STD	**7.0**	**0.1**	**0.09**	**2.0**		
Batch E						
LSE4	284	3.89	3.115	54	69.9	4.5 %
LSE5†	247	3.40	3.327	53		
LSE6	293	4.03	3.115	54		
Avg.	**288**	**3.96**	**3.115**	**54**		
STD	**5.8**	**0.1**	**0.00**	**0.0**		

* 1 kN = 224.8 lb. 1 MPa = 145.0 psi 1 mm = 3.94×10^{-2} in.

† Not included in average or standard deviation.

3.3 Strain Measurements

Strain gages were mounted on both axial compression and split cylinder specimens one day prior to testing. Two cylinders from each batch, one for axial compression testing and one for split tensile testing, were instrumented with gages. Two types of gages were used: (1) 1000 Ω resistance (WK-06-250BF-10C) strain gages having a gage factor of 2.04 and (2) 350 Ω resistance (WK-06-06ZAP-350) strain gages with a gage factor of 2.02. Each gage had a three-wire connection to compensate for temperature effects and was wired in a quarter bridge arrangement to a wheatstone bridge. An input voltage was supplied (20 and 6 volts for the 1000 Ω and 350 Ω gages, respectively) and the output voltage was recorded with an oscilloscope. The output voltage was then converted to strain with a standard quarter bridge completion equation.

3.3.1 Placement of Strain Gages

Axial compression specimens had a 1000 Ω and a 350 Ω gage mounted in the axial and transverse directions, respectively. Figures 3.10(a) and 3.10(b) show general gage placements for both axial compression and split tensile specimens. These gages were placed approximately in the middle of the cylinder, i.e., six inches from either end of the specimen. Split cylinder specimens had a 1000 Ω gage in the transverse direction while a 350 Ω gage in the axial direction. These gages were mounted on the flat end of the cylinder near the center where maximum tensile strain was expected to occur. In this report, the axial and transverse directions are parallel and perpendicular to the direction of loading, respectively. The specific location of the gages depended upon surface conditions. To eliminate stress concentration effects, strain gages were not mounted on rough surfaces or over holes. In some cases, split cylinder specimens had been lightly wet sanded to produce a desirable surface for mounting a gage. The procedure used for mounting strain gages follows.

Diametrical lines were drawn on the flat ends of each specimen using the jig described in Section 3.2. These lines were used for aligning the gages. A selected area was first dried locally with a hot air drier then cleaned with ethanol. An activator was sprayed on the surface of the cylinder, and then a small amount of adhesive (Loctite 330) was applied to the area. The gage was then aligned and pressed firmly into place, holding it down for approximately one minute. Because the adhesive needed at least two hours to cure, a piece of plastic was taped over the gages and the cylinders were returned to the curing room until they were tested.

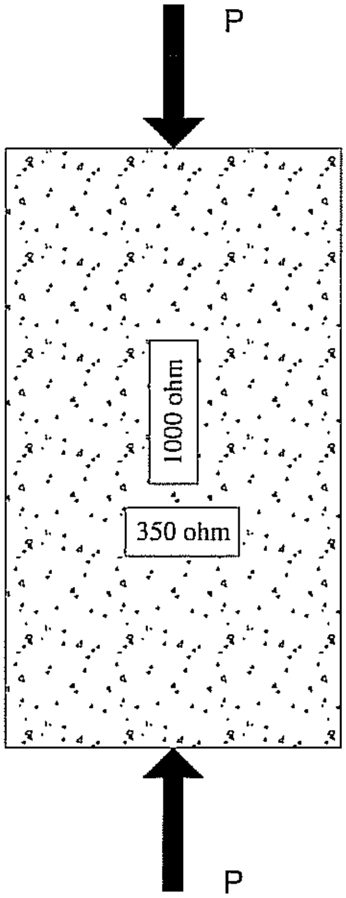

Figure 3.10(a). Axial Compression Test Specimen with Strain Gages.

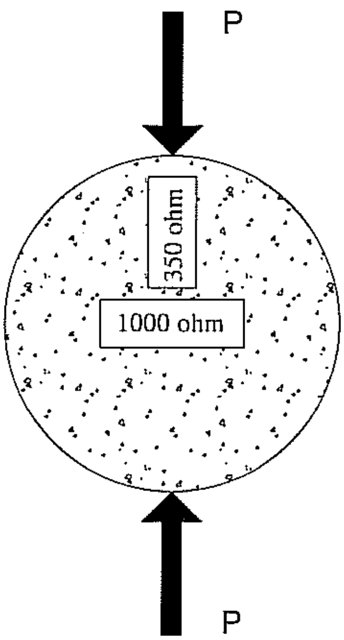

Figure 3.10(b). Split Tensile Specimen with Strain Gages.

3.3.2 Strain Measurement Results

Many factors affected the results for strain gaging, with the major contributor being the gage placement. Strain is not uniform through the specimen because concrete is not a homogenous material. If a gage was mounted over a large piece of aggregate just beneath the surface or away from the failure zone, not much if any strain was felt by the gage. Gages placed near the failure plane gave the best results.

In light of this, strain gage results proved to be unreliable; therefore the results are not presented and were not used in any analysis. One conclusion can be made from the results; strain is not uniform through the specimen, which is why strain gaging concrete specimens produces poor results. For future reference in regards to strain, a better method might be the use of circumferential strain.

4 Discussion and Conclusions

This phase of the research investigated the effects of three different types of coarse aggregate on several fresh and hardened concrete properties, such as unit weight, slump, air content, strength, modulus of elasticity, and fracture characteristics. Included in this chapter will be a discussion on the yield data. As stated in Chapter 2, there was one basic mix design with the types of coarse aggregate being the only intended variable.

4.1 Effects of Coarse Aggregate on Strength

The average strength results for the axial compression and split tensile tests are presented in Figures 4.1 and 4.2, respectively. In these figures load is plotted against crosshead displacement with an average curve for all cylinders tested per type of coarse aggregate, i.e., one curve per coarse aggregate type. Concrete mixes CA-B (basalt) and CA-G (glacial gravel) are the averages of two batches while mix CA-S (slag) is an average of four batches. From these figures it can be seen that concrete mix CA-S has an increase in both axial compression and split tensile strength over mixes CA-B and CA-G. These figures not only show that CA-S has a higher strength but also a higher average displacement at failure of the specimens tested in both axial compression and splitting tensile tests. In general, the shape of the curves is consistent for all mixes. This indicates that the curve's general shape appears to be independent of the coarse aggregate used.

Maximum axial compressive and split tensile strength, f'_c and f_{ct}, respectively are summarized in Table 4.1. All percent differences are based on concrete mix CA-B. Note that CA-S exhibits a 9.8% and a 12.6% increase in f'_c and f_{ct} over CA-B, respectively. Table 4.2 is a summary of crosshead displacements at failure of the specimens. It can be seen that mix CA-S has the largest axial displacement at failure over mixes CA-G or CA-B. Mixes CA-G and CA-S show more than a 10% increase in displacement at failure in split tensile tests when compared to CA-B.

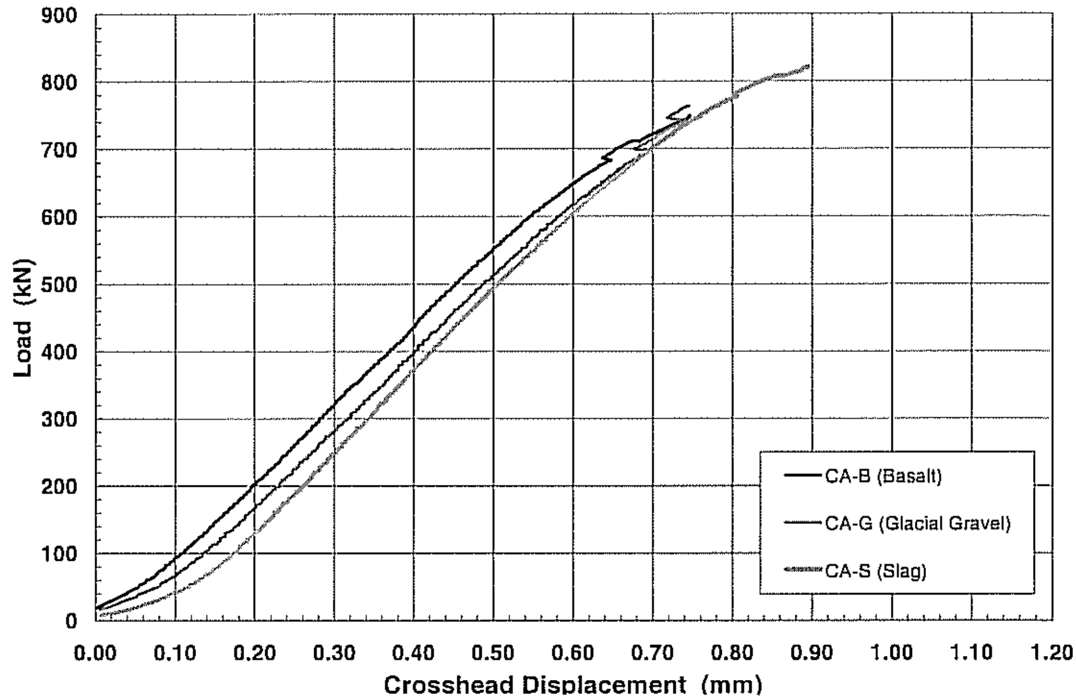

Figure 4.1. Average Axial Load versus Crosshead Displacement for All Concrete Mixes.

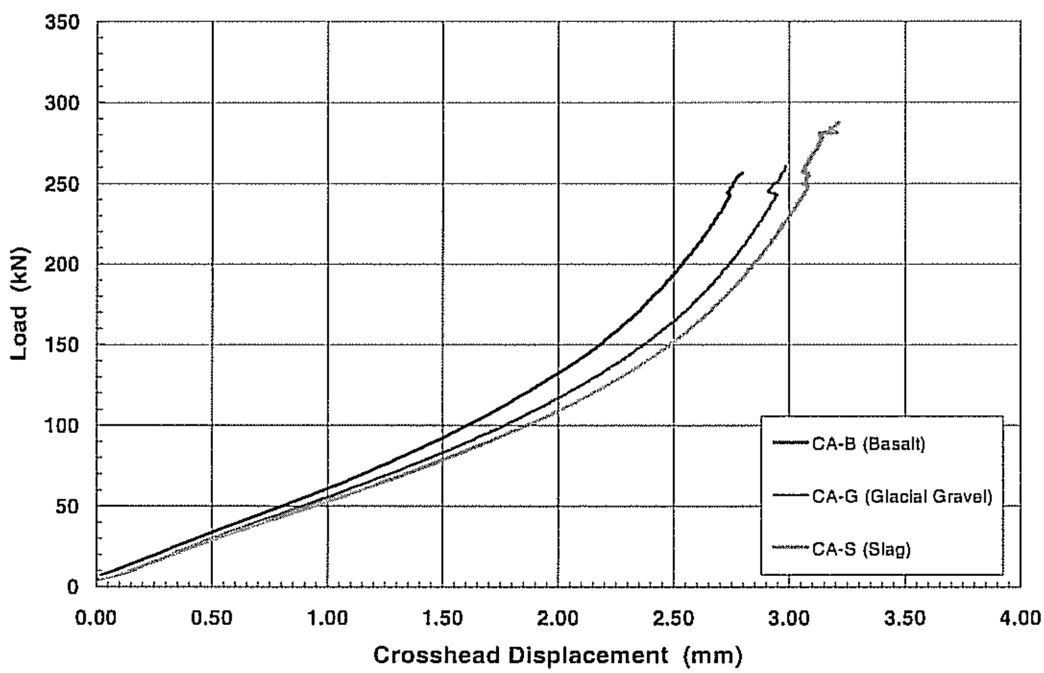

Figure 4.2 Average Axial Load versus Crosshead Displacement for All Concrete Mixes.

Table 4.1 Summary of Axial Compressive Strength and Split Tensile Strength

Aggregate Type	f'_c MPa (psi)	Percent Difference	f_{ct} MPa (psi)	Percent Difference
CA-B	41.0 (5948)	-	3.50 (508)	-
CA-G	41.8 (6066)	2.0	3.56 (518)	1.7
CA-S	45.0 (6523)	9.8	3.94 (572)	12.6

Table 4.2 Summary of Axial and Split Cylinder Displacements at Failure

Aggregate Type	Axial Displacement mm (in.)	Percent Difference	Split Cylinder Displacement mm (in.)	Percent Difference
CA-B	0.758 (0.030)	-	2.797 (0.110)	-
CA-G	0.812 (0.032)	7.1	3.087 (0.121)	10.4
CA-S	0.915 (0.036)	20.7	3.171 (0.125)	13.4

Figures 4.3 and 4.4 summarize the ultimate axial compressive and split tensile strengths per batch of concrete. In terms of each batch, concrete mixes CA-B and CA-S give fairly consistent results for both axial compression and split tensile strength, while CA-G has more variability. CA-B has the most consistent results with respect to axial compressive strength. Concrete mix CA-S consistently shows higher axial compressive and split tensile strengths than either of the other two concrete mixes.

In an attempt to understand strength variations between the concrete mixes made with different coarse aggregates, the yield data was reviewed. Yield data provides unit weight, actual cement content, and water-cement ratio for the freshly mixed concrete. In reviewing the unit weight data, the lowest unit weight was the CA-S (slag) at 2250 kg/m^3 (140 pcf) followed by CA-G (gravel) at 2277 kg/m^3 (148 pcf) and CS-B (basalt) at 2390 kg/m^3 (149 pcf). While this trend would be expected based on the lower bulk density of the slag, it is not clear as to whether or not unit weight affected the strength or stiffness of the concrete. However, a better correlation of strength variation in concrete is the water-cement ratio. The average water-cement ratio for all concrete batches was 0.46, and only varied from 0.45 to 0.47 for individual concrete cylinders tested regardless of coarse aggregate type. This is a fairly tight range making it difficult to draw conclusions concerning strength variations based on water-cement ratio. All of the unit weight data and water-cement ratios for each batch are presented in Appendices IV-B through IV-D.

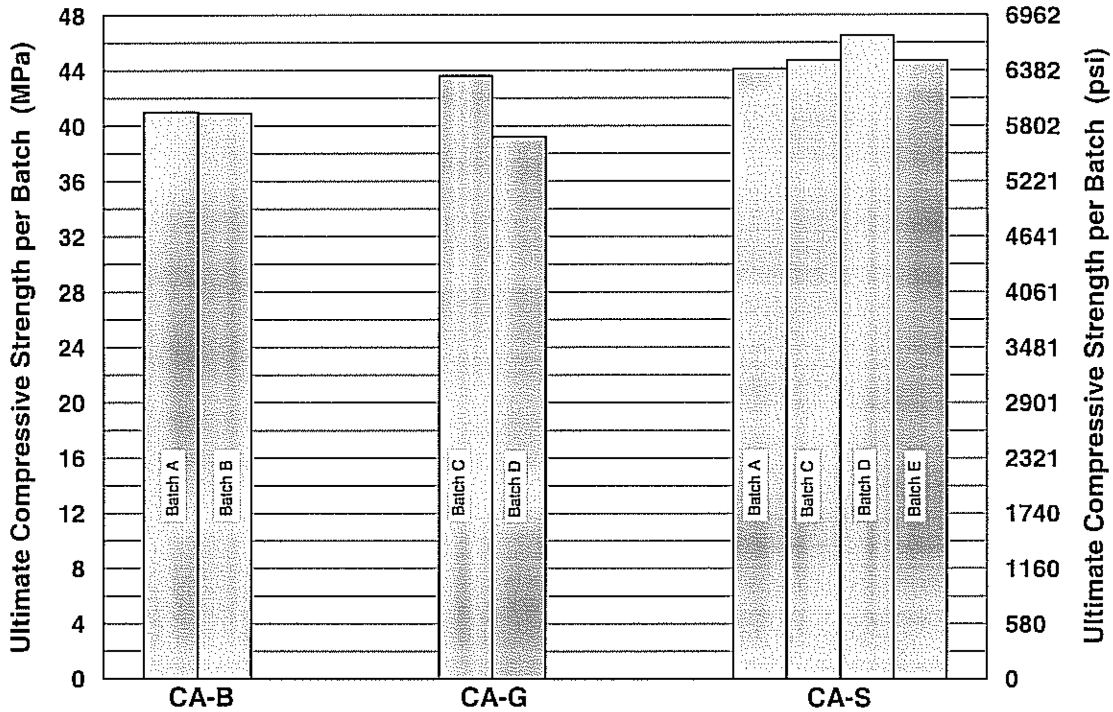

Figure 4.3. Summary of Axial Compressive Strength per Batch of Concrete.

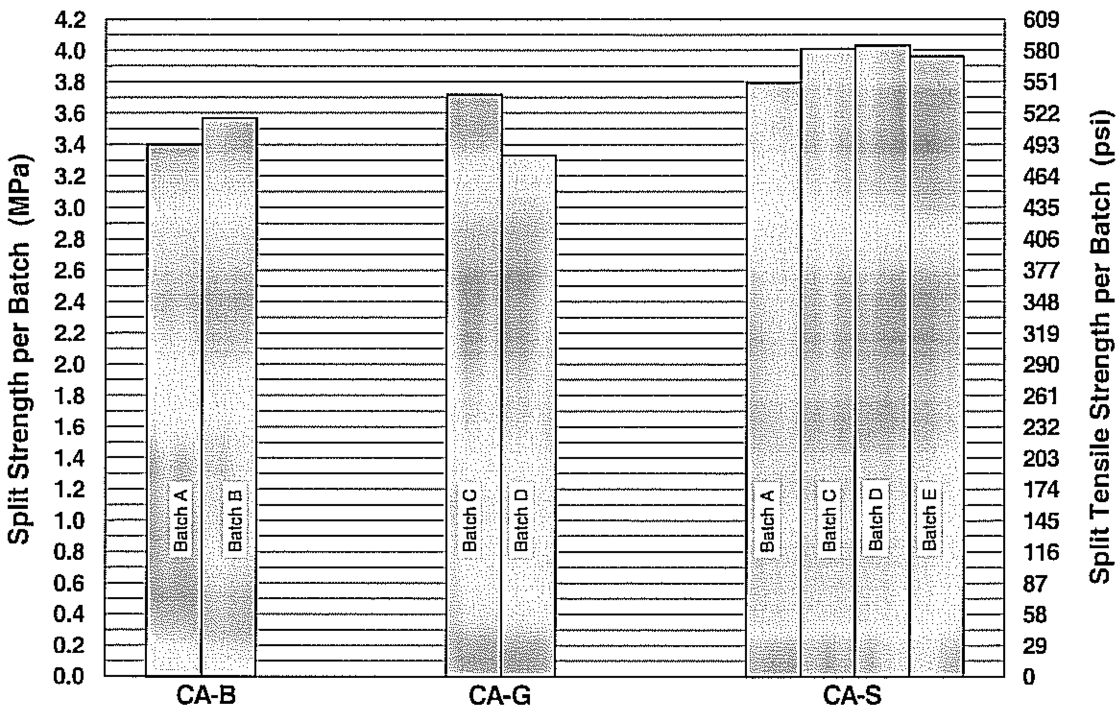

Figure 4.4. Summary of Ultimate Split Tensile Strength per Batch of Concrete.

Apparent cement content for each batch was computed and provided on the "Yield Data" worksheet provided in Appendices IV-B, IV-C and IV-D for the three respective mixes, CA-B, CA-G and CA-S. The design cement content was 335 kg/m^3, i.e., the equivalent of 335 kg of cement was used to produce a cubic meter of concrete. The average measured cement content for CA-B was 334 kg/m^3, CA-G was 336 kg/m^3, and CA-S was 342 kg/m^3. Figure 4.5 shows the actual measured cement content per batch of concrete used in this study. It is observed that each batch of concrete mix CA-S has a higher cement content than the remaining batches for mixes CA-B or CA-G. The actual measured cement content is plotted with compressive strength in Figure 4.6, and Figure 4.7 compares it for the average split tensile strength. From these figures it is shown that concrete mix CA-G, Batch C yields greater strength in terms of both axial compressive and split tensile than does Batch D. Batch C also has higher cement content than batch D. However, a closer review of the yield data also indicates that the measured batch volumes of concrete mix CA-S did not compare with the design volume. Table 4.3 is a summary of measured batch volumes, actual cement content, and axial compressive and split tensile strengths. In addition, the design values for batch volume, cement content and compressive strength are included. It can be seen from Table 4.3 that the batch volumes for CA-B (basalt) and CA-G (gravel) were relatively close to the design volume of 0.0780 m^3. However, the average batch volume for CA-S (slag) was 0.0764 m^3, which was 2.1% less than the nominal design volume. This volume reduction is the main reason for the apparent increase in the "actual cement content" reported in the yield data for CA-S. Because the nominal design quantity of 335 kg/m^3 of cement was used in each batch, there is no reason to believe that the cement content of the mortar varied between mixes (independent of aggregate type). Consequently, the increase in strength with "actual cement content" shown in Figures 4.6 and 4.7 is most likely due to the volume reduction and not necessarily a result of variation in cement content.

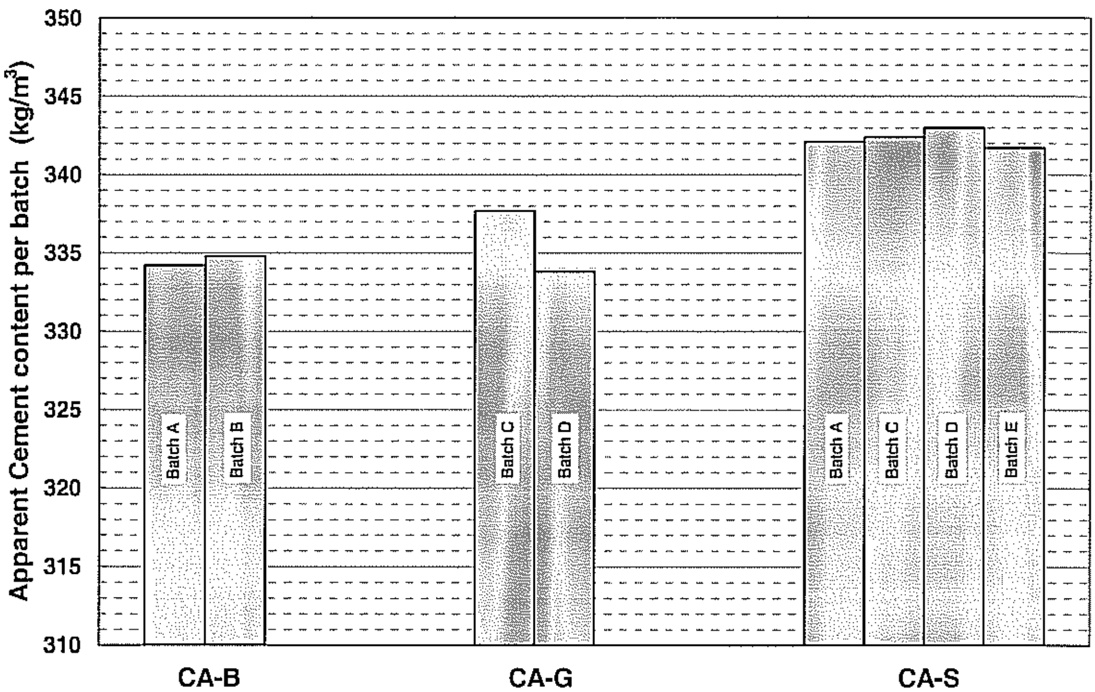

Figure 4.5. Apparent Cement Content per Batch of Concrete as Calculated in Yield Data.

Table 4.3 Summary of Batch Volumes, Apparent Cement Content per Batch, f'_c and f_{ct}.

Coarse Aggregate	Batch Name	Batch Volume m^3	Cement Content kg/m^3	f'_c MPa (psi)	f_{ct} MPa (psi)
CA-B	MA	0.0782	334.2	41.0 (5957)	3.40 (493)
	MB	0.0780	334.8	40.9 (5935)	3.57 (518)
CA-G	SSC	0.0772	337.7	43.6 (6323)	3.72 (540)
	SSD	0.0783	333.8	39.2 (5680)	3.33 (485)
CA-S	LSA	0.0764	342.1	44.1 (6403)	3.79 (550)
	LSC	0.0763	342.4	44.7 (6480)	4.01 (583)
	LSD	0.0762	343.0	46.5 (6740)	4.03 (585)
	LSE	0.0765	341.7	44.7 (6483)	3.96 (537)
Design values		**0.0780**	**335.0**	**24.1 (3500)**	-

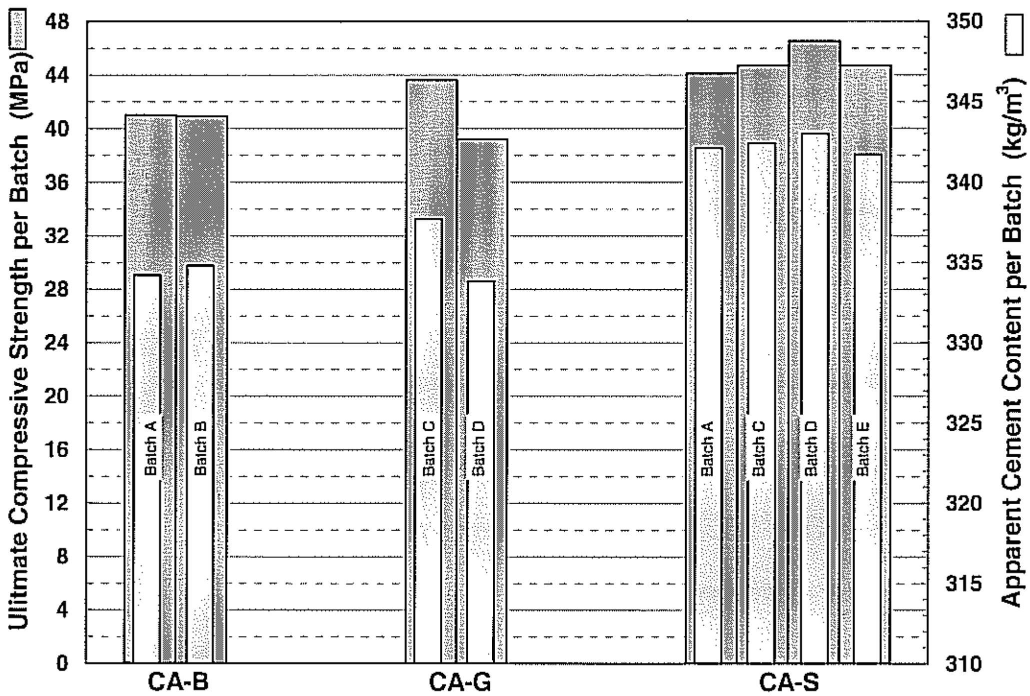

Figure 4.6. Axial Compressive Strength with Apparent Cement Content per Batch of Concrete.

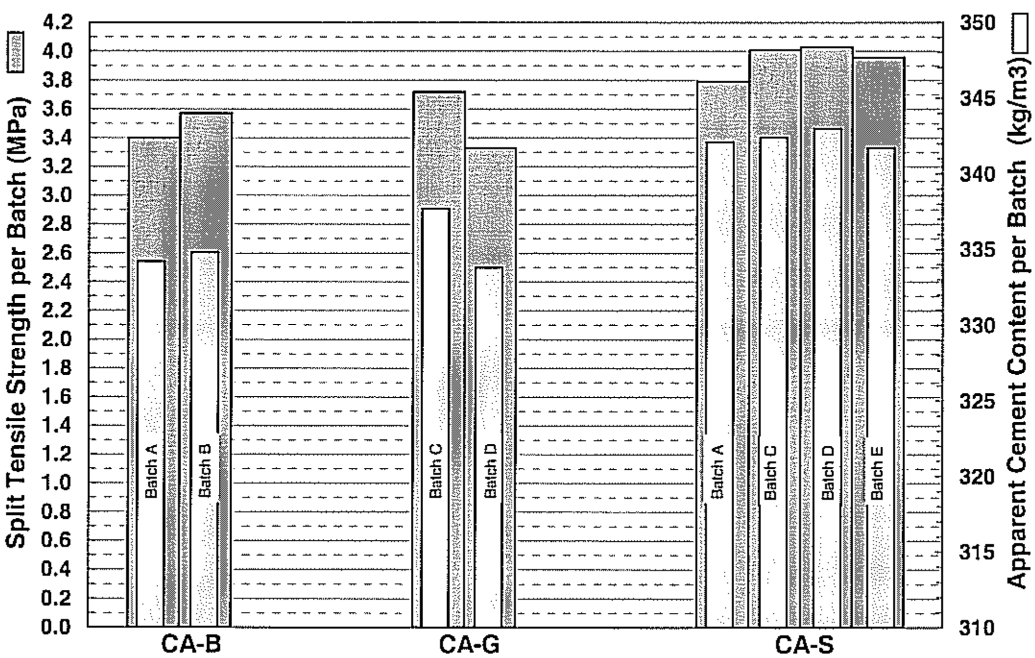

Figure 4.7. Split Tensile Strength with Apparent Cement Content per Batch of Concrete.

The volume reduction observed in mix CA-S (Table 4.3) can be explained by the physical properties of the coarse aggregate. Slag (mix CA-S) has a higher porosity (as noted indirectly by the higher percent absorption in Table 2.2) as well as larger surface pores than either the basalt (mix CA-B) or glacial gravel (mix CA-G). The increased porosity enables the mortar to penetrate the slag particles more readily. Therefore, it takes more mortar to fill the void space, including not only void spaces between coarse aggregate pieces, but also within the aggregate itself. This "higher mortar demand" phenomenon for concrete made with slag aggregate is believed to have an effect on strength and the type of failure observed with CA-S. This is also believed to be the reason why CA-S not only consistently "yields" low (in terms of volume) but also shows a slight increase in strength over both CA-B and CA-G. However, additional research will be required to confirm this possibility.

An additional observation was made concerning the fracture surface of the concrete. In general, the fracture surface of the CA-G (gravel) was the roughest, followed by CA-B (basalt) while CA-S (slag) was the smoothest. This indicated that the failure surface was a function of the coarse aggregate type. However, the roughest fracture surface did not correlate with the highest strength. In fact, the highest strength concrete CA-S had the smoothest fracture surface. A possible explanation for the higher strength CA-S is that the mortar penetrated into the surface pores of the slag, in effect reinforcing (strengthening) the slag aggregate. Because the slag has more surface area than the basalt and glacial gravel aggregate of the same diameter, the contact area between the aggregate and the mortar increases thereby increasing the load to cause failure. CA-S appeared to have no failures along the paste-to-aggregate interface in either the axial compression or split tensile specimens, whereas both CA-B and CA-G had approximately 20 to 30% bond failure present. A consequence of the greater reinforcement would be to force the fracture through the coarse aggregate increasing overall concrete strength.

Another interesting observation is in comparing the measured air content (ASTM C 173 Volumetric Method), presented in the "Report of Test" pages in Appendices IV-B, IV-C, and IV-D, and the back-calculated air content (ASTM C 138 Gravimetric Method) of the concrete for the three respective mixes. While an air content of 6.5% is generally required in design for durability, this study used a 5 ±1% target value. The measured air content percent using the Volumetric Method is presented with ultimate compressive and tensile strengths in Figures 4.8 and 4.9, respectively. In general, this method shows that an increase in air content results in a strength decrease.

The target value for air content was met based on the Volumetric Method (rollometer) as summarized in Table 4.4. Based on the Gravimetric Method, the back-calculated values for air content are considerably below the target value. However, the Gravimetric Method is based on bulk saturated surface dry specific gravity ($G_{B(SSD)}$) values. It can be questioned in this research whether the $G_{B(SSD)}$ values used to determine theoretical unit weights (air free basis) were correct. From Table 2.2, there was considerable variability in the measured $G_{B(SSD)}$ for the slag aggregate while the results for basalt and glacial gravel were relatively consistent between testing laboratories. Consequently, it is believed that the volumetric measurement is more representative of the actual air content because it is independent of coarse aggregate property measurements. It is interesting to note, however, the difference in the results between the two methods, which indirectly correlates with the absorption of the coarse aggregate. The absorption values used in the mix design were 3.55% for the slag, 1.45% for the basalt and 1.35% for the glacial gravel. This compares with an average difference of 3.2% for slag, 2.2% for basalt, and 1.2% for glacial gravel as seen in Table 4.4. It is not known why this difference occurs but it is speculated that a possible reason for the difference is due to the difficulty in measuring the correct specific gravity and absorption values of the coarse aggregate.

Table 4.4 Measured and Calculated Air Content

Coarse Aggregate	Batch Name	Measured Air Volumetric Method (%)	Calculated Air Gravimetric Method (%)	Direct Difference (Vol. – Grav.)
CA-B	MA	5.7	3.6	2.1
	MB	5.5	3.3	2.2
CA-G	SSC	4.1	2.9	1.2
	SSD	5.1	3.8	1.3
CA-S	LSA	4.2	1.0	3.2
	LSC	4.3	1.4	2.9
	LSD	4.1	1.0	3.1
	LSE	4.5	1.0	3.5
Nominal Design		5 ± 1%		

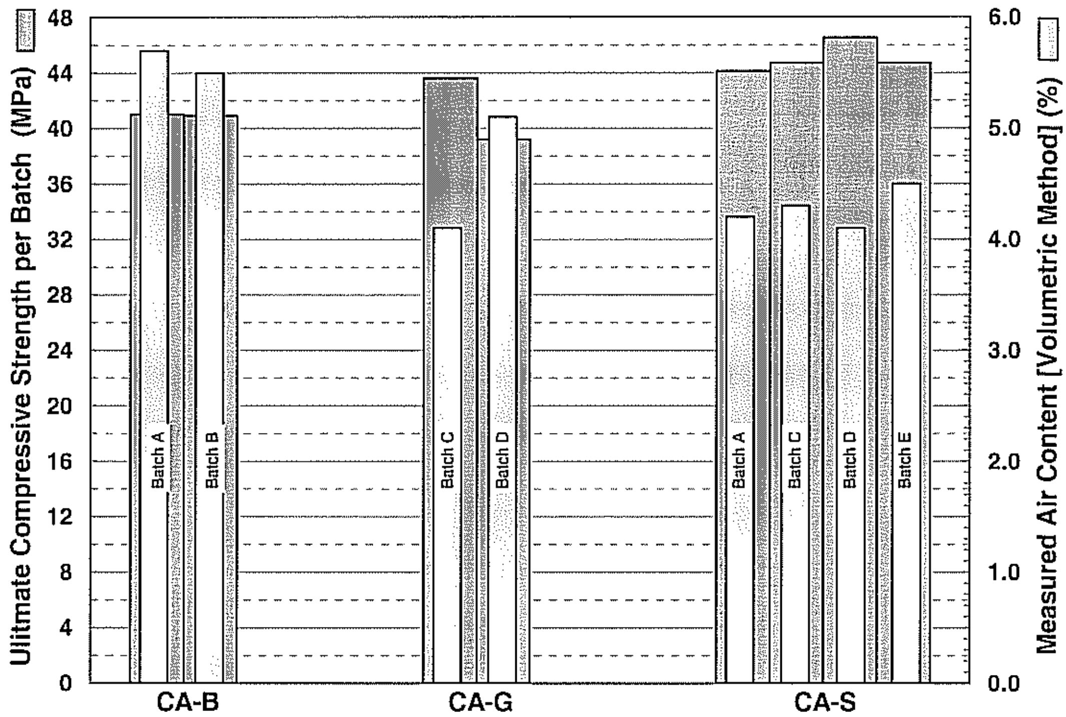

Figure 4.8. Axial Compressive Strength with Measured Air Content per Batch of Concrete.

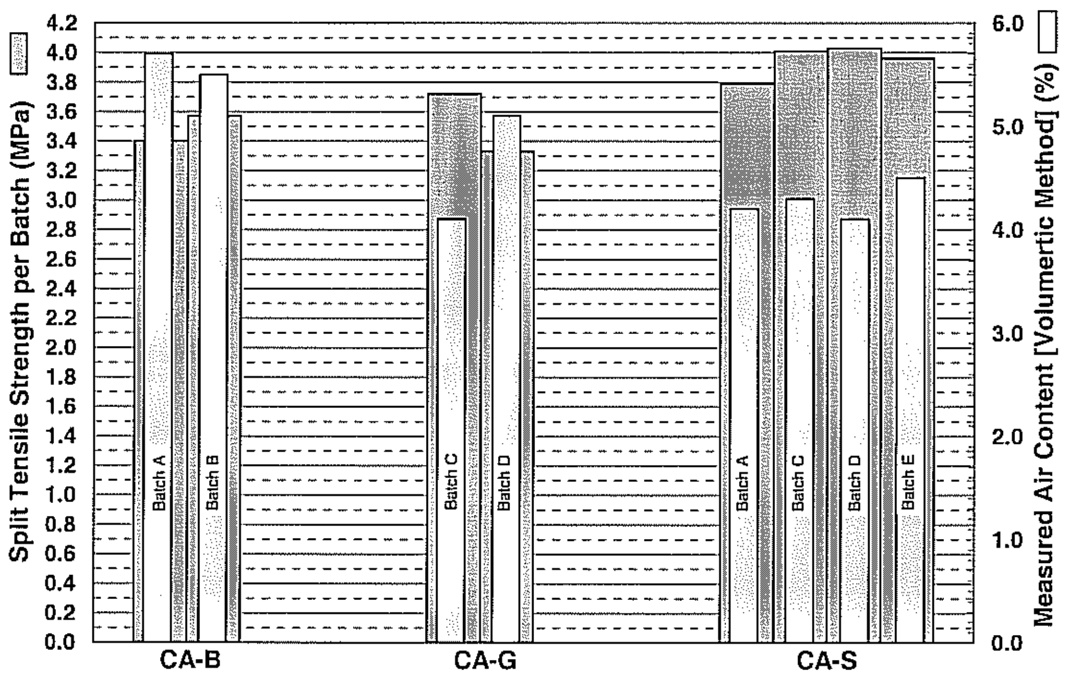

Figure 4.9. Split Tensile Strength with Measured Air Content per Batch of Concrete

Another reason why CA-S developed higher strength may be related to the absorption (water) characteristics of the slag. As discussed in Section 2.1, absorption measurements for the slag aggregate did not compare well between testing laboratories. The range for absorption was found to be approximately 2.5 to 8.5% (Table 2.2). If the actual absorption was larger than the 3.55% used in the initial mix design, then more water would be absorbed into the coarse aggregate. Less free water would be available to react with the cement, resulting in a lower water-cement ratio and thereby leading to higher strength. This would not be apparent in the calculation for water-cement ratio because the amount of absorbed water is a constant based on the absorption value of the coarse aggregate selected for the mix design.

4.1.1 Split Tensile Comparison

Split tensile strength data obtained from this study was compared to predictions from the ACI Concrete Building Code, ACI 318-95. The following ACI 318-95 relationship is for normal weight concrete.

$$f_{ct} = 0.56 \times \sqrt{f'_c} \quad \text{(SI)} \qquad f_{ct} = 6.7 \times \sqrt{f'_c} \quad \text{(USC)} \qquad 4.1$$

where

f_{ct} = split tensile strength of concrete (MPa, psi),
f'_c = axial compressive strength of concrete (MPa, psi).

Taking the split tensile strength obtained from test data and dividing it by the square root of the measured compressive strength gives a measured constant for comparing to the ACI factor 0.56 (SI units) or 6.7 (USC). Table 4.5 compares the factor calculated from the data to the empirical factor stated in ACI 318-95. The results are in good agreement as indicated in Table 4.5. Although CA-S has the largest percent difference, this was expected because CA-S has the largest relative difference between axial compressive and split tensile strengths (Table 4.3).

Table 4.5 Factor for Split Tensile Strength Data compared to ACI 318-95

Aggregate Type	f_{ct} Factor Calculated from Data SI (USC)	f_{ct} Factor from ACI 318-95 SI (USC)	Percent Difference from ACI 318-95 %
CA-B	0.547 (6.59)	0.56 (6.7)	-2.4
CA-G	0.551 (6.65)		-1.6
CA-S	0.587 (7.08)		4.8

4.1.2 Modulus of Elasticity

The modulus of elasticity, *E*, was calculated using a stiffness method because of a discrepancy associated with the true displacement of the specimen, as discussed in Section 3.1.1. The following stiffness method is used to develop a "calibration" type relationship to eliminate effects of the displacement discrepancy and to obtain *E* for each cylinder tested. Figure 3.1 illustrated the load frame used in this study. A system of two springs in series was used to model the specimen and the load frame including the bottom and top platens. From this model it was possible to isolate the stiffness of the specimen. As a result *E* was calculated using the relationship relating the specimen stiffness to *E*. The procedure and the assumptions used are described in the following paragraphs.

To obtain the overall system stiffness, a steel cylinder that was approximately the same size as a concrete cylinder was placed into the MTS load frame along with a digital dial gage with a readability of 0.0025 mm (0.0001 in.). The dial gage was placed between the top and bottom platen along side of the steel cylinder. In this configuration the dial gage gives the true displacement of the steel cylinder. The steel cylinder was then loaded and unloaded in axial compression several times to a maximum load of 1334 kN (300 kip), or approximately 23% of the ultimate steel strength. Load and crosshead displacement were recorded continuously throughout each of the tests using a personal computer. The crosshead displacement was measured using the LVDT as discussed in Chapter 3. The specimen displacement was manually recorded from the dial gage every 89 kN (20 kip) until a load of 623 kN (140 kip) was reached, and thereafter every 44.5 kN (10 kip) up to the maximum load. Figure 4.10 is a load versus displacement curve for the data obtained from the axial compressive loading of the steel cylinder. Included in

Figure 4.10 is curves obtained from the dial gage and LVDT displacement readings as well as the theoretical and corrected curves for the steel cylinder. The following discussion explains how the corrected and theoretical curves were obtained.

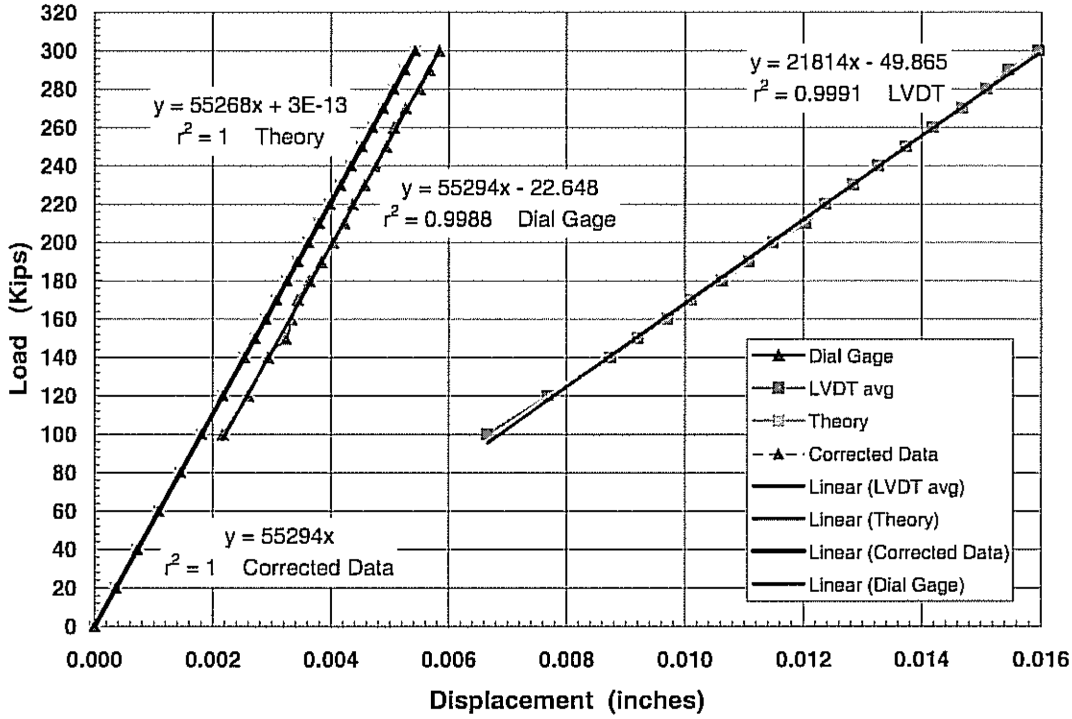

Figure 4.10. Axial Compressive Load versus Displacement for the Steel Cylinder Used for Compliance Testing.

A corrected load-displacement curve can be obtained from a combination of LVDT and dial gage data from the steel cylinder. The correction can later be applied to approximate the modulus of elasticity of the concrete cylinders tested. The slope of LVDT curve is the equivalent stiffness of the system when the steel cylinder was tested. The slope of the dial gage curve is the stiffness of the steel specimen. Using the relationship for springs in series, the stiffness of the top platen can be calculated from Equation 2,

$$\frac{1}{K_{syss}} = \frac{1}{K_{steel}} + \frac{1}{K_{TP}} \qquad 4.2$$

where

K_{syss} = system stiffness with the steel cylinder in place (measured by the LVDT),
K_{steel} = stiffness of steel specimen (measured by the dial gage),
K_{TP} = stiffness of the top platen.

The stiffness of the top platen can also be written as the load divided by the deflection such that

$$K_{TP} = \frac{P}{\Delta_{TP}} \qquad 4.3$$

where

P = applied load,
Δ_{TP} = displacement of top platen.

The top platen displacement, Δ_{TP}, is solved for at known load steps using measured LVDT and dial gage data in Equation 2 and substituting into Equation 3. Subtracting Δ_{TP} from Δ_{syss} (the LVDT measurement) gives the true displacement of the steel cylinder, Δ_s. The plot of load versus Δ_s is the "corrected" curve shown in Figure 4.10.

Assuming the modulus of elasticity of the steel cylinder, E_s, is 200 GPa (29,000 ksi), the theoretical cylinder stiffness, K_s, can be obtained directly from

$$K_s = \frac{P}{\Delta} = \frac{A \times E_s}{L} \qquad 4.4$$

where

K_s = steel specimen stiffness,
E_s = modulus of elasticity of steel cylinder,
A = cross sectional area of steel specimen,
L = length of steel specimen.

Plotting the theoretical stiffness (load versus displacement) yields the theoretical curve shown in Figure 4.10. The theoretical and corrected curves overlap each other indicating that they are in perfect agreement. This also indicates that the MTS testing machine is properly recording the load measurements.

The same principles were applied to the concrete specimens with the exception that E_c was calculated directly from the measured concrete stiffness, K_{con}. The following methodology was used to obtain the stiffness of the concrete specimen.

$$\frac{1}{K_{sysc}} = \frac{1}{K_{con}} + \frac{1}{K_{TP}} \qquad 4.5$$

where

K_{sysc} = system stiffness with concrete specimen in place (measured by LVDT),
K_{con} = stiffness of concrete cylinder (desired quantity),
K_{TP} = stiffness of top platen (from Eqn. 2).

The displacement of the top platen is assumed to be only a function of the applied load, and is therefore independent of the composition of the test specimen. Thus the stiffness of the top platen is not affected by the stiffness of the specimen. Equation 6 can then be written by solving Equations 2 and 5 for $1/K_{TP}$ and setting the results equal to one another.

$$\frac{1}{K_{syss}} - \frac{1}{K_{steel}} = \frac{1}{K_{sysc}} - \frac{1}{K_{con}} \qquad 4.6$$

Solving Equation 6 for $1/K_{con}$ results in

$$\frac{1}{K_{con}} = \frac{1}{K_{sysc}} + \frac{1}{K_{steel}} - \frac{1}{K_{syss}} \qquad 4.7$$

Now that the stiffness of the concrete specimen, K_{con}, is solved, E_c is related to the stiffness of the concrete specimen in the following manner. Solving Equation 4 and substituting concrete for steel gives the following expression for E_c.

$$E_c = \frac{K_{con} \times L}{A} \qquad 4.8$$

where

E_c = modulus of elasticity of concrete,
K_{con} = concrete specimen stiffness from Eqn. 7,
L = length of concrete specimen (12 in.),
A = cross sectional area of concrete specimen.

Modulus of elasticity was estimated for comparison using the relationships for normal weight concrete from the ACI Concrete Building Code 318-95.

$$E_c = 0.043 \times w^{1.5} \times \sqrt{f'c} \quad \text{SI} \qquad E_c = 33 \times w^{1.5} \times \sqrt{f'c} \ \text{USC} \qquad 4.9$$

where

E_c = modulus of elasticity of concrete specimen (MPa, psi),
w = unit weight of concrete (kg/m^3, lb./ft^3).

Table 4.6 is a summary of the modulus of elasticity for each of the three coarse aggregates used in this study and the percent difference from CA-B as well as from ACI 318-95. Moduli of elasticity shown are averages for all axial compression cylinders tested for that particularly type of coarse aggregate. Test data results did not compare well with ACI 318-95 predictions.

Table 4.6 Summary of Modulus of Elasticity Results

Aggregate Type	E_c Calculated from Data MPa (ksi)	Percent Difference from CA-B	E_c Estimated from ACI 318-95 MPa (ksi)	Percent Difference from ACI 318-95
CA-B	23,400 (3,387)	-	32,200 (4,640)	-27.4
CA-G	22,750 (3,299)	-2.6	32,250 (4,647)	-29.4
CA-S	24,950 (3,616)	6.7	30,800 (4,439)	-19.0

Caution needs to be taken when examination of modulus of elasticity is considered. Results presented were not obtained using the standard ASTM procedure. End effects may exist due to not only the barreling the specimen experiences during loading, but also the effect of end capping. Capping provides greater surface area in contact with the platens that translates to larger frictional forces holding the ends of the cylinder together.

4.2 Conclusions

The objective of this phase of the research was two-fold. The first objective was to become proficient in the preparation of concrete using the MDOT Mortar Voids method. The second objective was to determine if axial compressive and split tensile strength of concrete vary with coarse aggregate type based on a 28-day cure using the MDOT P1 mix design. Based on this research the following conclusions and observations are presented:

(1) Automated methods were used to determine the apparent specific gravity, bulk dry specific gravity and absorption. The results showed excellent agreement with standard ASTM methods for the basalt and glacial gravel aggregates. However, there was significant variation for the blast furnace slag aggregate.

(2) Based on the results of the strength testing and yield data results it is believed that consistent concrete was prepared using the MDOT Mortar Voids method.

(3) It was found that all concrete mixes gave superior strength results independent of coarse aggregate type (basalt, sand and gravel, or blast furnace slag) when compared to the design strength of 24 MPa (3500 psi) for a P1 mix design.

(4) There were, however, strength variations based on the coarse aggregate type. The slag concrete had a ten percent increase in axial compressive strength over the basaltic concrete. Similar results were found for split tensile strength with the slag concrete having a 12 percent increase over the basaltic concrete. The sand and gravel concrete was in between the slag and basalt concrete.

(5) From the yield data it was observed that the slag concrete had an overall volume reduction per concrete batch (and hence an apparent increase in cement content per cubic meter), which was believed to be due to the increased penetration of the mortar into the surface pores of the slag. It is believed that by increasing the contact area between the slag and the mortar provided increased strength in both compression and tension.

(6) It was observed that the concrete's facture surface, in relation to coarse aggregate fracture versus pullout, was dependent on the coarse aggregate type. The slag

coarse aggregate exhibited the very high surface fractures of approximately 80 to 100% of the coarse aggregate particles, while the bond failure for the basaltic concrete and sand and gravel concrete was estimated to be approximately 20 to 30 percent of the total. It was speculated that the higher mortar to aggregate interface caused the fracture surface to be forced through the slag as opposed at the interface.

(7) The air content of the slag concrete was much lower than the basaltic concrete or the sand and gravel concrete using both the Volumetric and Gravimetric Methods. The variability between the two methods was the greatest for the slag concrete because of difficulty in accurately measuring coarse aggregate properties (specific gravity and absorption) of the slag.

(8) The split tensile test results compared well with the ACI Concrete Building Code (ACI 318-95) predictions. However, the modulus of elasticity results did not compare well with ACI 318-95 predictions.

4.3 Recommendations for Future Work

(1) The automated specific gravity devices show excellent promise in quickly and accurately determining an aggregate's apparent specific gravity, bulk dry specific gravity and in estimating the maximum absorption. However, there was significant scatter estimating these properties for the slag aggregate. It is recommended that additional testing be considered to determine if the variation is due to the ASTM test method, which uses water to penetrate the aggregate, or with the helium pycnometer, which uses helium gas to penetrate the aggregate.

(2) It is apparent that the surface characteristics and shape of the coarse aggregate affect the overall strength of the concrete to a limited degree. While this level of strength increase may not be significant given the total strength of a concrete mix, it does provide an understanding of the fracture process, which can be important in studying the long-term durability of concrete. Therefore, it is recommended that additional research be conducted to better understand the effect of surface texture and shape.

Appendix 4A

Coarse Aggregate Specific Gravity and Absorption

Coarse Aggregate :	CA-B (Basalt)
Source Number :	31 - 76
Specification :	6AA
Test date:	4/17/98
Test laboratory:	MTU, B004 Dillman

Test number	M1	M2	M3	
Bucket Identification	X	Y	Z	
Pan Identification	X_1	Y_2	Z_3	
A. SSD Agg. + Bucket	7228.9	7267.5	7014.6	
B. Weight of Bucket	2181.6	2225.8	1974.2	
C. Weight of SSD Agg. (A - B)	5047.3	5041.7	5040.4	
D. Weight of SSD Agg. + Bucket in H_2O	4640.4	4659.4	4518.1	
E. Weight of Bucket in H_2O	1377.7	1405.6	1261.4	
F. Weight of SSD Agg. In H_2O (D - E)	3262.7	3253.8	3256.7	
G. Pan Weight + Oven Dry Agg.	5515.5	5264.9	6393.7	
H. Pan Weight	543.4	299.4	1431.1	
J. Weight of Oven Dry Agg. (G - H)	4972.1	4965.5	4962.6	
C - F (SSD Volume)	1784.6	1787.9	1783.7	
J - F (Dry Agg. - Dry Weight)	1709.4	1711.7	1705.9	
C - J (SSD - Dry Weight)	75.2	76.2	77.8	**Average**
Bulk Dry S.G. = J/(C -F)	2.79	2.78	2.78	**2.78**
Bulk SSD S.G. = C/(C - F)	2.83	2.82	2.83	**2.82**
Apparent S.G. = J/(J - F)	2.91	2.90	2.91	**2.91**
Absorption, % = [(C - J)/J]*100	1.51	1.53	1.57	**1.54**

Notes: All weights in grams

Coarse Aggregate Specific Gravity and Absorption

Coarse Aggregate :	**CA-G (Glacial Gravel)**
Source Number :	**31 - 45**
Specification :	**6AA**
Test date:	**4/15/98**
Test laboratory:	**MTU, B004 Dillman**

Test number	SSG1	SSG4	SSG5	
Bucket Identification	Y	Y	Z	
Pan Identification	Y_1	Y_4	Z_5	
A. SSD Agg. + Bucket	7270.2	7269.8	7011.4	
B. Weight of Bucket	2225.9	2225.8	1974.2	
C. Weight of SSD Agg. (A - B)	5044.3	5044.0	5037.2	
D. Weight of SSD Agg. + Bucket in H_2O	4622.7	4620.3	4468.9	
E. Weight of Bucket in H_2O	1405.6	1405.6	1261.4	
F. Weight of SSD Agg. In H_2O (D - E)	3217.1	3214.7	3207.5	
G. Pan Weight + Oven Dry Agg.	6354.0	5510.5	5504.8	
H. Pan Weight	1384.8	539.2	539.8	
J. Weight of Oven Dry Agg. (G - H)	4969.2	4971.3	4965.0	
C - F (SSD Volume)	1827.2	1829.3	1829.7	
J - F (Dry Agg. - Dry Weight)	1752.1	1756.6	1757.5	
C - J (SSD - Dry Weight)	75.1	72.7	72.2	**Average**
Bulk Dry S.G. = J/(C -F)	2.72	2.72	2.71	**2.72**
Bulk SSD S.G. = C/(C - F)	2.76	2.76	2.75	**2.76**
Apparent S.G. = J/(J - F)	2.84	2.83	2.83	**2.83**
Absorption, % = [(C - J)/J]*100	1.51	1.46	1.45	**1.48**

Notes: All weights in grams

Coarse Aggregate Specific Gravity and Absorption

Coarse Aggregate :	**CA-S(1) (Slag)**
Source Number :	**82 - 19**
Specification :	**6AA**
Test date:	**4/18/98 Trial 1**
Test laboratory:	**MTU, B004 Dillman**

Test number	LS1	LS2	LS3	
Bucket Identification	Z & Y	X & Y	X & Y	
Pan Identification	Z_1 & Y_1	X_2 & Y_2	X_3 & Y_3	
A. SSD Agg. + Bucket	9325.8	9471.2	9490.9	
B. Weight of Bucket	4200.0	4407.4	4407.4	
C. Weight of SSD Agg. (A - B)	5125.8	5063.8	5083.5	
D. Weight of SSD Agg. + Bucket in H_2O	5753.6	5906.8	5881.9	
E. Weight of Bucket in H_2O	2667.0	2783.3	2783.3	
F. Weight of SSD Agg. In H_2O (D - E)	3086.6	3123.5	3098.6	
G. Pan Weight + Oven Dry Agg.	6044.2	6041.9	6037.5	
H. Pan Weight	1090.9	1083.1	1083.4	
J. Weight of Oven Dry Agg. (G - H)	4953.3	4958.8	4954.1	
C - F (SSD Volume)	2039.2	1940.3	1984.9	
J - F (Dry Agg. - Dry Weight)	1866.7	1835.3	1855.5	
C - J (SSD - Dry Weight)	172.5	105.0	129.4	**Average**
Bulk Dry S.G. = J/(C -F)	2.43	2.56	2.50	**2.49**
Bulk SSD S.G. = C/(C - F)	2.51	2.61	2.56	**2.56**
Apparent S.G. = J/(J - F)	2.65	2.70	2.67	**2.68**
Absorption, % = [(C - J)/J]*100	3.48	2.12	2.61	**2.74**

Notes: All weights in grams

Coarse Aggregate Specific Gravity and Absorption

Coarse Aggregate :	**CA-S(2) (Slag)**
Source Number :	**82 - 19**
Specification :	**6AA**
Test date:	**7/7/98 Trial 2**
Test laboratory:	**MTU, B004 Dillman**

Test number	LS4	LS5	LS6	
Bucket Identification	X	Y	Z	
Pan Identification	X_4	Y_5	Z_6	
A. SSD Agg. + Bucket	4831.3	4885.4	4828.7	
B. Weight of Bucket	2178.9	2225.5	2178.9	
C. Weight of SSD Agg. (A - B)	2652.4	2659.9	2649.8	
D. Weight of SSD Agg. + Bucket in H_2O	2941.2	2973.8	2947.0	
E. Weight of Bucket in H_2O	1376.2	1405.1	1376.2	
F. Weight of SSD Agg. In H_2O (D - E)	1565.0	1568.7	1570.8	
G. Pan Weight + Oven Dry Agg.	3030.9	2883.8	2882.4	
H. Pan Weight	545.4	395.8	397.7	
J. Weight of Oven Dry Agg. (G - H)	2485.5	2488.0	2484.7	
C - F (SSD Volume)	1087.4	1091.2	1079.0	
J - F (Dry Agg. - Dry Weight)	920.5	919.3	913.9	
C - J (SSD - Dry Weight)	166.9	171.9	165.1	**Average**
Bulk Dry S.G. = J/(C -F)	2.29	2.28	2.30	**2.29**
Bulk SSD S.G. = C/(C - F)	2.44	2.44	2.46	**2.44**
Apparent S.G. = J/(J - F)	2.70	2.71	2.72	**2.71**
Absorption, % = [(C - J)/J]*100	6.71	6.91	6.64	**6.76**

Notes: All weights in grams

Fine Aggregate Specific Gravity and Absorption

Coarse Aggregate :	FA-Y (Sand)
Source Number :	31 - 45
Specification :	2NS
Test date:	7/7/98
Test laboratory:	MTU, B004 Dillman

Test number	1	2	4	
Flask Number	M	N	N	
Pan Identification	M_1	N_2	N_4	
A. SSD Agg. + Flask	695.4	688.5	679.3	
B. Weight of Flask	180.7	171.2	171.2	
C. Weight of SSD Agg. (A - B)	514.7	517.3	508.1	
D. Weight of SSD Agg. + Flask + H_2O	1001.9	993.9	988.3	
E. Weight of Flask + H_2O	678.8	669.2	669.2	
F. Weight of SSD Agg. In H_2O (D - E)	323.1	324.7	319.1	
G. Pan Weight + Oven Dry Agg.	1005.0	1027.4	1040.3	
H. Pan Weight	496.7	516.5	539.1	
J. Weight of Oven Dry Agg. (G - H)	508.3	510.9	501.2	
C - F (SSD Volume)	191.6	192.6	189.0	
J - F (Dry Agg. - Dry Weight)	185.2	186.2	182.1	
C - J (SSD - Dry Weight)	6.4	6.4	6.9	**Average**
Bulk Dry S.G. = J/(C -F)	2.65	2.65	2.65	**2.65**
Bulk SSD S.G. = C/(C - F)	2.69	2.69	2.69	**2.69**
Apparent S.G. = J/(J - F)	2.74	2.74	2.75	**2.75**
Absorption, % = [(C - J)/J]*100	1.26	1.25	1.38	**1.30**

Notes: All weights in grams

Coarse Aggregate Unit Weight (Dry Loose)

CA-B (Basalt) Source No. 31-76	English		SI	
	Test 1	Test 2	Test 1	Test 2
A. Bucket weight lbs,kg	17.95	17.95	8.14	8.14
B. Bucket + Agg. lbs,kg	63.80	63.75	28.94	28.92
C. Weight of Agg. (B - A) lbs,kg	45.85	45.80	20.80	20.78
D. Bucket Volume ft^3,m^3	0.4863	0.4863	0.0138	0.0138
E. Bulk Density {dry loose} (C/D) ft^3,m^3	94.29	94.18	1510.63	1509.18
F. Average	94.2 lbs/ft^3		1509.9 kg/m^3	

CA-G (Glacial Gravel) Source No. 31-45	English		SI	
	Test 1	Test 2	Test 1	Test 2
A. Bucket weight lbs,kg	17.95	17.95	8.14	8.14
B. Bucket + Agg. lbs,kg	64.90	65.45	29.44	29.68
C. Weight of Agg. (B - A) lbs,kg	46.95	47.50	21.30	21.54
D. Bucket Volume ft^3,m^3	0.4863	0.4863	0.0138	0.0138
E. Bulk Density {dry loose} (C/D) ft^3,m^3	96.55	97.68	1546.95	1564.38
F. Average	97.1 lbs/ft^3		1555.7 kg/m^3	

CA-S (Slag) Source No. 82-19	English		SI	
	Test 1	Test 2	Test 1	Test 2
A. Bucket weight lbs,kg	17.95	17.95	8.14	8.14
B. Bucket + Agg. lbs,kg	54.90	54.60	24.90	24.75
C. Weight of Agg. (B - A) lbs,kg	36.95	36.65	16.76	16.61
D. Bucket Volume ft^3,m^3	0.4863	0.4863	0.0138	0.0138
E. Bulk Density {dry loose} (C/D) ft^3,m^3	75.98	75.37	1217.22	1206.33
F. Average	75.7 lbs/ft^3		1211.8 kg/m^3	

Fine Aggregate Unit Weight (Dry Loose)

FA-Y (Sand) Source No. 31-45	English		SI	
	Test 1	Test 2	Test 1	Test 2
A. Bucket weight lbs,kg	17.95	17.95	8.14	8.14
B. Bucket + Agg. lbs,kg	70.35	70.45	31.92	31.95
C. Weight of Agg. (B - A) lbs,kg	52.40	52.50	23.78	23.81
D. Bucket Volume ft^3,m^3	0.4863	0.4863	0.0138	0.0138
E. Bulk Density {dry loose} (C/D) ft^3,m^3	107.76	107.96	1727.06	1729.24
F. Average	107.9 lbs/ft^3		1728.2 kg/m^3	

Appendix 4B

CA-B Mix Design Worksheets

Basalt

MICHIGAN DEPARTMENT OF TRANSPORTATION

FORM 1830 CONCRETE PROPORTIONING DATA FILE 300

CONTROL SECTION ID: GENERAL
JOB NUMBER: MTU
LAB NUMBER:
GRADE OF CONCRETE: P1
INTENDED USE OF CONCRETE: Pavement (Conv. Form)

MDOT mix design for CA-B

DATE: 4/27/1998
SPECIFICATION: 1996 STD SPECS
MIX DESIGN NUMBER:

CONCRETE MATERIALS

MATERIAL	SOURCE	PIT NUMBER	CLASS	SPECIFIC GRAVITY	ABSORPTION PERCENT
CEMENT	(SEE REMARKS)		I/IA	3.15	
FINE AGG.	SUPERIOR SAND & GRAVEL	31-45	2NS	2.67	0.87
COARSE AGG.	MOYLE	31-76	6AA	2.79	1.45
FLY ASH					

CEMENT CONTENT, kg/m^3 335
AIR CONTENT (DESIGN): 6.5% (SPECIFIED): 6.5%
R.W.C: 1.15
FLY ASH CONTENT, kg/m^3: 0

B/Bo : 0.72
SPECIFICATION TOLERANCE (±): 1.5%
THEORETICAL YIELD: 100.00%

WEIGHT OF COARSE AGG. (DRY/LOOSE) kg/m^3	AGGREGATE AND WATER PROPORTIONS QUANTITIES, kg/m^3 OF CONCRETE		
	FINE AGG (OVEN DRY)	COARSE AGG (OVEN DRY)	TOTAL WATER
1460	821	1051	167
1470	815	1058	167
1480	809	1066	166
1490	803	1073	166
1500	797	1080	166
1510	791	1087	165
1520	785	1094	165
1530	779	1102	165
1540	773	1109	165
1550	767	1116	164
1560	761	1123	164

REMARKS:
THIS CHART FOR USE WITH CEMENTS OF THE CLASS SHOWN FROM APPROVED SOURCES.

TYPICAL UNIT WEIGHT (DRY, LOOSE) OF COARSE AGGREGATE AS DESCRIBED ABOVE IS 1510 kg/m^3

SPECIAL MESSAGES:

CC:
MTU

JOHN F. STATON
MATERIALS RESEARCH ENGINEER

MIX PROPORTIONS WORKSHEET

	Laboratory No	Bulk Dry Specific Gravity	% Absorption
Cement: Lafarge (Alpena) Type 1		3.15	–
Coarse Aggregate: CA-B (Basalt) Source No. 31-76 Specification 6AA	MTU	2.79 ★	1.45 ★
Fine Aggregate: FA-Y Source No. 31-45 Specification 2NS		2.67 ★	0.87 ★

batch size

Material	Weight, kg/m^3	Batch Proportions kg 0.0779779 m^3	
Cement	335 ★	26.12	**Total cement** (C)
Coarse Aggregate (DRY)	1087 ★	84.76	**Total Coarse Agg.** (a)
Fine Aggregate (DRY)	791 ★	61.68	**Total Fine Agg.** (b)
Total Water	165 ★	12.87	**Total Water per Batch** (d)
Absorbed Water		22.64	**Absorbed water kg/m^3** (W)

Coarse aggregate gradation:

		Pass	Ret	%
21.190	21.19	25.0mm	19.0mm	25
21.190	21.19	19.0mm	12.5mm	25
21.190	21.19	12.5mm	9.5mm	25
21.190	21.19	9.5mm	4.75mm	25
	84.76			

Absorbed water:

		agg*absorption =	absorbed $h_2 0$
Coarse Agg	1087	0.0145	15.76
Fine Agg	791	0.0087	6.88
			22.64

Total Aggregate Contains 42.1 % Fine Aggregate

Note: ★ Provided by MDOT (Form 1830, File 300) and listed in Table 2.3

BATCH COMPUTATIONS WORKSHEET

WEIGHT IN kg

Coarse Aggregate

84.76 Coarse Agg (a)

Pail tare	1.65	1.64	3.29 + pails
			88.05 = total
25.0 - 19.0mm	21.19	0.00	
19.0 - 12.5mm	0.00	21.19	
12.5 - 9.5mm	0.00	21.19	
9.5 - 4.75mm	21.19	0.00	
Sub total	44.03	44.02	88.05 Total

Fine Aggregate

61.68 Fine Agg (b)

Moisture content

wet	dry
335.38	323.37
0.0371	MC

0.0371 MC

2.29 Moisture

Dry weight 61.68

\+

Moisture 2.29

Total 63.97

Cement

26.12 Cement (C)

Pail ID K, L

Tare weight 0.83 — 1.66 tare

Tare weight 0.83 — 27.78 Pail + cement

Total tare 1.66

Air Entraining Admixture

28 ml

Batch Summary

(a)	Coarse Aggregate as Designed	84.76 kg
(b)	Fine Aggregate as Designed	61.68 kg
(C)	Cement as Designed	26.12 kg
(D)	Total Water of Batch	14.12 kg
(e)	**Total Weight of Batch**	**186.68** kg

BATCH NO. MA

COARSE AGG CA-B (Basalt)

DATE: 6/3/98

Batch Made WED @ 9:30am

WATER MEASUREMENT

Coarse Agg +pail	44.03		
Coarse Agg +pail	44.02		
Total	88.05		
+ Total Batch Water	12.87	(d)	12.87
- Reserve Water	3.00		3.00
= Pails, Agg&Water	97.92	H_20	9.87

RESERVE WATER

Res water 3.00	1.33	surplus & Tare
+ Tare 0.29	0.29	- tare
= Total 3.29	1.04	= surplus

Reserve Water	3.00		
- Surplus Water	1.04		
=	1.96	H_2O +	9.87
Subtotal of water in batch		=	11.83
+ Moisture in Fine Aggregate		+	2.29
Total Water in Batch		**(D) =**	**14.12**

UNIT WEIGHT

Weight of Concrete & Bucket	41.03
- Weight of Bucket	8.14
= Weight of Concrete in Bucket	32.89 (f)

SLUMP = 2.25 " — 57.2 mm

AIR CONTENT

- Factor of Aggregate Porosity
= Percent Air 5.7

CONCRETE TEMPERATURE, C 19

Note: a,b,C,d come from mix proportions worksheet

BATCH COMPUTATIONS WORKSHEET **WEIGHT IN kg**

Coarse Aggregate

84.76 Coarse Agg (a)

Pall tare	1.65	1.65	3.30	+ pails
			88.06	= total
25.0 - 19.0mm	21.19	0.00		
19.0 - 12.5mm	0.00	21.19		
12.5 - 9.5mm	0.00	21.19		
9.5 - 4.75mm	21.19	0.00		
Sub total	44.03	44.03	88.06	Total

BATCH NO.	MB
COARSE AGG	CA-B (Basalt)
DATE:	6/3/98
Batch Made	WED @ 11:30am

Fine Aggregate

61.68 Fine Agg (b)

Moisture content

wet	dry
335.38	323.37
0.0371	MC

0.0371 MC

2.29 Moisture

Dry weight 61.68

\+

Moisture 2.29

Total 63.97

WATER MEASUREMENT

Coarse Agg +pail	44.03		
Coarse Agg +pail	44.03		
Total	88.06		
+ Total Batch Water	12.87	(d)	12.87
- Reserve Water	3.00		3.00
= Pails, Agg&Water	97.93	H_2O	9.87

RESERVE WATER

Res water	3.00	1.29 surplus & Tare
+ Tare	0.29	0.29 - tare
= Total	3.29	1.00 = surplus

Reserve Water	3.00		
- Surplus Water	1.00		
=	2.00	H_2O +	9.87
Subtotal of water in batch		=	11.87
+ Moisture in Fine Aggregate		+	2.29
Total Water in Batch		**(D) =**	**14.16**

Cement

26.12 Cement (C)

Pail ID	M , N		
Tare weight	1.16	2.37	tare
Tare weight	1.21	28.49	Pail + cement
Total tare	2.37		

UNIT WEIGHT

Weight of Concrete & Bucket	41.09	
- Weight of Bucket	8.14	
= Weight of Concrete in Bucket	**32.95**	**(f)**

Air Entraining Admixture

28 ml

Batch Summary

(a)	Coarse Aggregate as Designed	84.76 kg
(b)	Fine Aggregate as Designed	61.68 kg
(C)	Cement as Designed	26.12 kg
(D)	Total Water of Batch	14.16 kg
(e)	**Total Weight of Batch**	**186.72** kg

SLUMP = 3.00 " **76.2** mm

AIR CONTENT

- Factor of Aggregate Porosity	
= Percent Air	**5.5**

CONCRETE TEMPERATURE, C 19

Note: a,b,C,d come from mix proportions worksheet

YIELD DATA

Coarse Aggregate :	CA-B (Basalt)
Source Number :	31-76
Specification :	6AA

Formulae for Computation		Batch Identification MA	Batch Identification MB	Yield Data MA	Yield Data MB	Units
g	Unit Weight of Concrete $\frac{f}{\text{Volume of unit weight bucket}}$	$\frac{32.89}{0.01377}$	$\frac{32.95}{0.01377}$	2388.5	2392.9	kg/m^3
h	Batch Volume of Concrete $\frac{e}{g}$	$\frac{186.68}{2388.5}$	$\frac{186.72}{2392.9}$	0.07816	0.07803	m^3 batch
i	Cement used for one m^3 of concrete $\frac{C}{h}$	$\frac{26.12}{0.07816}$	$\frac{26.12}{0.07803}$	334.2	334.8	kg/m^3
j	Net water used for one m^3 of concrete $\frac{D}{h}$ - Absorbed Water (W)	$\frac{14.12}{0.07816}$ minus 22.64	$\frac{14.16}{0.07803}$ minus 22.64	157.98	158.78	kg/m^3
k	Water / Cement Ratio $\frac{j}{i}$	$\frac{157.98}{334.23}$	$\frac{158.78}{334.77}$	0.47	0.47	w/c

Note: C,D,e,f,W come from batch computations worksheet

REPORT OF TEST

Coarse Aggregate :	CA-B (Basalt)
Source Number :	31-76
Specification :	6AA

Properties of Coarse Aggregate

Bulk Specific Gravity (dry basis)	2.79
Absorption % (24 hour soak)	1.45
Unit weight (dry loose) kg/m^3	1510

Concrete Mixture Data

	Batch Identification				
	MA	MB			Average
Date of Batch	6/3/98	6/3/98			
Slump (mm)	57	76			**67**
Unit weight of Concrete (kg/m^3)	2389	2393			**2391**
Apparent Cement Content (kg/m^3)	334	335			**334**
Water/Cement Ratio (by weight)	0.47	0.47			**0.47**
Air Content (%)	5.7	5.5			**5.6**

Compressive Strength (MPa)

28 Days	41.1	40.9			**41.0**

Split Tensile Strength (MPa)

28 Days	3.40	3.57			**3.49**

Appendix 4C
CA-G Mix Design Worksheets
Glacial Gravel

MICHIGAN DEPARTMENT OF TRANSPORTATION

FORM 1830 CONCRETE PROPORTIONING DATA FILE 300

CONTROL SECTION ID: GENERAL
JOB NUMBER: MTU
LAB NUMBER:
GRADE OF CONCRETE: P1
INTENDED USE OF CONCRETE: Pavement (Conv. Form)

MDOT mix design for CA-G

DATE: 4/27/1998
SPECIFICATION: 1996 STD SPECS
MIX DESIGN NUMBER:

CONCRETE MATERIALS

MATERIAL	SOURCE	PIT NUMBER	CLASS	SPECIFIC GRAVITY	ABSORPTION PERCENT
CEMENT	(SEE REMARKS)		1/IA	3.15	
FINE AGG.	SUPERIOR SAND & GRAVEL	31-45	2NS	2.67	0.87
COARSE AGG.	SUPERIOR SAND & GRAVEL	31-45	6AA	2.73	1.35
FLY ASH					

CEMENT CONTENT, kg/m^3 335
AIR CONTENT (DESIGN): 6.5% (SPECIFIED): 6.5%
R.W.C: 1.15
FLY ASH CONTENT, kg/m^3: 0

B/Bo : 0.72
SPECIFICATION TOLERANCE (±): 1.5%
THEORETICAL YIELD: 100.00%

WEIGHT OF COARSE AGG. (DRY/LOOSE) kg/m^3	AGGREGATE AND WATER PROPORTIONS QUANTITIES, kg/m^3 OF CONCRETE		
	FINE AGG (OVEN DRY)	COARSE AGG (OVEN DRY)	TOTAL WATER
1506	773	1084	163
1516	767	1092	163
1526	761	1099	163
1536	755	1106	162
1546	749	1113	162
1556	743	1120	162
1566	737	1128	161
1576	731	1135	161
1586	724	1142	161
1596	718	1149	160
1606	712	1156	160

REMARKS:
THIS CHART FOR USE WITH CEMENTS OF THE CLASS SHOWN FROM APPROVED SOURCES.

TYPICAL UNIT WEIGHT (DRY, LOOSE) OF COARSE AGGREGATE AS DESCRIBED ABOVE IS 1556 kg/m^3

SPECIAL MESSAGES:

CC:
MTU

JOHN F. STATON
MATERIALS RESEARCH ENGINEER

MIX PROPORTIONS WORKSHEET

	Laboratory No	Bulk Dry Specific Gravity	% Absorption
Cement: Lafarge (Alpena) Type 1		3.15	-
Coarse Aggregate: CA-G (Glacial Gravel) Source No. 31-45 Specification 6AA	MTU	2.73 ★	1.35 ★
Fine Aggregate: FA-Y Source No. 31-45 Specification 2NS		2.67 ★	0.87 ★

batch size

Material	Weight, kg/m³	Batch Proportions kg 0.0779779 m³						
Cement	335 ★	26.12			Total cement			(C)
Coarse Aggregate (DRY)	1120 ★			Pass	Ret	%		
		21.834	21.84	25.0mm	19.0mm	25		
		21.834	21.83	19.0mm	12.5mm	25		
		21.834	21.84	12.5mm	9.5mm	25		
		21.834	21.83	9.5mm	4.75mm	25		
			87.34					
		87.34			Total Coarse Agg.			(a)
Fine Aggregate (DRY)	743 ★	57.94			Total Fine Agg.			(b)
Total Water	162 ★	12.63			Total Water per Batch			(d)

Absorbed Water	agg	*absorption	= absorbed h_2O			
Coarse Agg	1120	0.0135	15.12	21.58	Absorbed water kg/m³	(W)
Fine Agg	743	0.0087	6.46			
			21.58			

Total Aggregate Contains 39.9 % Fine Aggregate

Note: ★ Provided by MDOT (Form 1830, File 300) and listed in Table 2.3

BATCH COMPUTATIONS WORKSHEET

WEIGHT IN kg

BATCH NO. SSC

COARSE AGG CA-G (Glacial Gravel)

DATE: 6/4/98

Batch Made Thur @ 9:30am

Coarse Aggregate

87.34 Coarse Agg (a)

Pail tare	1.64	1.65	3.29 + pails
			90.63 = total
25.0 - 19.0mm	21.84	0.00	
19.0 - 12.5mm	0.00	21.83	
12.5 - 9.5mm	0.00	21.84	
9.5 - 4.75mm	21.83	0.00	
Sub total	45.31	45.32	90.63 **Total**

Fine Aggregate

57.94 Fine Agg (b)

Moisture content

wet	dry
344.74	332.36
0.0372	MC

0.0372 MC

2.16 Moisture

Dry weight 57.94

\+

Moisture 2.16

Total 60.10

Cement

26.12 Cement (C)

Pail ID O , P

Tare weight 1.19

Tare weight 1.29

Total tare 2.48

2.48 tare

28.60 Pail + cement

Air Entraining Admixture

28 ml

Batch Summary

(a)	Coarse Aggregate as Designed	87.34 kg
(b)	Fine Aggregate as Designed	57.94 kg
(c)	Cement as Designed	26.12 kg
(D)	Total Water of Batch	13.55 kg
(e)	**Total Weight of Batch**	**184.95** kg

WATER MEASUREMENT

Coarse Agg +pail 45.31

Coarse Agg +pail 45.32

Total 90.63

\+ Total Batch Water 12.63 **(d)** 12.63

\- Reserve Water 3.00   3.00

= **Pails, Agg&Water** **100.26** H_20 9.63

RESERVE WATER

Res water	3.00	1.53 surplus & Tare
+ Tare	0.29	0.29 - tare
= Total	3.29	1.24 = surplus

Reserve Water 3.00

\- Surplus Water 1.24

= 1.76 H_2O + 9.63

Subtotal of water in batch = 11.39

\+ Moisture in Fine Aggregate + 2.16

Total Water in Batch (D) = 13.55

UNIT WEIGHT

Weight of Concrete & Bucket 41.06

\- Weight of Bucket 8.14

= Weight of Concrete in Bucket **32.92** **(f)**

SLUMP = 2.00 "   **50.8** mm

AIR CONTENT

\- Factor of Aggregate Porosity

= Percent Air **4.1**

CONCRETE TEMPERATURE, C 19

Note: a,b,C,d come from mix proportions worksheet

BATCH COMPUTATIONS WORKSHEET **WEIGHT IN kg**

BATCH NO.	SSD	
COARSE AGG	CA-G (Glacial Gravel)	
DATE:	6/4/98	
Batch Made	Thur @ 11:30am	

Coarse Aggregate — 87.34 Coarse Agg (a)

Pail tare	1.65	1.65	3.30 + pails
			90.64 = total
25.0 - 19.0mm	21.84	0.00	
19.0 - 12.5mm	0.00	21.83	
12.5 - 9.5mm	0.00	21.84	
9.5 - 4.75mm	21.83	0.00	
Sub total	45.32	45.32	90.64 Total

Fine Aggregate — 57.94 Fine Agg (b)

Moisture content

wet	dry
344.74	332.36
0.0372	MC

0.0372 MC

2.16 Moisture

Dry weight 57.94
\+
Moisture 2.16
Total 60.10

Cement — 26.12 Cement (C)

Pail ID Q , R

Tare weight	1.31	2.50 tare
Tare weight	1.19	28.62 Pail + cement
Total tare	2.50	

Air Entraining Admixture 28 ml

Batch Summary

(a)	Coarse Aggregate as Designed	87.34 kg
(b)	Fine Aggregate as Designed	57.94 kg
(c)	Cement as Designed	26.12 kg
(D)	Total Water of Batch	13.59 kg
(e)	**Total Weight of Batch**	**184.99** kg

WATER MEASUREMENT

Coarse Agg +pail	45.32		
Coarse Agg +pail	45.32		
Total	90.64		
+ Total Batch Water	12.63	(d)	12.63
- Reserve Water	3.00		3.00
= Pails, Agg&Water	100.27	H_2O	9.63

RESERVE WATER

Res water	3.00	1.49 surplus & Tare
+ Tare	0.29	0.29 - tare
= Total	3.29	1.20 = surplus

Reserve Water	3.00		
- Surplus Water	1.20		
=	1.80	H_2O +	9.63
Subtotal of water in batch		=	11.43
+ Moisture in Fine Aggregate		+	2.16
Total Water in Batch		**(D) =**	**13.59**

UNIT WEIGHT

Weight of Concrete & Bucket	40.69	
- Weight of Bucket	8.14	
= Weight of Concrete in Bucket	32.55	(f)

SLUMP = 3.00 " 76.2 mm

AIR CONTENT

- Factor of Aggregate Porosity	
= Percent Air	5.1

CONCRETE TEMPERATURE, C 19

Note: a,b,C,d come from mix proportions worksheet

YIELD DATA

Coarse Aggregate :	CA-G (Glacial Gravel)
Source Number :	31-45
Specification :	6AA

Formulae for Computation		Batch Identification SSC	Batch Identification SSD	Yield Data SSC	Yield Data SSD	Units
g	**Unit Weight of Concrete** $\frac{f}{\text{Volume of unit weight bucket}}$	32.92 / 0.01377	32.55 / 0.01377	2390.7	2363.8	kg/m^3
h	**Batch Volume of Concrete** $\frac{e}{g}$	184.95 / 2390.7	184.99 / 2363.8	0.07736	0.07826	m^3 batch
i	**Cement used for one m^3 of concrete** $\frac{C}{h}$	26.12 / 0.07736	26.12 / 0.07826	337.7	333.8	kg/m^3
j	**Net water used for one m^3 of concrete** $\frac{D}{h}$ - Absorbed Water (W)	13.55 / 0.07736 minus 21.58	13.59 / 0.07826 minus 21.58	153.58	152.08	kg/m^3
k	**Water / Cement Ratio** $\frac{j}{i}$	153.58 / 337.67	152.08 / 333.81	0.45	0.46	w/c

Note: C,D,e,f,W come from batch computations worksheet

REPORT OF TEST

Coarse Aggregate :	CA-G (Glacial Gravel)
Source Number :	31-45
Specification :	6AA

Properties of Coarse Aggregate

Bulk Specific Gravity (dry basis)	2.73
Absorption % (24 hour soak)	1.35
Unit weight (dry loose) kg/m^3	1556

Concrete Mixture Data

	Batch Identification				
	SSC	SSD			Average
Date of Batch	6/4/98	6/4/98			
Slump (mm)	51	76			64
Unit weight of Concrete (kg/m^3)	2391	2364			2377
Apparent Cement Content (kg/m^3)	338	334			336
Water/Cement Ratio (by weight)	0.45	0.46			0.46
Air Content (%)	4.1	5.1			4.6

Compressive Strength (Mpa)

28 Days	43.6	39.2			41.4

Split Tensile Strength (Mpa)

28 Days	3.72	3.33			3.53

Appendix 4D
CA-S Mix Design Worksheets
Slag

MICHIGAN DEPARTMENT OF TRANSPORTATION

FORM 1830 CONCRETE PROPORTIONING DATA FILE 300

CONTROL SECTION ID: GENERAL
JOB NUMBER: MTU
LAB NUMBER:
GRADE OF CONCRETE: P1
INTENDED USE OF CONCRETE: Pavement (Conv. Form)

MDOT mix design for CA-S

DATE: 4/27/1998
SPECIFICATION: 1996 STD SPECS
MIX DESIGN NUMBER:

CONCRETE MATERIALS

MATERIAL	SOURCE	PIT NUMBER	CLASS	SPECIFIC GRAVITY	ABSORPTION PERCENT
CEMENT	(SEE REMARKS)		I/IA	3.15	
FINE AGG.	SUPERIOR SAND & GRAVEL	31-45	2NS	2.67	0.87
COARSE AGG.	LEVY SLAG	82-19	6AA	2.27	3.55
FLY ASH					

CEMENT CONTENT, kg/m^3 335
AIR CONTENT (DESIGN): 6.5% (SPECIFIED): 6.5%
R.W.C: 1.15
FLY ASH CONTENT, kg/m^3: 0

B/Bo : 0.72
SPECIFICATION TOLERANCE (±): 1.5%
THEORETICAL YIELD: 100.00%

WEIGHT OF COARSE AGG. (DRY/LOOSE) kg/m^3	AGGREGATE AND WATER PROPORTIONS QUANTITIES, kg/m^3 OF CONCRETE		
	FINE AGG (OVEN DRY)	COARSE AGG (OVEN DRY)	TOTAL WATER
1162	840	837	183
1172	832	844	182
1182	825	851	182
1192	818	858	182
1202	810	865	182
1212	803	873	181
1222	796	880	181
1232	788	887	181
1242	781	894	181
1252	774	901	181
1262	766	909	180

REMARKS:
THIS CHART FOR USE WITH CEMENTS OF THE CLASS SHOWN FROM APPROVED SOURCES.

TYPICAL UNIT WEIGHT (DRY, LOOSE) OF COARSE AGGREGATE AS DESCRIBED ABOVE IS 1212 kg/m^3

SPECIAL MESSAGES:

CC:
MTU

JOHN F. STATON
MATERIALS RESEARCH ENGINEER

MIX PROPORTIONS WORKSHEET

	Laboratory No	Bulk Dry Specific Gravity	% Absorption
Cement: Lafarge (Alpena) Type 1		3.15	-
Coarse Aggregate: CA-S (Slag) Source No. 82-19 Specification 6AA	MTU	2.27 ★	3.55 ★
Fine Aggregate: FA-Y Source No. 31-45 Specification 2NS		2.67 ★	0.87 ★

Batch size 0.0779779 m^3

Material	Weight, kg/m^3	Batch Proportions kg					
Cement	335 ★	26.12	Total cement (C)				
Coarse Aggregate (DRY)	873 ★				Pass	Ret	%
		17.019	17.01		25.0mm	19.0mm	25
		17.019	17.02		19.0mm	12.5mm	25
		17.019	17.02		12.5mm	9.5mm	25
		17.019	17.02		9.5mm	4.75mm	25
			68.07				
		68.07	Total Coarse Agg. (a)				
Fine Aggregate (DRY)	803 ★	62.62	Total Fine Agg. (b)				
Total Water	181 ★	14.11	Total Water per batch (d)				

Absorbed Water	agg*absorption =		absorbed h_2O		
Coarse Agg	873	0.0355	30.99	37.98	Absorbed water (W) kg/m^3
Fine Agg	803	0.0087	6.99		
			37.98		

Total Aggregate Contains 47.9 % Fine Aggregate

Note: ★ Provided by MDOT (Form 1830, File 300) and listed in Table 2.3

BATCH COMPUTATIONS WORKSHEET **WEIGHT IN kg**

Coarse Aggregate

68.07 Coarse Agg (a)

Pail tare	1.65	1.65	3.30 + pails
			71.37 = total
25.0 - 19.0mm	17.01	0.00	
19.0 - 12.5mm	0.00	17.02	
12.5 - 9.5mm	0.00	17.02	
9.5 - 4.75mm	17.02	0.00	
Sub total	35.68	35.69	71.37 Total

Fine Aggregate

62.62 Fine Agg (b)

Moisture content

wet	dry
329.69	317.54
0.0383	MC

0.0383 MC

2.40 Moisture

Dry weight 62.62
\+
Moisture 2.40
Total 65.01

Cement

26.12 Cement (C)

Pail ID A', B'

Tare weight 0.85 — 1.70 tare

Tare weight 0.85 — 27.82 Pail + cement

Total tare 1.70

Air Entraining Admixture

19 ml

Batch Summary

(a)	Coarse Aggregate as Designed	68.07 kg
(b)	Fine Aggregate as Designed	62.62 kg
(c)	Cement as Designed	26.12 kg
(D)	Total Water of Batch	15.00 kg
(e)	**Total Weight of Batch**	**171.81** kg

BATCH NO. LSA

COARSE AGG CA-S (Slag)

DATE: 6/5/98

Batch Made Fri @ 9:30am

WATER MEASUREMENT

Coarse Agg +pail	35.68		
Coarse Agg +pail	35.69		
Total	71.37		
+ Total Batch Water	14.11	(d)	14.11
- Reserve Water	3.00		3.00
= Pails, Agg&Water	**82.48**	H_2O	11.11

RESERVE WATER

Res water	3.00	1.80	surplus & Tare
+ Tare	0.29	0.29	- tare
= Total	3.29	1.51	= surplus

Reserve Water	3.00		
- Surplus Water	1.51		
=	1.49	H_2O +	11.11
Subtotal of water in batch		=	12.60
+ Moisture in Fine Aggregate		+	2.40
Total Water in Batch		**(D) =**	**15.00**

UNIT WEIGHT

Weight of Concrete & Bucket	39.12	
- Weight of Bucket	8.14	
= Weight of Concrete in Bucket	**30.98**	**(f)**

SLUMP = 2.25 " **57.2** mm

AIR CONTENT

- Factor of Aggregate Porosity
= Percent Air **4.2**

CONCRETE TEMPERATURE, C 20

Note: a,b,C,d come from mix proportions worksheet

BATCH COMPUTATIONS WORKSHEET **WEIGHT IN kg**

Coarse Aggregate

68.07 Coarse Agg (a)

Pail tare	1.64	1.65	3.29 + pails
			71.36 = total
25.0 - 19.0mm	17.01	0.00	
19.0 - 12.5mm	0.00	17.02	
12.5 - 9.5mm	0.00	17.02	
9.5 - 4.75mm	17.02	0.00	
Sub total	35.67	35.69	71.36 Total

BATCH NO.	LSC
COARSE AGG	CA-S (Slag)
DATE:	6/8/98
Batch Made	Monday@10:30am

WATER MEASUREMENT

Coarse Agg +pail	35.67		
Coarse Agg +pail	35.69		
Total	71.36		
+ Total Batch Water	14.11	(d)	14.11
- Reserve Water	3.00		3.00
= Pails, Agg&Water	82.47	H_2O	11.11

Fine Aggregate

62.62 Fine Agg (b)

Moisture content

wet	dry
313.09	301.21
0.0394	MC

0.0394 MC

2.47 Moisture

Dry weight 62.62

\+

Moisture 2.47

Total 65.09

RESERVE WATER

Res water	3.00	2.26	surplus & Tare
+ Tare	0.29	0.29	- tare
= Total	3.29	1.97	= surplus

Reserve Water	3.00		
- Surplus Water	1.97		
=	1.03	H_2O +	11.11
Subtotal of water in batch		=	12.14
+ Moisture in Fine Aggregate		+	2.47
Total Water in Batch		**(D) =**	**14.61**

Cement

26.12 Cement (C)

Pail ID K, G'

Tare weight 0.83 — 1.68 tare

Tare weight 0.85 — 27.80 Pail + cement

Total tare 1.68

UNIT WEIGHT

Weight of Concrete & Bucket	39.08	
- Weight of Bucket	8.14	
= Weight of Concrete in Bucket	**30.94**	**(f)**

Air Entraining Admixture 20 ml

Batch Summary

(a)	Coarse Aggregate as Designed	68.07 kg
(b)	Fine Aggregate as Designed	62.62 kg
(c)	Cement as Designed	26.12 kg
(D)	Total Water of Batch	14.61 kg
(e)	**Total Weight of Batch**	**171.43** kg

SLUMP = 2.25 " **57.2** mm

AIR CONTENT

- Factor of Aggregate Porosity	
= Percent Air	**4.3**

CONCRETE TEMPERATURE, C 21

Note: a,b,C,d come from mix proportions worksheet

BATCH COMPUTATIONS WORKSHEET **WEIGHT IN kg**

Coarse Aggregate 68.07 Coarse Agg (a)

Pail tare	1.65	1.65	3.30 + pails
			71.37 = total
25.0 - 19.0mm	17.01	0.00	
19.0 - 12.5mm	0.00	17.02	
12.5 - 9.5mm	0.00	17.02	
9.5 - 4.75mm	17.02	0.00	
Sub total	35.68	35.69	71.37 Total

BATCH NO. LSD

COARSE AGG CA-S (Slag)

DATE: 6/8/98

Batch Made Monday@11:00am

Fine Aggregate 62.62 Fine Agg (b)

Moisture content

wet	dry
313.09	301.21
0.0394	MC

0.0394 MC

2.47 Moisture

Dry weight 62.62
+
Moisture 2.47
Total 65.09

WATER MEASUREMENT

Coarse Agg +pail	35.68		
Coarse Agg +pail	35.69		
Total	71.37		
+ Total Batch Water	14.11	(d)	14.11
- Reserve Water	3.00		3.00
= Pails, Agg&Water	82.48	H_2O	11.11

RESERVE WATER

Res water	3.00	2.14	surplus & Tare
+ Tare	0.29	0.29	- tare
= Total	3.29	1.85	= surplus

Reserve Water	3.00		
- Surplus Water	1.85		
=	1.15	H_2O +	11.11
Subtotal of water in batch		=	12.26
+ Moisture in Fine Aggregate		+	2.47
Total Water in Batch		**(D) =**	**14.73**

Cement 26.12 Cement (C)

Pail ID A" , B"

Tare weight 0.85 — 1.70 tare

Tare weight 0.85 — 27.82 Pail + cement

Total tare 1.70

UNIT WEIGHT

Weight of Concrete & Bucket	39.16	
- Weight of Bucket	8.14	
= Weight of Concrete in Bucket	31.02	(f)

Air Entraining Admixture 21 ml

SLUMP = 2.00 " 50.8 mm

Batch Summary

(a)	Coarse Aggregate as Designed	68.07 kg
(b)	Fine Aggregate as Designed	62.62 kg
(c)	Cement as Designed	26.12 kg
(D)	Total Water of Batch	14.73 kg
(e)	**Total Weight of Batch**	**171.55** kg

AIR CONTENT

- Factor of Aggregate Porosity
= Percent Air 4.1

CONCRETE TEMPERATURE, C 21

Note: a,b,C,d come from mix proportions worksheet

BATCH COMPUTATIONS WORKSHEET

WEIGHT IN kg

Coarse Aggregate

68.07 Coarse Agg (a)

Pail tare	1.64	1.65	3.29 + pails
			71.36 = total
25.0 - 19.0mm	17.01	0.00	
19.0 - 12.5mm	0.00	17.02	
12.5 - 9.5mm	0.00	17.02	
9.5 - 4.75mm	17.02	0.00	
Sub total	35.67	35.69	71.36 Total

BATCH NO. LSE

COARSE AGG CA-S (Slag)

DATE: 6/8/98

Batch Made Monday@12:00am

Fine Aggregate

62.62 Fine Agg (b)

Moisture content

wet	dry
313.09	301.21
0.0394	MC

0.0394 MC

2.47 Moisture

Dry weight 62.62

\+

Moisture 2.47

Total 65.09

WATER MEASUREMENT

Coarse Agg +pail	35.67		
Coarse Agg +pail	35.69		
Total	71.36		
+ Total Batch Water	14.11	(d)	14.11
- Reserve Water	3.00		3.00
= Pails, Agg&Water	82.47	H_2O	11.11

RESERVE WATER

Res water	3.00	1.80	surplus & Tare
+ Tare	0.29	0.29	- tare
= Total	3.29	1.51	= surplus

Reserve Water	3.00		
- Surplus Water	1.51		
=	1.49	H_2O +	11.11
Subtotal of water in batch		=	12.60
+ Moisture in Fine Aggregate		+	2.47
Total Water in Batch		**(D) =**	**15.07**

Cement

26.12 Cement (C)

Pail ID D", E"

Tare weight	0.84	1.69	tare
Tare weight	0.85	27.81	Pail + cement
Total tare	1.69		

UNIT WEIGHT

Weight of Concrete & Bucket	39.10	
- Weight of Bucket	8.14	
= Weight of Concrete in Bucket	30.96	(f)

Air Entraining Admixture

21 ml

Batch Summary

(a)	Coarse Aggregate as Designed	68.07 kg
(b)	Fine Aggregate as Designed	62.62 kg
(c)	Cement as Designed	26.12 kg
(D)	Total Water of Batch	15.07 kg
(e)	**Total Weight of Batch**	**171.89** kg

SLUMP = 2.75 " 69.9 mm

AIR CONTENT

- Factor of Aggregate Porosity
= Percent Air 4.5

CONCRETE TEMPERATURE, C 21

Note: a,b,C,d come from mix proportions worksheet

YIELD DATA

Coarse Aggregate :	CA-S (Slag)
Source Number :	82-19
Specification :	6AA

	Formulae for Computation	Batch Identification				Yield Data				Units
		LSA	LSC	LSD	LSE	LSA	LSC	LSD	LSE	
g	Unit Weight of Concrete f / Volume of unit weight bucket	30.98 / 0.01377	30.94 / 0.01377	31.02 / 0.01377	30.96 / 0.01377	2249.8	2246.9	2252.7	2248.4	kg/m³
h	Batch Volume of Concrete e / g	171.81 / 2249.8	171.43 / 2246.9	171.55 / 2252.7	171.89 / 2248.4	0.07637	0.07629	0.07615	0.07645	m³ batch
i	Cement used for one m³ of concrete C / h	26.12 / 0.07637	26.12 / 0.07629	26.12 / 0.07615	26.12 / 0.07645	342.1	342.4	343.0	341.7	kg/m³
j	Net water used for one m³ of concrete D / h - Absorbed Water (W)	15.00 / 0.07637 minus 37.98	14.61 / 0.07629 minus 37.98	14.73 / 0.07615 minus 37.98	15.07 / 0.07645 minus 37.98	158.44	153.56	155.50	159.19	kg/m³
k	Water / Cement Ratio j / i	158.44 / 342.06	153.56 / 342.39	155.50 / 343.04	159.19 / 341.70	0.46	0.45	0.45	0.47	w/c

Note: C,D,e,f,W come from batch computations worksheet

REPORT OF TEST

Coarse Aggregate :	CA-S (Slag)
Source Number :	82-19
Specification :	6AA

Properties of Coarse Aggregate

Bulk Specific Gravity (dry basis)	2.27
Absorption % (24 hour soak)	3.55
Unit weight (dry loose) kg/m^3	1212

Concrete Mixture Data

	Batch Identification				
	LSA	LSC	LSD	LSE	Average
Date of Batch	6/5/98	6/8/98	6/8/98	6/8/98	
Slump (mm)	57	57	51	70	**59**
Unit weight of Concrete (kg/m^3)	2250	2247	2253	2248	**2249**
Apparent Cement Content (kg/m^3)	342	342	343	342	**342**
Water/Cement Ratio (by weight)	0.46	0.45	0.45	0.47	**0.46**
Air Content (%)	4.2	4.3	4.1	4.5	**4.3**

Compressive Strength (Mpa)

28 Days	44.1	44.7	46.5	44.7	**45.0**

Split Tensile Strength (Mpa)

28 Days	3.79	4.01	4.03	3.96	**3.95**

References

ACI Committee 318. "Building Code Requirements for Reinforced Concrete and Commentary." ACI 318-95, American Concrete Institute (ACI), Detroit, Michigan. (1995).

American Society for Testing and Materials. *Annual Book of ASTM Standards.* Vol. 04.01, Cement; Lime; Gypsum. (1998).

ASTM C 150-97a, Standard Specification for Portland Cement

American Society for Testing and Materials. *Annual Book of ASTM Standards.* Vol. 04.02, Concrete and Aggregates. (1998).

ASTM C 29/C 29M-97, Standard Test Method for Bulk Density (Unit Weight) and Voids in Aggregates

ASTM C 39-96, Standard Test Method for Compressive Strength of Cylindrical Concrete Specimens

ASTM C 127-88 (Reapproved 1993), Standard Test Method for Specific Gravity and Absorption of Coarse Aggregate

ASTM C 128-97, Standard Test Method for Specific Gravity and Absorption of Fine Aggregate

ASTM C 136-96a, Standard Test Method for Sieve Analysis of Fine and Coarse Aggregate

ASTM C 138-92, Standard Test Method for Unit Weight, Yield, and Air Content (Gravimetric) of Concrete

ASTM C 143/C 143M-97, Standard Test Method for Slump of Hydraulic-Cement Concrete

ASTM C 173-94a, Standard Test Method for Air Content of Freshly Mixed Concrete by the Volumetric Method

ASTM C 192/C 192M-95, Standard Practice for Making and Curing Concrete Test Specimens in the Laboratory

ASTM C 260-97, Standard Specification for Air-Entraining Admixtures for Concrete

ASTM C 470-94, Standard Specification for Molds for Forming Concrete Test Cylinders Vertically

ASTM C 496-96, Standard Test Method for Splitting Tensile Strength of Cylindrical Specimens

ASTM C 566-97, Standard Test Method for Total Evaporable Moisture Content of Aggregate by Drying

ASTM C 617-94, Standard Practice for Capping Cylindrical Specimens

ASTM C 1064-86 (Reapproved 1993), Standard Test Method for Temperature of Freshly Mixed Portland Cement

Grove, Gail H., *Concrete Mix Design Process Manual*, Final Report Prepared for Michigan Department of Transportation, Department of Civil and Environmental Engineering, University of Michigan, Ann Arbor, Michigan. (August, 1998).

Michigan Department of Transportation (MDOT), *1996 Standard Specifications for Construction*, Sections 601 and 902. MDOT Engineering Print Office, Lansing, Michigan. (May, 1996).

Michigan State Highway Laboratory, *Report of Investigation I 205-2.* Comparative Strength Tests of Pavement Concrete Using Slag and Gravel Coarse Aggregates, Ann Arbor, Michigan. (September, 1933).

Shehan, E.L., "The Mortar Voids Method of Proportioning Concrete as Used by the Michigan Department of State Highways", MDOT. (September, 1970).

U.S. Department of Transportation, "User Guidelines for Waste and By-Product Materials in Pavement Construction", Publication No. FHWA-RD-97-148, pp 3-1, 3-9 (Blast Furnace Slag: Material Description). (April 1998).

Vitton, S.J., Lehman, M.A., and Van Dam, T.J., (1998) "Automated Soil Particle Specific Gravity Analysis Using Bulk Flow and Helium Pycnometry," *Nondstructive and Automated Testing for Soil and Rock Properties, ASTM STP 1350,* W.A. Marr and C.E. Fairhurst, Eds., American Society for Testing and Materials, pp. 3-13.

Vitton, S.J., Personal Communication, Michigan Technological University, Department of Civil and Environmental Engineering, Houghton, Michigan. (August 1998 b).

SECTION 5

Dynamic and Quasi-Static Strength Testing

1 Introduction and Background

1.1 Introduction

The focus of this section is the strength evaluation of aggregate, cement matrix (mortar) and PCC under static and dynamic loading conditions. Typically, the duration of pavement loading is in the order of 50 to 60 milliseconds and in some cases faster depending on the condition of the joint. For example, joints that are faulted may experience shock loading due to the vertical weight of the vehicles crossing the joint. Hence the proposed approach views the loading process as a dynamic event to capture the strain rate dependent response of aggregate, mortar and concrete. It is well established in high strain rate literature that when bodies/structures are subjected to rapidly changing loads, their response differs significantly from those under static or quasi-static conditions. Generally, brittle materials fail by means of crack nucleation and growth, with limited plastic flow. Under compressive loading, failure consists of the eventual coalescence of multitude microcracks. It has been shown that compressively loaded brittle materials actually fail in tension at a multiplicity of sites where the overall compressive stress field is distributed into highly localized tensile regions (Lee and William, 1997).

The failure and fracture characteristics of many quasi-brittle and brittle materials have been found to be strongly rate dependent (e.g., Lankford 1983, Ravichandran and Subhash 1995). In considering the rate dependency of materials, the following three technical factors are important:

1. *Dependence of fracture strength and toughness on strain rate:* Compressive failure strength of brittle materials (ceramics and rocks) increases dramatically at strain rates greater than 10^2/sec (e.g., Lankford 1981, 1983, Grady and Lipkin 1980). This rate sensitivity is generally attributed to the inertia dominated dynamic crack growth from

pre-existing flaws (Lankford, 1983) and can be seen in the increase in compressive strength with an increasing strain rate as illustrated in Fig. 1.1 for limestone. Moreover, Suresh, et al. (1990) and Yang and Kobayashi (1990) have observed an increase in fracture toughness of ceramics with strain rate. However, not all brittle materials demonstrate an increase in compressive strength with increased strain rate. Figure 1.2 illustrates four materials in which one of the materials shows a flat or slightly decreasing compressive strength with increased strain rate (Lankford, 1983). It is speculated by Lankford that the reason for this occurring is a possible change in the failure mode through a grain boundary phase transformation induced by high stresses. Lankford further speculates that the brittleness of the transformed grain boundary could alter the failure process to the extent that the strength is lowered. This may also apply to aggregates since there are significant variations in grain and crystalline structure of aggregates.

2. *Variation of Fragment Size with Strain Rate:* Investigations under dynamic loading conditions of brittle materials have revealed that fragmentation size is inversely proportional to strain rate (Kipp and Grady 1985). That is, as the strain rate increases the fragment size at failure decreases. This effect is shown in Fig. 1.3 (Lankford and Blanchard, 1991). Smaller fragment size and narrow distribution imply nucleation and rapid coalescence of numerous micro-cracks at high strain rates. Such a phenomenon may have profound implications on rock blasting and fragmentation studies as well as for natural and man-made materials used as aggregate.

3. *At higher strain rates, the damage tends to be more local:* This is seen for example, when a large structure is slowly loaded the influence of the load is felt simultaneously at distances far away from the region where the load is applied. However, when a load is applied rapidly to the same structure damage concentrates around a very localized region of the structure. Consequently, the fracture strength may increase with strain rate (as illustrated in Figure 1.1), but the concentration of the stresses under dynamic loading may initiate damage and influence crack propagation and load transfer characteristics in a more localized area.

The study of material rate dependency has been investigated using a split Hopkinson pressure bar (also called Kolsky bar) technique, which has been widely used at high strain rates in the range of 10^2-10^4 s^{-1}. The split Hopkinson Pressure bar (SHPB) consists of a striker bar, an incident bar and a transmission bar, as shown schematically in Fig.1.4. The specimen to be characterized is placed between the incident and transmission bars. The free end of the incident bar is impacted by the striker bar, which is launched from a gas gun at a predetermined velocity. The impact generates a compression loading pulse in the incident bar which travels towards the specimen, subjecting it to the required compressive loading. A part of this pulse is transmitted into the transmission bar and the rest is reflected back into the incident bar as a tensile pulse. Strain gages are mounted at the center of each bar to measure the magnitude and duration of the strain pulses as they pass by. Based on one-dimensional calculations (Meyers, 1994; Follansbee, 1985), it can be shown that the magnitude of the transmitted pulse gives a measure of stress to which the specimen is subjected and the magnitude of the reflected wave gives a measure of strain rate within the specimen. Integrating the strain rate with respect to time yields the strain in the specimen. Thus, the stress-strain response of a material can also be obtained at high strain rates. The equations for calculating stress, strain rate and strain within the specimen are given by

$$\sigma_s(t) = \frac{A_b E_b \varepsilon_T(t)}{A_S} \qquad 1.1$$

$$\dot{\varepsilon}_S = -\left(\frac{2c_o \varepsilon_R(t)}{l}\right) \qquad 1.2$$

$$\varepsilon_S(t) = \int_0^t \dot{\varepsilon}_S(\tau) d\tau \qquad 1.3$$

where, A, E, σ, ε and $\dot{\varepsilon}$ refer to area, Young's modulus, stress, strain and strain rate respectively, and the subscripts b, s, T, and R refer to the bar, specimen, transmitted pulse and reflected pulse, respectively. The length of the specimen is *l*; c_o is the longitudinal bar wave velocity and *t* is time.

There are, however, some drawbacks to the traditional SHPB for testing brittle materials when studying the way in which fracture develops in brittle materials. The main problem is that a reflected tensile pulse (generated from the specimen) travels back through the incident bar reaching the striker-end and then is reflected back as a compression pulse reloading the specimen. This process is repeated several times causing multiple loading on the specimen and subsequent additional damage to the specimen. While the stress-strain response and fracture strength can be obtained from the first transmitted load pulse, the multiple loading further damages the specimen making it very difficult to investigate the fracture process. Therefore, correlations between the actual energy input and the microstructural changes (such as crack density, energy absorbed, etc.) are difficult to obtain. Therefore, when investigating the fracture characteristics of a material the specimen must only receive a single compression pulse. This is achieved by designing a momentum trap (MT) at the impact end of the incident bar. The MT is designed in such a way that when the reflected tensile pulse reaches the striker-end of the incident bar, it absorbs the tensile wave energy and does not allow subsequent compression pulses to travel towards the specimen. Thus, the specimen is subjected to a single compression loading. A SHPB with a momentum trap is referred to as a Modified Split Hopkinson Pressure Bar (MSHPB) and is shown schematically in the Fig. 1.5.

The amplitude of the input stress pulse depends on the impact velocity of the striker bar as it contacts the incident bar while the length of the striker bar governs the pulse's duration. Choosing suitable lengths of the striker bar can generate compressive stress pulses with durations between 100-400 μs. Longer compressive stress pulses with duration of up to 0.5 ms are possible with a larger SHPB system using longer striker bars. A strain gage, mounted on the incident bar measures the complete history of the input loading pulse. A unique aspect of this technique is that a well-defined and controlled loading of a specimen can be achieved by controlling the amplitude and the duration of the input loading pulse. This is similar to a "quick-stop" technique so that a controlled amount of damage can be induced for further microstructural characterization. Moreover, the loading and unloading rates of the input pulse can be customized through insertion of a work hardening material e.g., Cu or Al, between the striker and the incident bar (Nemat-Nasser et al 1991, Subhash and Nemat-Nasser 1993). Such customization capabilities facilitate initiation and propagation of microcracks to desired stages, while preventing their coalescence and subsequent macro-scale failure. This then allows the specimen to be investigated for further microstructural observations of induced crack morphology.

By properly adjusting the incident wave amplitude, one can induce controlled amount of damage and then study, after the impact, the amount of damage and the damage initiation and propagation characteristics. The damage also can be quantified by using ultrasonic measurements techniques. The input amplitude can also be adjusted to cause complete fracture of the specimen to obtain fracture strength at a specific strain rate. Since the specimen is subjected to a single pulse in MSHPB, the signals not only reveal the fracture strength of the specimen, but also allow for comparison of fracture characteristics to the energy absorbed in the fracture process. The above technique can also be used to conduct indirect tension tests (split tensile) on short cylindrical specimens. By conducting tests at a range of strain rates, one can also obtain the variation of failure strengths with strain rate, which will be used for damage quantification as a function of rate. An additional possibility is that specimens may also be tested in various environmental conditions, e.g., moisture, temperature or in triaxial confinement.

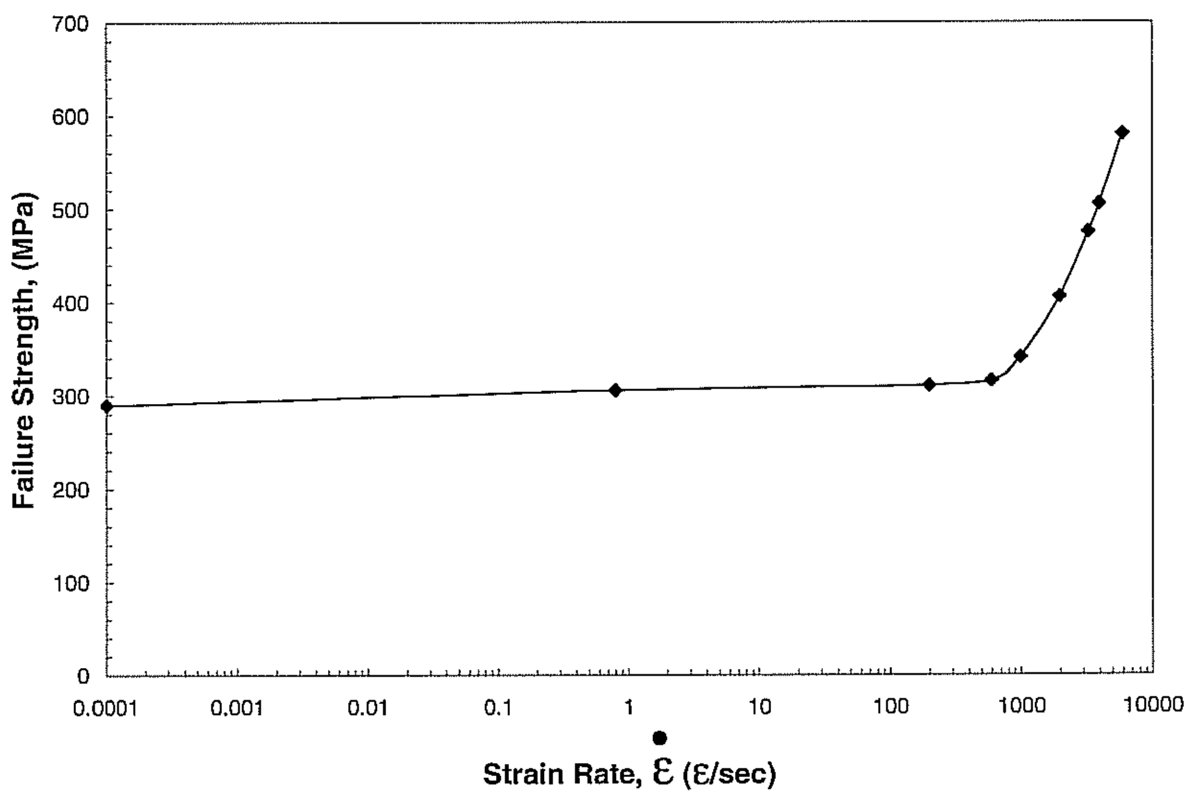

Figure 1.1 Compressive strength versus strain rate for limestone (after Lankford, 1983).

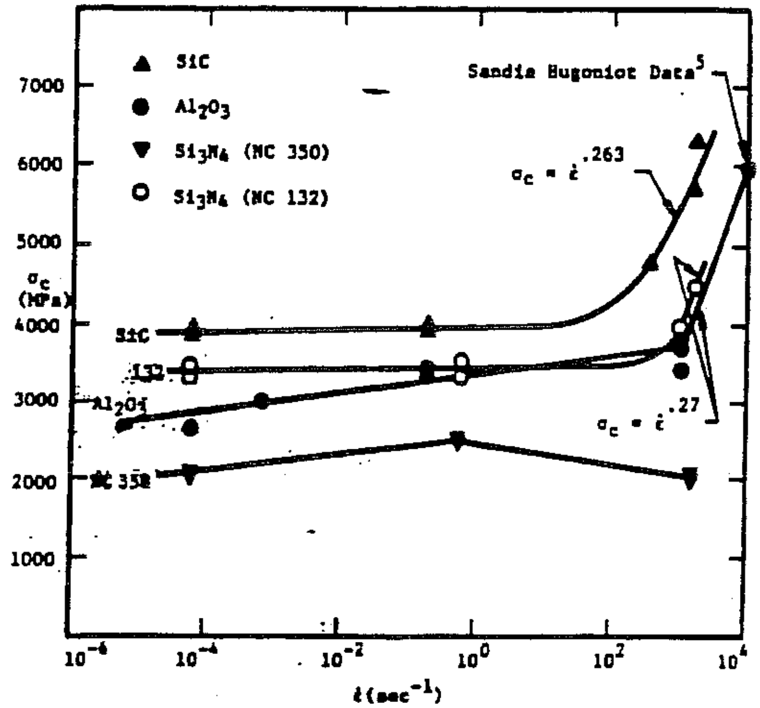

Figure 1.2 Compressive strength of various ceramic materials versus strain rate (from Lankford, 1983).

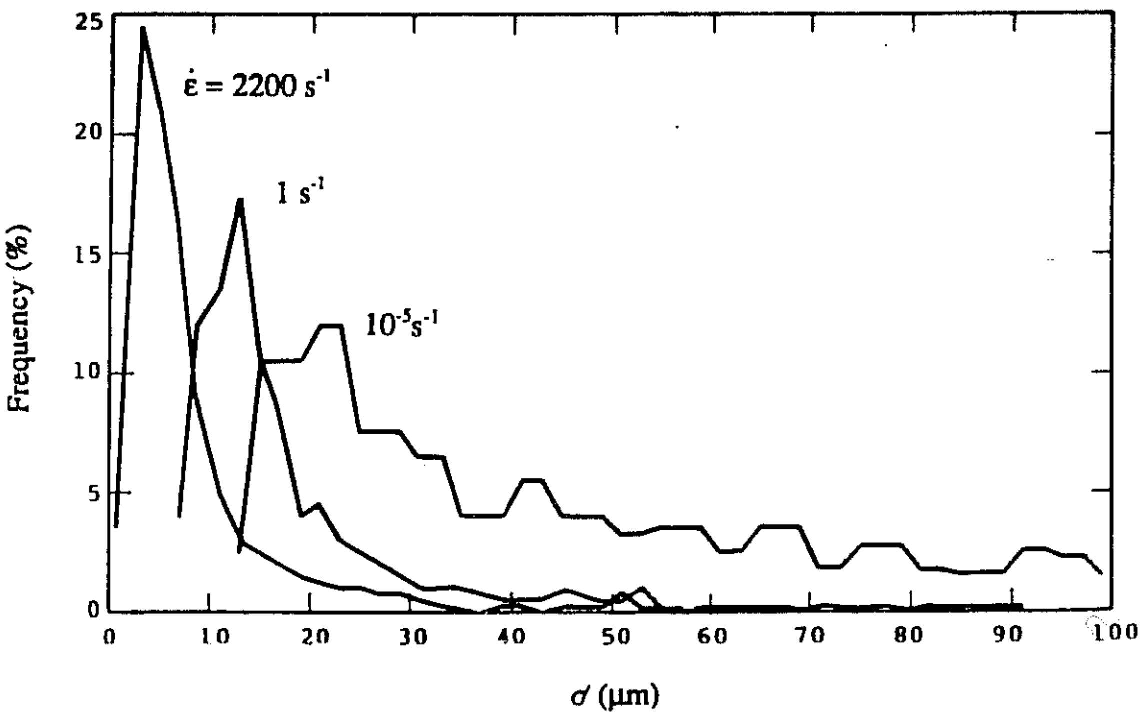

Figure 1.3. Affect of fragment size versus strain rate (From Lankford and Blanchard, 1991)

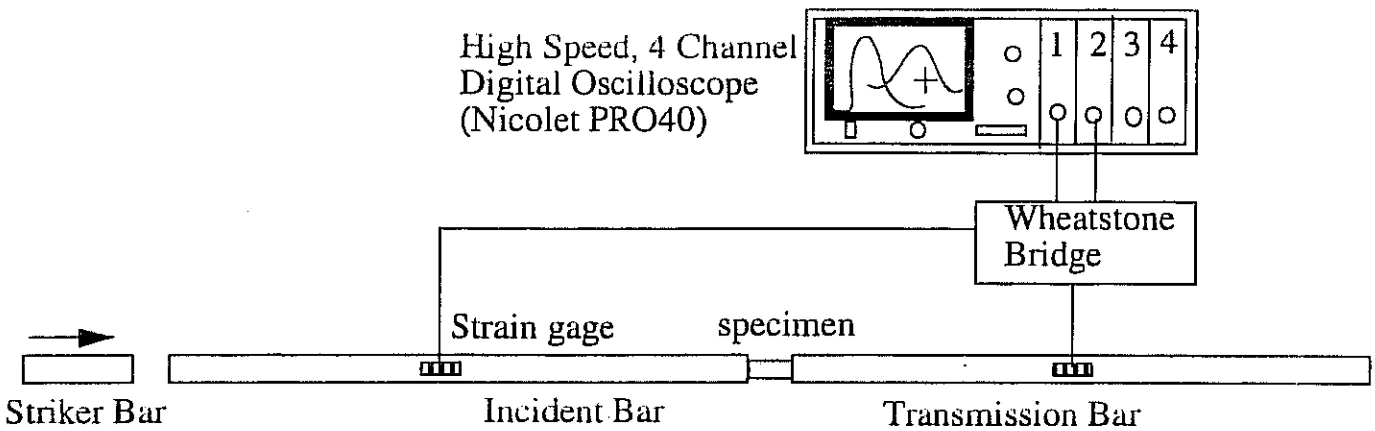

Figure 1.4 Split Hopkinson pressure bar.

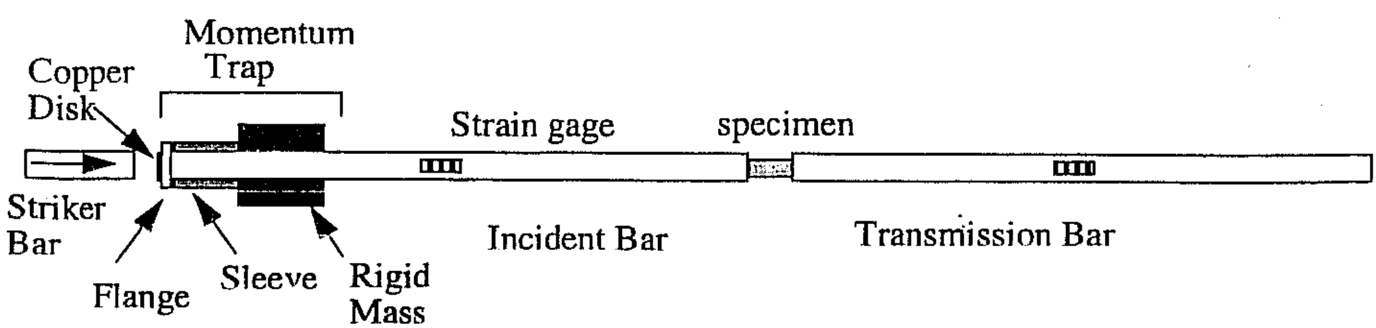

Figure 1.5 Modified Split Hopkinson pressure bar with momentum trap.

1.2 Background

1.2.1 Geological Materials

While the study of rate effects in ductile metals occurred in the late 1940s' and 1950s', the study of rate effects in geologic materials was not investigated until the 1960s' when Kumar (1968) studied the effects of both strain rate and temperature on the strength of basalt and granite. It was found that increased strain (and stress) rates increased the strength and stiffness of rock, as did decreasing temperature. Mellor (1971) conducted an extensive study into the effects of temperature on the strength and deformability on a wide range of igneous and sedimentary rocks and found that decreasing temperature caused an increase in both strength and stiffness of the rocks tested. Although the rate of increase varied for different rock types, all of the research indicates a marked increase in strength and deformation characteristics with decreasing temperature and increasing strain rate of loading.

The effects of temperature on the strength and fracture characteristics of rock were also investigated in the 1970s' as a result of a dramatic decrease in the grinding efficiency at iron ore mines located in northern climates during winter months by Vitton (1977) and later by Kawatra and Eisele (1989). Vitton investigated the effects of cold temperatures on the strength of various iron ore types as well as granite, sandstone and shale in both dry and saturated conditions. He found that cold temperatures increased the strength of the sandstone and granite tested, but not for all of the iron ore types tested or for the saturated shale samples. Vitton attributed the lack of increase in strength of some of the iron ore types to the lack of pore structure or the lack of softer mineral inclusion that can blunt the propagation of microcracks. In the case of saturated shale, he cited the inability of the pore water to freeze, which was due to the shale's small pore size, thus preventing a strength increase. Dutta and Kim (1993) investigated the effect of both temperature and strain rate on rocks and found that tensile strength and deformability of rock was significantly more sensitive to increasing loading rate than to decreasing temperature.

In the 1970s' and 1980s', with the introduction of the Split Hopkinson Pressure Bar for testing brittle materials, significant research was conducted at high strain rates for both rock and ceramic materials by Janach (1976), Grady (1982), Grady and Kipp (1980), Lankford (1981) and others.

1.2.2 Concrete

The U.S. Corps of Engineers conducted research on concrete for military applications, which included the effect of strain rate on concrete from impact loading (Mellinger and Birkimer, 1966). Later, Oh (1987), as well as others, investigated the strain rate effect on concrete using a SHPB. The most extensive study on the rate effect on concrete, however, was conducted under a research program sponsored by the U.S. Air Force and reported in a series of four papers (Ross et al., 1989, Ross et al., 1995, Ross, et al., 1996, and Malvar and Ross, 1998). In this research the dynamic strength data results are presented as a ratio of dynamic strength to static strength and plotted as a function of strain rate. The strain rate in the quasi-static range (standard compression testing range) was 10^{-7} to 10^{-5}/sec, while the dynamic strain rates went as high as 1000/sec (10^{3}/sec). Since the strain rate is plotted on a log (10) basis in these results, the abscissa (x-axis) values for 10^{-7}/sec for example would be plotted as a –7 and 10^{3}/sec would be plotted as a 3. As a comparison the strain rate loading used in this research testing was approximately 10^{-5}/sec for static loading and 10 to 100/sec (10^{1} to 10^{2}/sec) for the dynamic loading, which would be plotted on the abscissa as –5 and 1 to 2, respectively.

Ross et al. (1989) investigated the dynamic and quasi-static strength of mortar and concrete using a two-inch diameter SHPB. A series of tests were conducted on mortar and concrete in compression, direct tension and split tensile (indirect tension) testing. In the SHPB the indirect tension test is conducted by placing the cylindrical side of the mortar or concrete specimen directly between the loading bars, thus placing a line load diametrically opposed to each other. As a load is applied the specimen is forced to split apart in tension. While this test is an indirect measure of a materials tensile strength, it has become the standard test for tension in both concrete and rock testing at least for static testing conditions. The results of the tensile testing on mortar are shown in Figure 1.6. Ross et al. found that the dynamic tensile strength of mortar, at strain rates of 1/sec to 100/sec, is approximately 1.5 to 3 times that of the tensile strength at quasi-static strain rates. In addition, they found that there is close agreement in the test results between the direct and the indirect tension testing of mortar, which can be seen in Figure 1.6. Since indirect tension testing is significantly easier to conduct than direct tension, this is an important finding. In effect, since the indirect tension testing uses cylindrical specimen both tensile and compressive strength can be determined from cylindrical specimens, which can more easily be prepared in a laboratory. Interestingly, Ross et al. only presented the uniaxial compression results for mortar (in Figure 11 in Ross et al., 1989) but did not provide any discussion or evaluation of the results. However, from Figure 11 the unaixial compression tests for mortar show a dynamic/static ratio of 1.1 to 2.0 in the strain rate range of 1 to 300/sec.

Ross et al., (1995) conducting tests on the dynamic tensile and compressive strength of concrete (tested at similar strain rates) found that concrete is significantly more rate sensitive in tension than in compression. This can be seen in Figure 1.7 (from Ross et al., 1995) where, above a strain rate of 1/sec, the increase in dynamic strength over the static strength increases dramatically in tension, but not as much for compression. For example, at a strain rate of 100/sec (2 on Figure 1.7) the ratio of dynamic to static strength ratio is 8 for tension, but approximately only 1.2 to 1.8 for compression. However, it should be noted that the majority of the test results presented by Ross et al., are below a ratio of 4 and only a few data points, which were taken from other researchers, have higher ratio values (6 to 8) in the strain rate range of 10 to 100/sec.

Ross et al., (1996) also studied the effect of moisture and strain rate on concrete strength, i.e., they studied at what critical strain rate the strength and stiffness of concrete start increasing as the strain rate is increased. The main finding of this investigation was that for concrete the critical strain rate occurs at a lower strain rate for tension than for compression. This can be seen in Figure 1.8 for tension and Figure 1.9 for compression. It can also be seen in Figures 1.8 and 1.9 that the ratio of dynamic to static strength is significantly higher in tension than compression. The critical strain rate range for concrete begins between 1 and 10/sec and 60/sec for tension and at a higher strain rate of 60 to 80/sec for compression. The effect of moisture was also investigated in this study where they found that moisture increases the rate sensitivity of concrete. However, no percent of increase was provided.

Malvar and Ross (1998) conducted a literature review to characterize the available stain rate data that exists for concrete in tension and compression. The data was presented as a dynamic increase factor (DIF) versus strain rate, where DIF is the ratio of dynamic strength to static strength. From this data it was observed that the strain rate data fits more of a bilinear model than a gradual increase model. This indicates, unlike the initial research, that there is a gradual increase in the DIF for strain rates up to a point and then more of a rapid increase. The data also indicates that there is no increase in strain rate below 10^{-6}/sec.

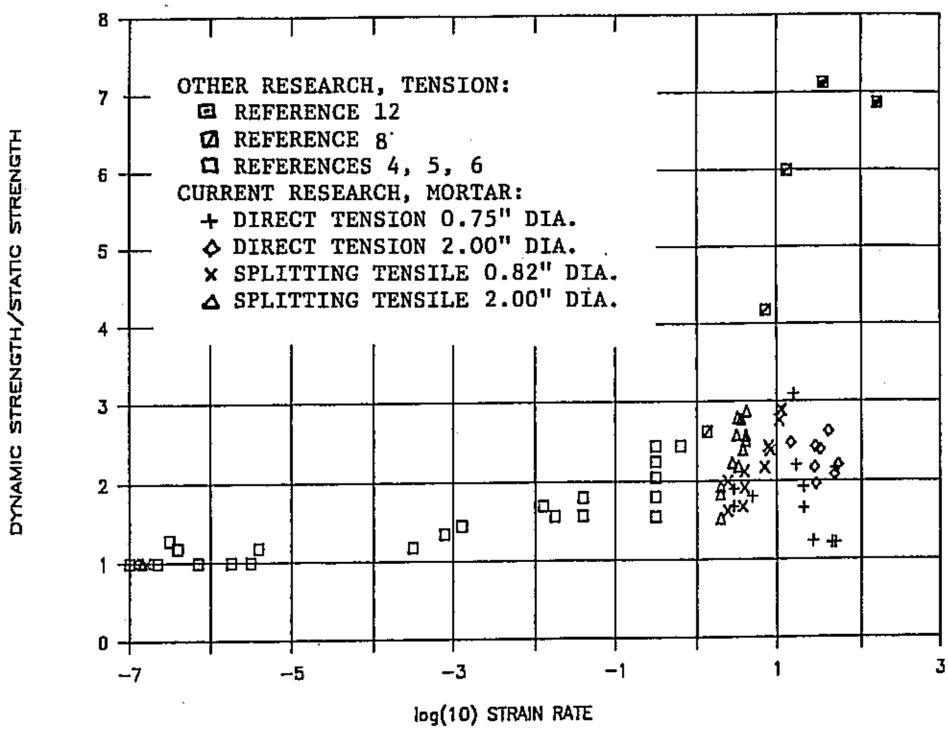

Figure 1.6. Tensile strength ratios of mortar versus $\log_{10}$ (from Ross et al., 1989).

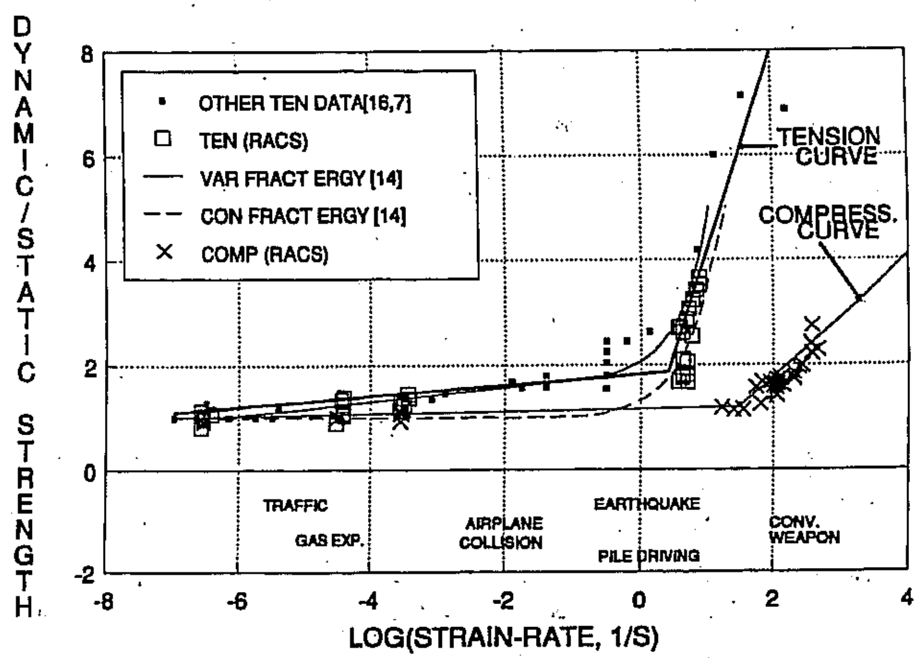

Figure 1.7 Ratio of concrete dynamic to static strength as a function of strain rate, based on a log 10, (from Ross et al., 1995).

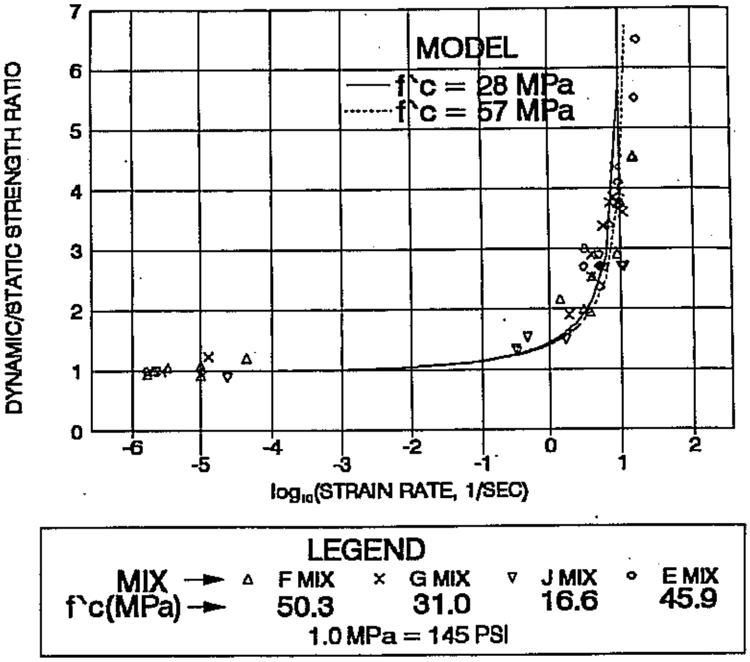

Figure 1.8 Ratio of dry concrete tensile strength to static strength as a function of strain rate log 10 (from Ross et al., 1996)

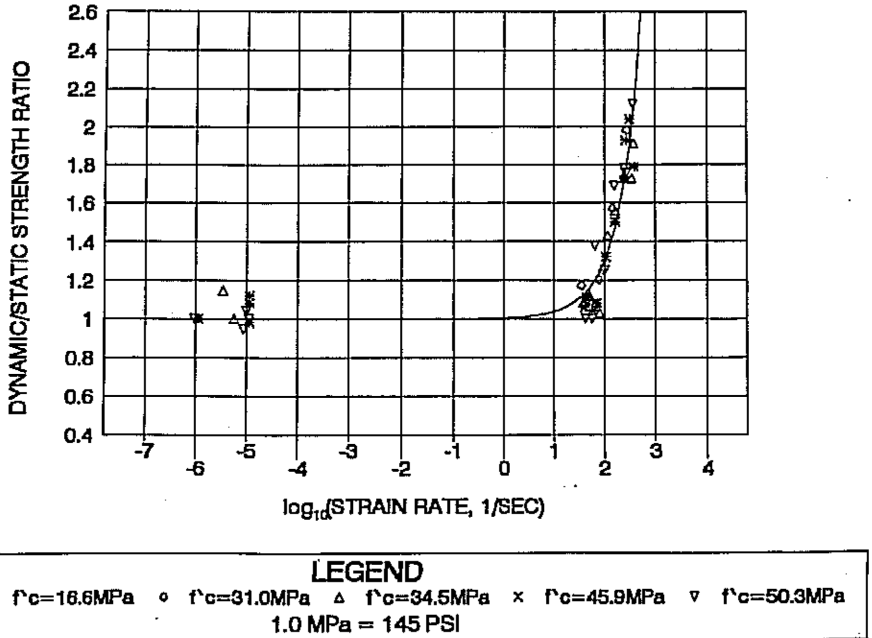

Figure 1.9 Ratio of dry concrete compressive strength to static strength as a function of strain rate log 10 (from Ross et al., 1996)

2 Specimen Preparation

2.1 Aggregate

All of the natural aggregate speciemens were obtained from active quarries, while the blast furnace slag specimens were obtained directly from steel production plants. A number of blocks were obtained from each source weighting between 20 to 100 pounds. The blocks were cored with a SE2025 Solberga direct drive drill and a 3/8 inch ID diamond tip core bit using water as coolant. Initially some basalt specimens were cored with a lightweight (#10) cutting oil as a coolant. The 3/8 inch diameter core was selected, since this dimension falls within the range of coarse aggregate used in PCC as well as the size of the half-inch dynamic uniaxial compression testing equipment, which has a maximum testing size of 0.5 inches. After coring, the specimens were cut to a 2:1 length to diameter ratio using a ISOMET 1000 precision saw. Samples were tested for end parallelism, which must be within 0.001 inch according to ASTM's procedures for compression testing. For aggregates that showed distinct bedding planes, specimens were cored both parallel and perpendicular to the bedding in order to investigate the strength variations that might result from the texture present in the rocks. Specimens were also extracted from a range of blocks and locations to represent the statistical variations typically present in geological materials. A minimum ten specimens were prepared for each test condition, e.g., dynamic, static, dry and saturated.

2.2 Mortar

In addition to the dynamic and static testing of aggregate, mortar was also prepared and tested. Two batches of mortar were mixed and formed into beams using fabricated metal forms. The beams were extracted from the metal forms and placed in the MTU curing room for moisture control. The initial mortar mix was prepared at an air content of 5%. However, discussions with MDOT personnel indicated that this air content was too low giving the mortar an unrealistically high strength. Consequently, an additional batch of mortar was mixed into beams with a target air content of 9 to 10%. The mix proportioning worksheet, batch computations and yield data for the mortar are provided in Appendix A of this section.

The mortar was also cored using the SE2025 Solberga direct drive drill with a 3/8 inch ID diamond tip core bit using water as coolant. Approximately ten specimens were tested each week for 18 weeks. All of the specimens were cored from the two mortar beams prior to the first week of testing. After coring, the samples were cut to a 2:1 length to diameter ratio using the ISOMET 1000 precision saw. Samples were tested for end parallelism, which had to be within 0.001 inches, using a digital micrometer. Also, there was some concern as to the possibility of unequal curing of the mortar beam, i.e., the surfaces of the mortar beam may have cured differently than in the center of the beam. To avoid possible variations in the mortar properties, all of the cored samples were placed in a container and randomly mixed prior to being separated and placed into plastic bags. It was hoped that this would provide a more statistical representation of the entire mortar beam. Water was added to the plastic bags to assist in the curing process.

2.3 Portland Cement Concrete (PCC)

2.3.1 Indirect Tension and Uniaxial Compressive Strength PCC Specimens

Two batches of PCC were prepared for a given coarse aggregate type. The first set was prepared for the static and dynamic indirect tension and compressive strength testing while the second set was prepared for the aggregate interlock testing. For the compressive strength testing the following five coarse aggregate types were selected:

Bruce Mines Diabase	95-010
Port Inland #1, Limestone	75-005
Presque Isle Stone, Limestone	71-047
Superior Sand & Gravel	31-045
Levy Steel Dix #1, Slag	82-019

An important aspect of the PCC was that it be consistent between batches and that the only variable be the coarse aggregate type. The mixing procedures used to produce the PCC for the strength testing followed the procedures outlined in Section Four. The fine aggregate used in the PCC was from Superior Sand and Gravel of Hancock, MI, the same fine aggregate that was used in Section Four. In addition, the same cement and air entrainer was used as in Section Four.

The specimen test size for the static and dynamic strength testing was three-inch diameter by six-inch long specimens. In addition, three six-inch by twelve-inch cylinders from each batch were also cast for 28-day strength testing. While plastic forms were available for casting the three-inch by six-inch specimens, it was thought that the coarse aggregate arrangement within the PCC could be affected by the side constraint of the plastic molds and that variations in the test results may result. Consequently, it was decided to cast the PCC into beams and to core the beams with a diamond core bit, creating the three-inch by six-inch specimens. Special metal forms were, therefore, fabricated for casting the PCC beams. The metal forms were designed such that ten specimens could be cored from each PCC beam. The depth of the beam was seven inches so that a six-inch length specimen could be cut from the cored sample. Each PCC batch produced two PCC beams. The beams were cored using a portable electric Milwaukee heavy-duty Model 4004 Dymodrill drill with a three-inch diamond core barrel. The cored specimens were cut on a diamond cut-off saw to a six-inch length for a 2:1 length-to-diameter ratio for compression testing and 1:1 for indirect tension testing. Water was used as the coolant during the coring and cutting operations. After cutting, the specimen's ends were surface ground to a parallelism of 0.001 inch, which is required under ASTM for uniaxial testing, using a Reid Model 618 PF surface grinder shown in Figure 2.1. A dilute water solution with water solvable oil was used to cool the specimens during the grinding operation. A special jig was design and machined to hold the concrete specimens during the grinding process. In general, the grinding operation took approximately ten to fifteen minutes per specimen, with each side of the specimen being surfaced. The grinding wheel was periodically dressed to ensure proper grinding efficiency. Overall, the grinding operation went well, with the exception of a couple of the blast furnace slag PCC specimens in which the specimens failed in shear failure during grinding.

In addition to the three-inch diameter PCC specimens prepared, compression testing was also conducted on two existing PCC pavements, which have been referred to as "aged concrete." One aged pavement had been made with natural sand and gravel coarse aggregate while a second pavement consisted of a blast furnace slag coarse aggregate. These pavements were obtained from MDOT in six-inch diameter cores. Due to the size of the core as well as observable microcracking, only two-inch diameter specimens could be cored. Consequently, a two-inch diameter high precision diamond core barrel was obtained and used to extract the two-inch cores from the six-inch cores.

Tests were conducted in both a moist condition and a dry condition. The moist condition were essentially the moisture condition of the PCC at 30 day, i.e., the moisture added during concrete mixing and the humidity from the curing room, while the dry conditions were obtained by drying the PCC in an oven until there was no moisture loss, i.e., moisture content was zero. A drying temperature of 110° C was used to dry the PCC. In general, the drying time took approximately three days and was determined by periodically taking representative PCC specimens out of the oven and weighting them to determine when moisture loss was complete.

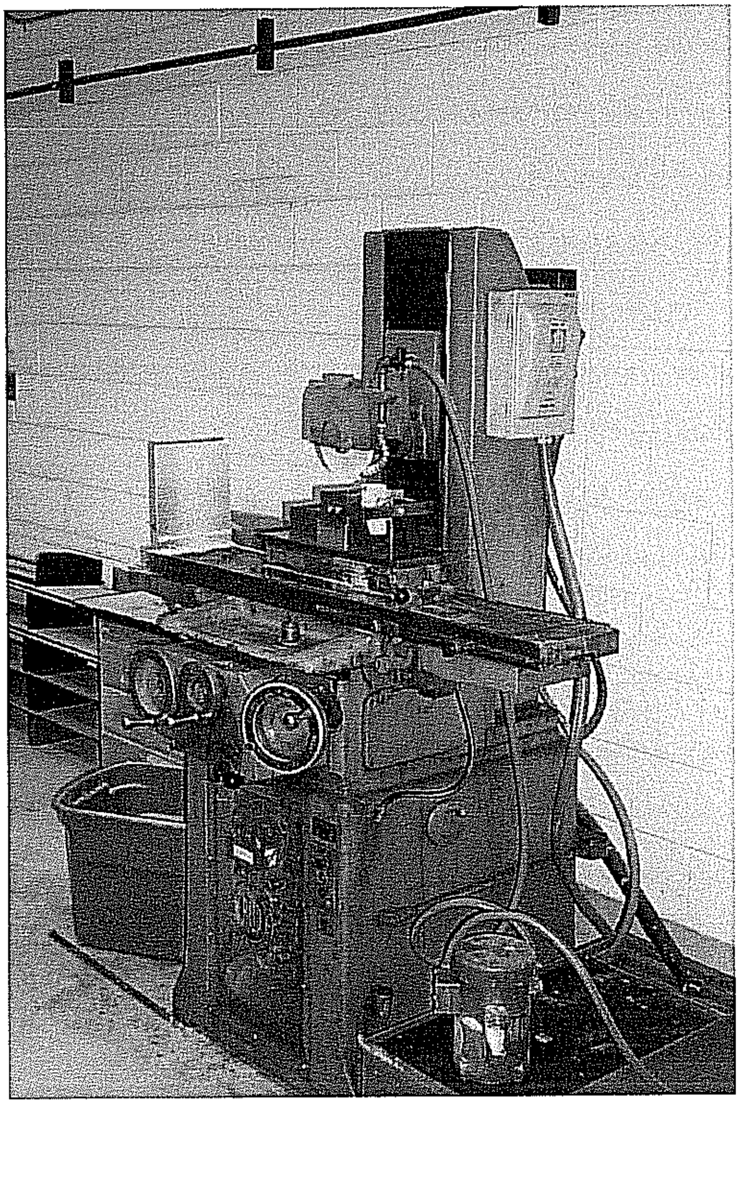

Figure 2.1 Reid surface grinder used for paralleling PCC test specimens.

3 Experimental Procedures

3.1 Aggregate and Mortar

The aggregate specimens were tested in both dry and water saturated conditions. The dry specimens were maintained at room temperature and humidity prior to testing and were not dried in an oven. It was assumed that the moisture content of the specimens would be relatively low and were considered as being "dry." The saturated specimens were submerged in water for approximately 30 days prior to testing. No vacuum saturation was used to saturate any of the test specimens. Although the specimens were described as saturated, it is unlikely that they were at 100% saturation, but were believed to be a relatively close to being saturated.

Approximately one-half of the test specimens were tested at a quasi-static strain rate, while the other half was tested at a high strain rate. The quasi-static tests were conducted on a 5 kip MTS system with a TestStar II digital controller. The 5-kip testing system has a 22 kip rated frame and a three-gallon per minute hydraulic pump supply. The system is located in the Soil Dynamics Laboratory in the Civil & Environmental Engineering Department at Michigan Tech. The system is configured to conduct resilient modulus test with the hydraulic actuator positioned on the top of the system applying vertical loaded downward. The tests were conducted in displacement control and conducted according to ASTM standards for uniaxial compression testing of rock.

The high strain rate tests were conducted using a half-inch diameter modified split Hopkinson pressure bar (MSHPB) located in the Engineering Mechanics and Mechanical Engineering Department at Michigan Tech. A schematic of the half-inch modified Split Hopkinson Pressure Bar and measurement system is shown in Figure 1.12. A Nicolet digital oscilloscope was used to collect and store the dynamic fracture information. To start the testing, the striker bar is placed in the gas gun and pressurized to approximately 30 psi. The specimen is then placed between the incident bar and the transmission with the two bars being butted up against the specimen to hold it in place. After the specimen is in place, a piece of thin copper plate is placed at the end of the incident bar for the striker bar to hit. The purpose of the copper plate is to alter the loading pulse from a square wave to more of a triangular wave. The triangular loading pulse has been found to produce better results on brittle material than the traditional square wave pulse (Subhash and Nemat-Masser, 1993). Once the specimen and copper plate are in place, the trigger system of the oscilloscope is set and the system fired. The initial load pulse travels through the incident bar where it triggers the oscilloscope to start collecting data. The loading pulse then contacts the specimen where energy is released in the fracture process. Part of the energy will travel back into the incident bar, where it is recorded by the strain gages on the bar and part of the energy will travel into the transmission bar where it is also recorded by strain gages. The data are recorded and stored for later analysis. The testing and data reduction and analysis procedures are more fully described in Ravichandran and Subash (1995).

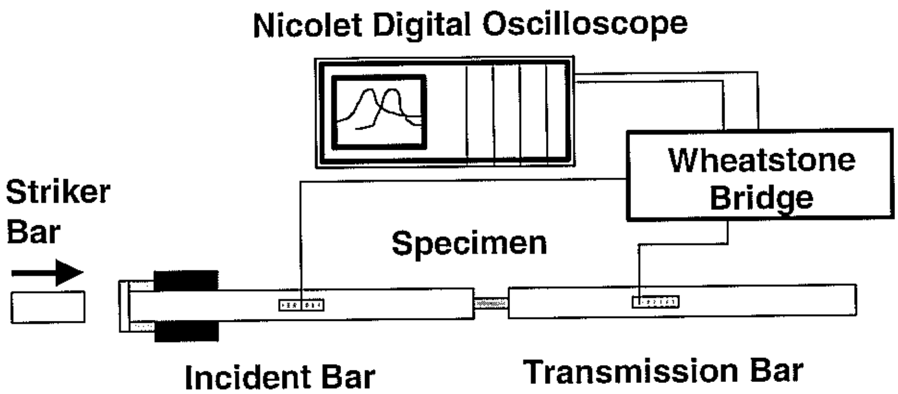

Figure 3.1 Half-inch diameter Split Hopkinson Pressure Bar schematic.

3.2 Portland Cement Concrete

The PCC specimens were tested in both quasi-static and at high strain rates and consisted of both uniaxial compression and indirect tension testing. In addition, PCC specimens were tested in both moist and dry conditions at 30 days instead of 28 to be more consistent with the research conducted at Eglin Air Force Base (Ross et al., 1985, 1995, 1996, and 1998) on the dynamic fracture of concrete. The quasi-static tests were conducted on a 55 kip MTS system with a TestStar II digital controller. The 55-kip testing system has a 55 kip rated frame and a six-gallon per minute hydraulic pump supply. The hydraulic actuator in this system is located on the bottom of the testing system in the traditional configuration with the load being applied upward. The system is located in the Structural Testing Laboratory in the Civil & Environmental Engineering Department at Michigan Tech. Approximately half of the PCC specimens were tested in quasi-static conditions and half at a high strain rate.

The high strain rate tests were conducted using a three-inch diameter Split Hopkinson Pressure Bar (SHPB) located in the Concrete Testing Laboratory at Michigan Tech. The system functions in basically the same way as the half-inch diameter system but has not been modified for single load testing, which is not required for measuring the dynamic strength of materials. A modified system would be needed when investigating the microfracture of brittle materials. A Nicolet digital oscilloscope is used to collect the data during testing in the same fashion as in the half-inch MSHPB. The SHPB system is shown in Figure 3.2 and the instrumentation in Figure 3.3. The uniaxial compression tests were conducted using the same procedures as with the half-inch MSHPB. However, the indirection tension tests used fabricated platens to apply the line load to the specimen. Figure 3.4 illustrates the set up of the indirect tension platens.

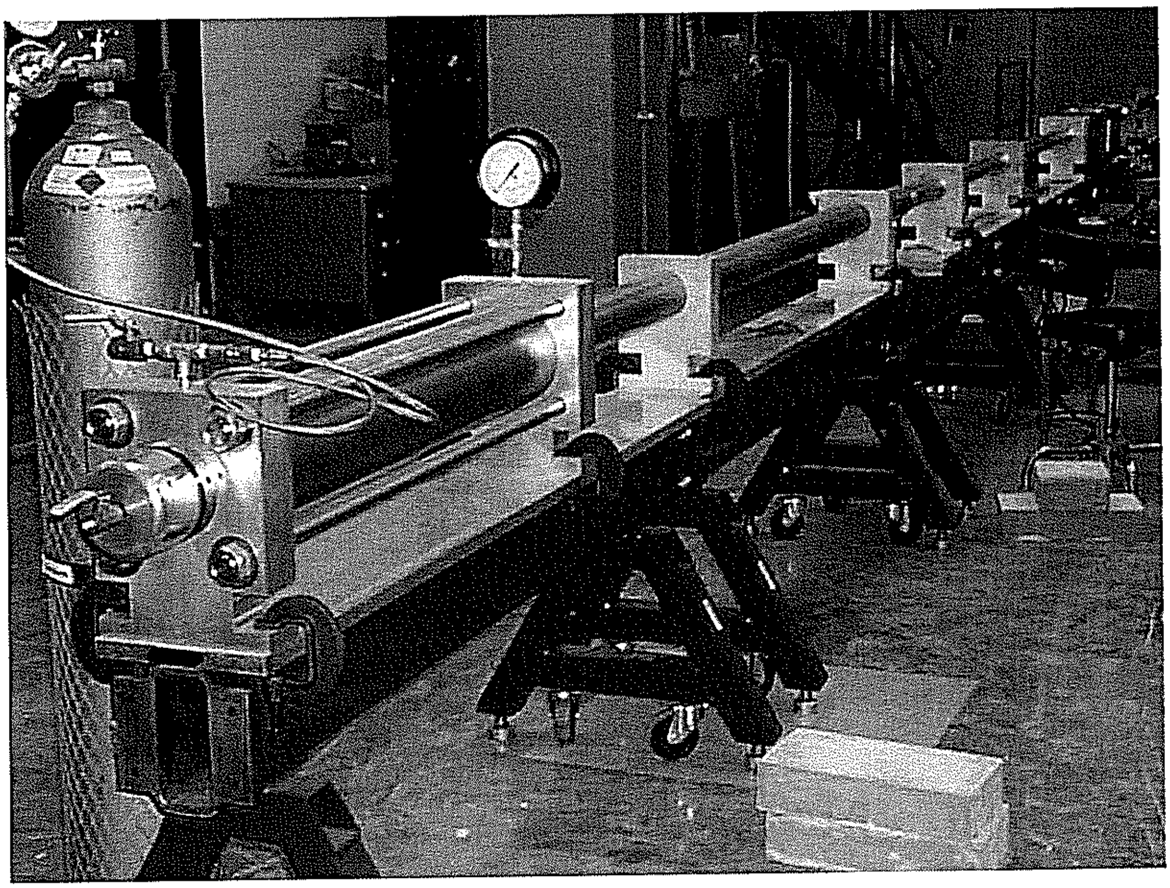

Figure 3.2 Three inch Split Hopkinson Pressure Bar.

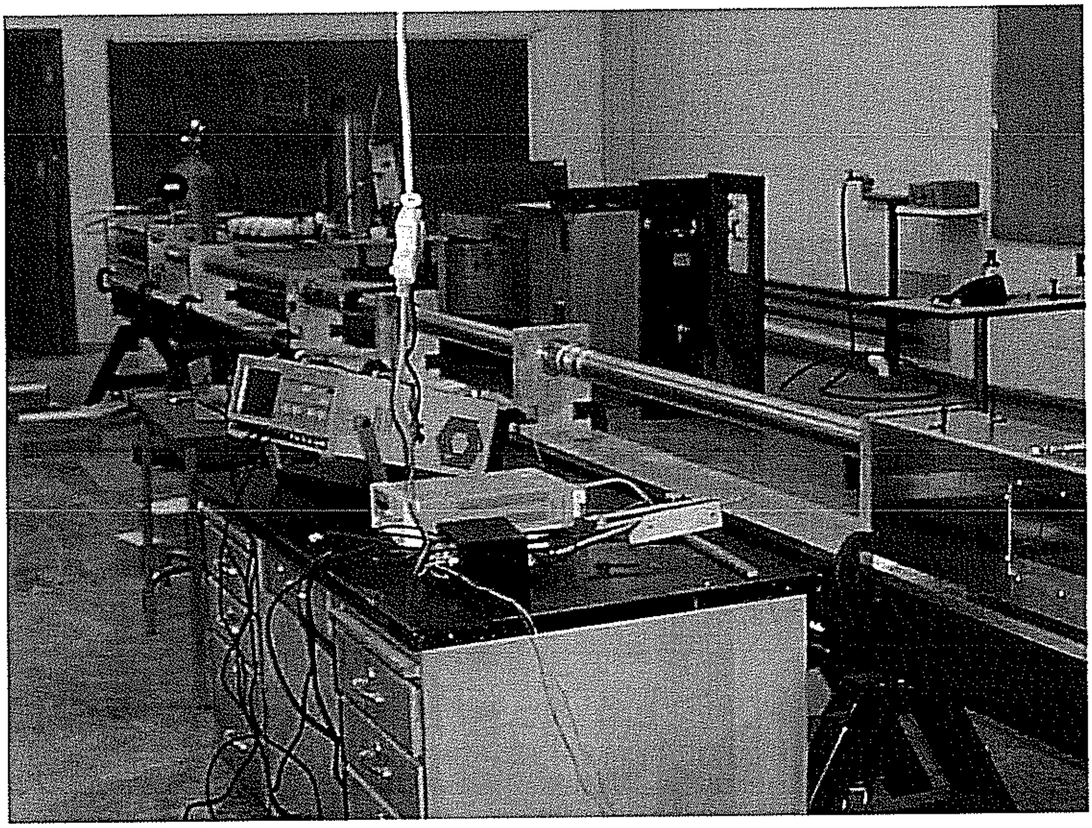

Figure 3.3 SHPB measurement equipment.

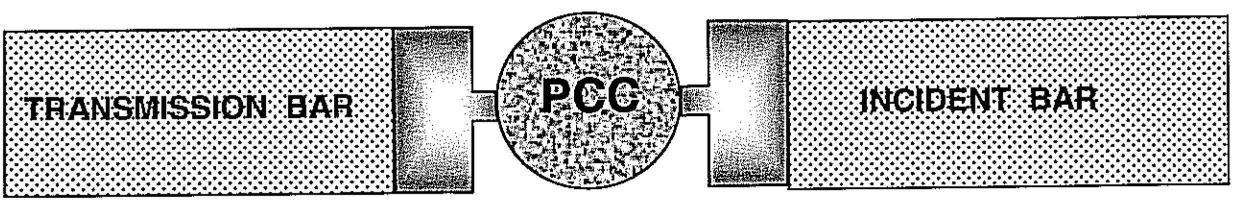

Figure 3.4 Indirect test platens for the SHPB.

4 Experimental Results

4.1 Aggregates

Uniaxial compression tests were conducted at both a quasi-static strain rate of approximately 10^{-6}/sec (following ASTM standards) and at a high strain rate near 10^{2}/sec for each aggregate type. Approximately eight to ten specimens were tested for each test condition, i.e., quasi-static, dynamic, dry, and saturated. Table 4.1 summarizes the compressive strength data for all the aggregates in dry and saturated conditions. The raw data for the static and dynamic uniaxial fracture strength in dry and saturated conditions, respectively, is presented in Figures 4.1(a) and 4.1(b). However, for ease of comprehension, the same data are presented in terms of mean and standard deviation in Figs. 4.2(a) and 4.2(b). It is clear from the plots that the dynamic fracture strength of aggregates is consistently greater than the static strength in both dry and saturated conditions. In general, the slag aggregates exhibited the lowest compressive strength, followed by the carbonates (limestone and dolomite families) with an intermediate strength. The mafic igneous aggregates (Bruce Mines and Moyle) exhibited the highest compressive fracture strength. The air-cooled slag consists of two distinct structures: one extremely porous region and the other a dense structure with considerably lower porosity. The denser structure (slag specimen 1.2) exhibited strength comparable to that of carbonates. It is interesting to note that there is no significant difference in the uniaxial compression strength of limestones and dolomites when the specimens were cored either parallel or perpendicular to the bedding (see specimen nos. 5, 8 and 10). The minor differences may be due to the limited number of specimens tested, since the data also falls within the statistical variations of the carbonate.

The above data is replotted in Figures 4.3(a) and 4.3(b), so as to compare the static and dynamic strengths separately in dry and saturated conditions, respectively. The plots clearly reveal that no significant strength variations occur under saturated conditions compared to the dry conditions. However, in the case of the mafic igneous aggregates, slightly higher compressive strength was noticed in dry condition than in the saturated condition in static loading. A plot of aggregate density versus the mean uniaxial compressive strength is shown in

Figures 4.4(a) and 4.4(b) for dry and saturated aggregates, respectively. In these plots, the data for specimens cored parallel and perpendicular to the bedding are combined since there is no significant variation in uniaxial strength as discussed before. Both static and dynamic values are plotted on the same graph. Although there is considerable scatter in the experimental data, it can be seen that, in general, the compressive strength increases with density and the dynamic strength data shows a steeper slope compared to the static data.

Figures 4.5(a) and 4.5(b) illustrate the axial stress-strain curves obtained from the strain gage measurements under static and dynamic loads for all the aggregates except slag. Almost all the rocks exhibit initially a linear elastic response followed by a non-linear response just before failure. The inelastic response is more pronounced in stiffer (higher strength) rocks under dynamic loads than static loads. The inelastic strain is a representation of the strain associated with the onset of microcracks, their growth and coalescence leading to eventual failure of the specimen. From these experiments, one can more accurately estimate the strain rate during a test, which will be discussed later in Chapter Five of this section.

4.2 Cement Matrix

Ten mortar specimens were tested approximately each week for 18 weeks at seven-day intervals, i.e., the first set of tests were conducted seven days after PCC mixing. The dynamic strength tests were conducted on the half-inch MSHPB while the static tests were conducted on the 5 kip closed loop servo-hydraulic MTS system. All of the static tests were conducted in displacement control. As reported previously the mortar air content was approximately 9%. The results of the combined mortar testing are shown in Figure 4.6 in a raw date from while the statistical analysis showing the mean and standard deviation of the data is shown in Figure 4.7.

4.3 Portland Cement Concrete

Approximately forty PCC specimens were prepared from each aggregate type PCC while twenty were prepared for the aged concrete. Ten specimens were tested under indirect tension and uniaxial compression loading in each condition, i.e., static, dynamic, moist and dry. The raw data indirect tension results are shown in Figure 4.8 for the 30 day concrete while the statistical analysis of the data providing the mean and standard deviation are presented in Figure 4.9. Figure 4.10 provided the raw data for uniaxial compression results for the 30-day PCC, while Figure 4.11 presents the mean and standard deviation for the test data. In addition, aged concrete was also tested in uniaxial compression from cores extracted from highway pavement. The highway pavements consisted of two different coarse aggregates, a natural aggregate PCC and a blast furnace slag PCC. The aged concrete cores were only tested in a dry condition. The mean and standard deviation of the test data are plotted in reference to the 30-day PCC results in Figure 4.12.

Table 4.1 Compressive strength data for all the aggregates in dry and saturated conditions.

			Compressive Fracture Strength (MPa)			
ID No. Pit ID	Aggregate/ (Quarry)	Orientation and Batch	Static Dry	Static Saturated	Dynamic Dry	Dynamic Saturated
1 95-006	AC Slag (Algoma)	Batch 1 Batch 1.2	12.1 ± 4.1 97.6 ± 34.1	16.3 ± 5.0	33.2 ± 10.1 163.1 ± 32.8	39.5 ± 5.3
2 95-006	WC Slag (Algoma)	Batch 2.0 Batch 2.1	22.8 ± 6.7	19.1 ± 8.6 10.0 ± 3.9	43.4 ± 26.4	52.6 ± 11.1 34.9 ± 33.6
3 82-019	WC Slag (Levy)	Random	21.1 ± 8.4	33.5 ± 11.3	30.0 ± 10.2	68.7 ± 19.6
4 71-047	Limestone (Presque Is.)	Random	77.7 ± 17.1	43.9 ± 17.0	147.5 ± 37.5	117.0 ± 38.9
5 06-008	Limestone (Bay Co.)	Normal Parallel	91.6 ± 37.3 65.4 ± 21.5	94.1 ± 31.8 73.4 ± 24.3	186.8 ± 24.2 165.9 ± 37.3	177.3 ± 40.2 168.5 ± 33.7
6 75-005	Limestone (Port In.)	Random	103.6 ± 31.8	107.9 ± 16.2	282.2 ± 43.2	221.3 ± 4.2
7 49-065	Dolomite (Cedarville)	Random	85.2 ± 43.9	86.8 ± 34.6	157.1 ± 27.8	186.8 ± 22.5
8 58-009	Dolomite (Denniston)	Normal Parallel	92.8 ± 29.2 76.6 ± 29.1	90.0 ± 59.8 75.0 ± 27.6	154.2 ± 22.2 149.1 ± 22.3	139.2 ± 57.0 153.5 ± 82.4
9 58-008	Dolomite (Rockwood)	Normal Parallel	124.4 ± 22.1	99.9 ± 33.3 74.6 ± 39.6	156.0 ± 37.9	181.5 ± 31.9 150.3 ± 33.1
10 93-003	Dolomite (France St.)	Normal Parallel	131.2 ± 27.8 134.9 ± 30.5	 148.3 ± 43.2	206.8 ± 46.5 212.9 ± 25.2	 211.1 ± 69.8
11 31-076	Basalt (Moyle)	Random	183.6 ± 23.6	121.3 ± 34.7	371.9 ± 35.5	352.8 ± 53.1
12 95-010	Diabase (Ontario Traprock)	Water Cut Oil Cut	270.5 ± 59.1 226.8 ± 46.2	203.9 ± 106.8	489.5 ± 57.9 342.8 ± 65.9	445.3 ± 99.5

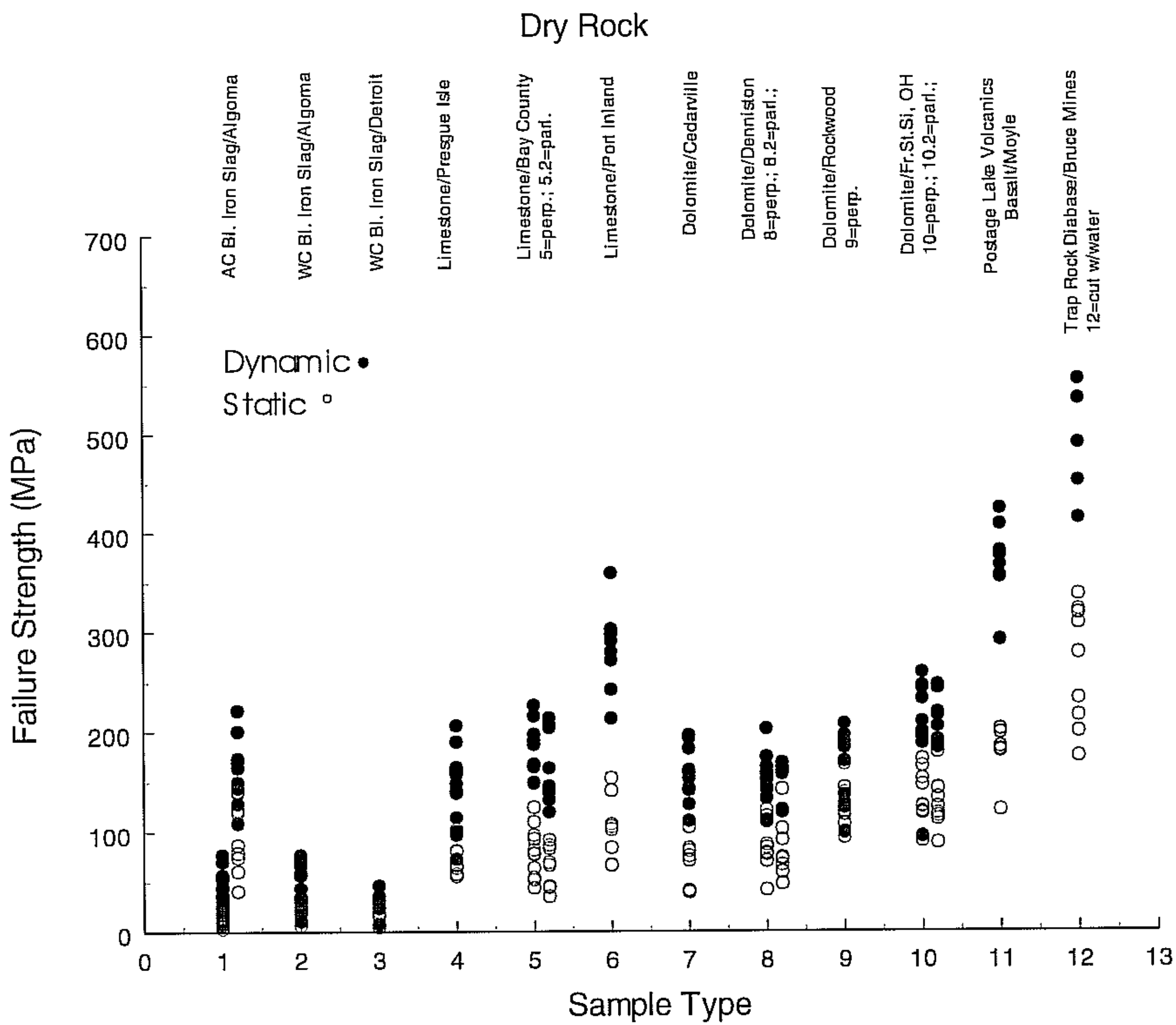

Figure 4.1(a) Raw data for static and dynamic compressive strengths for dry aggregate results.

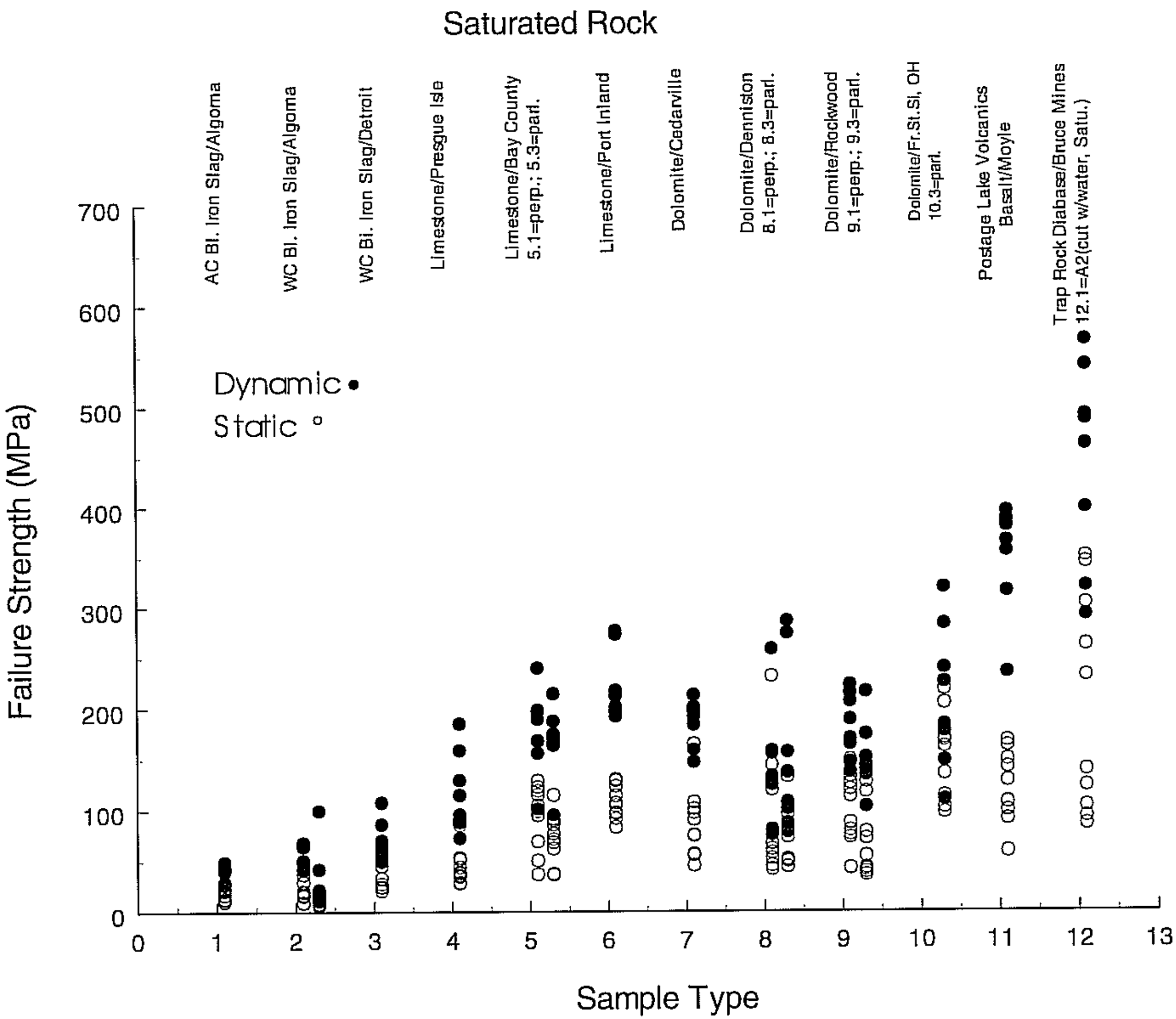

Figure 4.1(b) Raw data for static and dynamic compressive strengths for saturated aggregate results.

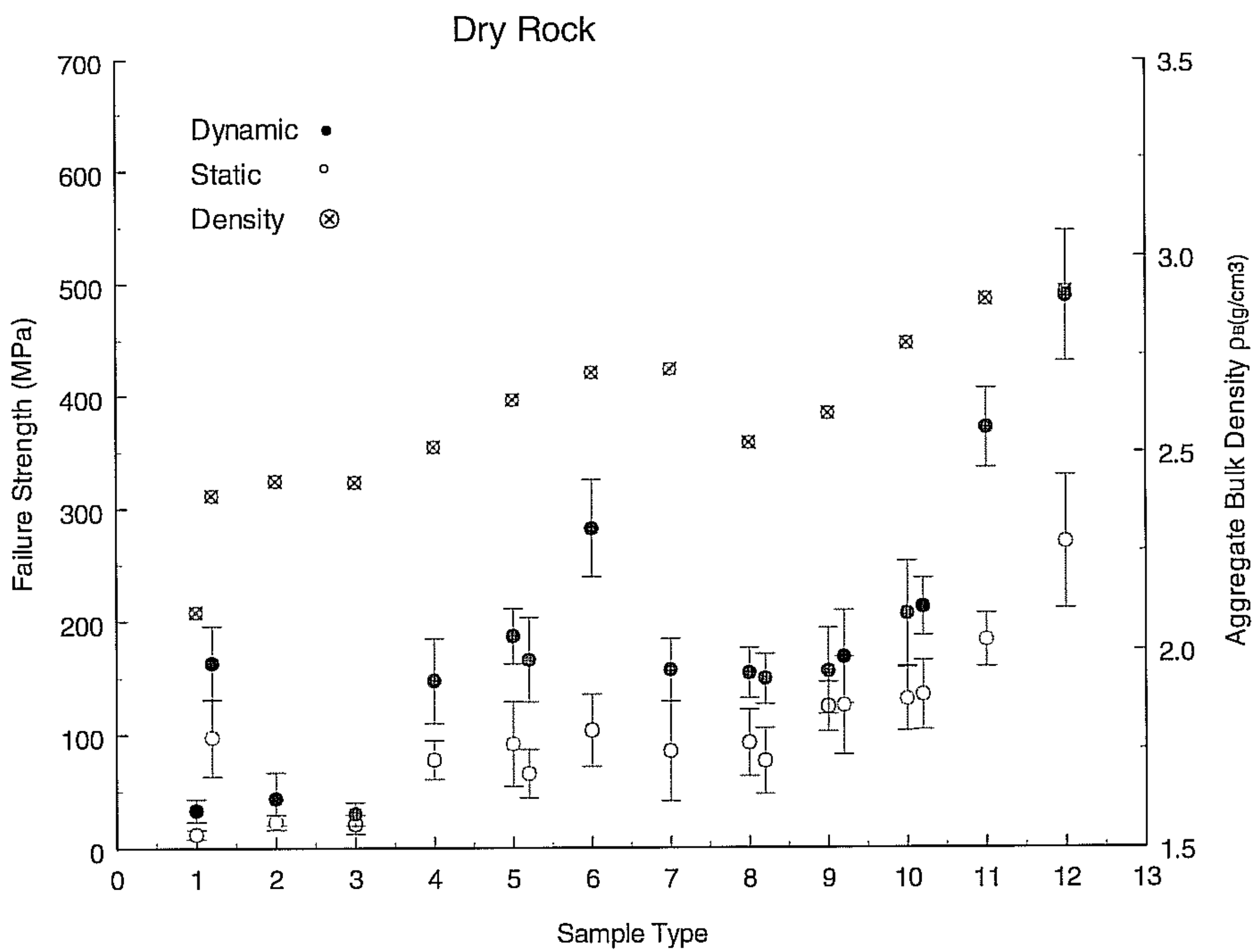

Figure 4.2(a) Statistical analysis showing mean and standard deviation of static and dynamic compressive strength of dry aggregate including aggregate dry bulk density.

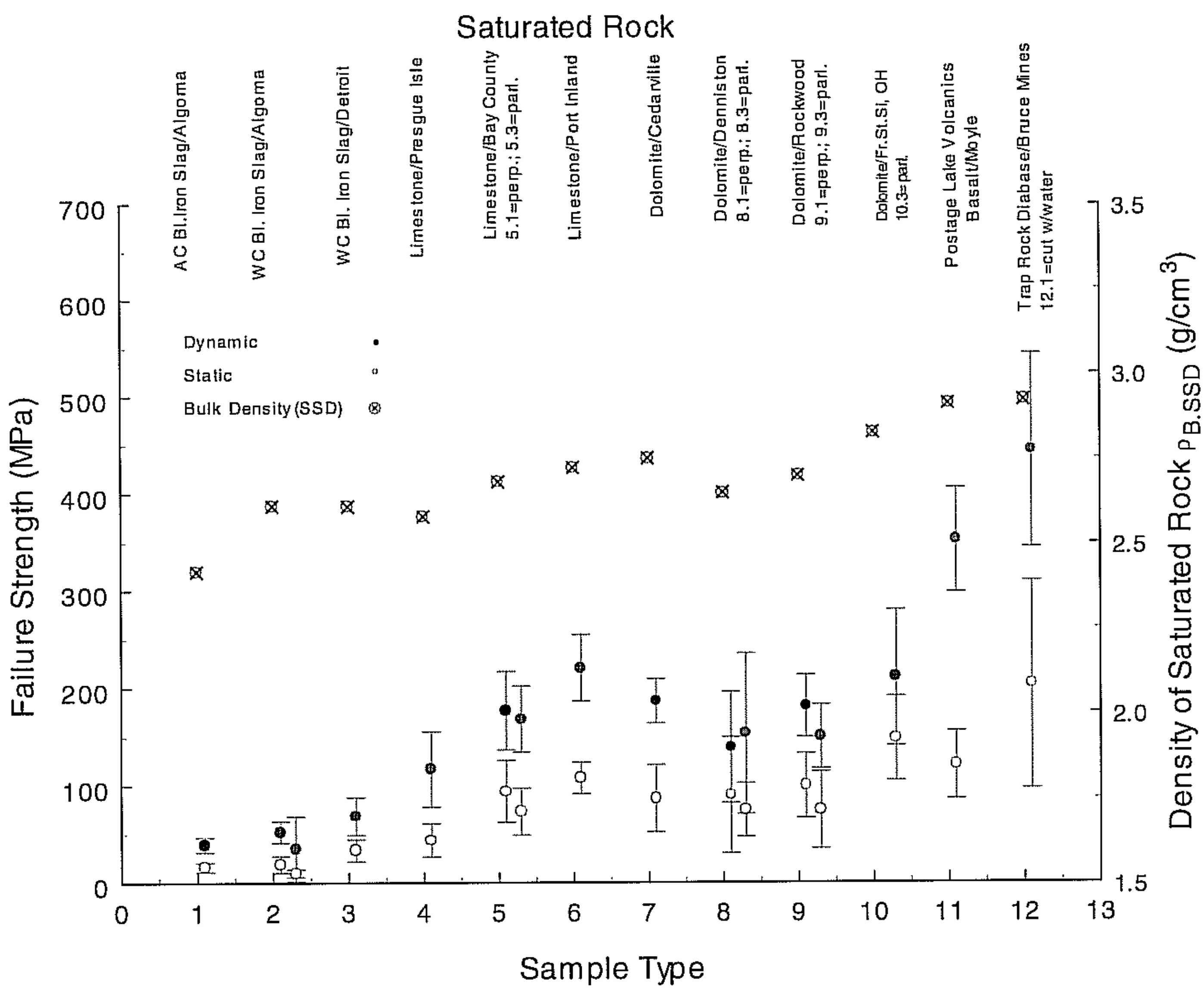

Figure 4.2(b) Statistical analysis showing mean and standard deviation of static and dynamic compressive strength of saturated aggregate including aggregate bulk dry density.

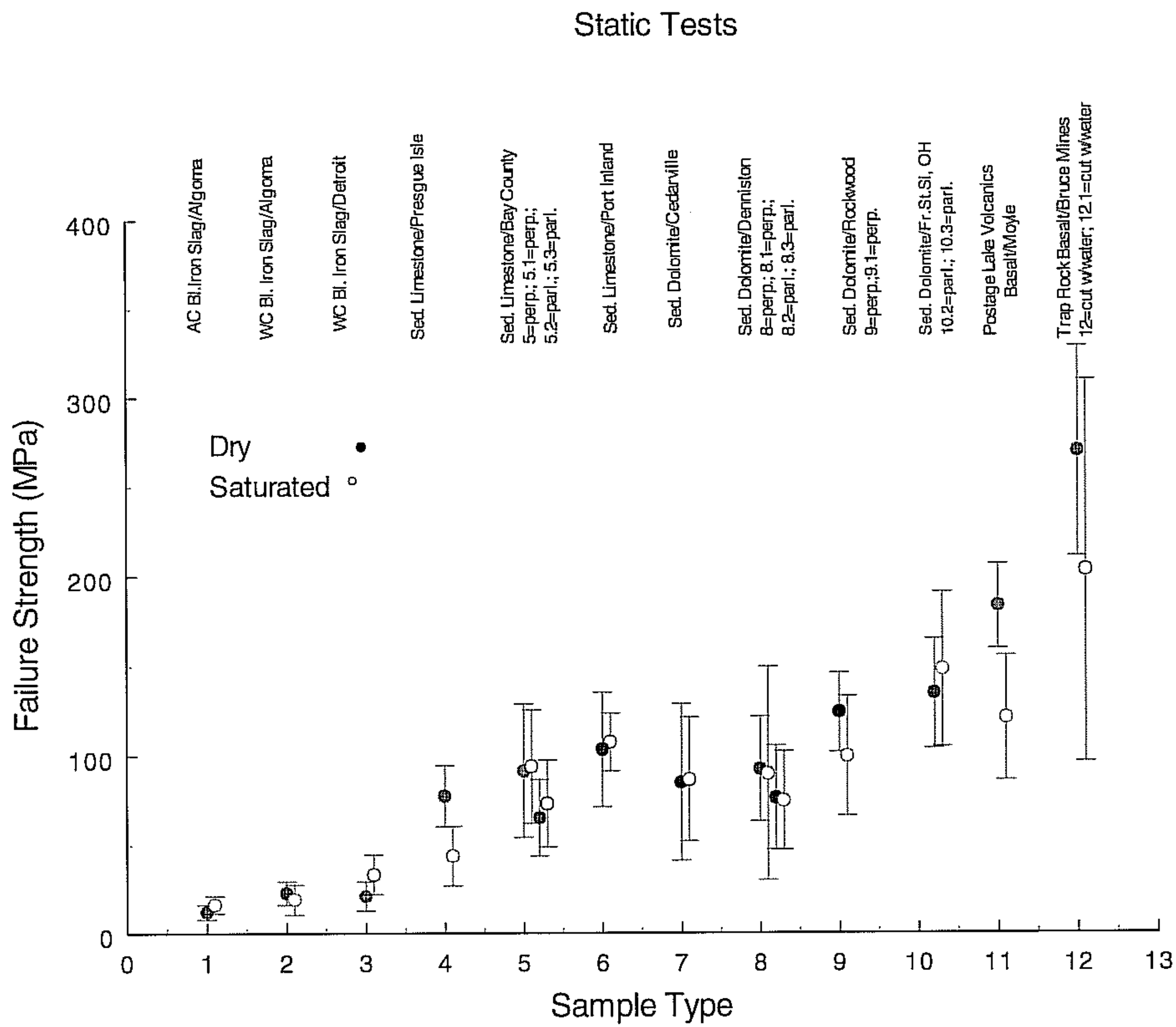

Figure 4.3(a) Comparison of dry and saturated strength results for static test results.

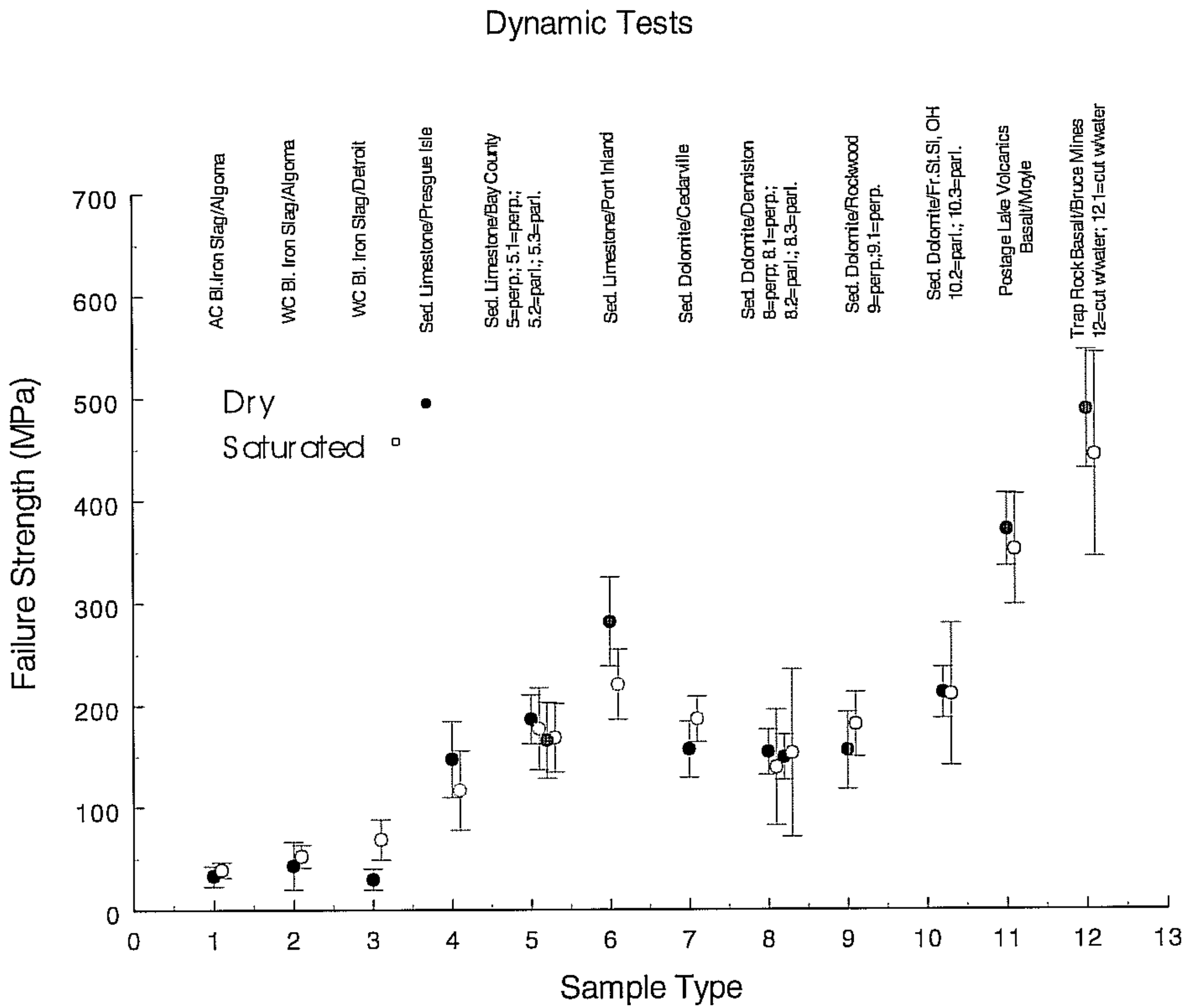

Figure 4.3(b) Comparison of dry and saturated strength results for dynamic test results.

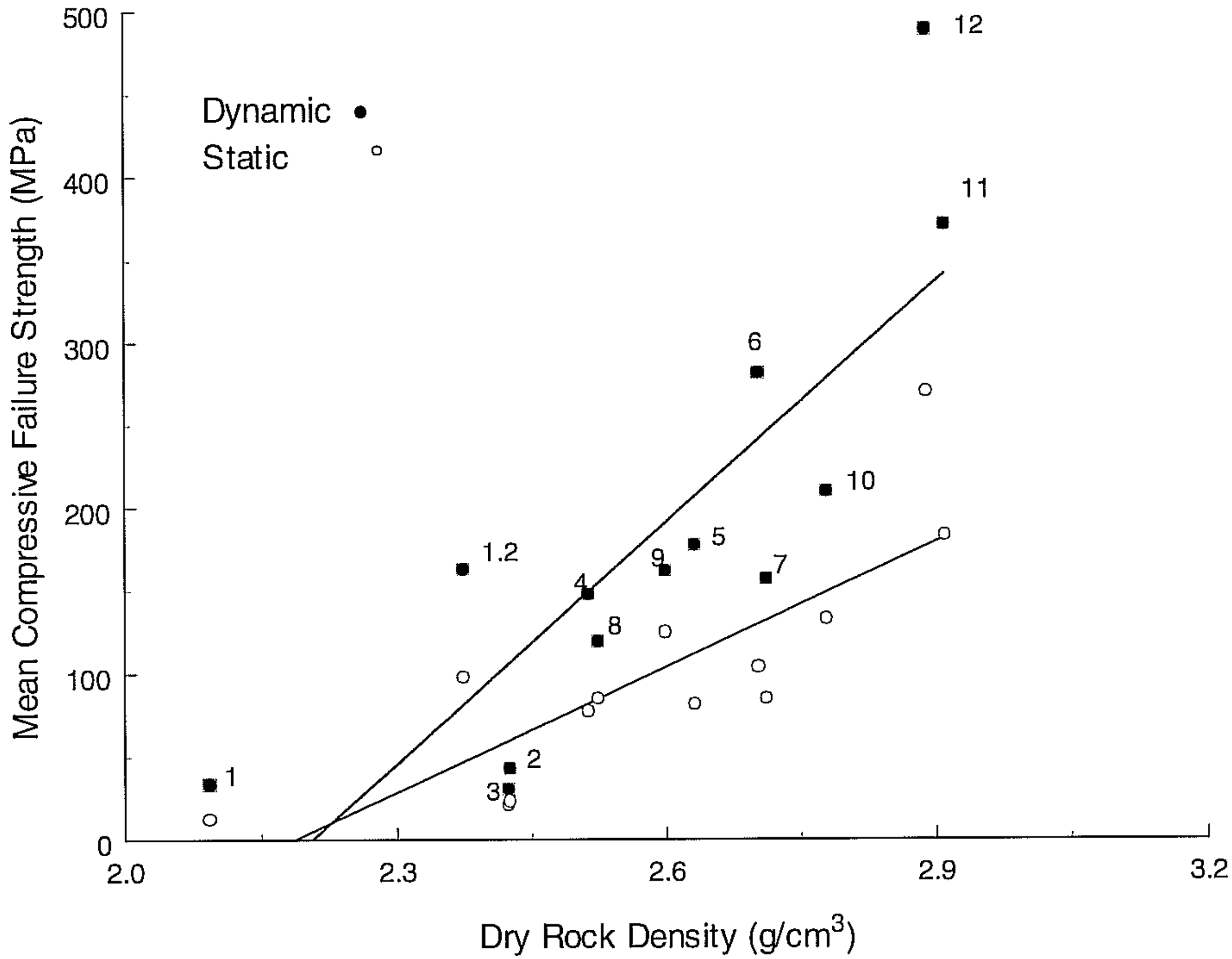

Figure 4.4 (a) Comparison of static and dynamic failure strength with dry bulk density.

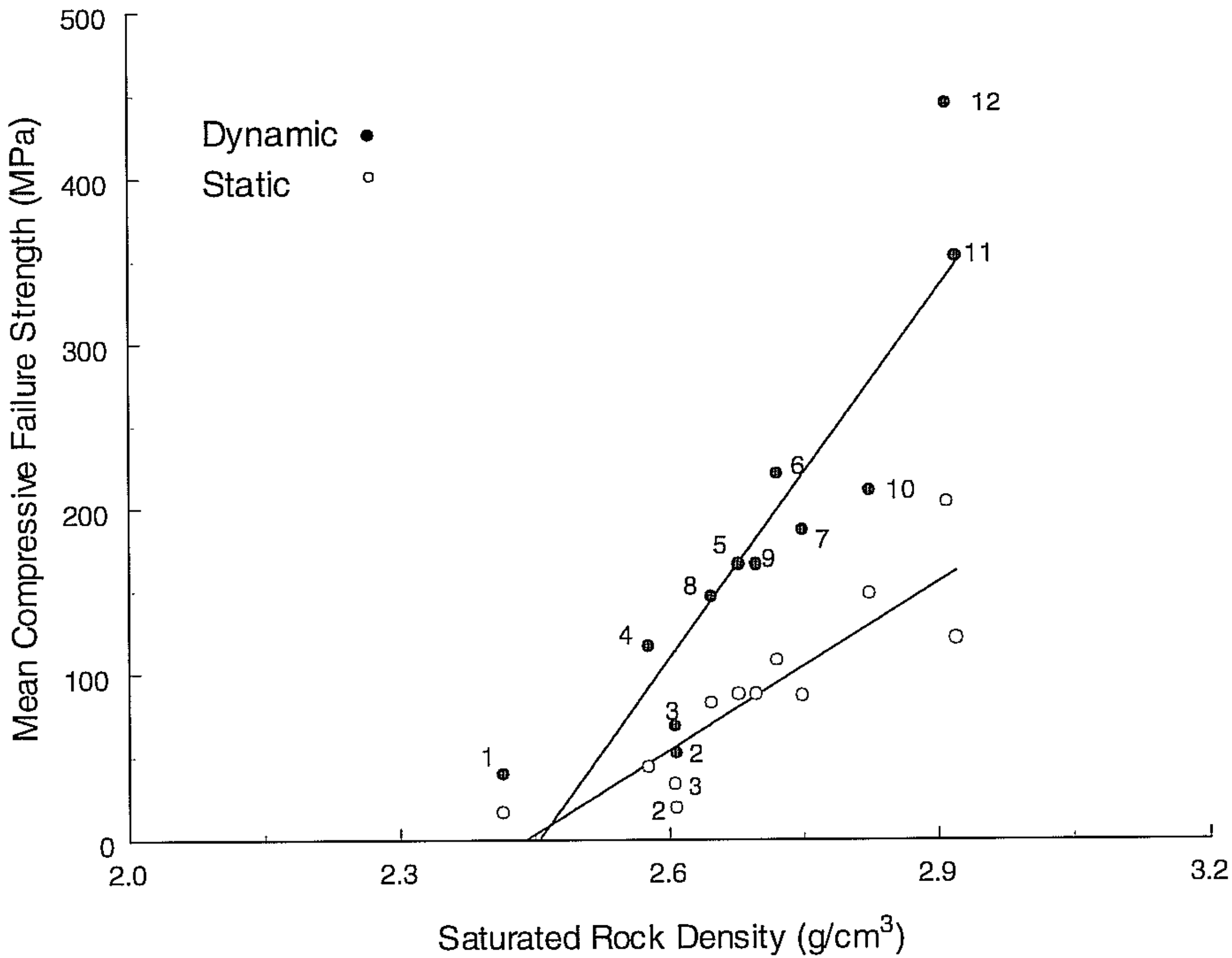

Figure 4.4 (b) Comparison of static and dynamic failure strength with saturated bulk density.

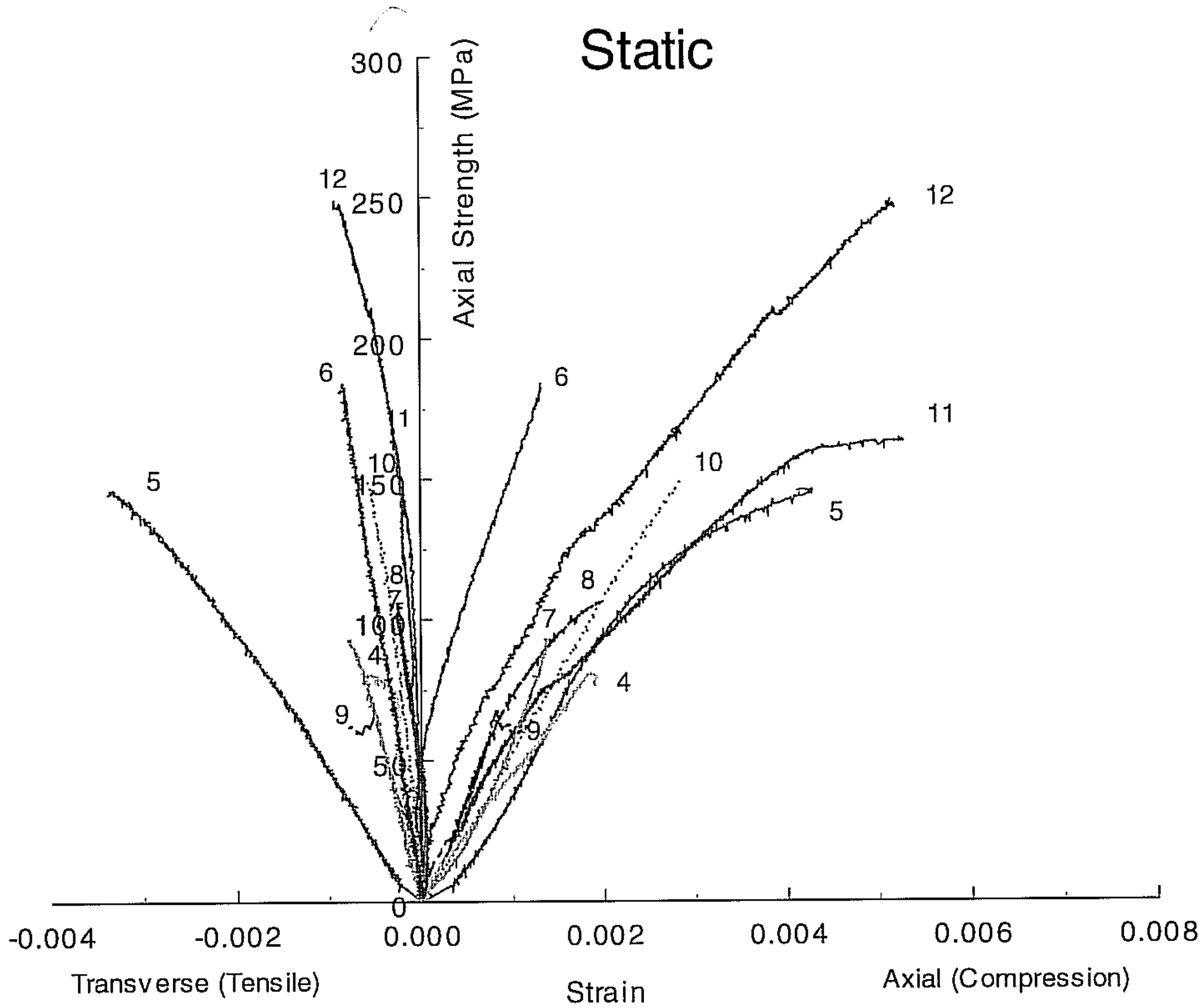

Figure 4.5(a) Axial stress-strain curves for static compressive strength test results.

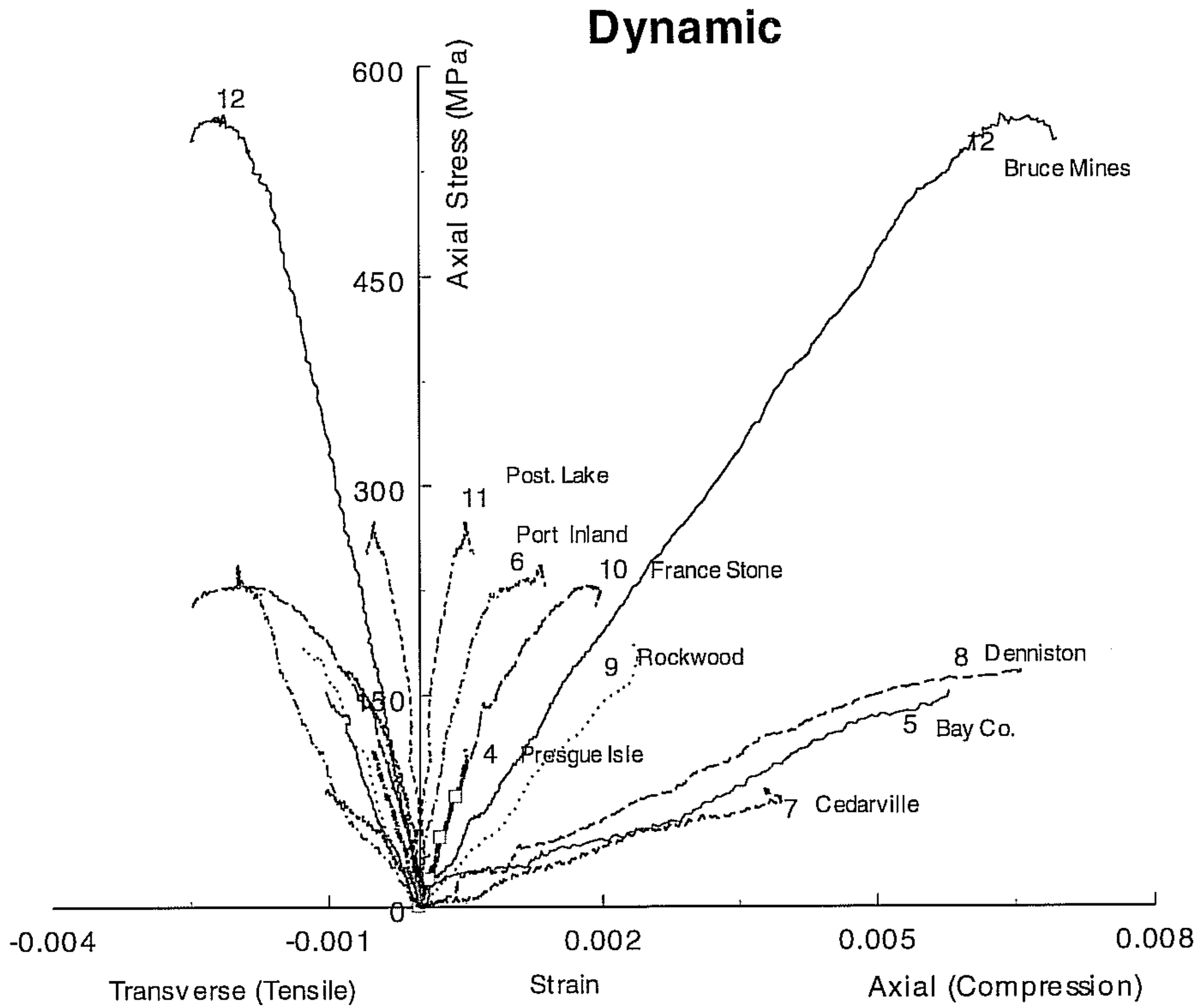

Figure 4.5(b) Axial stress-strain curves for dynamic compressive strength test results.

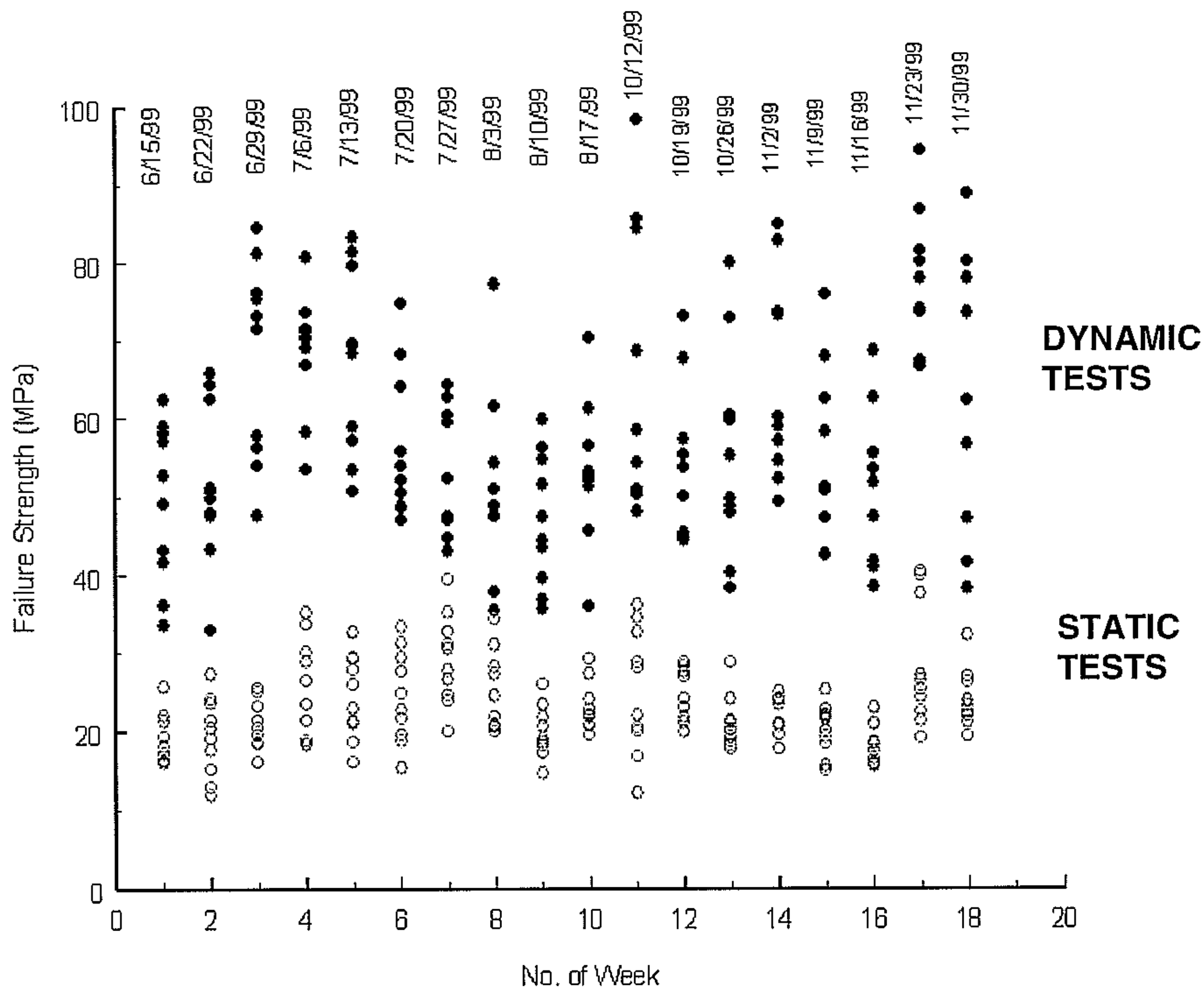

Figure 4.6 Raw data for static and dynamic mortar testing.

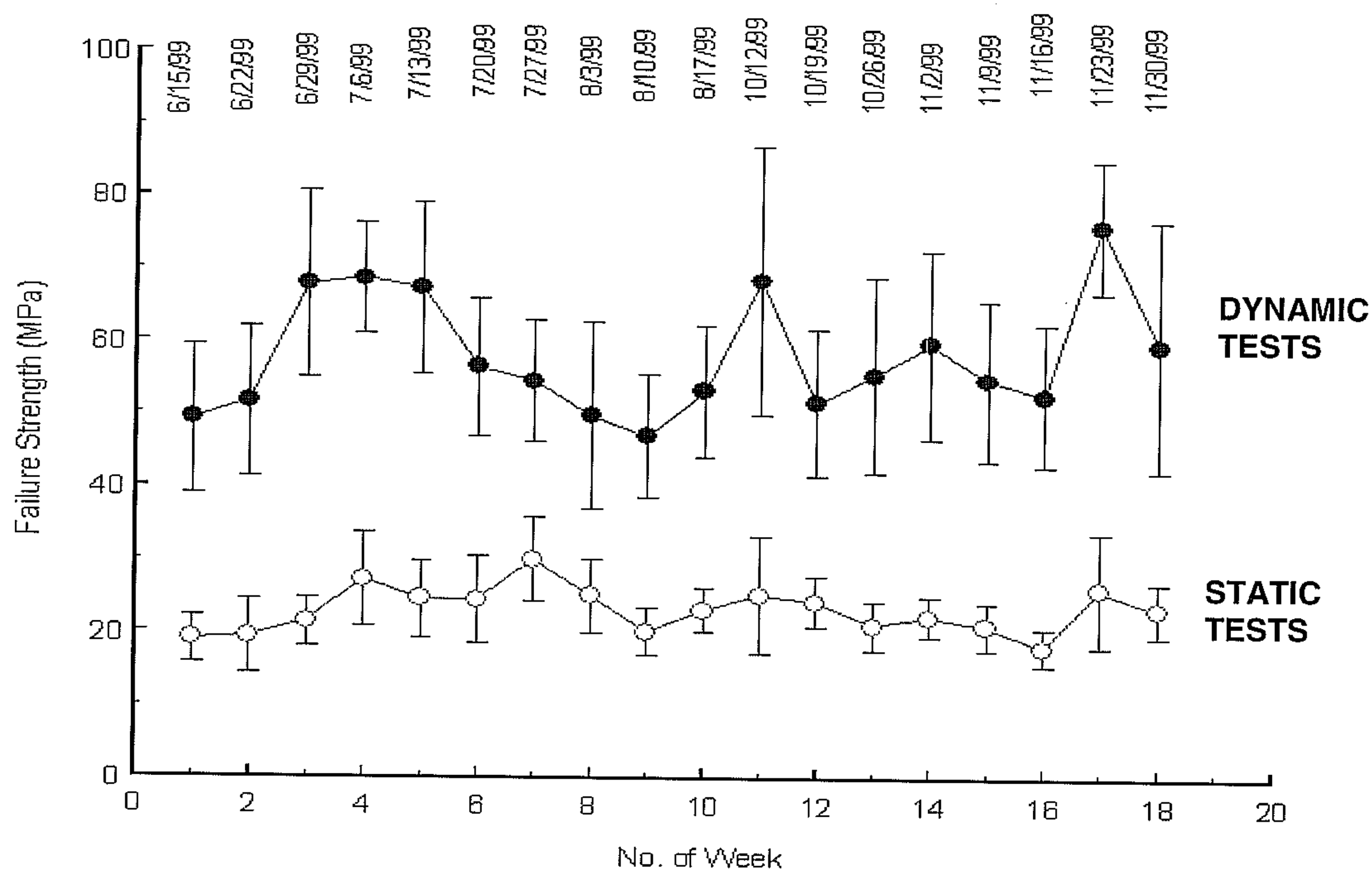

Figure 4.7 Results of mortar static and dynamic uniaxial compression testing.

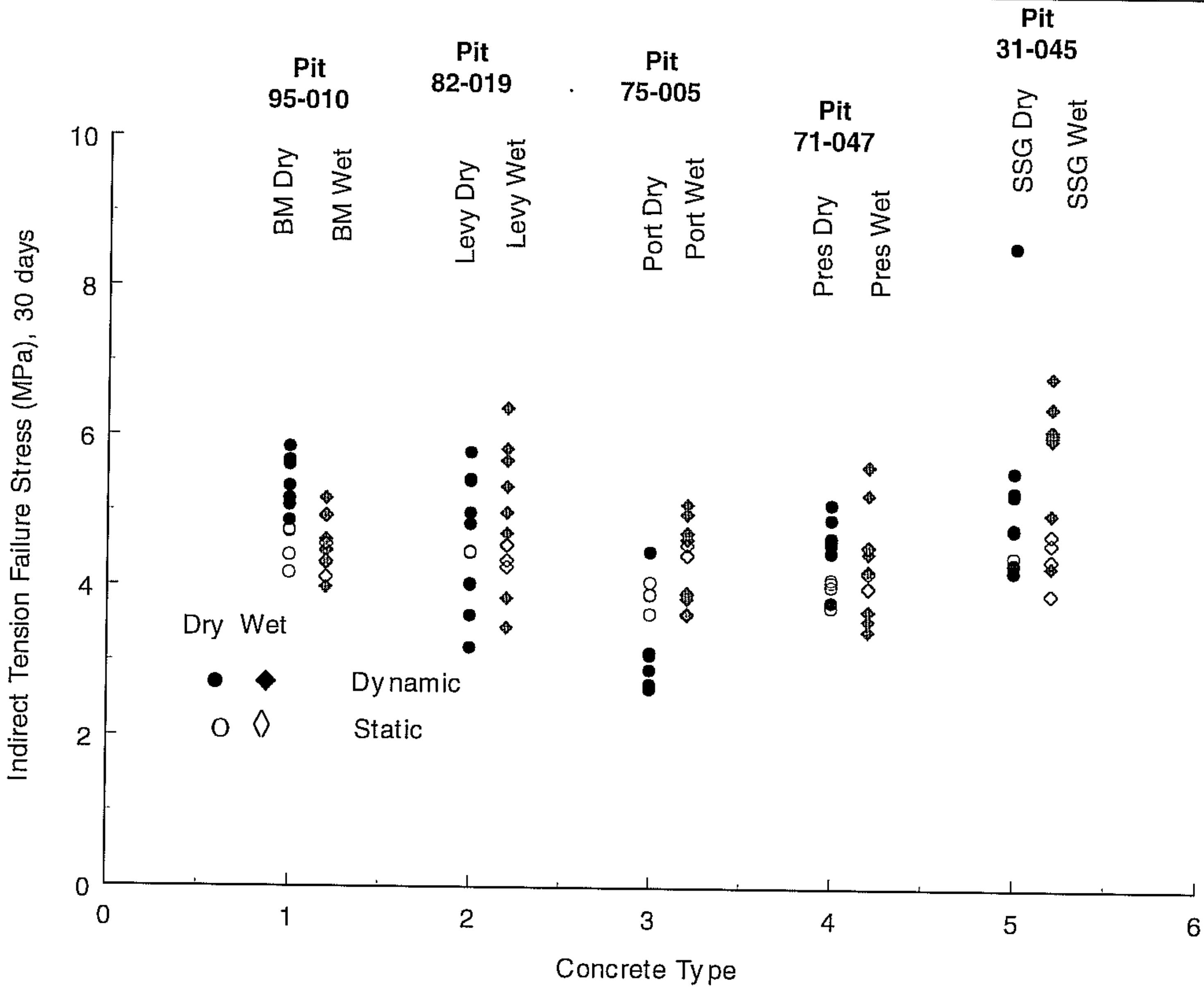

Figure 4.8 Raw data from static and dynamic indirect tensile testing of concrete with different coarse aggregate types.

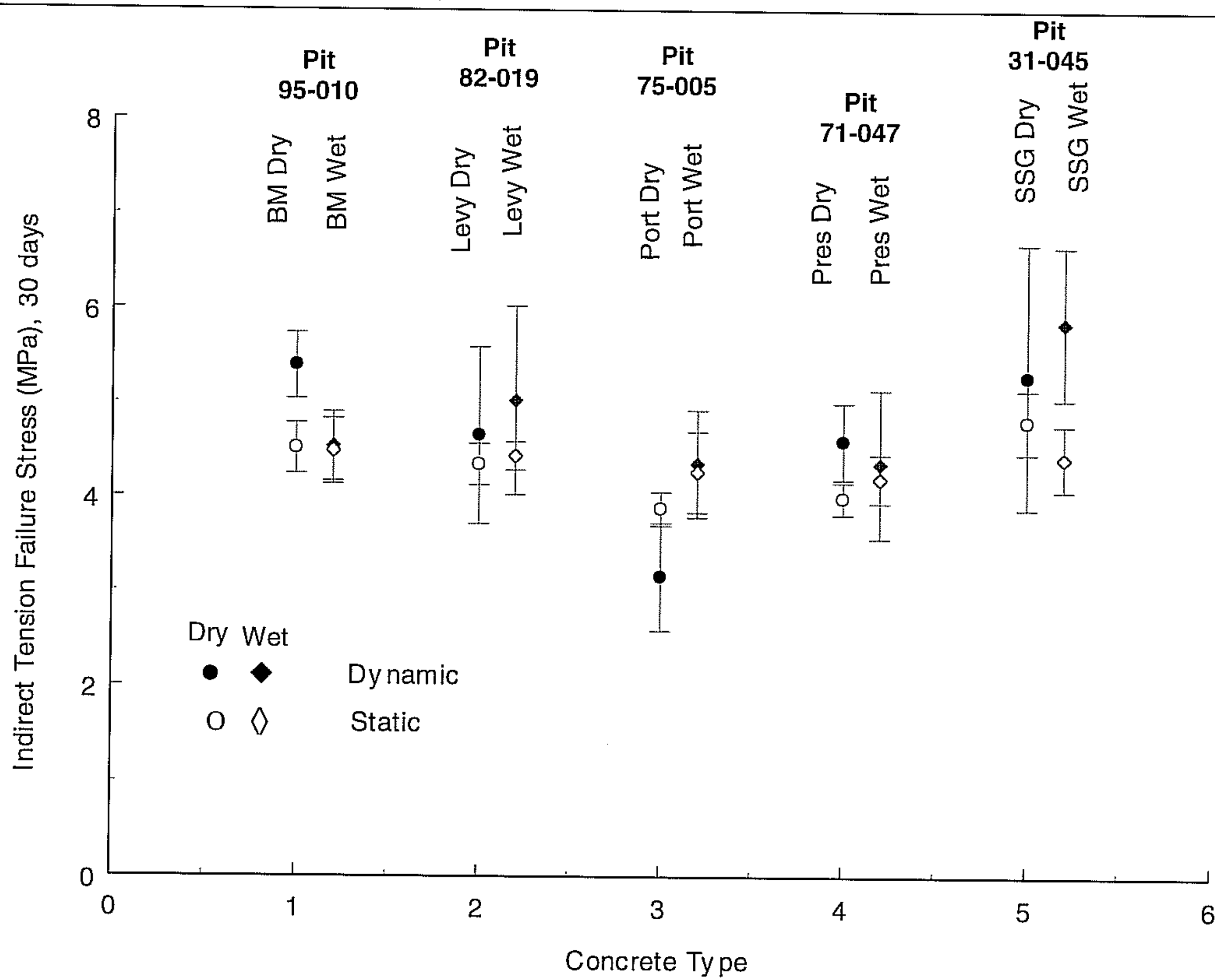

Figure 4.9 Statistical analysis showing mean and standard deviation of the static and dynamic tensile testing of concrete with different coarse aggregate types.

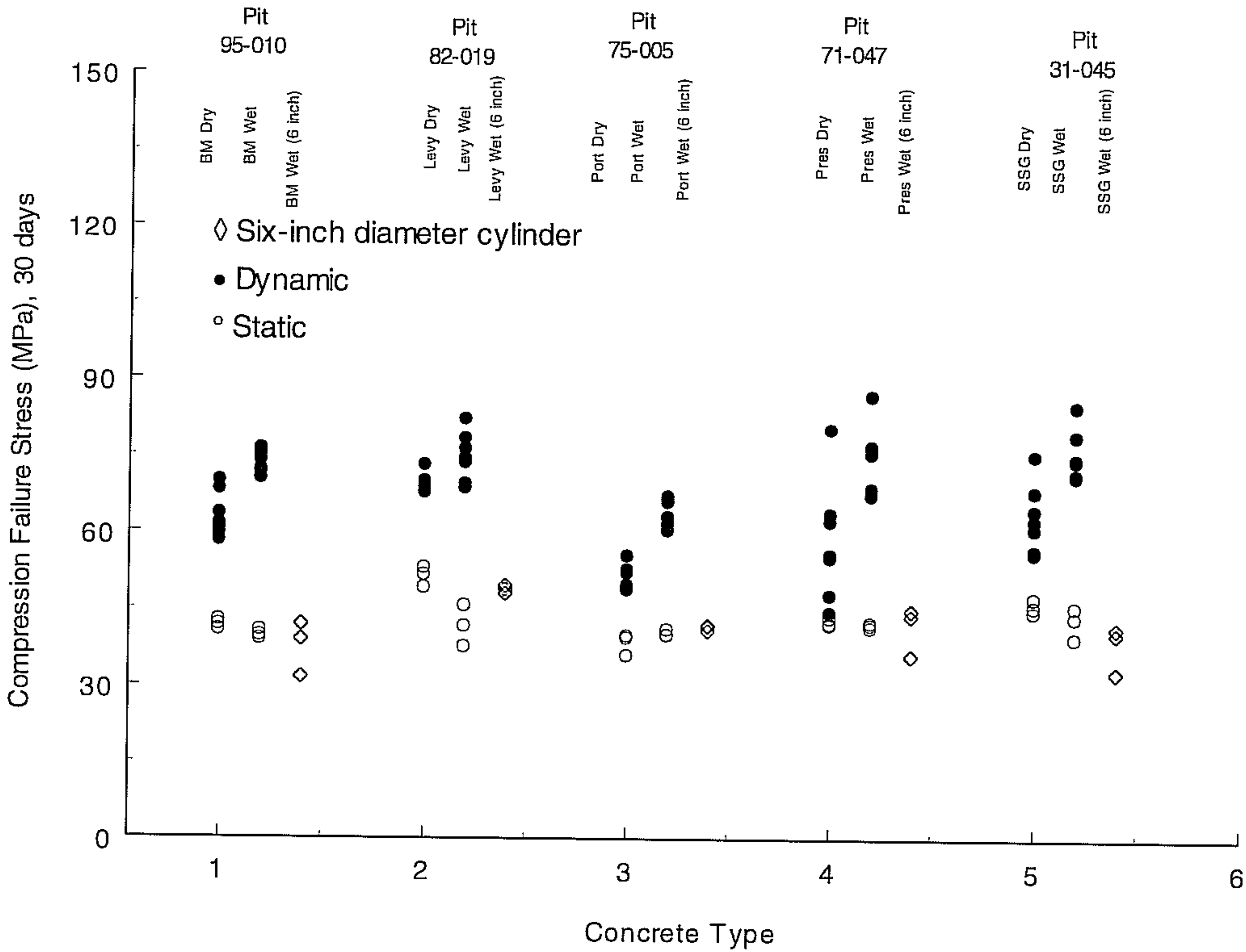

Figure 4.10 Raw data from static and dynamic uniaxial compression testing of concrete with different coarse aggregate types.

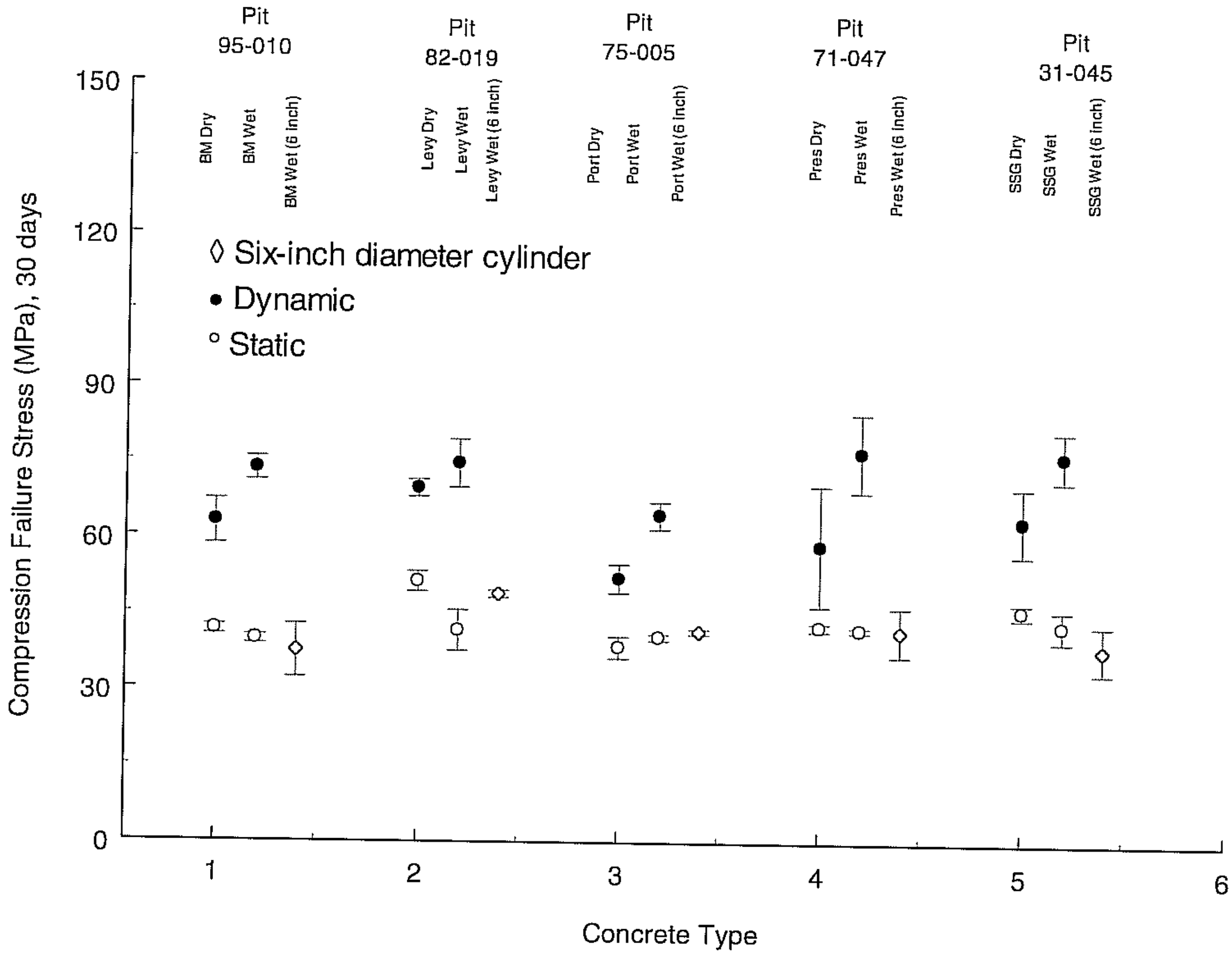

Figure 4.11 Statistical analysis showing mean and standard deviation of the static and dynamic uniaxial compression testing of concrete with different coarse aggregate types

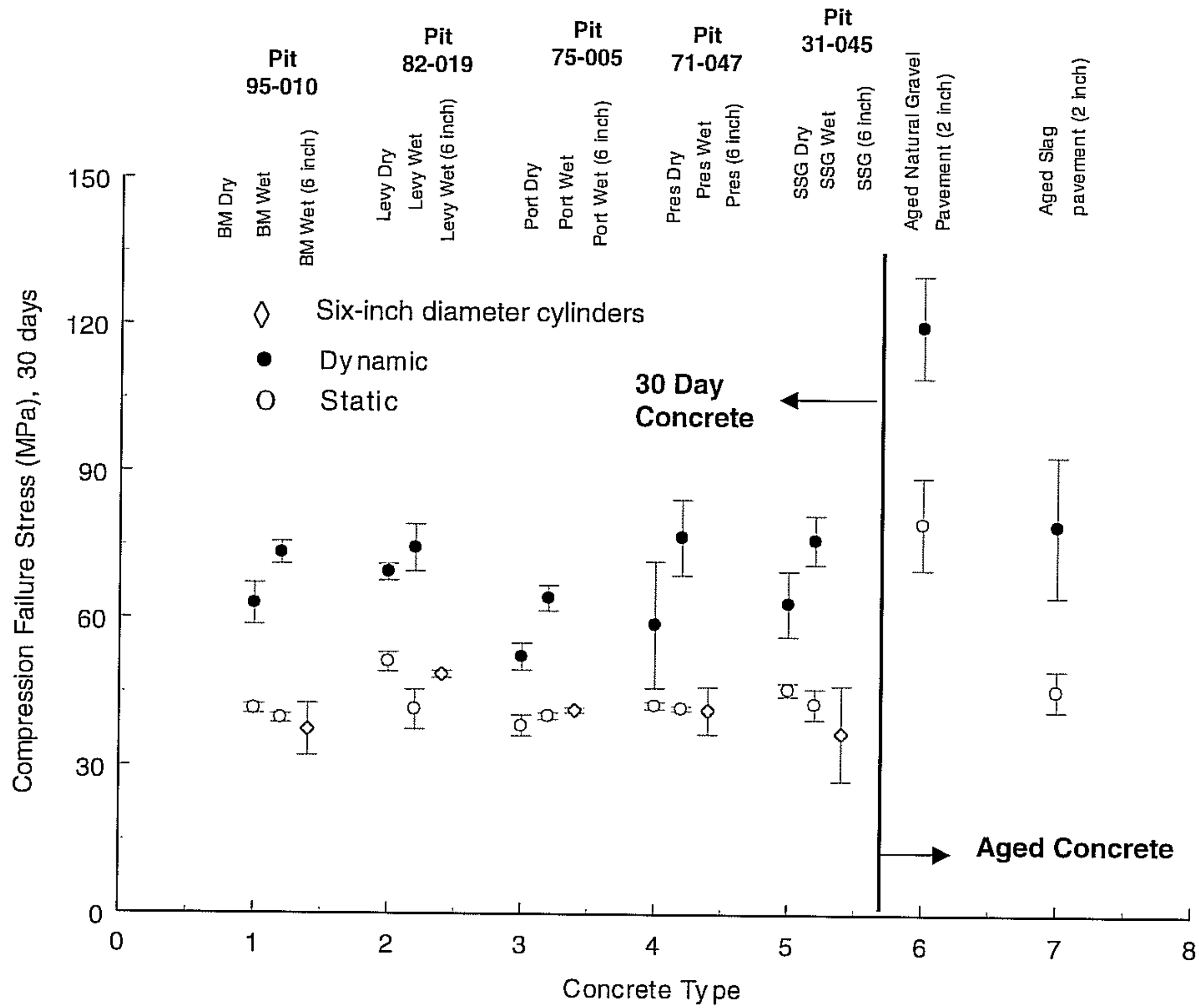

Figure 4.12 Statistical data for the dry and moist PCC static and dynamic compression testing including aged concrete data.

5 Discussion

5.1 Aggregates

5.1.1 Static and Dynamic Strength

Deere and Miller (1966) produced an engineering classification for intact rock based on uniaxial compressive strength that has gained wide acceptance in engineering practice. This classification categorizes rocks from very high strength (Category A) through very low strength (Category E) using a geometric progression of uniaxial static compressive strength values. Accordingly, the Deere and Miller classification (from Jumikis, 1983) has been applied to the uniaxial compression results obtained in this research for the dry testing conditions given in Figure 4.2(a). The correlation of uniaxial failure strength between this research and the Deer and Miller classification is presented in Figure 5.1, along with the aggregate's bulk density.

Starting with the slag specimens 1 through 3, it can be seen that the static test results of three out of the four slag specimens lie in the very low strength category **E**, while the higher density air-cooled slag specimen 1.2 lies in the medium strength category **C**. However, in both cases the dynamic results move into the next higher strength category, low strength **D** and high strength **B**, respectively. The increase in the dynamic strength over the static strength can also be seen in the results of static testing of limestone and dolomite specimens 4 through 8, which lie in the medium strength category **C**, and aggregates 9 and 10, which just lie in the high strength category **B**. Again, the dynamic test results lie in the next higher strength category; high strength **B** for aggregates 4 through 8, except 6, which moves two categories higher into category **A** "very high strength." However, the results for aggregates 9 and 10 stay in the same strength category of the static strength category **B** but are at the lower and upper boundaries of this category. Following this general pattern, aggregate 11 (basalt) moves from high strength category **B** to very high strength category **A**. Moreover, the static strength of aggregate 12 (diabase) is already in the highest strength category **A** (very high strength) while the dynamic strength is considerably higher. Continuing the geometric progression sequence of uniaxial compressive strength 440 MPa would be the start of the next category. The dynamic strength of aggregate 12

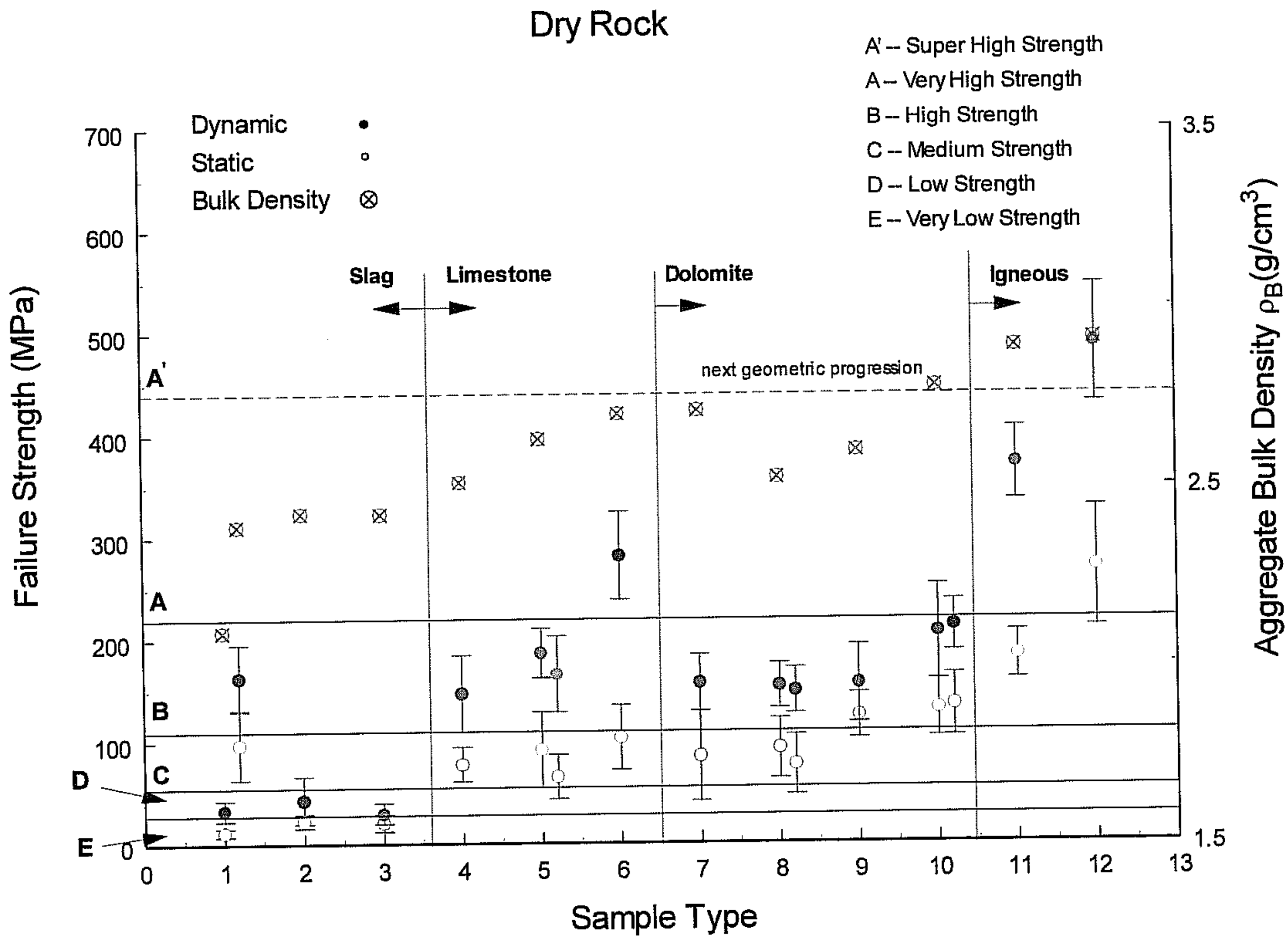

Figure 5.1 Uniaxial compression strength classification system for static and dynamic tests.

at 490 MPa would place this aggregate above the 440 MPa boundary into a new category that has been labeled **A'** and identified as "super high strength."

Comparing all of the aggregates, the blast furnace slag specimens have the lowest overall strength, which originates from a combination of factors including extensive porosity and compositional and the microstructural variations. Since slag is produced during the metallurgical treatment of iron ore, it consists of gangue and the secondary constituents from iron ores including, coke residue and limestone with a chemical composition consisting primarily of CaO, SiO_2, $A1_2O_3$ and MgO and trace amounts of sulfur and some alkalis (Lea, 1971). The final structure of the slag depends on available chemical constituents and the cooling conditions of the molten slag. Since slag melt has a high thermal energy of about 1700 kJ/kg, slow cooling conditions facilitate full dissipation of this energy and results in a stable dense crystalline structure with high density and mechanical properties close to that of natural aggregates (Lea, 1971). When the molten slag is quickly air-cooled or water-quenched with limited amounts of water, it traps steam in the mass and produces a relatively porous, glassy material with poorer mechanical properties. In this research both air-cooled (specimen 1) and water-quenched slag (specimen 2 and 3) were tested. The Algoma air-cooled slag (specimen 1), however, consisted of two distinct regions, a porous lighter colored region (listed as specimen 1.0) and a darker colored denser region (listed as specimen 1.2). While the air-cooled slag specimen 1.0 had approximately the same strength as the water-quenched specimens 2 (also from the Algoma Steel mill) and 3 (from the Levy Company) at approximately 20 MPa, specimen 1.2 had significantly higher strength at 98 MPa, which was in the range of the carbonates aggregates. Three possible explanations can be given for the higher strength for the denser air-cooled specimen 1.2. First, and most likely is that the denser slag had less porosity then specimen 1.0, 17 versus 30%. However, the bulk density of specimen 1.2 is approximately the same as the water-quenched slag specimens 2 and 3 at approximately 2.4 g/cm^3 and has basically the same porosity at 17% versus an average of 18% for specimen's 2 and 3. Interestingly, the air-cooled slag specimen 1.0, which only had a bulk density of 2.09 g/cm^3 and a significantly higher porosity at 30%, has about the same strength as the water-quenched slag specimen's 2 and 3. A second reason as mentioned previously is that the air-cooled slag may have had more time to cool since water was not used to increase the cooling rate of the slag by inducing thermal cracking in the slag mass. A longer cooling time would allow a denser crystalline structure to form resulting in higher strength.

However, the climatic conditions between an air-cooled site and a water-quenched site may not differ substantially and therefore the cooling rate may be approximately the same whether water quenching is used or not. A more significant factor, though, may be the subsequent breaking and crushing of the slag soon after placement in the cooling trench, which is conducted typically within 48-hours. Breaking up and crushing the slag reduces the thermal mass and greatly increases thermal cooling since the surface area of the slag exposed to the atmosphere is significantly increased. Air-cooled slag on the other hand, is deposited in a disposal area and left for a longer period of time prior to breakage and crushing and in some cases such as with the Algoma slag many years. A third possible reason, which was speculated in Section Three, is that the air-cooled slag due to its transportation and deposition may have been better mixed allowing improved chemical association and nucleation sites for crystal development. In general, the molten air-cooled slag was placed in large metal crucibles and transported to the disposal area by heavy equipment. The slag was then dumped down a slope providing additional mixing and onto other slag that would act as an insulator allowing slower cooling and better crystal development. A difference in crystalline structure between the air-cooled slag and the water-quenched slag can also be seen in Figure's A.1 and A.2 in Section Three of this report. The air-cooled slag, while also having numerous pores, appears the have a more developed crystalline structure as opposed to the water-quenched slag, which has a more glassy structure. It is probable that the more developed crystalline structure of the air-cooled slag, even at a porosity of 30% and a bulk density of 2.09 g/cm^3, gives the air-cooled slag an equivalent strength to the water-quenched slags, which has a higher bulk density at 2.40 g/cm^3 and a lower porosity of approximately 17%. Moreover, the higher density air-cooled slag specimen 1.2 with approximately an equivalent bulk density and porosity of the water-quenched slag has strength similar to that of carbonates. One likely reason for a denser region in the air-cooled slag is the higher density minerals will settle in the molten slag while the gas bubbles and lighter minerals will rise in the molten slag, thus forming the two regions in the slag. This is also seen in the water-quenched slags, where a lighter region forms at the top of the slag and a darker region towards the base of the slag. However, there was no discernable difference in bulk density and strength in the specimens cored and tested from either region. Based on these observations, it is recommended that additional research be conducted to better understand the factors that affect the development of slag's mechanical strength.

Inspecting the limestone and dolomite test results in Figure 5.1 a number of observations can be made. First, Jumikis (1983) indicates that dolomites are typically stronger than limestones in static strength, although not by a large margin. This relationship is confirmed in this research with the average dry static strength of limestones (aggregates 4, 5, and 6) equal to 84.6 MPa and the dolomites (aggregate types 7 through 10) equal to 107.5 MPa. However, the reverse occurs in the dynamic test results, where the average dynamic dry strength of the limestones are equal to 195.6 MPa while the dolomites are equal to 170.4 MPa. Second, while the static strengths of the three limestones tested (specimens 4, 5 and 6) are relatively close in value, the dynamic strength shows a strong increase that correlates well with the aggregate's bulk density. The dolomites also show an increase in dynamic strength with bulk density, however, this increase is also seen in the static strength results with the exception of specimen 7 (Cedarville dolomite). The Cedarville dolomite has a lower static and dynamic strength but has a relatively high bulk density. Consequently, by excluding the Cedarville dolomite it can be seen that there is a good correlation in dynamic strengths with bulk density for the carbonate aggregates. Inspecting the microstructure of the four dolomite aggregates from the thin sections shown in Figures A.6 through A.9 (Section Three), it can be observed that specimen 7 (Cedarville) and specimens 10 (France Stone) have relatively large grain structures, compared to specimens 8 (Denniston) and 9 (Rockwood), which have relatively fine grain structures. Although only four dolomites were investigated, the larger gain size appears to correlate with higher bulk density and conversely the finer grained dolomites with lower bulk density. What appears noticeably different, however, between the Cedarville and France Stone dolomite is that while the Cedarville dolomite has a larger grain size, it also has a more random and non-uniform grain size distribution. It is not clear as to how this microstructure controls the mechanical properties of the Cedarville dolomite; however, it possible that the more irregular nature of the crystalline grain structure may cause some of the deviations in the static and dynamic test results.

Finally, the igneous aggregates had the highest strength as expected. It is also interesting to note that although only two igneous aggregates were tested, their strengths to a smaller degree also correlated with bulk density. From this data it appears that in general dynamic strength correlates well with bulk density for the aggregate tested with the exception of the Cedarville Dolomite. In addition, it is also apparent that microstructural variations within aggregate types, e.g., carbonates, will influence this relationship.

5.1.2 Rate Sensitivity

A material's rate sensitivity is an important parameter that quantifies the ability of the material to resist higher dynamic versus static loads and is observed by an increase in compressive strength at higher applied strain rates. Many researchers provide the rate sensitivity for a material as a ratio of the dynamic to static strength (D/S). A material with a D/S of one would not be rate sensitive while a D/S greater than one would be rate sensitive. The D/S ratios for all of the aggregate tested in this research are presented in Table 5.1.

Table 5.1 Dynamic/Static strength (D/S) ratio data for dry and saturated aggregates.

			Compressive Fracture Strength Dynamic/Static Strength (D/S) Ratio			
ID No. Pit ID	**Aggregate/ (Quarry)**	**Orientation and Batch**	**Dry**	**Aggregate Average**	**Saturated**	**Aggregate Average**
1 95-006	AC Slag (Algoma)	Batch 1 Batch 1.2	2.74 1.67	**Slag** 1.93	2.42	**Slag** 2.68
2 95-006	WC Slag (Algoma)	Batch 2.0 Batch 2.1	1.90		2.75 3.49	
3 82-019	WC Slag (Levy)	Random	1.42		2.05	
4 71-047	Limestone (Presque Isle)	Random	1.90	**Limestone** 2.30	2.67	**Limestone** 2.23
5 06-008	Limestone (Bay Co.)	Normal Parallel	2.04 2.54		1.88 2.30	
6 75-005	Limestone (Port Inland)	Random	2.72		2.05	
7 49-065	Dolomite (Cedarville)	Random	1.84	**Dolomite** 1.64	2.15	**Dolomite** 1.83
8 58-009	Dolomite (Denniston)	Normal Parallel	1.66 1.95		1.55 2.05	
9 58-008	Dolomite (Rockwood)	Normal Parallel	1.25		1.82	
10 93-003	Dolomite (France St.)	Normal Parallel	1.58 1.58		1.42	
11 31-076	Basalt (Moyle)	Random	2.03	**Igneous** 1.78	2.91	**Igneous** 2.55
12 95-010	Diabase (Ontario)	Water Cut Oil Cut	1.81 1.51		2.18	

In reviewing the D/S results in Table 5.1, it can be seen that the aggregates all have a D/S greater than one, and consequently are considered to be rate sensitive. However, the amount of increase varied between aggregate types, ranging from 1.33 to 2.68. There was a noticeable increase in D/S between saturated and dry conditions for the blast furnace slag and the igneous aggregates with an average of 1.86 and 2.62 respectively. On the other hand, there was essentially no difference between saturated and dry conditions for the carbonate aggregates with limestones at a D/S of 2.30 and 2.23 respectively and the dolomites an average D/S of 1.64 and 1.83 respectively. However, there is a noticeable difference in the D/S between limestones and dolomites with the limestones having an average D/S of 2.26 and the dolomites an average of 1.73. The difference between the average D/S for limestone is relatively significant considering that the D/S ranged from 1.33 to 2.68, thus representing a variation of approximately 40% of the total range. It is also interesting to note that the high strength igneous and the very low strength blast furnace slag had similar D/S ratios of 1.93 and 1.78 for dry conditions and 2.68 and 2.55 for saturated conditions, respectively. The comparable D/S ratios may be an indication of the similarity of the microstructure of these materials since both made of igneous materials.

Another parameter that is used to assist in evaluating the applicability (or the effectiveness) of a specific aggregate to resist dynamic loads, e.g., impact or blasting, is the strain rate sensitivity (of fracture strength) parameter 'λ'. This parameter is also used in the development of rate dependent constitutive models for aggregates. From the strain gage data provided in Fig. 4.5(a) and (b) the strain rate ($\dot{\varepsilon}$) can be estimated during a test based on the measured strain (ε) and the time to fracture (t), i.e., $\dot{\varepsilon} = \varepsilon/t$. The strain rate for quasi-static tests was determined to be approximately in the range of 10^{-5}/s and for dynamic tests it was measured to be in the range of 10^{2}/s. The strain rate sensitivity parameter 'λ' is defined as follows:

$$\lambda = \frac{d\sigma_f}{d\left(\log\dot{\varepsilon}\right)} = \frac{\sigma_d - \sigma_s}{\log\left(\frac{\dot{\varepsilon}_d}{\dot{\varepsilon}_s}\right)} \qquad \textbf{5.1}$$

where, σ_d and σ_s refer to dynamic and static fracture strengths, $\dot{\varepsilon}_d$ and $\dot{\varepsilon}_s$ refer to corresponding dynamic and static strain rates, respectively. The numerator can be calculated from the average static and dynamic fracture strengths of the aggregates provided in Table 4.1. Since all the tests were performed either at a constant static strain rate 10^{-5}/s or a constant dynamic strain rate 10^{2}/s, the denominator is approximately 7. The strain rate sensitivity λ values are tabulated in Table 5.2. In this table it can be seen that the low strength slag aggregates also have the lowest rate sensitivity (λ<l0), ranging from 1.17 to 3.00 but 9.29 for the dense portion of the air-cooled slag (specimen 1.2). The high strength basalts have the highest rate sensitivity (λ>25), ranging from 26.90 to 31.30, while the carbonates have the intermediate values ranging from 4.52 to 25.52.

Table 5.2 Strain rate sensitivity λ values.

ID Number	Strain Rate Sensitivity, λ Aggregate	λ	λ Average
1.0	Algoma air cooled blast furnace slag – porous section	3.00	
1.2	Algoma air-cooled blast furnace slag – dense section	9.81	
2	Algoma water-quenched blast furnace slag	2.93	4.2
3	Levy water-quenched blast furnace slag	1.27	
4	Limestone, Presque Isle	9.97	
5	Limestone, Bay County	13.59	16.4
6	Limestone, Port Inland	25.52	
7	Dolomite, Cedarville	10.27	
8	Dolomite, Denniston	8.77	
9	Dolomite, Rockwood	4.52	8.6
10	Dolomite, France Stone	10.81	
11	Basalt, Portage Lake Lava Series, Moyle	26.90	
12	Diabase, Ontario Traprock	31.30	29.1

In crystalline brittle solids, such as ceramics, the rate sensitivity has been found to originate from microstructural inhomogenieties such as pores, cracks and impurities that exist along the grain boundaries (Lankford, 1981; Grady and Lipkin, 1980; Lankford and Blanchard, 1991; Ravichandran and Subhash, 1995). Typically these inhomogenieties form a small fraction of the overall material volume. Although it is known that inhomogenieties control the fracture characteristics of brittle materials, an important aspect of brittle failure is that resistance to crack growth from these inhomogenieties varies with strain rate. At low strain rates (traditional static testing rates), the rate sensitivity has been found to originate from the thermally activated stable sub-critical crack growth from these pores, cracks, and geologic discontinuities. But beyond a critical strain rate of 10^2/s, the compressive fracture strength increases dramatically with strain rate, which is attributed mainly to inertia dominated crack growth, i.e., as the loading rate increases, the time available for crack to initiate and grow reduces. The inertia associated with the crack growth acceleration will inhibit early fracture while the applied stress continues to rise rapidly, thus elevating the compressive failure strength under dynamic loads. Similar situation can be envisioned for the aggregates tested in this investigation. All the aggregates consist of highly inhomogeneous microstructure with small amounts of porosity (with the exception of slag) and impurities, which are potential sites for crack nucleation and growth under applied loads. Therefore, at higher loading rates, the stress level rises rapidly before the crack growth is initiated thus resulting in a higher compressive strength and rate sensitivity. In the case of slag aggregates, which are highly porous, it is believed that this porosity and lack of a well-defined crystalline structure (rather than impurities and inhomogeneities) dominate the deformation process and therefore, the failure strength is relatively low at both static and dynamic loading rates as seen in this research. However, a significant increase in strain rate sensitivity was seen in the dense air-cooled slag specimen 1.2, with a $\lambda = 9.81$ for the dense air-cooled compared to a $\lambda = 2.10$ for the water-quenched slag specimen 1.0. The primary reason for the increase in strength and rate sensitivity is believed to be due to the better developed crystalline structure of the air-cooled slag versus the water quenched slag. This can be seen in Figures A.1 and A.2, which show the difference in microstructure between the two slags. It is also interesting to compare the strain rate parameter λ results with the D/S results for both slags and igneous aggregates. Basically, the D/S results are similar for slag and the igneous aggregates, while the strain rate parameter results are significantly different for the two aggregate types. This indicates that while the strain rate parameter λ provides a measure of strength (and potentially a classification method), the normalization of the static and dynamic strength results, i.e., D/S, may possibly provide an indication of an aggregate's microstructural characteristics, e.g., igneous versus sedimentary or within a specific geologic category such as limestones.

Another significant feature of the strain rate sensitivity parameter λ is that it summarizes the results of both the static and dynamic testing results into one parameter. One correlation already discussed is strength (both static and dynamic) with bulk density. A plot of bulk density versus strain rate sensitivity parameter λ for all the aggregates is plotted in Figure 5.2. From this figure it can be seen that there is a general increase in λ with respect to bulk density with a linear correlation coefficient (trendline) of 0.61. Also, it is interesting to note in Figure 5.2 that some of the aggregates tend to group together. For example, the air-cooled slag lie on one side of the

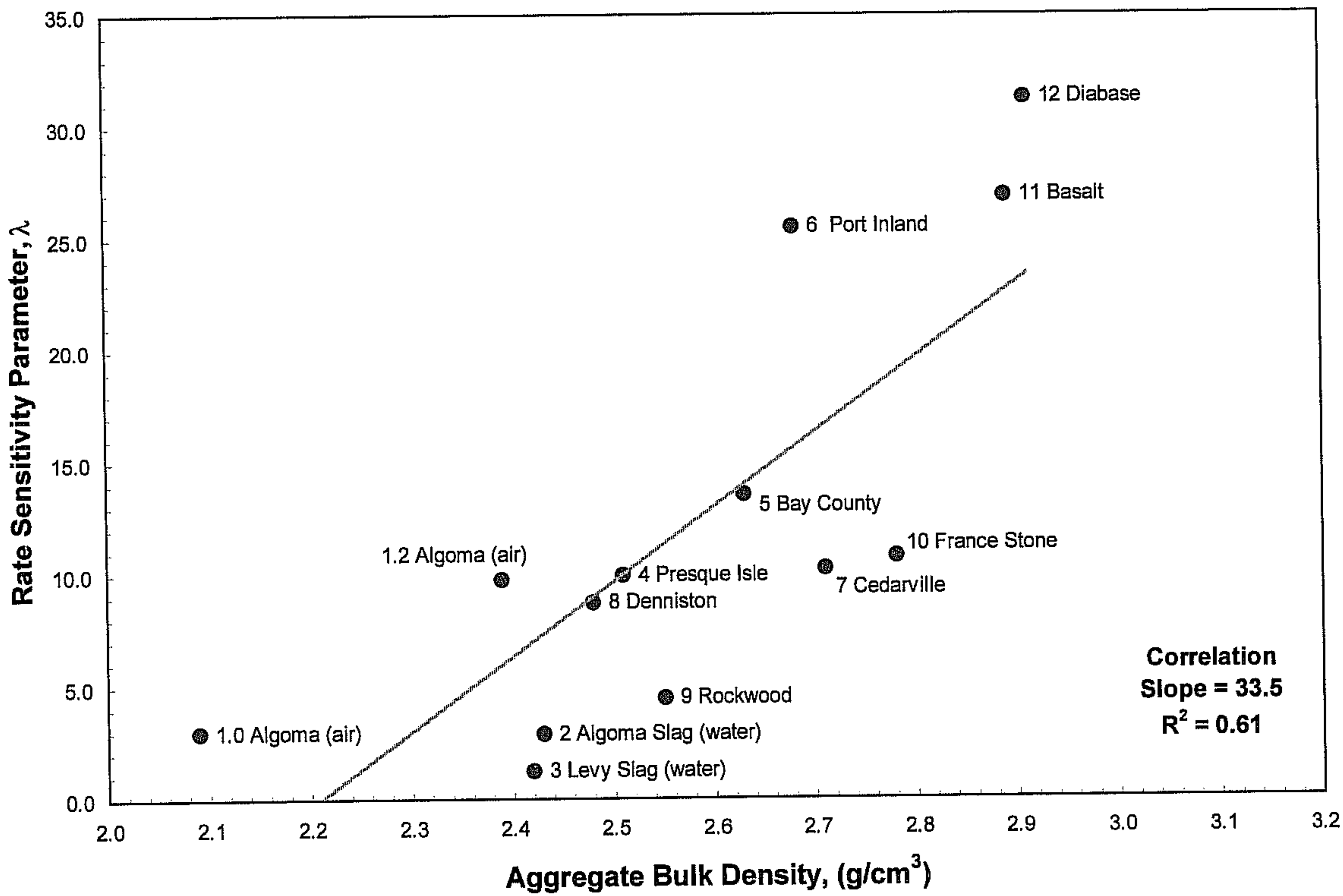

Figure 5.2 Strain rate versus aggregate bulk density for compression testing.

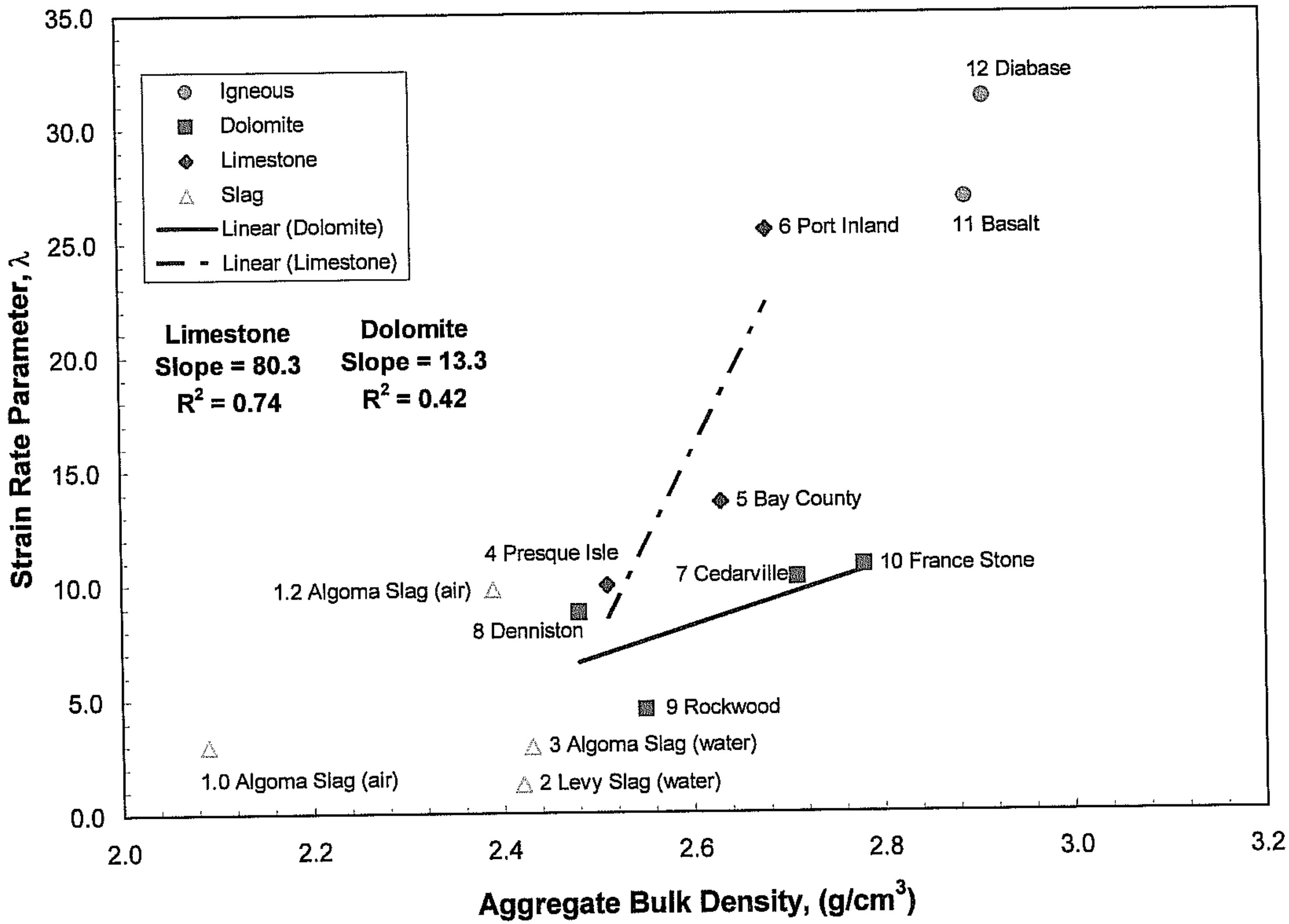

Figure 5.3 Rate sensitivity versus aggregate bulk density grouped by aggregate type.

trendline while the water-quenched slag are grouped on the other side. Further grouping based on geologic types is presented in Figure 5.3. From this figure it can be seen that there are more or less linear increases in strain rate sensitivity for both the limestone and dolomite aggregates. Therefore, trendlines were also added for the limestone and dolomites carbonates. The dolomite had the lowest linear correlation of 0.42 while the limestones had a linear correlation of 0.74. No correlation is provided for the igneous aggregate since only two aggregates types were tested. Also, no correlation was provided for the slag since there is such a large difference between the dense air-cooled specimen 1.2 and the other lower strength slags. However, excluding specimen 1.2 it can be seen that the general trend would be approximately level suggesting that there is limited to no increase in the rate sensitivity with bulk density for the slag aggregates.

Inspecting the strain rate sensitivity of the carbonate aggregates, the limestones range from 9.97 to 25.52 with an average of 16.4, while the dolomites on the other hand range from a low of 4.52 to a high of 10.81, with an average of 8.6. Thus, the limestones have average rate sensitivity almost twice that of dolomites. The limestone aggregates not only have higher strain rate sensitivity but also have a greater increase in strain rate sensitivity with bulk density. This same trend can be seen in the D/S results with the limestones having a higher D/S than the dolomites (2.30 versus 1.64). These results suggest that there may be a greater difference in microstructure between the limestone and dolomite aggregates than may have been previously considered given the similarity in static compressive strengths.

Inspecting the carbonate's microstructure shown in the thin-sections provided in Figures A.3 through A.9 (Section Three) a couple of generalization can be made concerning the testing results and the aggregate's microstructure[1]. In considering the limestone aggregates, it appears based on the size and uniformity of the grain size that the limestones are composed primarily of micrite or microcrystalline calcite and fossils. According to Blatt et al., (1972), micrite is by far the most common constituent in carbonate rocks with the individual crystals in ancient rocks usually less than 5 um in diameter. Micrite in turn commonly converts to calcite grains. From the thin-sections it can be seen that the Presque Isle limestone has the largest and most disorganized grain structure along with skeletal remains. The Bay County limestone has a smaller and somewhat more uniform grain size as well as skeletal fragments compared to the

[1] The following discussion provides only provide possibilities, since not enough information is available to make conclusive statements.

Presque Isle limestone. The Port Inland limestone has the smallest and most uniform grain size of the three limestones in addition to skeletal remains. Comparing the grain size of the limestones to its bulk density and rate sensitivity λ, it can be seen that as the grain size decreases both the bulk density and rate sensitivity parameter λ increase. In addition, the D/S values also increase from 1.90 for Presque Isle, to 2.3 for Bay County and finally to 2.7 for Port Inland limestone, which also corresponds to increasing dynamic strength. Interestingly, in ceramic engineering, it has been shown that for a given material the smaller the grain size and uniformity of the grain size the harder and higher dynamic strength of the material. This appears to fit with the general trend in the limestones, with the smaller grain size limestones having the higher strength. The benefit of the smaller grain size in increasing the strength of the material is that the failure cracks must fracture along a greater number of grains boundaries. As noted above, the strength (and rate sensitivity) of a material is a function of the microstructural inhomogenieties such as pores, cracks and impurities that exist along the grain boundaries. However, if the strength of the grain boundary is low due to significant inhomogenieties and other defects, the overall strength of the material will likely also be low regardless of grain size.

While there is wide agreement on the formation of limestone carbonates, there has been significant controversy over the formation of dolomitic rocks. The controversy centers on whether the dolomite develops as a primary mineral, i.e., that form naturally in bodies of water or whether the dolomites form as a secondary replacement product of limestone carbonates. That is, where limestones ($Ca\text{-}CO_3$) forms and then later transition into dolomite ($Mg\text{-}CO_3\text{-}Ca\text{-}CO_3$) due to migrating groundwater or changes in ocean chemistry. In general, the evidence suggests that dolomite forms as a replacement product of limestone. This is seen in thin sections of ancient dolomites where the individual dolomite crystals or clusters of crystals penetrate the original calcite carbonate particles. It has also been observed in the field where layered carbonate rocks abruptly change from limestone to dolomite with the change cutting across the carbonate bedding indicating that the dolomite is secondary. Another issue involving the formation of dolomites is that the dolomite crystals depart significantly from ideal conditions as opposed to calcite crystal formation. According to Blatt et al. (1972), dolomite is not stoichiometric but ranges in composition from approximately 56 mole % calcium and 44 moles % magnesium instead of an ideal value of 50%. A secondary problem in the formation of dolomite crystals during replacement of calcite crystals is the isomorphus substitution of other divalent ions such as magnesium, iron and aluminum ions for calcium in the structure. Typically, the most common and abundant substitute for calcium other than magnesium is ferrous iron, e.g., $Ca(Mg, Fe)(CO_3)_2$. This is the primary reason that dolomites have a higher absolute density than limestones due to the inclusion of the heavier magnesium and iron ions.

The above discussion on limestone and dolomite suggests two possibilities related to the results of this research. First, Blatt et al. (1972) points out that due to the depositional and environmental formation of carbonates, they tend to be relatively uniformed in composition and structure as opposed to other sedimentary rock types. This is primarily due to carbonates forming in basins as opposed to being transported as in the case of sand and other clastic sediments. This can be seen to some degree in the results from Table 1.2 (Section Three) for the absolute density (G_{ab}) values for the carbonate aggregates. The absolute density measurements were made using a Micromeritics 1330 helium pycnometer, which can provide accurately a material density to four significant digits due to the use of helium gas to penetrate the internal structure of the material. The results from Table 1.2 are as follows:

		G_{ab}		
Limestones:	Presque Isle	2.687	Average:	2.691
	Bay County	2.697	Standard deviation:	± 0.005
	Port Inland	2.690		
Dolomites:	Cedarville	2.770	Average:	2.813
	Denniston	2.828	Standard Deviation:	± 0.296
	Rockwood	2.836		
	France Stone	2.818		

Clearly, the limestone aggregates have a very constant density value with relatively little variation. This is somewhat surprising since the geological age of the limestone ranges from Silurian (France Stone) to Mississippian (Bay County) as well as in geographic location. The dolomites, on the other hand, show a larger variation in absolute density with the Cedarville aggregate lying between the limestone and dolomite carbonates although the remaining three dolomites are reasonably close in value. While certainly not conclusive, the variation may also suggest the secondary nature of the dolomite and may also help explain why there appears to be more variability in the dolomites results as opposed to the limestone results. It may also help explain the variation in the Cedarville dolomite in relation to the other dolomites. Although speculative, it is possible that the lower absolute density of the Cedarville dolomite may indicate that the replacement process was significantly different than for the other dolomites. That is, less magnesium and ferric iron ions were involved since the higher absolute densities of the dolomites is due to the replacement of calcium with heavier magnesium and iron ions. It is also interesting to note that there is an inverse relationship between the absolute density and the bulk density for the Rockwood, Denniston and France Stone dolomites. That is, as the absolute density increased the overall bulk density decreased. However, an important aspect of bulk density is the size and distribution of the pores and fractures within the aggregate, which can dramatically affect an aggregate's performance in a number of areas such as strength and freeze-thaw durability.

A second possibility is that the mechanism of dolomitic replacement would obviously affect the development of new grain boundaries and pore spaces during and after transition of limestone to dolomite. Cleary, if migrating ground waters or ocean waters are resulting in the growth of new minerals within the existing structure of the limestone, grain boundaries and pore spaces will change. Again, while speculative it is possible that a net result in the replacement process is an overall decrease in the stability and strength of the grain boundaries, especially if the crystal development is to result in larger crystal or clusters of crystals. Inspecting Figures A.6 through A.9, it can be seen that the structure of the four dolomites are generally different than the limestones. In particular, it is interesting to examine the Cedarville dolomite, which has very large grains and a somewhat irregular and disorganized structure as compared to the France Stone dolomite, which has a somewhat smaller grain size but is also much more uniform. The grain size of the Denniston and Rockwood dolomites, however, are even smaller and equally uniform, with Rockwood somewhat smaller than the Denniston dolomite. In reviewing the rate sensitivity parameters for the dolomites, i.e., France Stone $\lambda=10.81$, Cedarville, $\lambda=10.27$, Denniston $\lambda=8.77$ and Rockwood $\lambda=4.52$, the apparent trend is for the larger grain size dolomites to have higher rate sensitivity. This trend is opposite to what was observed with the limestones in which the strain rate parameter increased with smaller grain size. As noted above, the rate sensitivity of a material is a function of the microstructural inhomogenieties such as pores, cracks and impurities that exist along the grain boundaries. Clearly, due to the secondary nature of dolomite as a replacement product it is possible that there could be a change in the microstructure of the dolomite after transition from a limestone with the development and growth of new crystals. As a consequence, there may also be a marked difference in the dynamic response between limestones and dolomites. This is seen in the D/S results where the average D/S = 2.30 for limestones and D/S = 1.64 for the dolomites. While it is speculative that the variations in dynamic test results are a result of the replacement process of limestones into dolomites, it does suggest that the dynamic testing may provide a means of characterizing some aspects of the microstructural features of carbonates and in turn providing a means of better classifying carbonate aggregates.

The igneous aggregates tested, while both mafic in composition, also represent two very different formational environments. The basalt (specimen 11) is from the Portage Lake Lava Series and is known as a flood basalt. That is, the molten rock (magma) flowed out onto the earth's surface as lava, thus being exposed to the earth's atmosphere. Consequently, the cooling of the basalt was relatively rapid as compared to magmas that are trapped within the earth. This is seen by a large number of gas bubbles trapped in the rock as well as a differentiation of the lighter and heavier minerals due to gravity. The diabase, on the other hand, (Specimen 12) while primarily composed of the same chemical composition as the basalt, formed as a traprock (the reason for the quarries name Ontario Traprock). A traprock is a magma that is trapped below the surface of the earth where it crystallized under higher pressures and temperatures than the temperature and pressure at the earth's surface. Consequently, the crystal size of the diabase is considerably larger than the basalt. The difference in microstructure between the basalt and the diabase can be seen in Figures A.10 and A.11 (Section Three). As would be expected the diabase, with a slower cooling environment, forms a more stable crystalline structure. Although the grain structure is larger, it is likely that the strength of the grain boundaries is also higher with less inhomogenieties and defects due to the more stable cooling environment. This is seen in both higher strength and in higher rate sensitivity for the diabase with λ=31.30 versus λ=26.90 for the basalt. It is also interesting to compare the structure of the Algoma air-cooled slag with that of the basalt in that both have a similar splinter-like crystalline structure. The diabase, on the hand, has very well developed crystals. Although only two igneous aggregates in addition to the slag aggregate were tested, the dynamic testing results tend to indicate variations in microstructure. However, as note above additional research will be required to fully explore this relationship.

5.1.3 Aggregate Index Correlations

The primary aggregate index correlations used to classify aggregates used in PCC are the dilation and durability index values, which are used to assess freeze/thaw susceptibility and the LA abrasion index. These index values were obtained from the Michigan Department of Transportation (MDOT, 1997) and are presented in Table 5.3. These index values were than compared to the static and dynamic compressive strength results from this research. It should be noted, however, that while the index values are generally representative of the aggregate from each quarry, there might be some variation in these index values when applying them to the aggregates investigated in this research. This is due in part to the MDOT index values being derived from quarry samples taken at a specific point in time but where natural variations can occur as mining progresses over a longer period of time. Consequently, additional deviations are associated with comparing the MDOT index data with the results from this research. In general, the index values were compared to the static and dynamic strength, the D/S ratio, and the rate sensitivity parameter λ of the aggregates tested. Overall, the rate sensitivity parameter λ had a better correlation with the index values than the other research results. However, there also were some variances within the index values themselves. For example, the Bay County limestone (5) has very poor dilation, durability, and LA abrasion values. Moreover, its index values differ significantly from the other two limestones, the Presque Isle (4) and Port Inland (6) limestone, which were investigated in this research. However, the strength, bulk density and porosity values as well as the microstructure observed in the Bay County limestone thin section compared very well with the other two other limestone aggregates investigated. [2]

The first correlation investigated was between the dilation and durability index values and the strain rate parameter λ. This correlation is plotted in Figure 5.4 where it can be seen that there is considerable scatter when all of the data is plotted together. However, as with previous data sets there are data that group together. In particular, data with rate sensitivity parameters less than 15 and those greater than 25, which are also identified on Figure 5.4. Inspecting the

[2] It should be noted, though, that when initially coring the test samples of the Bay County limestone with an oil-based coolant, it was observed that unlike the other aggregates the Bay County limestone absorbed the coolant into its pores. It is speculated that the absorption was due, in part, to the fossils incorporated in to the limestone and not necessarily from the limestone matrix itself.

index values based on geologic origin it can be seen that if the carbonate data for rate sensitivity less than 15 are plotted together while excluding the Port Inland limestone, which has a high rate sensitivity and the Bay County limestone, which appears to have erratic index values, there is an excellent correlation between both dilation and durability with the strain rate parameter λ. This plot is presented in Figure 5.5 along with the linear correlation lines plotted on the figure and having a linear regression coefficient of 0.98 for the dilation data and a linear regression coefficient of 0.99 for the durability data[3]. The data includes all four dolomites and the Presque Isle limestone. This is particularly interesting result, since the dilation and durability index tests are performed on concrete specimens.

Table 5.3 Relevant aggregate index properties from MDOT.

Aggregate	Dilation	Durability	LA Abrasion Max	LA Abrasion Min	LA Abrasion Last
1 AC Algoma Slag	---	----	41	28	32
3 WQ Levy Slag	0.001	99	43	36	40
4 Limestone, Presque Isle	0.005	88	31	25	24
5 Limestone, Bay County	0.131	6	44	23	44
6 Limestone, Port Inland	0.004	86	28	26	26
7 Dolomite, Cedarville	0.002	95	38	28	31
8 Dolomite, Denniston	0.008	80	35	30	30
9 Dolomite, Rockwood	0.035	41	38	21	21
10 Dolomite, France Stone	0.002	96	42	26	26
11 Basalt, Moyle	0.008	80	16	15	15
12 Diabase, Ontario Trap.	0.000	100	14	12	13

In regards to the LA abrasion index values, a relatively linear inverse relationship (dashed lines) exists between the maximum LA abrasion index values and the unconfined compressive strength (both static and dynamic) as shown in Figure 5.6. While both the static and dynamic compressive strength data exhibit an inverse relationship with LA abrasion index, the dynamic strength data gives a much broader slope and is able to separate the aggregates (or spread the

[3] The two correlations are basically equal in value since the durability index is calculated from the dilation results.

data) for better correlation. For example, the static data for all the carbonates is clustered and provides only limited information for comparison of one aggregate against the other based on this property. However, the dynamic data provides a broader range allowing for separation of the data, which may better assist in ranking of these materials based on this property. It can also be noted that the dynamic values should in some way correlate with the LA abrasion since the abrasion process (or material fracture) during the test occurs typically in milliseconds and hence one can argue that the use of dynamic strength data as a more realistic representation of the process. Therefore, the relationship between the strain rate sensitivity parameter, λ, and the maximum LA abrasion values for the aggregates are plotted in Figure 5.7. Again a relatively linear relationship is also observed in this figure illustrated by the gray trend line, although the correlation coefficient is only 0.74. However, the carbonates taken collectively clearly do not fit a linear relationship and in fact appear to have a reverse relationship if the Port Inland limestone (λ=25) is excluded. This relationship is presented in Figure 5.8 where the linear correlation coefficient is only 0.23 and where the relationship indicates that the LA abrasion values increase with increasing strain rate parameter.

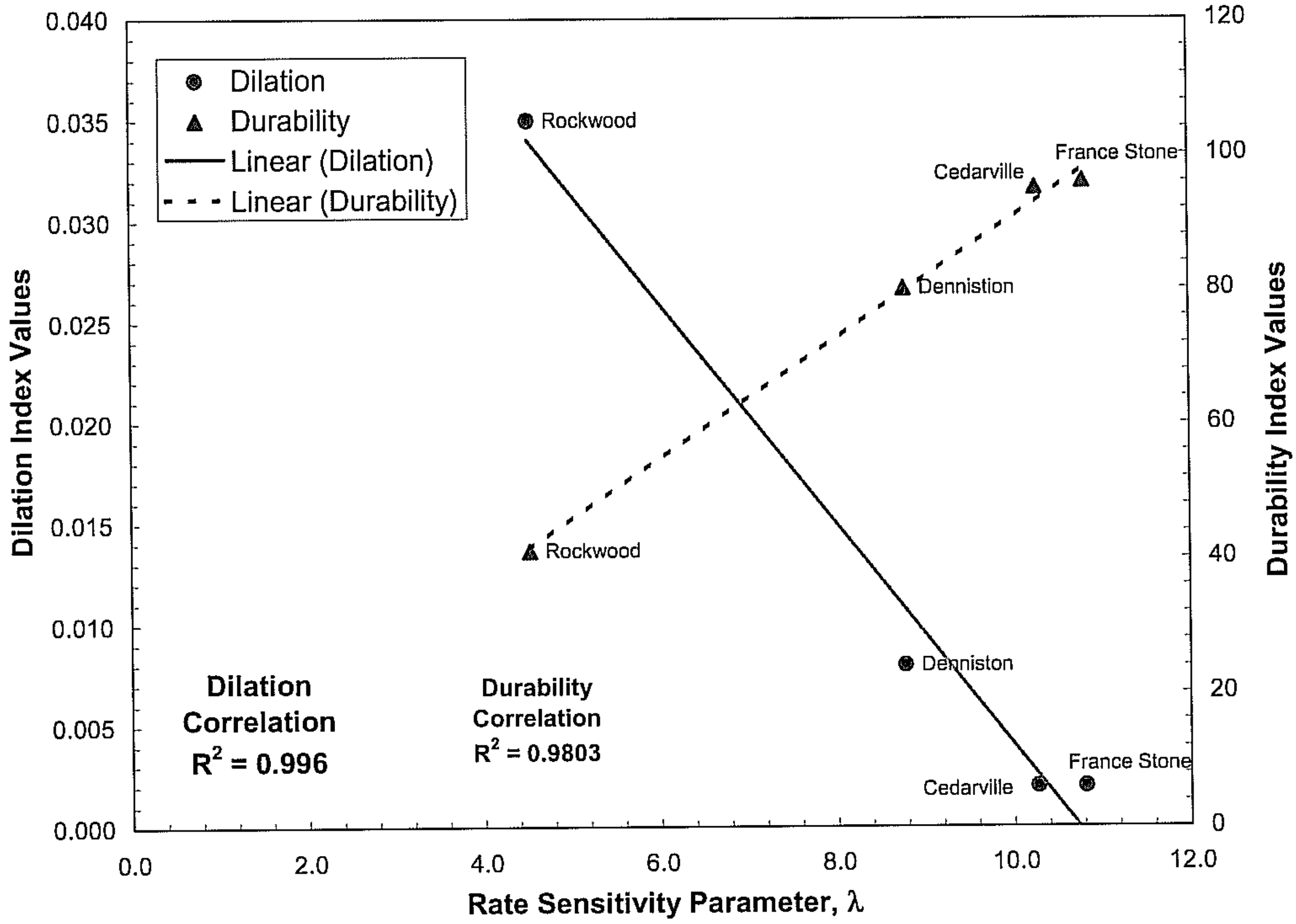

Figure 5.5 Dilation and durability index values for carbonate aggregates versus strain rate parameter λ.

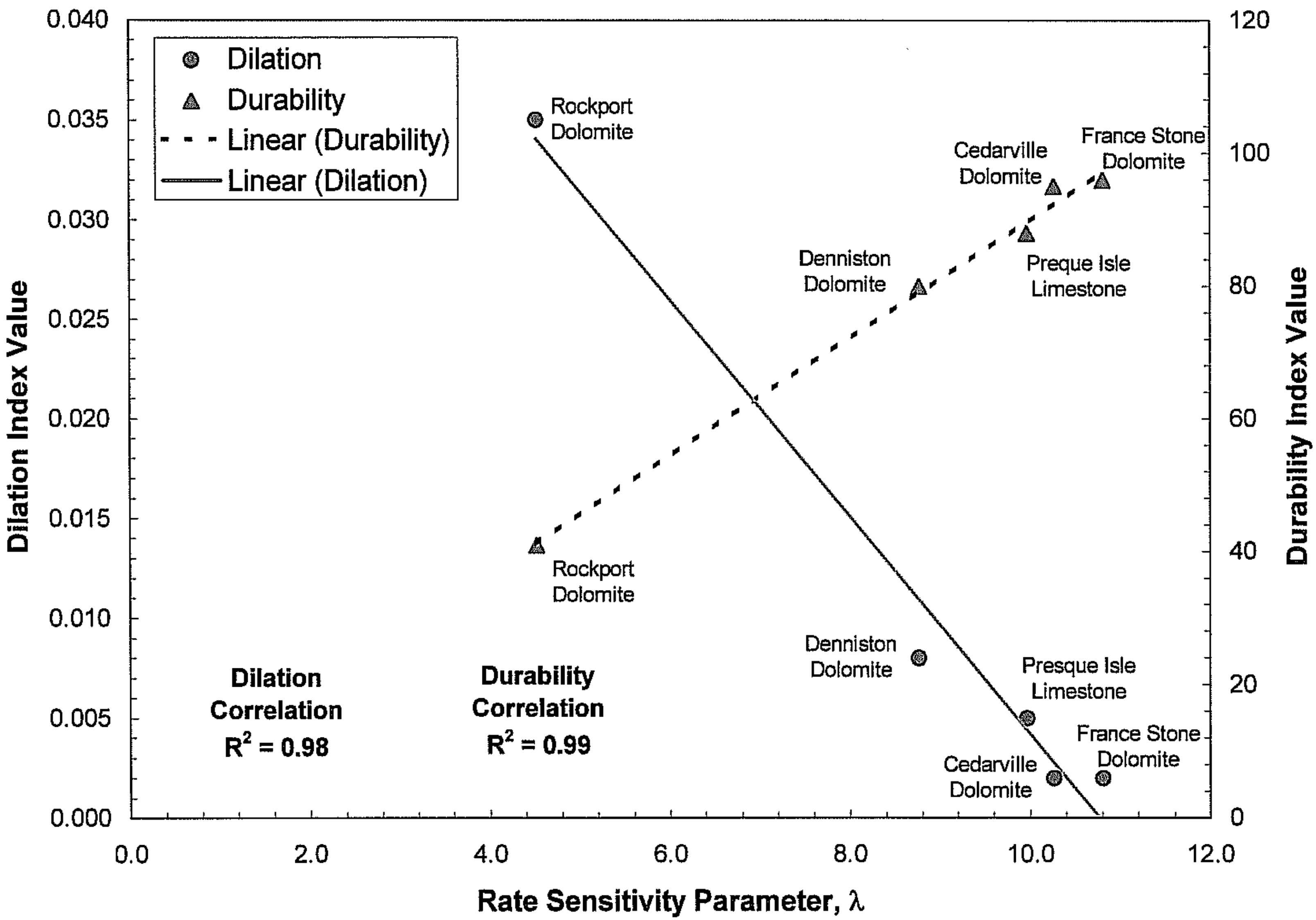

Figure 5.5 Dilation and durability index values for carbonate aggregates versus strain rate parameter λ.

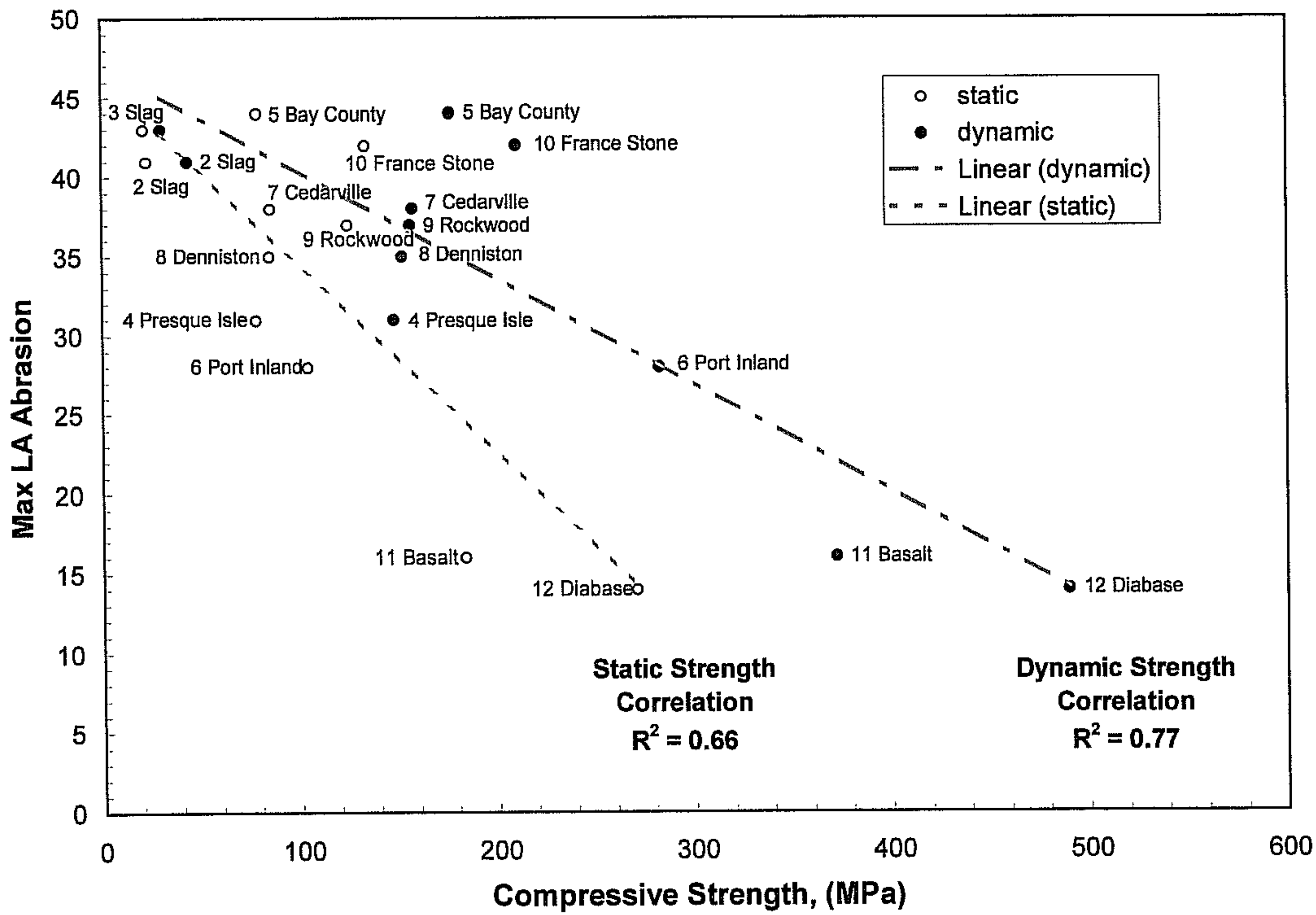

Figure 5.6 Maximum LA Abrasion values versus compressive strength.

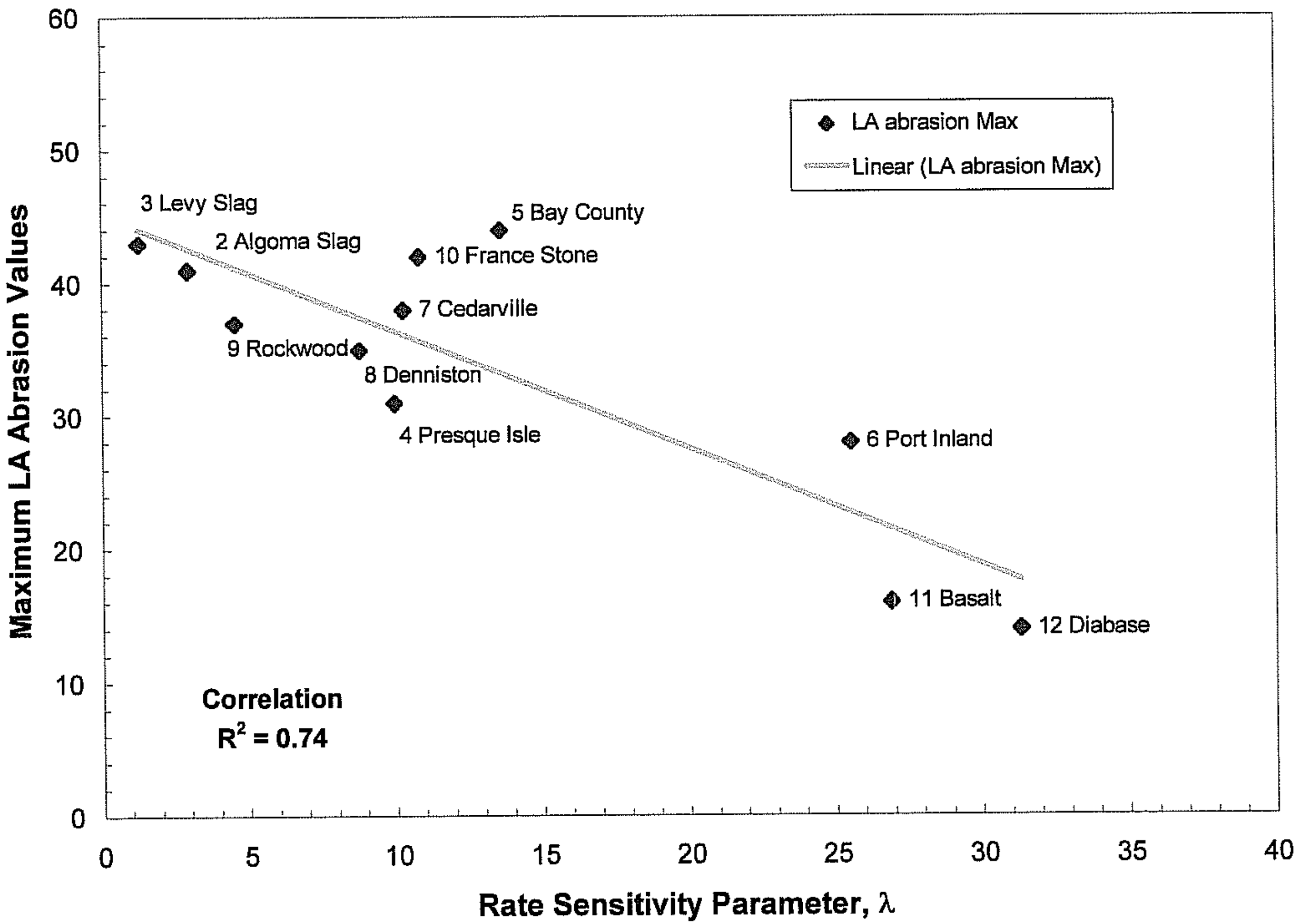

Figure 5.7 Maximum LA abrasion values versus the rate sensitivity parameter.

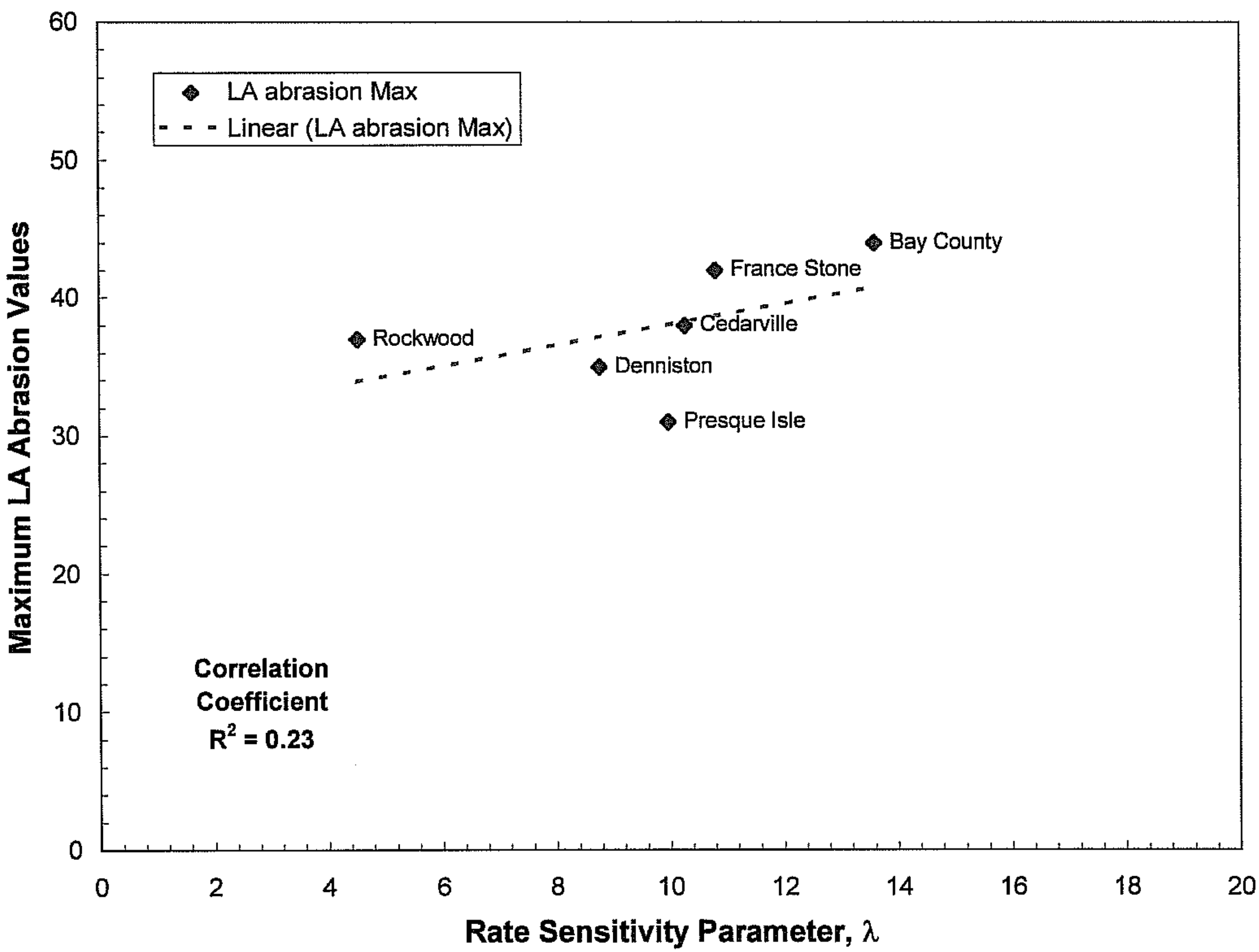

Figure 5.8 Maximum LA abrasion values for the carbonate aggregate versus the rate sensitivity parameter.

5.2 Cement Matrix

The uniaxial compression test results, shown in Figure 4.7, indicates that the cement matrix (mortar) is also rate sensitive. In general, the results show a dynamic strength to static strength (D/S) ratio of 1.5 to 3.5 in uniaxial compression. This compares well with the research by Ross et al., (1985) who also reported a 1.5 to 3 increase for mortar. However, the details concerning the mixing method and curing of the mortar tested in Ross's et al. research were not provided. As mentioned in Chapter Three of this section, the mortar's air content is critical to correctly representing the actual mortar in PCC. The mortar was mixed following the MDOT mortar voids method discussed in Section 4 at a 5% air. However, this produced a stronger mix than exists in PCC. A second batch was then prepared at 9% air, which was believed to be more representative of the mortar in PCC. In general, the average static strength of the mortar (over the testing period) was 24 MPa while the dynamic strength was approximately 58 MPa. It is interesting to compare the mortar's static and dynamic strengths versus the aggregate strengths, which is provided in Table 5.4 and grouped by geologic categories. From these data it can be seen that the mortar and slag are relatively close in compressive strength with the mortar's dynamic strength higher than the dynamic strength of the slag. Otherwise, all of the aggregate types tested are (at a minimum) four times stronger than the mortar in both static and dynamic strength. As discussed in Section Four, since the 28-day strength of PCC is primarily a function of the mortar strength; the strength of the coarse aggregate does not play as important a role in overall strength. However, it is unclear what the effects (if any) to PCC are when the coarse aggregate strength is approximately or somewhat lower than the mortar strength.

Table 5.4 Average static and dynamic compressive strengths of mortar and aggregates.

Material Type	Static[4] Strength Mpa	Dynamic[4] Strength MPa
Mortar	24	58
Slag	22 (20)	37 (52)
Limestone	85 (80)	195 (170)
Dolomite	107 (106)	173 (162)
Igneous	226 (162)	430 (398)

[4] Compressive strengths are from dry testing conditions while the compressive strengths for saturated test conditions are in parenthesis. No saturated mortar samples were tested.

Another interesting aspect of the mortar testing presented in Figure 4.7 is the variations in strength over the 18-week testing period with both increases and decreases in static and dynamic strengths. The static strengths increase during the first four weeks and then decrease slightly in weeks five and six and then increase again to about a maximum in week seven to approximately 30 MPa. However, after seven weeks the static strength levels off to about 20 MPa (±5 MPa).

The dynamic strength results mirror to some degree the static results in general overall increases and decreases. The fact that both the static and dynamic tests have similar variations is important since it verifies that the variations are occurring in the mortar instead of due to experimental errors since the static and dynamic tests were independent tests. The most obvious dynamic strength increase occurs after the first two weeks where the mortar, at around 50 MPa, reaches a maximum dynamic strength of approximately 70 MPa and maintains this strength over three weeks. This three-week period of time is also when the standard 28-day PCC tests, i.e., fourth week, are conducted. After the fifth week the strength drops dramatically off to a low of 50 MPa at week nine. Interestingly, this is also accompanied by a decrease in the static strength to the minimum strength reached in the static test of 20 MPa. At this point the D/S ratio has dropped from a high of 3 at 28-days to a low of 1.5 at week nine. This occurs two more times throughout the testing at 11 and 15 weeks where the mortar reaches a maximum dynamic strength of 70 MPa followed by a decrease. It is unclear as to the reasons for these variations in both static and dynamic strength during curing, which was conducted in the same manner as the concrete specimens tested in this research. One possibility for the variations is that the mortar specimens, which were cored from two larger mortar blocks, may have been taken at different locations within the blocks that were at different points of curing. For example, core specimens taken near the edge of the blocks may be at a different point of curing than specimens taken in the middle of the mortar blocks. However, during testing all of the cores were mixed together in an attempt to minimize this problem. A second possibility is that during cement hydration some micro cracking may be occurring, thus indicating that the developing microstructure of the mortar is altering during the curing time. It was speculated in the aggregate section that the D/S ratio might be a function of a material's microstructure. If this is the case, the D/S changing from a low of 1.5 to a high of 3.5 (week 11) may indicate that microstructural changes are occurring; resulting in both increases and decreases in strength. However, additional testing along with petrographic analysis would be required to confirm this hypothesis.

5.3 Portland Cement Concrete

Concrete specimens with the coarse aggregate as the only variable were tested in indirect tension and uniaxial compression at both static and dynamic loading rates. In addition, the tests were performed under both moist and dry conditions while being tested at 30 days[5]. The following materials were used as coarse aggregates in the PCC: Bruce Mines diabase (BM) 95-101, Levy Slag 82-019, Presque Isle limestone 71-047, Port Inland limestone 75-005 and Superior Sand and Gravel (SSG) 31-045. As discussed in Chapter Four of this section, the dry test conditions were achieved by oven drying the specimens at a temperature of 110° C for approximately three days. In addition, PCC from two older concrete pavements (aged PCC), which had been test cored, were also tested in uniaxial compression. One of the PCC pavements had a natural coarse aggregate while the other pavement had a slag coarse aggregate. However, the aged concrete, which was originally cored from six-inch diameter cylinders in the field, was later cored to two-inch diameter cores in the lab. This is a smaller diameter than the three-inch diameter specimens, which were prepared for testing the PCC with different coarse aggregates and tested after a 30-day cure. Consequently, in analyzing the test results the diameter of the specimens should be kept in mind since smaller diameter specimens tend to result in higher strengths. Also, the size of the maximum aggregate in the PCC compared to the diameter is also a factor in the strength of the PCC when testing smaller size cores.

5.3.1 Indirect Tension Testing

The indirect tension testing results were presented in Figures 4.8 and 4.9, in which Figure 4.8 provided the raw results and Figure 4.9 provided statistically processed data. From these figures the following observations were made. First, the indirect tensile strength results ranged from a low of 3 MPa to a high of 6 MPa. The static tensile strengths vary from 3.9 MPa to 4.9 MPa, a difference of only 1 MPa, while the dynamic tensile strength results ranged from 3 MPa to 6 MPa, a difference of 3 MPa. Therefore, the difference in the static and dynamic strength indicated that the concrete was rate sensitive in tension but not by a wide margin. The exception was the Port Inland PCC, which had a negative result with the dynamic strength being

[5] The 30-day cure time was selected to be consistent with the research by Ross et al. (1985, 1995 and 1996).

less than the static strength for dry conditions but essentially the same for moist conditions. It is believed that the Port Inland PCC was incorrectly prepared (as will be discussed in the uniaxial compression test discussion section) since the Port Inland PCC data had a rate sensitivity increase in uniaxial compression but none in tension. It is highly unlikely that the PCC would have no rate sensitivity in tension but have rate sensitivity in compression. Third, the results varied between dry and moist conditions for the PCC aggregate types. The Bruce Mines PCC and Presque Isle PCC had higher rate sensitivity in the dry condition then in the moist condition, whereas, the Levy slag and Superior Sand & Gravel PCC had higher rate sensitivity in the moist condition than in the dry condition. Finally, there was no statistical correlation between PCC strength and coarse aggregate strength with either the static or dynamic strengths.

While the results of the indirect tension tests were variable, the dynamic to static strength ratio (D/S) ranged from 1.0 to 1.35 at a strain rate of 80/sec. These results, however, do not compare with the D/S ratios by Ross et al., (1989, 1996) who found a D/S ratio between 6 to 8 for PCC in indirect tension; clearly a significant difference in D/S ratios. The results of the Ross et al. (1996) research were previously presented in Figure 1.9. It is unclear as to the reason for this lower rate sensitivity or the variations in the dry and moist conditions in this research, since both the dry and moist specimens were tested at the same time, which eliminated (to some degree) variations between testing the dry and moist PCC specimens. However, European researchers (Comité Euro-International du Béton, 1990) also investigated the rate sensitivity of concrete in tension. In this research they developed a model known as the CEB model to predict the D/S factors for concrete in tension based on the concrete's static compressive strength. According to the CEB model, the D/S at a strain rate of 80/sec is 1.8 (for a concrete with a static compressive strength of 70 MPa) and 2.4 (for a concrete at a static compressive strength of 30 MPa). The average static compressive strength of the PCC used in this research was approximately 45 MPa, which by interpolating the CEB model between a D/S of 1.8 and 2.4 would predict a D/S ratio of 2.2, which is considerably closer to the indirect tension results in this research, i.e., between 1.0 and 1.35 versus the results from Ross et al., at between 6 and 8. The CEB model showing the predicted dynamic to static ratio (termed a dynamic increase factor) along with the model developed by Malvar and Ross (1998) is shown in Figure 5.9. Malvar and Ross, however, in analyzing the CEB model stated that the strain rate at which rate sensitivity begins to increase was too high and that a lower strain rate should be used. By readjusting the

CEB model to a lower starting strain rate value Malvar and Ross were able to raise the predicted rate sensitivity of concrete in tension to a D/S of 6 to 8, which would be comparable to the results of Ross et al. and other researchers. In effect, they simply moved the CEB curves to the left to match their model curves. However, the CEB model, regardless of the model readjustment by Malvar and Ross was based on experimental results. As noted above, the CEB model also varied based on concrete uniaxial compressive strength, e.g., 30 MPa and 70 MPa, which show that the D/S ratios increase for lower compressive strength concrete at a given strain rate than for higher strength concrete.

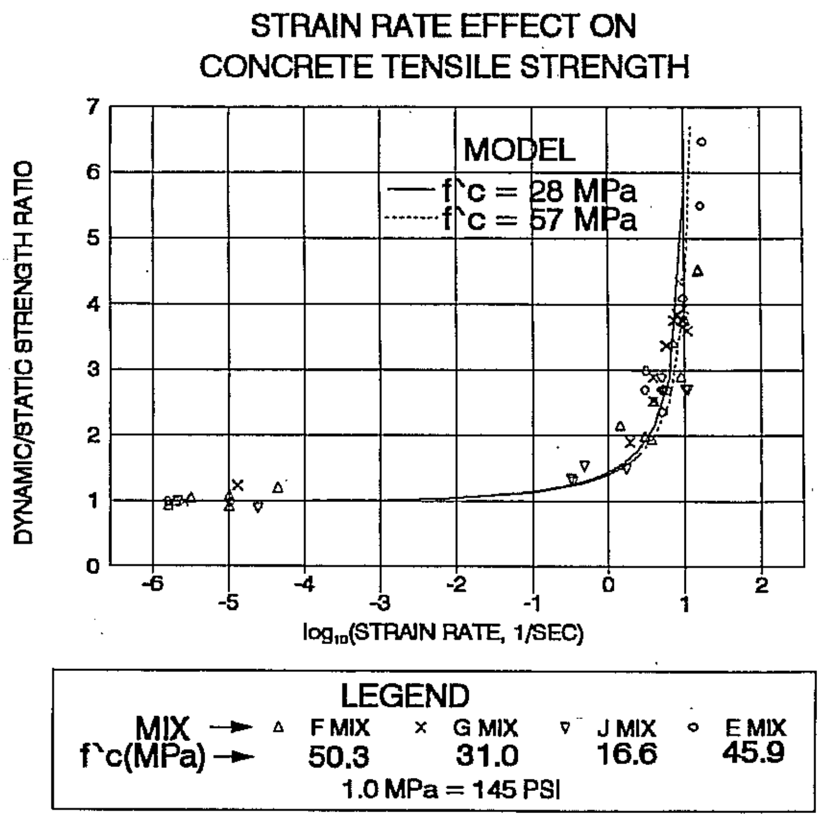

Figure 5.9 CEB and Ross et al. models for the rate sensitivity of concrete in tension, (From Malvar and Ross (1998).

It appears, however, that even discounting Malvar and Ross readjustment of the CEB model that the rate sensitivity of concrete found in this research was still lower than that predicted by the CEB model. In addition, according to Ross et al., (1996) the moist tensile strength of concrete is greater than the dry strength at high strain rates. This was seen in the Levy slag and Superior Sand & Gravel PCC but not the remaining PCC specimens tested. Ross et al. attributes the increase in dynamic tensile strength due to moisture to a tendency of the moisture to amplify the inertia effects (resistance to cracking) of the concrete. Again, the results of this research were not consistent in regard to moisture. However, the indirect tension tests procedures used in this research were based on those provided in Ross et al. (1996). For example, the same specimen length to diameter ratio of one was used, i.e., three-inch diameter by three-inch length. In addition, platens were machined in the same configuration as the platens used by Ross et al. Finally, a strain rate of 80/sec was used in this research while Ross et al. conducted the indirect tension tests in the strain rate range of 1 to 100/sec. The primary difference in the testing procedures was that Ross et al. used two-inch diameter specimens while this research used three-inch diameter specimens. This introduces a "size effect" between the two tests results with the smaller diameter two-inch specimens more likely stronger and stiffer than the larger three-inch specimens. However, as will be discussed in the following section on the PCC compression results, the difference between two and three-inch specimens should not be that large, although the difference may be larger in tension than in compression due to the lower tensile strength of PCC. Consequently, it is unclear as to what caused the lower D/S ratios and variations in moisture conditions in this research. One possible explanation, however, may be how the platens, which were used to apply a line load to the sample, were kept in alignment with respect to the test specimen. While in the static indirect tension testing the specimen can be carefully aligned as the loading platens make vertical contact with the specimen. In effect, the static test is self-aligning. However, in the dynamic testing it was harder to maintain the alignment since the specimen had to be held horizontally between the platens through friction (see Figure 3.4) from the SHPB bars. In this situation it was possible to misalign the specimen and therefore care had to be taken to align each specimen. If any misalignment did occur than the line load would not be applied diametrically across the specimen and lower failure strength would result since a smaller area across the specimen would fail in tension. However, there was no mention by Ross et al. (1996) concerning using an alignment fixture. If the dynamic indirect tension testing is continued it is highly recommended that a self-aligning fixture mechanism to hold the sample correctly in place be designed, tested, and used in future research.

In considering the results of the Ross et al. (1996) research, it is also unclear as to why the PCC is more rate sensitive in tension than in compression in regards to concrete failure. It is possible that the significantly lower tensile strength of concrete (both static and dynamic strength) compared to the compressive strength may account for this increase rate sensitivity. That is, lower strengths would be more affected by the rate of loading than higher strength materials. This is in fact seen in the CEB model where the lower strength concrete, as determined by the concrete's static compressive strength, had higher rate sensitivity than the higher strength concrete. In considering tensile testing, the main difference between the indirect tension test and the uniaxial compression test is that in tension, failure is forced to occur along a predefined surface, i.e., diametrically through the center of the concrete disk. In the uniaxial compression test, failure occurs along many surfaces (resulting in significantly higher material strength), which may mask higher rate sensitivity since each surface has a greater potential to find a surface of lower fracture strength. It should also be noted that the length of the failure surface in uniaxial compression is typically twice as long as in the indirect tension test, since failure takes place along the length of the sample in compression but only has to travel through the diameter of the sample in tension. Taking into account the higher rate sensitivity of concrete in tension and that failure is forced through a predefined surface, coarse aggregate strength may in fact have an influence on rate sensitivity, although this was not observed in the testing in this report. It was observed, however, that failure occurred through both pop outs and coarse aggregate fracture, but that the majority of failures appeared to be through aggregate fracture, possibly due to forcing the failure surface through the diameter of the specimen. While Ross et al. (1996) tested concrete of different strengths; it appears that they used the same coarse aggregate in all of their mixes so no variation in strength would have been observed due to coarse aggregate strength. It is suggested that additional dynamic indirect tension testing may be warranted considering the large variation in coarse aggregate strength.

Lastly, it should be noted that the conclusion given in Ross et al. (1996) that the rate sensitivity of PCC in tension is independent of the PCC compressive strength appears to be incorrect. This conclusion is based on the results presented in Figure 1.9 where four different concrete mixes were tested in tension. After plotting the results for these mixes, the data is curve-fitted by two equations, one for PCC with a compressive strength of 28 MPa and one for PCC at 57 MPa. As seen in Figure 1.9 the two curve-fitted equation essentially overlap. However, the CEB model, which was discussed above and will be further discussed in the following section, as well as in a paper by Malvar and Ross (1998) clearly show that the rate sensitivity of concrete in tension is in fact a function of the PCC compressive strength.

5.3.2 *Uniaxial Concrete Compression Testing*

The results of uniaxial concrete compression testing were presented in Figure 4.10 through 4.12 for the following concrete test specimens: six-inch diameter cylinders (required ASTM cylinders for strength testing), 30-day (fresh) three-inch diameter specimens, which were cored from freshly cast PCC blocks, and the two-inch diameter PCC cored from the six-inch concrete pavement cores and referred to as "aged" concrete in this report. The three-inch diameter fresh PCC specimens were also tested in both dry and moist (curing room) conditions, while the aged PCC specimens were only tested in dry conditions.

Overall, the static compressive strength results for the fresh PCC ranged from 40 to 50 MPa (5,800 to 7,250 psi), while the dynamic compressive strength results ranged from 50 to 75 MPa (7,250 to 10,875 psi). Consequently, all of the fresh PCC tested are rate sensitive in compression. Remarkably, the aged natural aggregate (sand and gravel) PCC had a static strength of 80 MPa (11,600 psi) and was higher then all of the dynamic compressive strength results for the fresh PCC. Moreover, its dynamic compressive strength was even significantly higher at 120 MPa (17,400 psi). The aged highway slag PCC had a static compressive strength approximately equal to the average static strength of the fresh PCC while its dynamic strength was higher than the dynamic compressive strength of the fresh PCC. The high strength of the aged natural aggregate PCC, however, was somewhat surprising given the environmental factors and vehicle loading that the concrete experienced over its history. It would be expected that these factors would have reduced the concrete strength due to micro-cracking and other possible distresses. Still, both the aged natural aggregate and slag aggregate concrete were also rate sensitive with the dynamic strength greater than their static strength.

In comparing test cylinders of different diameters the size effect must also be considered. In the case of the aged highway PCC, the specimens were cored at a two-inch diameter while the 30-day PCC specimens were cored at a three-inch diameter. According to Sender (1997), smaller diameter specimens may be stronger and stiffer than larger diameter specimens given geometrical similar specimens, i.e., the same diameter to length ratio. Sender investigated the strength difference between 37.5 mm (1.5 in.), 75 mm (3 in.) and 150 mm (6 in.) diameter concrete specimens and found that there was at most a 20% between the 37.5 mm (1.5 in.) and 150 mm (6 in.) specimens. The difference between the 1.5-inch and three inch diameter specimens, however, was significantly lower at only 4%. This suggests that the size effect is not significant in comparing the two and three inch diameter specimens in this research. The size effect in compressive strength between the three-inch and six-inch diameter specimens in this research resulted in a 6% difference for the Bruce Mines PCC, 2% for the Presque Isle PCC, 2% for the Port Inland PCC, 15% for the Levy Slag PCC and 14% for the Superior Sand & Gravel PCC. On average, the Bruce Mines, Presque Isle, and Superior Sand and Gravel PCC six-inch diameter specimens had lower strength then the three-inch diameter specimens, while Levy Slag and Port Inland PCC the reverse occurred, with the larger specimens sizes having a higher strength. However, in all cases, the values were within 15%, which is lower then the variation cited by Sender (1997) of 20%. It is unclear as to why the Levy slag and Superior Sand and Gravel PCC had a higher strength for the larger six-inch specimens than the three-inch specimens.

An important part of this research was to investigate the degree that coarse aggregate strength plays in concrete's overall static and dynamic strength. In comparing the coarse aggregate strength (both static and dynamic) to the strength of the concrete it was found that there was no statistical correlation between either the static and dynamic strength of the coarse aggregate and the static and dynamic strength of the fresh PCC (after a 30 day cure) in either dry or moist conditions. While there was some concern about the quality of the mixing operations for the Port Inland PCC, the results confirm the generally held belief that the strength of fresh PCC is not strongly dependent on coarse aggregate strength. This supports the research results presented in Section Four that indicated that the concrete mixes gave adequate strength independent of coarse aggregate type, although there was up to a 10% variation is strength with the slag PCC being somewhat higher in strength than the basalt PCC followed by the natural aggregate PCC. For the strength results in this section, however, there was no clear order to the strength increases or decreases in either the dynamic or static results or in the dry and moist conditions with respect to coarse aggregate type. Taken as a whole, the average static compressive strength of the PCC in Section Four was 48.1 MPa (6,975 psi) while in this section it was 45 MPa (6,525 psi). There were, however, larger variations in strength between the PCC specimens tested in this section than in the PCC tested in Section Four. Again, it is unclear for the increase in variation between the PPC tested in this section and Section Four, since the same mixing procedures were used.

A very consistent trend in the uniaxial compressive strength results, however, was the difference in dynamic strength between moist and dry conditions. Essentially, all of the fresh PCC specimens[6] had greater dynamic strength in moist conditions than in dry conditions. In contrast, the fresh PCC static strength had both increases and decreases between moist and dry conditions, with the difference between the two conditions relatively small. Again, this agrees well with the findings of Ross et al. (1996) where a significant difference in the dynamic strength in moist and dry conditions was also observed. Moreover, Ross et al., found that the strain rate at which concrete becomes rate sensitive, i.e., the strain rate at which the dynamic strength starts to increase over the static strength, was at a lower strain rate for moist conditions than for dry conditions. This clearly indicates that water in the concrete's pore structure plays an important function during dynamic fracture and failure. Ross et al. attributes the increase in strength from moisture to inertial effects, i.e., the more mass in a specimen the more resistance to failure. Since moisture increases the concrete's overall mass, it therefore increases the concrete's resistance to failure at higher strain rates. While this is reasonable, another significant factor that must be considered is the water's state of stress in the concrete's pore space. When concrete's saturation is less than 100% and in an unsaturated state, the free water is in tension (also referred to as suction or capillary stress). The tension stress of water places an effective tension stress on the concrete specimen that in effect pulls the concrete pores together thus increasing the concrete's overall strength. This is the same concept as in soil and rock mechanics where capillary stresses act to increase the soil or rock's overall strength. Moreover, when dynamically loaded, the pores in the concrete will slightly compress reducing further the pore volume and resulting in even higher tension stresses (capillary stress). The net effect is to increase the concrete strength. However, if the concrete (or soil) become fully saturated the capillary stress is lost along with the increased strength component. The same situation will occur in soil when it becomes 100% saturated. As the dynamic stress moves through a fully saturated soil, the soil structure will attempt to compress the pore space within the soil. But since the water will not be able to escape due to the speed of the loading as well as the low permeability of the soil, the net

[6] The moisture condition of the PCC at 30-day during testing was the moisture content of the PCC immediately after curing. It was based on the water added to the concrete during mixing plus the moisture that migrated into the concrete during the 30-day curing process. The plastic molds were removed after 24 hours and the specimens exposed to 100% humidity in the curing room for 30 days. However, the concrete would still not be at 100% saturation but at a somewhat lower saturation.

effect is to increase the pore water pressure. Increasing the pore water pressure in turn causes a decrease in the soil's effective stress resulting in a decrease in soil strength, since the pore water pressure is now positive and pushing the soil grains apart. It is speculated that this same phenomenon may occur in concrete. That is, while there is an increase in dynamic strength with moisture in unsaturated conditions, the reverse may occur at 100% saturation where a strength decrease can result. This may be very important in concrete pavement performance during the springtime of the year or when concrete pavements become saturated. However, a more useful role for the dynamic testing of concrete in moist conditions is the possibility that it may provide a better means of quantifying a concrete's pore structure such as pore size, distribution and connectivity. Essentially, a majority of a concrete's pore system is in the mortar with a smaller amount (in general) in the coarse aggregate. Therefore, by changing a concrete's air content and subsequently the size and distribution of the air voids, its response to dynamic loading in unsaturated and fully saturated conditions may be different indicating important aspects of the air-void system. In addition, since the dynamic loading tests the entire concrete specimen, it may better quantify the properties of the concrete than can be done with testing smaller parts of the concrete such as for example with thin-sections. However, additional research will have to be conducted to verify this hypothesis. If Ross's hypothesis is correct, then fully saturated concrete should have the highest dynamic strength and then decreasing with decreasing moisture content. However, if the hypothesis presented in this research is correct then the dynamic strength should increase to just near full saturation but then decrease when fully saturation is reached due to a loss of capillary stress. Again, if the hypothesis presented above is correct it may also provide significant information concerning the size, distribution and connectivity of the concrete's pore structure.

As discussed above, all of the PCC specimens tested in uniaxial compression were rate sensitive, i.e., the dynamic to static strength ratios were greater than one. The dynamic to static strength ratios (D/S) for the compressive test results varied from an average 1.4 to 1.9 at a strain rate of 25/sec and compare extremely well to the results from Ross (1989, 1995 and 1996). As noted above, moisture affects the rate sensitivity of concrete, with moisture increasing the concrete's rate sensitivity. Accordingly, Table 5.5 provides the D/S of the PCC for dry and moist conditions. Table 5.5 clearly shows the difference between dry and moist conditions with the average D/S for dry conditions 1.41 and for moist conditions 1.79. While the results for dry condition are relatively consistent, the main deviation in the moist D/S results is the Port Inland PCC. However, as noted above it is believed that there were possible problems in the preparation of this concrete. While it had adequate static strength, although somewhat low, its failure mode during static compression was also different than the other PCC tested. The primary difference in failure was that it did not exhibit a brittle failure such as in a double cone or planar failure. Instead, the PCC failed in a plastic crushing manner with very limited failure surfaces developing. The concrete is also suspect when reviewing the yield work sheets in Appendix A. While the PCC mixing procedures developed and used in Section Four resulted in very consistent concrete performance, the same procedures were also followed in preparing the PCC for concrete preparation in this section. During concrete preparation, all of the data concerning the individual components were recorded. However, the only data sheet lacking complete information was the Port Inland PCC, where the surplus water was not recorded and consequently the total water in the batch could not be determined to complete the records. Although this data was missing, the unit weight (145 pcf), percent air (4.5%) and slump (2 inches) for the Port Inland PCC were all within range of the other PCC prepared and tested. Since all of this data was within the range of the other PCC, it was believed that the PCC was acceptable for testing. However, the results from the indirect tension testing also show that the Port Inland PCC was problematic in that the dynamic strength results were lower than the static strength results. If in fact there was a problem with the preparation of the Port Inland PCC, it is interesting that the difference did not show up in the dry D/S, but only in the moist conditions D/S ratio data. As discussed in the aggregate D/S results, the D/S appears to be strongly a function of the material's microstructure. For example, the basalt and slag aggregates had similar D/S ratios suggesting a similar microstructure. Freshly prepared concrete therefore should also have a similar microstructure or pore structure if prepared in similar proportions and manner. In fact, this is seen in the relative consistency of the dry and moist D/S results. The obvious contradiction to this trend is the Port Inland PCC, which appears to have been improperly made. However, if the D/S ratio is sensitive to the microstructure of the mortar and it is assumed that the Port Inland PCC had some form of variation in its microstructure due to the improper mixing, than the moist D/S results would have provided an indication of this problem. That is, the D/S ratio would indicate a deviation in the performance of the PCC, while the unit weight, percent air and slump all indicated acceptable PCC.

Table 5.5 Ratio of dynamic to static strength tests for uniaxial compression test in dry and moist conditions.

PCC Type		Dry Dynamic/Static	Moist Dynamic/Static
Bruce Mines	(95-101)	1.50	1.86
Levy Slag	(82-019)	1.38	1.80
Port Inland	(75-005)	1.38	1.59
Presque Isle	(71-047)	1.40	1.84
Superior Sand & Gravel	(31-045)	1.40	1.79
Natural Aggregate:	Aged PCC	1.50	Not Tested
Slag Aggregate:	Aged PCC	1.73	Not Tested

In reviewing the D/S results of the aged PCC, the natural aggregate PCC had a D/S ratio of 1.50 in the range of the fresh PCC dry conditions, while the slag PCC a 1.73 ratio in the range of the fresh PCC moist conditions. It was assumed prior to testing that the aged PCC would most likely have decreased in strength due to environmental and loading factors. However, the aged natural aggregate PCC had the highest strength of any of the PCC tested. While this may be due to difference in mix design, preparation, placement and curing, the D/S ratio was still in the range of the fresh PCC again suggesting that the microstructure of the fresh PCC and aged PCC were similar. Interestingly, the slag coarse aggregate PCC has a higher D/S, which may again be the result of a different PCC mix design, PCC preparation, placement and curing. But another possibility may be that there was a difference in the microstructure between the natural aggregate and the slag aggregate PCC, resulting in a different D/S ratio between the two.

The above discussion suggests (but does not prove) that the rate sensitivity of concrete in compression, as defined by the D/S ratio, is relatively independent of the concrete's static or dynamic compressive strength and more a function of the concrete's microstructure. Ross et al., (1996) also presented data strongly showing that the D/S ratio is independent of concrete strength. This data is presented in Figure 5.10 and has also been annotated with the uniaxial compression results from this research for both dry and moist test conditions. The data presented in Figure 5.10 represents uniaxial compression results concrete at five different strengths: 16.6, 31.0, 34.5, 45.9 and 50.3 MPa and tested over a strain rate range of 10^{-6} to 300/sec. Although not clearly stated in the Ross et al. research, it is assumed that the same coarse and fine aggregates as well as cement type were used to create the different mixes with the only variation in the water-to-cement ratio. It can be observed in Figure 5.10 that regardless of the concrete's static strength, the D/S ratio appears to increase at the same rate for the different strength concrete with increasing strain rate. In addition, since the results of this research are relatively close to Ross et al. results, it suggests that the D/S is basically independent of overall concrete strength. In support of this, Ross et al. also provides the following statement:

> "In all of the strain work by the authors (Ross et al., 1989, 1995 and 1996) all data is usually normalized with respect to data obtained at low strain rate (static test) using the same kind of specimens. This results in the use of the dynamic increase factor, defined as the ratio of dynamic strength to static strength. Hopefully, by using this one may eliminate problems such as different maturates relative to each cure time and different mix strengths. Also, it is believed that the effects of scale due to specimen size and aggregate may also be minimized by the use of the dynamic increase factor."

In regards to the issue of maturity and specimen size it is interesting to note that in the results presented in Table 5.5 show that the aged natural slag PCC had approximately the same D/S ratio as the fresh PCC indicating that maturities and specimen size may not be a factor. However, it should also be noted that moisture affects the D/S of concrete, which has been shown in both the results in this research as well as in the results of Ross et al.

As discussed previously, in crystalline brittle material the rate sensitivity originates from the microstructural inhomogenieties such as pores, cracks, and impurities that exists along grain boundaries. Although these inhomogenieties only form a small fraction of the overall volume of material, it is known that the resistance to crack growth from these inhomogenieties is a function of strain rate. In regards to concrete, previous research as well as the results in this research indicates that for concrete the mortar's microstructure and its bonding characteristics with the coarse aggregate primary control the strength of concrete. Consequently, it is the formation of the mortar's microstructure, which includes the pore structure and bonding of the coarse aggregate, that controls its dynamic failure characteristics. This also helps explain, at least in part, the significant influence moisture has on the D/S ratio, since water in the pore space affects the state of stress during dynamic failure as was discussed previously. It was also shown that the D/S results were very consistent with a D/S ratio of 1.4 (±0.05) for dry conditions and 1.8 (±0.11) for moist conditions. However, the D/S ratio for the mortar uniaxial compression results presented in Figure 4.7 showed that the D/S ratio varied between 1.5 and 3 over the 18 weeks after mixing. One possible reason for the variations in the mortar D/S results may be due to the curing procedure used. After mixing, the mortar blocks were placed in the curing room and cored after one week of curing. The mortar test specimens were then placed in a plastic bag with water. In contrast, the PCC blocks while also placed in a curing room were cored throughout the 30-day curing period. After coring the PCC specimens were placed back into the curing room until they were tested at 30 days. Consequently, the mortar specimens may have had better access to water. It was suggested that the variation in D/S ratios over the 18-week period might have also been from microstructural changes due to cement hydration, which also may have been affected by the availability to water during the curing process. However, additional research will be needed to determine if in fact the D/S ratio is changing during the curing of the mortar and how this affects the D/S ratio of PCC.

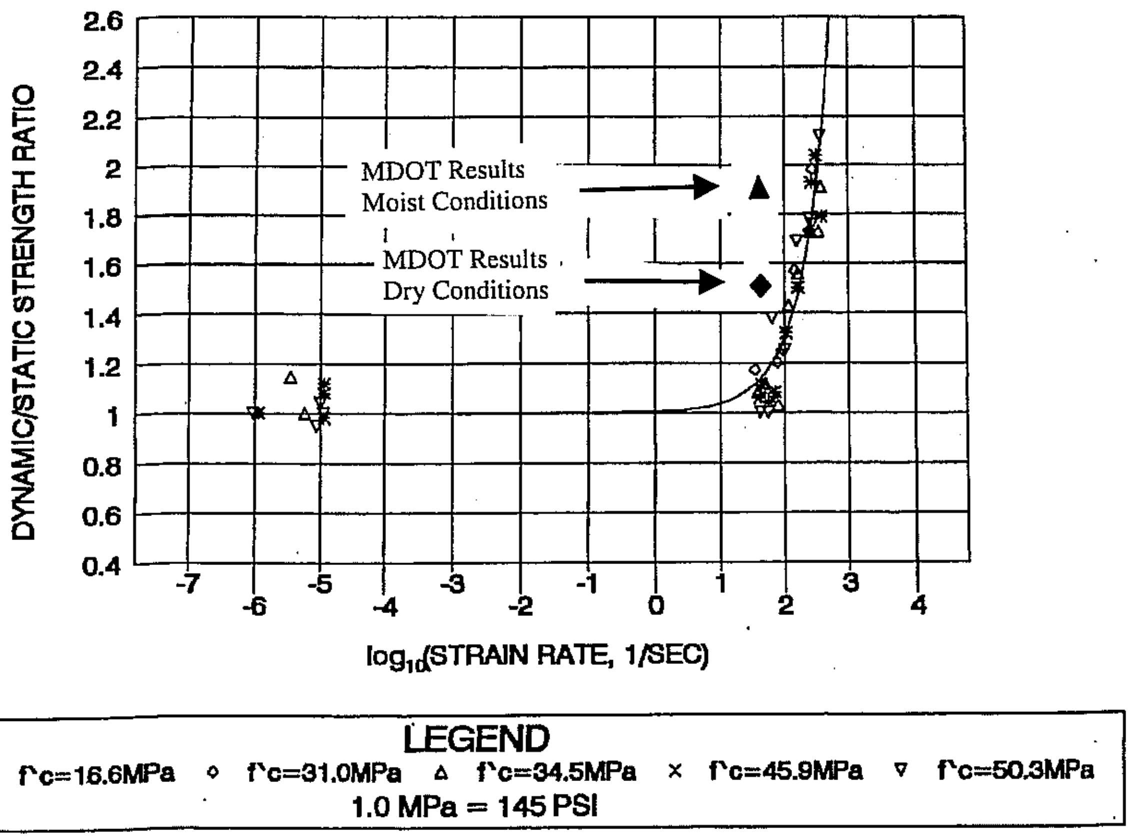

Figure 5.10 Dynamic to static compressive strength ratio for concrete compressive strength from Ross et al. (1996) and annotated with the results from this research.

Another interesting observation discussed previously is that Ross et al. (1996) states that the D/S ratio for concrete in *tension* is independent of the concrete's original static strength. However, in a later paper by Malvar and Ross (1998) it is basically shown that tension is in fact a function of the concrete's static strength. Although this point is not explicitly stated in the paper, they cite the CEB model (Comité Euro-International du Béton, 1990), which is considered the most comprehensive model for strain for the strain rate enhancement of concrete, to compare dynamic strain rate data from their research as well as others. According to the CEB model, the D/S ratio in *tension* at high strain rates is *not* independent of the static compressive strength of concrete, which was also discussed in indirect tension results. This is shown mathematically (for the CEB model) for strain rates above 30/sec as follows:

$$\frac{D}{S} = \beta\left(\frac{\dot{\varepsilon}}{\dot{\varepsilon}_s}\right)^{1/3} \qquad \textbf{5.2}$$

where:

D	=	dynamic strength
S	=	static strength
$\log \beta$	=	$7.11\delta - 2.33$
δ	=	$1/(10 + 6f'_c/f'_{co})$
f'_c	=	Concrete static compressive strength
f'_{co}	=	10 MPa
ε	=	dynamic strain rate
ε_s	=	dynamic strain rate

Equation 5.2 from the CEB model shows that the tensile D/S ratio for concrete is directly a function of concrete's static compressive strength, since the δ variable is a function of the concrete's static compressive strength. Since this data was based on experimental test results, it can be assumed that tensile D/S ratio does vary with the concrete's compressive strength. This then suggests that static and dynamic tension testing of concrete may provide more information concerning the characteristics of the concrete then compression testing does. For example, it has been pointed out by a number of researchers that compression testing is in fact a series of tensile failures as the concrete barrels and splits apart. This may also explain why there is a greater range in tension D/S ratios with respect to strain rate than for compression D/S ratios, i.e., in tension there is only generally one failure surface while in compression there are many making the failure more complex and stochastic in nature. Consequently, direct or indirect tensile testing

of concrete may better describe the overall concrete strength and possibly durability and may provide a better indication of the significance of the characteristics of the coarse aggregate in the concrete.

An estimate of the rate sensitivity parameter λ for the PCC in compression is given in Table 5.6[7]. As in the D/S ratio results, the effect of moisture can clearly be seen in these results with the moist condition at an average strain rate parameter value of 5.3 (excluding the Port Inland PCC) and the dry condition at an average value of 2.7. However, the Port Inland PCC had a similar λ value in the dry condition, as the does the other PCC specimens, but the λ value is noticeably lower in the moist condition. Again, it is in the moist test conditions that give an indication that the Port Inland PCC was different than the other concrete. It can also be seen that the dried condition λ for the aged PCC is almost double the fresh PCC results. It is also interesting to compare the strain rate parameters from Table 5.5 with the strain rate results for aggregate presented in Table 5.2. Essentially, the strain rate parameters for dry and moist condition PCC (2.3 to 5.4) are within the range of strain rate parameters for water-quenched slag aggregate while the carbonate and igneous aggregates are considerably above. However, due to the relatively consistent values in the two testing conditions, it appears that the strain rate parameter for the PCC again indicates that the mortar controls the strength of the PCC. It appears that both the D/S ratio and the strain rate parameter λ provide additional information regarding the characteristics of concrete. However, additional research will be required to better understand if and how they relate ultimately to concrete field performance.

Table 5.6 Rate sensitivity parameter λ for dry and moist conditions.

PCC Type		Dry Dynamic/Static	Moist Dynamic/Static
Bruce Mines	(95-101)	3.3	5.3
Levy Slag	(82-019)	2.8	5.2
Port Inland	(75-005)	2.3	3.6
Presque Isle	(71-047)	2.4	5.4
Superior Sand & Gravel	(31-045)	2.7	5.1
Natural Aggregate:	Aged PCC	6.2	Not Tested
Slag Aggregate:	Aged PCC	5.1	Not Tested

[7] Strain gages were not placed on the PCC specimens to measure exact strain rates. Instead, the strain rates were based on the strain readings measured from the strain gages placed on the bars of the Split Hopkinson Pressure Bar.

6 Conclusions and Recommendations for Future Research

The research focus in this section was to investigate the static and dynamic strength of coarse aggregate, mortar and concrete with a primary emphasis on the relationship between coarse aggregate strength and concrete performance. In particular, the research was focused on the development of an improved aggregate classification system that would relate the properties of coarse aggregate with concrete performance. The conclusions reached in this research are presented in the following sections followed by recommendations for future research.

6.1 Strength Conclusions

6.1.1 Aggregates

1) The static uniaxial compression test results for the igneous and carbonates had excellent agreement with the commonly used Deere & Miller rock strength classification system, verifying the static uniaxial compression testing procedures used in this research.

2) The mafic igneous aggregates had the highest uniaxial compressive strength under static loading conditions and are rated as "high strength" (Category A) according to the Deere and Miller Rock Classification System. The carbonate aggregates had average strength and are rated as "medium strength" (Category C), although three of the dolomites carbonates are in the next higher category "high strength" (Category B). The blast furnaces slag had the lowest strength of all the aggregate tested and are rated as "very low strength" (Category E). However, the dense portion of the air-cooled slag (specimen 1.2) had significantly higher strength and is rated as "medium strength" (Category C). This strength was just below the "high strength" boundary and was close to the strength of dolomites.

3) The dynamic strength for most of the aggregates increased by one strength category on the Deere & Miller Rock Strength Classification System over the aggregate's static strength. Since the static strength of the Bruce Mines aggregate was already in the "high

strength category," an additional strength category needed to be added to the Deer & Miller classification system. This was accomplished by creating the next higher strength category following the geometric progression used to generate the existing categories. The new category is termed "super high strength" (Category A') and is the category where the dynamic strength of the Bruce Mine aggregate (95-010) lies. The static strengths of the limestones are "medium strength," while the dynamic strength of the Presque Isle (71-047) and Bay County (06-008) limestones are rated as "high strength." However, the Port Inland aggregate (75-005) increased two categories to the "very high strength" category. The static strength of the Cedarville (49-065) and Denniston (58-009) dolomites are "medium strength" while their dynamic strengths increased to "high strength". However, both the static and dynamic strength of the Rockwood (58-008) and France Stone (93-003) dolomite are in the same category "high strength."

4) Both the Algoma (95-006) and Levy (82-019) water-quenched slag had the lowest aggregate strength tested and is rated as "Very Low Strength." The Algoma air-cooled slag is also rated as "Very Low Strength." However, the dense portion of the Algoma air-cooled slag (specimen 1.2) is significantly stronger and is two strength categories higher at "Medium Strength" and is approximately equivalent to the carbonate strength. It was also observed that even at very low bulk density of 2.09 g/cm^3 the porous air-cooled slag had strength equal to the water-quenched slag, which had a significantly higher bulk density of 2.40 g/cm^3. It is speculated that the early crushing of the water-quenched slag may result in a more rapid cooling of the slag reducing the mechanical properties of the slag.

5) While the static dry strength of the dolomite aggregates are higher than the limestone aggregate, the opposite occurs for the dynamic strength with the limestone having a higher strength than dolomites.

6) There is a very good correlation with dynamic strength and bulk density for the limestone aggregate and similarly for the dolomites with the exception of the Cedarville dolomite. It appears that the random and non-uniform grain size distribution of the Cedarville

dolomite, which is believed due to the secondary replacement nature of dolomite, may account for this discrepancy.

7) Rate sensitivity is defined as the increase in dynamic strength of a material over its static strength. All of the aggregate types tested are rate sensitive, although the amount of increase varied between aggregate types. The dynamic to static strengths ratios (D/S) ranged between 1.33 and 2.68 for all of the aggregates tested. There was a noticeable increase in the average D/S value between saturated and dry conditions for the blast furnace slag and the mafic igneous aggregate with an average of 1.86 and 2.62 respectively. However, there was no noticeable difference in the carbonate aggregates between saturated and dry conditions. There was, though, a significant difference in the D/S between limestones and dolomites at 2.27 and 1.74, respectively. This represents a 40% difference in the total range in the D/S of the aggregates tested.

8) A strain rate sensitivity parameter λ was defined, which takes into account the difference in static and dynamic strength and normalizes it to the difference in strain rate between the static and dynamic loading rates. The low strength slag aggregates have the lowest rate sensitivity, ranging from 1.17 to 3.00 for the water quenched slag and 9.29 for the dense air-cooled slag (specimen 1.2) for an overall average of 4.2. The carbonates have the intermediate values ranging from 4.52 to 25.52, with an average of 11.9. The high strength igneous aggregates have the highest rate sensitivity, ranging from 26.90 to 31.30, with an average of 29.1. Based on the rate sensitivity parameter, the trend in highest to lowest rate sensitivity was as follows: diabase > basalt > limestone > dolomite > slag. Clearly there was significant differentiation between aggregate types and even within aggregate types to be used as a potential classification system.

9) The first correlation investigated was between the rate sensitivity parameter λ and bulk density. There is a general increase in the strain rate parameter λ and bulk density for all the aggregates tested, with the exception of the slag specimens, having a correlation coefficient of 0.61. Grouping the limestone aggregates increased the correlation coefficient to 0.74 but decreased the correlation coefficient for dolomite to 0.42. By

excluding the higher density slag specimen (1.2) it appears that there is no increase in rate sensitivity with increasing bulk density for the slag aggregates.

10) There was a significant difference in the average strain rate sensitivity parameter λ between the dense air-cool slag (specimen 1.2) at 9.8 and the remaining slag at 2.4, which is over a four-fold difference. The rate sensitivity of the air-cooled slag was even higher than the average rate sensitivity of the dolomite aggregates at 8.6.

11) The results of the dynamic testing as represented by the D/S and rate sensitivity parameter λ results, indicated a significant difference between limestones and dolomites. In general, dolomites were stronger in static strength than limestones. However, the situation is reversed with the limestones having a higher dynamic strength than the dolomites. In addition, the limestone had a D/S of 2.30 and the dolomites had a D/S of 1.64 while the average rate sensitivity parameter λ for limestone was 16.4 and 8.6 for dolomite. Inspecting the microstructure of the carbonates indicates that for the limestone the rate sensitivity increases (both in D/S and λ) for decreasing grain size while the opposite occurred for the dolomite where the D/S and λ decreased with decreasing grain size. It is hypothesized that the formational history of the limestone and dolomite may explain this observation. Basically, limestone forms as a primary rock while dolomite forms by chemically altering the structure of the limestone. This includes recrystallizing and replacing calcium with heavier magnesium and iron ions. It is speculated that this replacement results in a weakening of the grain boundaries of the dolomite and thus results in lower dynamic strength. However, it also likely that the higher *static* strength of the dolomites versus the limestones may results from a healing of some of the larger defects due to the replacement process. The larger defects such as bedding planes and fractures generally control the static strength of an aggregate. It was also noted that the D/S ratios for the igneous and slag aggregates were approximately equal indicating similar microstructures but had significantly different strain rate parameter values (4.2 versus 29.1) indicating that the grain boundary strength was significantly different between the igneous and slag aggregate. It was again speculated that the D/S ratio might provide an indication of microstructure type while the rate sensitivity parameter strength.

12) The rate sensitivity parameter λ was compared to the freeze/thaw susceptibility dilation and durability index values for all the aggregates tested. While there was considerable scatter in the data, the aggregates could be separated into two groups; those with rate sensitivity parameters greater than 25 and those less than 15. In addition, when correlating the carbonate aggregates with rate sensitivity parameters less than 15 and excluding the Bay County limestone, which is believed to have erratic values, there was an excellent agreement between rate sensitivity and the frost susceptibility index values dilation and durability with a linear correlation coefficient of 0.98.

13) There was a general linear inverse relationship between the LA abrasion index values and the static and dynamic compressive strength results. However, the dynamic strength results had a somewhat better correlation with a linear correlation coefficient of 0.77 versus 0.66 for the static strength results. In addition, the slope of the dynamic strength versus LA abrasion results was steeper providing a broader separation of dynamic strength and LA abrasion data.

14) There was also a linear inverse relationship between the strain rate sensitivity parameter and LA abrasion data, with a linear correlation coefficient of 0.74. However, this relationship does not necessarily hold for the carbonate aggregate, which already excludes the Port Inland limestone due to its high rate sensitivity value greater than 25. For the carbonates, it appears that the relationship is reversed with the LA abrasion values increasing with increasing rate sensitivity, which does not appear to be realistic.

6.1.2 Mortar Strength

1) The mortar was found to be rate sensitive with the dynamic to static strength ratio (D/S) ratio range between 1.5 and 3.5 over the 18-week testing period.

2) Both the static and dynamic strength of mortar varied over an 18-week period with both increases and decreases over the 18-week period. Interestingly, a high strength period

where the D/S was approximately 3 occurred at the 28-day testing period followed by a decrease to a D/S of 1.5 in week nine.

3) The D/S changes may indicate that the development of the mortar microstructure during the curing process may not be constant. However, it is possible that testing procedures may have also played a role in the increase and decrease in strength over the 18-week period, although the testing procedure attempted to minimize possible variations by pre-coring and mixing the test specimens prior to testing.

6.1.3 Concrete Strength

6.1.3.1 Indirect Tension Test Results

1) The PCC was found to be only slightly rate sensitive in tension. The dynamic to static strength ratio (D/S) ranged between 1 and 1.3. In addition, there was no statistical correlation between PCC strength and coarse aggregate type in either the static or dynamic indirect tension testing.

2) The results of the indirect tension did not correlate with the results of Ross et al., (1989) who found a 6 to 8 D/S ratio. However, similar research in Europe where a model known as the CEB model predicted that the rate sensitivity of the concrete tested in this research should have a D/S ratio of approximately 2.2, significantly closer to the results in this research.

3) It is believed, however, that the results of the indirect tension testing may not have been properly conducted although the reasons for this remain unclear since the same procedures that were used in this research were based on the research of Ross et al. (1989). It is suspected that one reason for the lower results may be attributed to not having proper alignment of the specimen in the split Hopkinson pressure bar device.

6.1.3.2 Uniaxial Compression Test Results

1) All of the 30-day cured PCC tested in uniaxial compression were rate sensitive. In general the PCC had an average static compressive strength of 45 MPa, while the dynamic compressive strength was approximately 67 MPa. The Dynamic to Static strength ratio (D/S) ranged between 1.4 and 1.9, which agrees extremely well with the results from Ross et al. (1989, 1995, and 1996).

2) The aged concrete was also found to be rate sensitive. Interestingly, the natural aggregate PCC had a static compressive strength at 80 MPa, which was higher than any of the 30-day cured PCC tested, while its dynamic strength was significantly higher at 120 MPa. On the other hand, the aged slag coarse aggregate PCC had a static compressive strength of 45 MPa, which was also close to the average strength of the 30-day cured PCC, while its dynamic strength was 78 MPa, which was approximately the same strength as the static strength of the aged PCC but higher than the dynamic strength of the 30-day cured PCC. The excellent strength of the aged PCC, especially the natural aggregate PCC, was surprising since it had been obtained from existing pavement and had been exposed to both loading and environmental stresses.

3) There was generally good agreement between the six-inch specimens and the three-inch specimens tested in static loading conditions with a 6% difference for the Bruce Mines PCC, 2% for the Presque Isle PCC, and 2% for the Port Inland PCC. However, the Levy slag and Superior Sand & Gravel PCC had a 15% and 14% difference respectively.

4) There was no statistical correlation found between either the static and dynamic strength of the coarse aggregate in the PCC and the static or dynamic strength of the concrete.

5) The dynamic strength of the concrete increased with moisture, which agrees with the research by Ross et al. The increase in dynamic strength was attributed to inertial effects where an increase in moisture increases the mass of the concrete and therefore increases its resistance to failure. However, it was also noted that the moisture's state of stress must also

be considered since in unsaturated concrete the moisture is in a state of tension, which increases the overall strength of a material. Dynamic loading would cause a volume decrease, which would further increase the tension stress in the concrete. It was speculated that a fully saturated concrete would act in the opposite manner, i.e., a decease in pore volume due to dynamic loading would decrease the strength of the concrete by increasing the pore's fluid pressure.

6) The dynamic to static strength ratio (D/S) for the fresh PCC was very consistent for the dry PCC at an average ratio of 1.41 while the moist conditions were at 1.79, excluding the Port Inland PCC, which is believed to have been mixed improperly. While the D/S ratio for dry Port Inland PCC was consistent with the other PCC tested, its moist D/S was 1.59, below the other moist D/S values. Since a material's rate sensitivity, as defined by the D/S ratio, has been found to originate from microstructural inhomogenieties such as pores, cracks and impurities that exist along the grain boundaries, the PCC D/S ratio results are a function of the concrete's microstructure. In addition, it has been shown that the presence of water in the pore space (Conclusion 5) also affects the rate sensitivity of concrete. Consequently, the D/S values for concrete are an indication or a possible quantification of the concrete's microstructure. The combined D/S results for aggregate, mortar and concrete *suggests* (but does not prove) that D/S value is primarily influenced by the microstructure of the mortar followed by the microstructure of the mortar-coarse aggregate bond and lastly by the structural characteristics of the coarse aggregate.

7) The compression testing of concrete indicates that the rate sensitivity (as defined as the D/S ratio) is relatively independent of the concrete's static or dynamic compressive strength. However, indirect tension testing of concrete clearly shows that the concrete's rate sensitivity *is* a function of the concrete's strength, which is more consistent with a stronger mortar and therefore a change in the mortar's microstructure. That is, if the concrete has a higher compressive strength than the mortar strength and consequently its microstructure characteristics must also be stronger, which should result in a different rate sensitivity value, e.g., D/S ratio. This conclusion suggests that indirect tension testing may provide a better estimate of a concrete's performance than the traditional uniaxial compression testing. In

addition, since a single fracture surface generally develops in tension failure, it may also provide a better indication of the significance of mortar-coarse aggregate bond as well as the coarse aggregate strength in concrete.

8) The results of the rate sensitivity parameter λ for concrete were similar to the D/S ratio results in that it shows a significant change in value between the dry and saturated conditions. In addition, it also indicated that there was a problem with the Port Inland PCC, which had a significantly lower λ value than the other PCC tested. However, a significant difference between the D/S ratio and the λ values was between the fresh (30-day cured) and the aged concrete in dry conditions. The average λ value for aged concrete was 5.6 and 2.7 for the fresh concrete, which was over a two-fold difference. This suggest that the λ is sensitive to the concrete's maturity while the D/S ratio appears to be more a function of the concrete's microstructure. However, it is unclear at this point the relationship between the D/S ratio and the λ and why the λ is sensitive to the maturity of a concrete, while the D/S ratio is not. It appears, though, that both the D/S ratio and λ may provide significant information to better predict the performance of concrete. However, additional research will be required to better understand this relationship.

6.2 Recommendation for Future Research

The primary objective of this research was essentially two-fold. The first objective was to develop a coarse aggregate classification system while the second objective was to relate this classification system to the performance of concrete. The first objective was met with the development of the strain rate parameter λ. This parameter, which is function of the static and dynamic strength of the aggregate, provides a very broad range for differentiating aggregates. However, the research also showed that there is no statistical relationship between the strength of the aggregate and the strength of concrete, although it appears that the surface characteristics between the coarse aggregate do influence the compressive strength of the concrete to some degree. In effect, the compressive strength of concrete, as is generally assumed, is primarily a function of the mortar. The second objective was not completely successful. However, the research did show very interesting results for the rate sensitivity of concrete and in particular its' relationship to the microstructure of the mortar, as seen in the dynamic response between saturated and unsaturated conditions. In addition, the research indicates that the strain rate parameter λ for the coarse aggregate may provide performance information in regards to issues such as freeze-thaw and long-term durability. To investigate these issues the following three research areas are suggested: (1) continued investigation on the strain rate parameter λ and dynamic to static (D/S) strength ratios, (2) investigation into the microstructural characteristics of mortar using the strain rate parameter λ and dynamic to static (D/S) strength ratios, and (3) investigation of tensile testing versus compression testing as a performance test for concrete. The specific recommendations for each area are provided below.

6.2.1 Aggregate Research Recommendations

a) The strain rate parameter λ provided a means to better differentiate coarse aggregates. This was particularly important for the carbonate aggregates, where a very wide range of values were obtained with some carbonates close in value to slag and one Port Inland in the range of igneous aggregate. However, this broad range was not observed in the traditional static compression test. In addition, the dynamic to static ratios (D/S) values clearly indicated the difference in formation of the limestones and dolomites and in turn the difference in microstructure, which can relate to durability issues in concrete, e.g., freeze-thaw durability. Consequently, it is recommended a broader range of carbonate aggregates be investigated to form a larger database for carbonate, which can then be related to concrete performance tests.

b) The research results also indicated that blast furnace slags have very low strain rate parameter values. While the research shows that this low strain rate parameter values do not affect concrete's uniaxial compressive strength, the strength of the aggregate may be important in functions such as aggregate interlock. The research indicated, however, the process by which the slag forms (air-cooled versus water-quenched) may dramatically affects its overall strength. Essentially, the air-cooled slag showed greater crystallinity then the water-quenched slag with its low-density portion having equal strength with the water-quenched slag while its dense portion had strength compatible with carbonates.

To improve the strength characteristics of slag it is recommended that research be conducted into the mechanism by which the air-cooled dense portion of the slag gained its strength. Knowing the limits of this strengthening process may provide information by which slag may still be processed by water quenching and crushing, but by altering the process to some degree may provide a stronger slag product.

6.2.2 *Concrete Research Recommendations*

a) As discussed in this chapter dynamic testing is used to study the fracture characteristics of brittle materials. This research has shown that in crystalline brittle solids, such as ceramics, the rate sensitivity has been found to originate due to the microstructural inhomogenieties such as pores, cracks and impurities that exist along the grain boundaries. In effect, dynamic testing provides a method to study the microstructural characteristics of these materials. The results of this research suggest that dynamic testing can also be used to study the microstructural characteristics of concrete. Both the rate parameters λ and dynamic to static ratio (D/S) indicated significant properties of concrete independent of the traditional testing methods. For example, the D/S results suggest that the D/S ratio is independent of concrete strength but a function of the microstructural framework or type, while the strain rate parameter appears to provide the strength of the microstructure of the mortar and secondarily to the mortar-coarse aggregate interface bond. In addition, both parameters are affected by the presence of water in the pore space. This may be a very important finding and one that could lead to a relatively straightforward test method in quantifying differing pore size and distribution within the mortar. It is also suggested that this may lead to a more definitive tests for the long-term durability of concrete in both strength and in freeze-thaw conditions. Based upon these findings the following research projects are suggested:

(i) Conduct static and dynamic tests on representative samples of concrete prepared by MDOT over a period of six months to obtain a database of strain rate parameter λ values and dynamic to static strength ratios. In addition, the coarse aggregate used in the PCC should also be tested for λ and D/S values as suggested in the recommendation on aggregates and compared to the results of the concrete testing.

(ii) Concrete that shows variation in λ or the D/S values should be investigated for microstructural characteristics using scanning electron microscopic techniques to determine the primary reason for the variation and to validate the dynamic testing results.

(iii) Concrete specimen subjected to freeze-thaw testing should be tested dynamically to determine whether there are changes in the λ or D/S values before and after freeze-thaw testing. This may indicate whether the freeze/thaw process affected the microstructure of the mortar and subsequently may be used as a test criteria for the effects of freeze/thaw on PCC.

(iv) The research suggested that there should be significant variations between partially saturated concrete, i.e., 28-day concrete, and fully saturated concrete. It is recommended that a series of tests be conducted on concrete consisting of three different coarse aggregate types, basalt, carbonate and a blast furnace slag. The saturated specimens can be saturated using standard pressure saturation techniques used to saturate low permeability soils. The primary emphasis of the saturation is to fully saturate the mortar. The significance of this testing may provide a means to differentiate the connectivity and pore size distribution of the mortar, which may provide a better estimate of a concrete's durability such as in its susceptibility to freeze-thaw conditions.

6.2.3 Compression, indirect tension and direct shear testing of concrete research recommendations

While the dynamic and static compression tests were successful, it was questioned whether the indirect tension tests were valid. Research by Ross et al and others indicate that indirect tension testing may be important in the analysis of concrete. The following recommendations are provided concerning this testing:

a) The indirect tension testing procedure used in this research should be improved and addition indirect tests conducted to provide a better estimate of the rate sensitivity of the

PCC tested in this research in tension. The research by Ross et al. (1985, 1995 and 1996), indicates that the rate sensitivity of concrete as described by the D/S ratio is independent of the concrete's compressive strength. However, research by Malvar and Ross (1998) and the European researchers show that the rate sensitivity of concrete (D/S) in *tension* is a function of the concrete's compressive strength. This dependency suggests that indirect tension testing of concrete may be more sensitive to variations in concrete composition and structure than is compression testing. It has been noted that compression failure is a combination of multiple tensile fractures as the specimen splits apart.

b) However, for higher strength concrete shear failure is also important. Consequently, direct shear tests should also be conducted on the concrete. While direct shear testing of concrete has not been established as a standard test for concrete, it is believed this testing may provide a more definitive test regarding the role of coarse aggregate in concrete. In addition, defining the dynamic rate sensitivity of concrete in direct shear may also be an important parameter in the analysis of aggregate interlock.

APPENDIX A

Concrete and Mortar Mix Sheets

BATCH COMPUTATIONS WORKSHEET **WEIGHT IN kg**

Coarse Aggregate

Coarse Agg (a)

Pail tare			+ pails
			= total
25.0 - 19.0mm	0.00	0.00	
19.0 - 12.5mm	0.00	0.00	
12.5 - 9.5mm	0.00	0.00	
9.5 - 4.75mm	0.00	0.00	
Sub total			Total

BATCH NO.	Motar1
COARSE AGG	None
DATE:	6/8/99
Batch Made	Tuesday @ 3:00

Fine Aggregate

23.71 Fine Agg (b)

Moisture content

wet	dry
173.3	165.7

0.0459 moisture content

0.0459 MC

1.09 Moisture

Dry weight 23.71
+
Moisture 1.09
Total 24.80

WATER MEASUREMENT

Coarse Agg +pail ____
Coarse Agg +pail ____

Total ____

+ Total Design Water 0.00 (d) 0.00
- Reserve Water 4.00 4.00
= Pails, Agg&Water ____ H_2O 0.00

Cement

10.20 Cement (C)

Pail ID L'

Tare weight 0.85 — 1.68 tare

Tare weight 0.83 — 11.88 Pail + cement

Total tare 1.68

RESERVE WATER

Res water	4.00	0.29 surplus & Tare
+ Tare	0.29	0.29 - tare
= Total	4.29	0.00 = surplus

Reserve Water 4.00
- Surplus Water 0.00
= 4.00 H_2O + 0.00

Subtotal of water in batch = 4.00
+ Moisture in Fine Aggregate + 1.09
Total Water in Batch (D) = 5.09

Air Entraining Admixture 10 ml

UNIT WEIGHT

Weight of Concrete & Bucket ____
- Weight of Bucket 8.14
= Weight of Concrete in Bucket ____ (f)

Batch Summary

(a)	Coarse Aggregate as Designed	0.00 kg
(b)	Fine Aggregate as Designed	23.71 kg
(c)	Cement as Designed	10.20 kg
(D)	Total Water of Batch	5.09 kg
(e)	**Total Weight of Batch**	**39.00** kg

SLUMP = ____ " ____ mm

AIR CONTENT ____

- Factor of Aggregate Porosity ____
= Percent Air 9

CONCRETE TEMPERATURE, C 21

Note: a,b,c,d come from mix proportions worksheet

BATCH COMPUTATIONS WORKSHEET

WEIGHT IN kg

Coarse Aggregate

Coarse Agg (a)

Pail tare ______ ______ + pails

= total

25.0 - 19.0mm 0.00 0.00

19.0 - 12.5mm 0.00 0.00

12.5 - 9.5mm 0.00 0.00

9.5 - 4.75mm 0.00 0.00

Sub total ______ ______ Total

BATCH NO. Motar 2

COARSE AGG None

DATE: 6/8/99

Batch Made Tuesday @ 5:30

Fine Aggregate

23.71 Fine Agg (b)

Moisture content

wet	dry
173.3	165.7

0.0459 moisture content

0.0459 MC

1.09 Moisture

Dry weight 23.71

\+

Moisture 1.09

Total 24.80

WATER MEASUREMENT

Coarse Agg +pail ______

Coarse Agg +pail ______

Total ______

\+ Total Design Water ______ (d) ______

\- Reserve Water 4.00 4.00

= Pails, Agg&Water ______ H_2O 0.00

RESERVE WATER

Res water 4.00	0.29 surplus & Tare
+ Tare 0.29	0.29 - tare
= Total 4.29	0.00 = surplus

Reserve Water 4.00

\- Surplus Water 0.00

= 4.00 H_2O + 0.00

Subtotal of water in batch = 4.00

\+ Moisture in Fine Aggregate + 1.09

Total Water in Batch (D) = 5.09

Cement

10.20 Cement (C)

Pail ID L', H'

Tare weight 0.85 — 1.68 tare

Tare weight 0.83 — 11.88 Pail + cement

Total tare 1.68

Air Entraining Admixture

11 ml

UNIT WEIGHT

Weight of Concrete & Bucket ______

\- Weight of Bucket 8.14

= Weight of Concrete in Bucket ______ (f)

Batch Summary

(a)	Coarse Aggregate as Designed	0.00 kg
(b)	Fine Aggregate as Designed	23.71 kg
(c)	Cement as Designed	10.20 kg
(D)	Total Water of Batch	5.09 kg
(e)	**Total Weight of Batch**	**39.00** kg

SLUMP = ______ " ______ mm

AIR CONTENT

______

\- Factor of Aggregate Porosity ______

= Percent Air 9.8

CONCRETE TEMPERATURE, C 21

Note: a,b,c,d come from mix proportions worksheet

YIELD DATA

Coarse Aggregate:	Source Number:	Specification:
Bruce Mines	95-10	6AA
Presque Isle	71-47	6AA
Port Inland	75-5	6AA
Superior Sand & Gravel	31-45	6AA
Levy Slag	82-19	6AA

	Formulae for Computation	Batch Identification					Yield Data					Units
		BM	Pr.Is.	Po.In.	SSG	LS	BM	Pr.Is.	Po.In.	SSG	LS	
g	Unit Weight of Concrete $\frac{f}{\text{Volume of unit weight bucket}}$	33.65 0.01377	32.00 0.01377	32.35 0.01377	32.39 0.01377	31.07 0.01377	2443.7	2323.9	2349.3	2352.2	2256.4	kg/m^3
h	Batch Volume of Concrete $\frac{e}{g}$	187.00 2443.7	178.77 2323.9	#VALUE! 2349.3	185.11 2352.2	172.05 2256.4	0.07652	0.07693	-	0.07870	0.07625	m^3 batch
i	Cement used for one m^3 of concrete $\frac{C}{h}$	26.12 0.07652	26.12 0.07693	26.12 -	26.12 0.07870	26.12 0.07625	341.4	339.6	-	331.9	342.6	kg/m^3
j	Net water used for one m^3 of concrete $\frac{D}{h}$ - Absorbed Water (W)	12.56 0.07652 minus 13.23	13.77 0.07693 minus 22.39	#VALUE! - minus 14.67	13.71 0.07870 minus 23.59	15.23 0.07625 minus 40.15	150.91	156.59	-	150.67	159.63	kg/m^3
k	Water / Cement Ratio $\frac{j}{i}$	150.91 341.38	156.59 339.58	- -	150.67 331.94	159.63 342.59	0.44	0.46	-	0.45	0.47	w/c

Note: C,D,e,f,W come from batch computations worksheet

BATCH COMPUTATIONS WORKSHEET — **WEIGHT IN kg**

BATCH NO.	BM
COARSE AGG	CA-B (Bruce M.)
DATE:	12/2/99
Batch Made	Thurs @ 4:30

Coarse Aggregate

84.53 Coarse Agg (a)

Pail tare	1.75	1.75	3.50 + pails
			88.03 = total
25.0 - 19.0mm	21.13	0.00	
19.0 - 12.5mm	0.00	21.14	
12.5 - 9.5mm	0.00	21.13	
9.5 - 4.75mm	21.13	0.00	
Sub total	44.01	44.02	88.03 Total

Fine Aggregate

63.79 Fine Agg (b)

Moisture content

wet	dry
128.69	125.83
0.0227	MC

0.0227 MC

1.45 Moisture

Dry weight 63.79

\+

Moisture 1.45

Total 65.24

Cement

26.12 Cement (C)

Pail ID A', B'

Tare weight 0.85

Tare weight 0.85

Total tare 1.70

1.70 tare

27.82 Pail + cement

Air Entraining Admixture

29 ml

Batch Summary

(a)	Coarse Aggregate as Designed	84.53 kg
(b)	Fine Aggregate as Designed	63.79 kg
(c)	Cement as Designed	26.12 kg
(D)	Total Water of Batch	12.56 kg
(e)	**Total Weight of Batch**	**187.00** kg

WATER MEASUREMENT

Coarse Agg +pail	44.01		
Coarse Agg +pail	44.02		
Total	88.03		
+ Total Batch Water	12.32	(d)	12.32
- Reserve Water	3.00		3.00
= Pails, Agg&Water	97.35	H_2O	9.32

RESERVE WATER

-1.012449

Res water	3.00	1.50 surplus & Tare
+ Tare	0.29	0.29 - tare
= Total	3.29	1.21 = surplus

Reserve Water	3.00		
- Surplus Water	1.21		
=	1.79	H_2O +	9.32
Subtotal of water in batch		=	11.11
+ Moisture in Fine Aggregate		+	1.45
Total Water in Batch		**(D) =**	**12.56**

UNIT WEIGHT

Weight of Concrete & Bucket	41.80	
- Weight of Bucket	8.15	
= Weight of Concrete in Bucket	33.65	(f)

SLUMP = 1.75 " 44.5 mm

AIR CONTENT

- Factor of Aggregate Porosity
= Percent Air 4.5

CONCRETE TEMPERATURE, C 20

Note: a,b,C,d come from mix proportions worksheet

BATCH COMPUTATIONS WORKSHEET

WEIGHT IN kg

Coarse Aggregate

77.35 Coarse Agg (a)

Pail tare	1.75	1.75	3.50 + pails
			80.85 = total
25.0 - 19.0mm	19.34	0.00	
19.0 - 12.5mm	0.00	19.33	
12.5 - 9.5mm	0.00	19.34	
9.5 - 4.75mm	19.34	0.00	
Sub total	40.43	40.42	80.85 Total

BATCH NO.	Pr.Is.
COARSE AGG	CA-I (Pres. Isle)
DATE:	12/6/99
Batch Made	Mon. @ 11:30

Fine Aggregate

61.52 Fine Agg (b)

Moisture content

wet	dry
89.44	86.95
0.0286	MC

0.0286 MC

1.76 Moisture

Dry weight 61.52

+

Moisture 1.76

Total 63.29

WATER MEASUREMENT

Coarse Agg +pail	40.43		
Coarse Agg +pail	40.42		
Total	80.85		
+ Total Batch Water	12.87	(d)	12.87
- Reserve Water	3.00		3.00
= Pails, Agg&Water	90.72	H_2O	9.87

RESERVE WATER

Res water	3.00	1.15 surplus & Tare
+ Tare	0.29	0.29 - tare
= Total	3.29	0.86 = surplus

Reserve Water	3.00		
- Surplus Water	0.86		
=	2.14	H_2O +	9.87
Subtotal of water in batch		=	12.01
+ Moisture in Fine Aggregate		+	1.76
Total Water in Batch		**(D) =**	**13.77**

Cement

26.12 Cement (C)

Pail ID A', B'

Tare weight 0.85 — 1.70 tare

Tare weight 0.85 — 27.82 Pail + cement

Total tare 1.70

UNIT WEIGHT

Weight of Concrete & Bucket	40.15	
- Weight of Bucket	8.15	
= Weight of Concrete in Bucket	32.00	(f)

Air Entraining Admixture

20 ml

Batch Summary

(a)	Coarse Aggregate as Designed	77.35 kg
(b)	Fine Aggregate as Designed	61.52 kg
(c)	Cement as Designed	26.12 kg
(D)	Total Water of Batch	13.77 kg
(e)	**Total Weight of Batch**	**178.77 kg**

SLUMP = 2.5 " 63.5 mm

AIR CONTENT

- Factor of Aggregate Porosity

= Percent Air 4.25

CONCRETE TEMPERATURE, C 19

Note: a,b,C,d come from mix proportions worksheet

BATCH COMPUTATIONS WORKSHEET

WEIGHT IN kg

Coarse Aggregate

83.67 Coarse Agg (a)

Pail tare	1.75	1.75	3.50 + pails
			87.17 = total
25.0 - 19.0mm	20.92	0.00	
19.0 - 12.5mm	0.00	20.91	
12.5 - 9.5mm	0.00	20.92	
9.5 - 4.75mm	20.92	0.00	
Sub total	43.59	43.58	87.17 Total

BATCH NO. Po.In.

COARSE AGG CA-P (Port In.)

DATE: 12/8/99

Batch Made Wed. @ 11:30

Fine Aggregate

59.26 Fine Agg (b)

Moisture content

wet	dry
126.47	122.71
0.0306	MC

0.0306 MC

1.82 Moisture

Dry weight 59.26

\+

Moisture 1.82

9.16

Total 61.08

Cement

26.12 Cement (C)

Pail ID A', B'

Tare weight 0.85

1.70 tare

Tare weight 0.85

27.82 Pail + cement

Total tare 1.70

WATER MEASUREMENT

Coarse Agg +pail	43.59		
Coarse Agg +pail	43.58		
Total	87.17		
+ Total Batch Water	12.16	(d)	12.16
- Reserve Water	3.00		3.00
= Pails, Agg&Water	96.33	H_2O	9.16

RESERVE WATER

Res water	3.00	-	surplus & Tare
+ Tare	0.29	0.29	- tare
= Total	3.29	#VALUE!	= surplus

Reserve Water	3.00		
- Surplus Water	#VALUE!		
=	#VALUE!	H_2O +	9.16
Subtotal of water in batch		=	######
+ Moisture in Fine Aggregate		+	1.82
Total Water in Batch		(D) =	#####

Air Entraining Admixture

25 ml

UNIT WEIGHT

Weight of Concrete & Bucket	40.50	
- Weight of Bucket	8.15	
= Weight of Concrete in Bucket	32.35	(f)

Batch Summary

(a)	Coarse Aggregate as Designed	83.67 kg
(b)	Fine Aggregate as Designed	59.26 kg
(c)	Cement as Designed	26.12 kg
(D)	Total Water of Batch	#VALUE! kg
(e)	**Total Weight of Batch**	###### kg

SLUMP = 2 " 50.8 mm

AIR CONTENT

- Factor of Aggregate Porosity

= Percent Air 4.5

CONCRETE TEMPERATURE, C 18

Note: a,b,C,d come from mix proportions worksheet

BATCH COMPUTATIONS WORKSHEET

WEIGHT IN kg

Coarse Aggregate

87.34 Coarse Agg (a)

Pail tare	1.71	1.73	3.44 + pails
			90.78 = total
25.0 - 19.0mm	21.84	0.00	
19.0 - 12.5mm	0.00	21.83	
12.5 - 9.5mm	0.00	21.84	
9.5 - 4.75mm	21.83	0.00	
Sub total	45.38	45.40	90.78 Total

BATCH NO.	SSG
COARSE AGG	CA-G (Glacial Gravel)
DATE:	12/13/99
Batch Made	Mon. @ 4:00

Fine Aggregate

57.94 Fine Agg (b)

Moisture content

wet	dry
321.5	312.8
0.0278	MC

0.0278 MC

1.61 Moisture

Dry weight 57.94

\+

Moisture 1.61

Total 59.55

WATER MEASUREMENT

Coarse Agg +pail	45.38		
Coarse Agg +pail	45.40		
Total	90.78		
+ Total Batch Water	12.63	(d)	12.63
- Reserve Water	3.00		3.00
= Pails, Agg&Water	100.41	H_2O	9.63

Cement

26.12 Cement (C)

Pail ID G , H

Tare weight 0.85

1.68 tare

Tare weight 0.83

27.80 Pail + cement

Total tare 1.68

RESERVE WATER

Res water	3.00	0.82 surplus & Tare
+ Tare	0.29	0.29 - tare
= Total	3.29	0.53 = surplus

Reserve Water	3.00		
- Surplus Water	0.53		
=	2.47	H_2O +	9.63
Subtotal of water in batch		=	12.10
+ Moisture in Fine Aggregate		+	1.61
Total Water in Batch		**(D) =**	**13.71**

Air Entraining Admixture

29 ml

UNIT WEIGHT

Weight of Concrete & Bucket	40.54	
- Weight of Bucket	8.15	
= Weight of Concrete in Bucket	32.39	(f)

Batch Summary

(a)	Coarse Aggregate as Designed	87.34 kg
(b)	Fine Aggregate as Designed	57.94 kg
(c)	Cement as Designed	26.12 kg
(D)	Total Water of Batch	13.71 kg
(e)	**Total Weight of Batch**	**185.11 kg**

SLUMP = 2.75 " 69.9 mm

AIR CONTENT

- Factor of Aggregate Porosity	
= Percent Air	5.25

CONCRETE TEMPERATURE, C 19

Note: a,b,C,d come from mix proportions worksheet

BATCH COMPUTATIONS WORKSHEET

WEIGHT IN kg

Coarse Aggregate

68.07 Coarse Agg (a)

Pail tare	1.74	1.74	3.48 + pails
			71.55 = total
25.0 - 19.0mm	17.01	0.00	
19.0 - 12.5mm	0.00	17.02	
12.5 - 9.5mm	0.00	17.02	
9.5 - 4.75mm	17.02	0.00	
Sub total	35.77	35.78	71.55 Total

Fine Aggregate

62.62 Fine Agg (b)

Moisture content

wet	dry
143.6	138.9

0.0338 MC

0.0338 MC

2.12 Moisture

Dry weight 62.62

+

Moisture 2.12

Total 64.74

Cement

26.12 Cement (C)

Pail ID A' , B'

Tare weight 0.85

Tare weight 0.85

Total tare 1.70

1.70 tare

27.82 Pail + cement

Air Entraining Admixture

22 ml

Batch Summary

(a)	Coarse Aggregate as Designed	68.07 kg
(b)	Fine Aggregate as Designed	62.62 kg
(c)	Cement as Designed	26.12 kg
(D)	Total Water of Batch	15.23 kg
(e)	**Total Weight of Batch**	**172.05 kg**

BATCH NO. LS

COARSE AGG CA-S (Slag)

DATE: 12/15/99

Batch Made Wed. @ 4:00

WATER MEASUREMENT

Coarse Agg +pail	35.77		
Coarse Agg +pail	35.78		
Total	71.55		
+ Total Batch Water	14.11	(d)	14.11
- Reserve Water	3.00		3.00
= Pails, Agg&Water	82.66	H_2O	11.11

RESERVE WATER

Res water	3.00	1.29 surplus & Tare
+ Tare	0.29	0.29 - tare
= Total	3.29	1.00 = surplus

Reserve Water	3.00		
- Surplus Water	1.00		
=	2.00	H_2O +	11.11
Subtotal of water in batch		=	13.11
+ Moisture in Fine Aggregate		+	2.12
Total Water in Batch		**(D) =**	**15.23**

UNIT WEIGHT

Weight of Concrete & Bucket	39.22	
- Weight of Bucket	8.15	
= Weight of Concrete in Bucket	31.07	(f)

SLUMP = 1.5 " 38.1 mm

AIR CONTENT

- Factor of Aggregate Porosity

= Percent Air 4.5

CONCRETE TEMPERATURE, C 18

Note: a,b,C,d come from mix proportions worksheet

References

Abdel-Maksoud, M.G., N. Hawkins, and Barenberg (1997): E. Behavior of Concrete Joints under Cyclic Shear. *Proceedings,* ASCE, Aircraft Pavement Technology: In the Mist of Change, pp. 190-204.

Anton, R.J. and Subhash, G. (1999): Dynamic Vickers Indentation of Brittle Materials. *Wear* (in Print).

Blatt, H., Middleton, G. and R. Murray: (1972), *Origins of Sedimentary Rocks*, Prentice-Hall, Inc., Englewood Cliifs, New Jersey, p. 634.

Cargill, J. S. and Shakoor, A. (1990): Evaluation of empirical methods for measuring the uniaxial compressive strength of rock. *Int. J. Rock Mech. Min. Sci. & Geomech. Abstr.,* 27, 495-503.

Cohee, G. V. (1965): Geologic History of the Michigan Basin, Washington Academy of Science Journal, Vol. 55, pp. 211-223.

Deere, D. U., and R. P. Miller (1966): Engineering Classification and Index Properties for Intact Rock. Technical Report No. AFWLTR-65 116, Air Force Weapons Laboratory, Kirkland Air Force Base, New Mexico.

Dutta, K. and Kim, K. (1993): High-Strain-Rate Tensile Behavior of Sedimentary and Igneous Rocks at Low Temperatures, U.S Army Corps of Engineers, CRREL Report 93-16, pp. 11.

Fairbanks, C. J. , Polvani,R. S. , Wiederhorn, S. M. , Hockey B. J., and Lawn, B. R. (1982): *J. Material Sci. Letts.,* 1982, 1, pp. 391-393.

Follansbee, P.S. (1985): The Hopkinson Bar, *Materials Testing, Metals Handbook,* 9th Edition, American Society of Metals, Metals Park, OH, Vol. 8, pp. 198-203.

Grady, D. E., and Lipkin, J. (1980): Criteria for Impulsive Rock Fracture. *Geophys. Res. Lett.,* 7, pp. 255-258.

ICE, (1976): Manual of Applied Geology for Engineers, Institution of Civil Engineers, London, p. 378.

Jumikis, A. R., (1983): Rock Mechanics, Second edition, Trans Tech Publications, Zellerfield, Germany, pp. 62-63.

Kawatra and Eisele (1989): Effect of temperature on the performance of an autogenous grinding circuit. Advances in Autogenous and Semiautogenous Grinding Technology (A. L. Mular and G. F. Agar, Eds.) Dept. of Mining and Mineral Process Engineering, University of British Columbia, Canada, pp. 485-499.

Koeppel, B. J. and Subhash,G. (1999): Characteristics of Residual Plastic Zone Under Static and Dynamic Indentations, *Wear* 224, pp. 56-67.

Lankford, J. (1981): Mechanisms Responsible for Strain-Rate Dependent Compressive Strength in Ceramic Materials, *J. Am. Cer. Soc.,* 64, c-33- c-35.

Lankford, J. and Blanchard, C. R. (1991): Fragmentation of Brittle Materials at High rates of Loading, *J. Material. Sci,* 26, pp. 3067- 3072.

Lankford, J.(1998): Predebon, W.W., Staehler, J.M. , Subhash,G. , Pletka, B. J. and Anderson, C.E. The Role of Plasticity as Limiting Factor in the Compressive Failure of High Strength Ceramics. *Mech. of Material* 29, pp. 205-218.

Lea, F. M. (1971): The Chemistry of Cement and Concrete, Third edition, Chemical Publishing Company, pp. 455-562.

Lee, Y. H. and Williams, K. (1997): Mechanical Properties of Concrete in Uniaxial Compression, ACI Materials Journal, V. 94, No. 6, pp. 457-471.

MDOT (1997): Aggregate Source Inventory, Materials Testing Section, Materials and Testing Division, Lansing, MI, February.

Malvar, L. J. and Ross, C. A. (1998): Review of Strain Rate Effects for Concrete in Tension, ACI Materials Journal, November/December, pp. 735-739.

Meyers, M. A. (1994): *Dynamic Behavior of Materials*, John Wiley & Sons, Inc., New York. Nemat-Nasser, S., Issacs, J. B., and Starrett, J. E. (1991): Hopkinson Techniques for Dynamic Recovery Experiments, *Proceedings of the Royal Society of London, A,* 435, 37 pp. 1-385.

Okubo S., Nishimatsu Y. and He C. (1990): Loading Rate Dependent of Class II Rock Behavior in Uniaxial and Triaxial Compression Tests-An Application of a Proposed New Control Method," *Int. J. Rock Mech. Min. Sci & Geomech. Abstr.* 27, pp. 559-562.

Ravichandran, G. and Subhash, G. (1994): Critical Appraisal of Limiting Strain Rates for Compression Testing of Ceramics in a Split Hopkinson Pressure Bar, *J. of the Am. Ceram. Soc.* 77, pp. 263-267.

Ravichandran, G. and Subhash, G. (1995): A Micromechanical Model for High Strain Rate Behavior of Ceramics, *Int. J. of Solids and Structures.* 32, pp. 2627-2646.

Ross, C.A., Thompson, P. Y. and J. W. Tedesco, (1985): Split-Hopkinson Pressure-Bar Tests on Concrete and Mortar in Tension and Compression, ACI Materials Journal, September/October, pp. 475-481.

Ross, C.A., Tedesco, J. W. and S. T. Kuennen, (1995): Effects of Strain Rate on Concrete Strength, ACI Materials Journal, January-February, pp. 37-47.

Ross, C.A., Jerome, D. M., Tedesco, J. W. and M. L. Hughes, (1996): Moisture and Strain Rate Effects on Concrete Strength, ACI Materials Journal, May-June, pp. 293-300.

Sender, S. (1997): Size Effect Tests of High Strength Concrete," Journal of Materials in Civil Engineering, ASCE, Vol. 9, No. 1, pp. 46-48.

Subhash, G. and Nemat-Nasser, 5. (1993): Dynamic Stress-Induced Transformation and Texture Formation in Uniaxial Compression of Zirconia Ceramics, *J. of the Am. Ceram. Soc., 76*, pp. 153-65.

Subhash G. and Ravichandran, G. (1998): Mechanical Behavior of Hot Pressed Aluminum Nitride Under Uniaxial Compression. *J. Material Sci.,* **33,** pp. 1933-1939.

Suresh, S., Nakamura, T., Yeshurun, Y., Yang, K.-H., and Duffy, J. (1990): Tensile Fracture Toughness of Ceramic Materials: Effects of Dynamic Loading and Elevated Temperatures," J. Am. Ceram. Soc., 73, pp. 2457-2466.

Vitton, S. J. and Subhash, G. (1999): Dynamic and Static Strength of Aggregates: An Estimate of Rate Sensitivity of Geologic Materials, Proceedings, Institute of Lake Superior Geology, 45th Annual Meeting, Marquette, MI, Vol. 45, part 1, pp. 54-56.

Wawersik W. R. and Fairhurst C. A.(1970): A study of brittle rock fracture in laboratory compression experiments, *Int. J. Rock Mech. Min. Sci.,* 7, pp. 56 1-575.